The interactions between inflammasome activation and induction of autophagy following Pseudomonas aeruginosa infection

Majid Sakhi Jabir

A thesis Submitted in fulfillment of the requirements for the degree of Doctor of Philosophy

College of Medicine, University of Glasgow Institute of infection, immunity and inflammation

June 2014

بسم الله الرحمن الرحيم

وقل رب زدني علما

طه (114)

صدق الله العلي العظيم

In the name of Allah, the beneficent, the merciful

(Say, My lord, grant me more knowledge)

TaHa (114)

Acknowledgements

PhD research often appears a solitary undertaking. However, it is impossible to maintain the degree of focus and dedication required for its completion without the help and support of many people.

First I would like to thank Professor Tom Evans for being my supervisor. He gave much help and support through my time as a PhD student and for that I am extremely grateful.

Professor Tom Evans has provided much support and has allowed me to join his group to develop my career. He is an inspiring clinical and scientific mentor and has always tried to help develop my career in the best possible ways.

I think I can honestly say through all the ups and downs, scientific and otherwise, I have never regretted the decision to embark on a PhD (or not much anyway!). This is almost entirely due to the people I've met along the way.

This thesis would not have been possible without the help and support from my laboratory and clinical colleagues. There were always plenty of people ready and willing to give advice and support.

Dr. Neil Ritchie has been a source of wealth of knowledge in FACS and *In vivo* work. I am grateful for his patience in teaching me all the techniques that I needed to conduct my work.

Jim Riley, Shauna Kerr for making me feel welcome and assisting me in different ways within the laboratory.

I would like to thank all previous and current members in the Prof. Tom Evans lab group for their continuous support and encouragment since the beginning of my career and who were always a source of advice.

Special thanks also to my family.

Author's declaration

I declare that, except where referenced to others, this thesis is the product of my own work and has not been submitted for any other degree at the University of Glasgow or any other institution.

Signature _____

Printed name   Majid Sakhi Jabir

Table of contents

List of figures

Chapter 1

Chapter 2

Chapter 3

Chapter 5

List of Abbreviations

2-ME	2-mercaptoethanol
3-MA	3-Methyl-adenine
7-AAD	7-amino-actinomycin
8-OHdG	8-Oxo-2-deoxyguanosine
Aim-2	Absent in melanoma 2
Ambra1	Activating molecule in Beclin-1 regulating autophagy
ASC	Apoptosis-associated speck-like protein containing a CARD
Atg	Autophagy- related gene
AIDS	Acquired immunodeficiency syndrom
APC	Antigen presenting cells
ATP	Adenosine triphosphate
ATPIF1	ATPase inhibitory factor 1
BIR	Baculoviral inhibitory repeat like domain
BM	Bone marrow
BMDM	Bone marrow derived macrophages
BrdU	Bromodeoxyuridine
BSA	Bovine serum albumin
CARD	Caspase recruitment domain
Cardif	Caspase recruitment domain adaptor inducing IFN-β
CD	Cluster of differentiation
CLRs	C-type lectin receptors
CMA	Chaperone mediated autophagy
CYBB	Cytochrome B(-24), beta subunit
DAMP	Danger associated molecular pattern
DAPI	4',6-diamidin-2-phenylindole
DC	D. cells
DMEM	Dulbecco's modified Eagle's medium
DNA	Deoxyribonucleic acid
dsDNA	Double strand Deoxyribonucleic acid
ECL	Enhanced luminol-based chemiluminescent
E.coli	Escherichia coli

EDTA	Ethylene-diaminetetraacidic acid
ELISA	Enzyme linked immunosorbent assay
ER	Endoplasmic reticulum
FACS	Fluorescence activated cell sorting
FCS	Foetal calf serum
FITC	Fluorescein isothiocynate
FSC	Forward scatter
GBP5	Guanylate binding protein 5
GBP	Guanylate binding protein
GFP	Green fluorescent protein
GM-CSF	Granulocyte macrophage colony stimulating factor
HEKs	Human embryonic kidney 293 cell line
HIV	Human immunodeficiency virus
HMGB	High mobility group box
HRP	Horseradish peroxidase
HSBSS	Hanks buffered salt solution
IF	Immunofluorescence
IFN	Interferon
IL	Interleukin
IP	Immunoprecipitation
IRF	Type I IFN regulatory transcription factor
IRG	Immunity related GTpase
JNK	Jun N-terminal kinase
KO	Knock-out
LB	Luria Bertani
LC3	Light chain 3
LDH	Lactate dehydrogenase
LDS	Lithum dodecyl sulphate
LIF	Lithium fluoride
LIR	LC3-interacting region
LPS	Lipopolysaccharide
MAPLC3	Microtubule-associated protein light chain 3
M-CSF	Macrophage colony-stimulating factor

MFI	Mean fluorescence intensity
MHC	Major Histocompatibility complex
MOI	Multiplicity of infection
mtDNA	Mitochondrial Deoxyribonucleic acid
mTOR	Mammalian target of rapamycin
MyD88	Myeloid differentiation primary response gene 88
NAC	N acetyl cysteine
NADPH	Nicotinamide adenine dinucleotide phosphate-oxidase
NAIP	Neural apoptosis inhibitory protein
NBR1	Neighbor of BRC1 gene 1 protein
NF-κB	Nuclear factor-κB
NGS	Normal goat serum
NK	Natural killer
NLRs	NOD-like receptors
NLRP3	NACHT,LRR,PYD domains containing protein 3
NLRC4	NLR family CARD domain containing protein 4
NO	Nitric oxide
NOD	Nucleotide-binding oligomerization domain
POLYI:C	Polyinosine-Polycytosine
P62	Nucleoporin 62
PAMP	Pathogen associated molecular pattern
PBS	Phosphate buffered solution
PCR	Polymerase chain reaction
PE	Phosphatidyl-ethanolamine
PFA	Paraformaldehyde
PINK-1	PTEN-induced putative kinase 1
PI(3)K	Phosphoinositide-3-kinase
PtdIns(3)p	Phosphatidylinositol 3-phophate
PVDF	Polyvinylidene difluoride membrane
RIPA	Radioimmuno precipitation assay
RLRs	Rig like receptors
ROS	Reactive oxygen species
PRRs	Pattern recognition receptors

RPMI-1640	Roswell Park Memorial Institute- 1640 medium
RT-PCR	Reverse transcriptase polymerase chain reaction
SEM	Standard error of mean
SDS	Sodium dodecyl sulphate
SLE	Systemic lupus erythematosus
SLR	Sequestasome like receptor
SNPs	Single nucleotide polymorphism
SQSTM1	Sequestosome-1
SSC	Side scatter
STAT3	Signal transducer and activator of transcription 3
T3SS	Type III secretion system
TBE	Tris - base EDTA
TBP	TATA-binding protein
TE	Tris-EDTA buffer
TGF	Transforming growth factor
TH2	T-helper 2
TH17	T-helper 17
TMB	Tetramethylbenzidine
Tor	Target of rapamycin
TRAF	TNF receptor activated factor
TRIF	TIR-containing adapter-inducing IFN-β
TLRs	Toll like receptors
TNF	Tumor necrosis factor
ULK	Serine-Threonine protein kinases
UV	Ultra violet
WB	Western blot
WT	Wild type

List of publications and presentation

Publications

1- Caspase-1 cleavage of the TLR adaptor TRIF inhibits autophagy and β–Interferon production during *Pseudomonas aeruginosa* infection. (2014), Cell and Host microbe, 15, 214-227.

2- Mitochondrial damage contributes to *Pseudomonas aeruginosa* activation of the inflammasome and is down-regulated by autophagy (will publish soon in Autophagy).

Meeting Abstract

1- Majid Jabir and Tom Evans. Inflammasome activation following Pseudomonas infection inhibits autophagy. Scottish society for experimental medicine. March 2013, oral presentation.

Presentation

1- Majid Jabir and Tom Evans. Role of the bacterial type III Secretion system in autophagy. Poster presentation (2011).

2- Majid Jabir and Tom Evans. Relationship between autophagy and inflammasome activation. Poster presentation (2012).

Abstract

Introduction

Autophagy is a cellular process whereby elements within cytoplasm become engulfed within membrane vesicles and trafficked to fuse with lysosomes. This is a common cellular response to starvation, allowing non-essential cytoplasmic contents to be recycled in times of energy deprivation. However, autophagy also plays an important role in immunity and inflammation, where it promotes host defence and down-regulates inflammation. A specialised bacterial virulence mechanism, the type III secretion system (T3SS) in *Pseudomonas aeruginosa* (PA), an extracellular bacterium, is responsible for the activation of the inflammasome and IL-1β production, a key cytokine in host defence. The relationship between inflammasome activation and induction of autophagy is not clear.

Hypothesis and aims

The central hypothesis is that induction of autophagy occurs following PA infection and that this process will influence inflammasome activation in macrophages.

Our aims were to determine the role of the T3SS in the induction of autophagy in macrophages following infection with PA, and to investigate the effects of autophagy on inflammasome activation and other pro-inflammatory pathways following infection with these bacteria.

Materials and methods

Primary mouse bone marrow macrophages BMDMs were infected with PA, *in vitro*. Induction of autophagy was determined using five different methods: - electron microscopy, immunostaining of the autophagocytic marker LC3, FACS, RT-PCR assays for autophagy genes, and post-translational conjugation of phosphatidyl-ethanoloamine (PE) to LC3 using Western blot. Inflammasome activation was measured by secretion of active IL-1β and caspase-1 using ELISA and Western blot. Functional requirements of proteins were determined using knockout animals or SiRNA mediated knockdown.

Result and Conclusions

PA induced autophagy that was not dependent on a functional T3SS but was dependent on TLR4 and the signaling molecule TRIF. PA infection also strongly induced activation of the inflammasome which was absolutely dependent on a functional T3SS. We found that inhibition of inflammasome activation increased autophagy, suggesting that the inflammasome normally inhibits this process. Further experiments showed that this inhibitory effect was due to the proteolytic action of caspase-1 on the signaling molecule TRIF. Using a construct of TRIF with a mutation in the proteolytic cleavage site, prevented caspase-1 cleavage and increased autophagy. TRIF is also involved in the production of interferon-β following infection. We also found that caspase-1 cleavage of TRIF down-regulated this pathway as well.

Caspase-1 mediated inhibition of TRIF-mediated signaling is a novel pathway in the inflammatory response to infection. It is potentially amenable to therapeutic intervention.

Recognition of a pathogen infection is a key function of the innate immune system that allows an appropriate defensive response to be initiated. One of the most important innate immune defences is provided by a multi-subunit cytoplasmic platform termed the inflammasome that results in production of the cytokine IL-1β.

The human pathogen *Pseudomonas aeruginosa* activates the inflammasome following infection in a process that is dependent on a specialized bacterial virulence apparatus, the type III secretory system (T3SS). Here, we report the novel finding that this infection results in mitochondrial damage and release of mitochondrial DNA into the cytoplasm. This initiates activation of an inflammasome based on the protein NLRC4. Autophagy induced during infection removes damaged mitochondria and acts to down-regulate NLRC4 activation following infection. Our results highlight a new pathway in innate immune activation following infection with a pathogenic bacterium that could be exploited to improve outcomes following infection.

1 Introduction

1.1 *Pseudomonas aeruginosa*

Pseudomonas aeruginosa is a Gram negative pathogen which can cause opportunistic infections in the host. It belongs to the family of Pseudomonadacae. It is a common environmental organism, widely found in the soil and water. *Pseudomonas aeruginosa* can survive in many different types of environmental conditions and metabolise a wide range of carbon containing sources for its nutritional requirements. This bacterium can survive in high temperature even up to 42°C (Berthelot et al., 2001).

1.1.1 *Pseudomonas aeruginosa* infections

P. aeruginosa can cause serious infections in the healthy tissues but it more typically causes acute and chronic infections in almost any immuno-deficient individual where it takes advantage of a deficient host immune system, such as a breach in mucosal continuity or skin injury (Lyczak et al., 2000). *P. aeruginosa* can cause urinary tract infections, respiratory system infections, dermatitis, soft tissue infections and a variety of systemic infections in severely immuno- compromised patients. Patients with cystic fibrosis are particularly at risk, and virtually all affected patients develop chronic pseudomonal respiratory infections (Lyczak et al., 2000) (Gaspar et al., 2013).

P. aeruginosa pneumonia is a very common cause of healthcare-associated infections responsible for almost 10 % of all hospital acquired infection in the USA: this number is much higher in developing countries. The natural properties of this pathogen are suitable for an opportunistic and nosocomial infection (Weber et al., 2007), as it shows resistance to high

concentrations of salts, dyes, weak antiseptics and many antibiotics. It has been successfully isolated in the hospital environment from disinfectants, respiratory equipment, food, sinks, taps, toilets, showers and mops (Sadikot et al., 2005).

In general, *P. aeruginosa* is resistant to a wide range of common antimicrobial agents which makes its treatment often difficult. Resistance may or may not be plasmid-mediated but can be explained by the permeability barrier afforded by its Gram-negative outer membrane and its tendency to form a biofilm layer on colonized surfaces, which results in resistance to therapeutic concentration of antibiotics. Due to its natural habitat of soil it has developed resistance to naturally occurring antibiotic from bacilli, actinomycetes and molds. In addition it possess several multidrug efflux pumps which also contributes to the resistance (Yoshihara and Eda, 2007). *P. aeruginosa* can also undergo horizontal gene transfer such as transduction and conjugation which enables transfer of antibiotic resistance plasmids. The antibiotics still effective against *P. aeruginosa* include agents such as Imipenem, Gentamicin, and Fluoroquinolones (Poole and McKay, 2003).

1.1.2 *Pseudomonas aeruginosa* virulence factors

P. aeruginosa produces several extracellular products that after colonization can cause extensive tissue damage, bloodstream invasion, and disseminated systematic disease. *P. aeruginosa* has a wide array of virulence factors, which results in a multifactorial pathogenesis where normal host defences are altered or circumvented. This wide array of virulence factors contribute to the ability of *P. aeruginosa* to cause such a

3

wide variety of diseases throughout the body. *P. aeruginosa* has several cell- associated and secreted proteins which contribute to its virulence. Examples are elastase A, phospholipase C and other effector proteins translocated via the type III secretory system (T3SS), and considered further below (Travassos et al., 2005). Some *P. aeruginosa* strains have a single polar flagellum, which contributes to the motility of the bacterium, but it is also an important virulence factor (Soscia et al., 2007). All *P. aeruginosa* strains have multiple pili structure belonging to the type IVa pilin class (Woods et al., 1980). *P. aeruginosa* has two isoform of LPS , smooth and rough (Pier and Ames, 1984). In addition, *P. aeruginosa* has a wide range of other virulence factors such as iron acquisition proteins (Poole and McKay, 2003). Invasion of tissues by *P. aeruginosa* is dependent on production of extracellular enzymes and toxins such as LasA protease, protease IV, elastase and alkaline protease and pyocyanin (Bejarano et al., 1989). *P. aeruginosa* also produces exotoxin A (Allured et al., 1986). *P. aeruginosa* also produce haemolycin, phospholipase C (PlcHR) and Rhamnolipid, which results in degradation of host cell phospholipids (Terada et al., 1999) . Some strains of *P. aeruginosa* produces alignate, a mucoid exopolysacchadide which contributes to biofilm formation (Lau et al., 2004).

1.1.3 *Pseudomonas aeruginosa* type III secretion system

The type III secretion system (T3SS) is exclusive to Gram-negative bacteria and is structurally related to the flagellum (Desvaux et al., 2006). T3SS are essential for the pathogenicity of many Gram-negative bacteria. It allows the bacteria to inject protein effectors into the host cell in one single

step altering the function of the host cell and promoting survival of the bacteria (Salmond and Reeves, 1993). The T3SS of *P. aeruginosa* is similar to that found in *Yersinia* species at both a structural and functional level (Keizer et al., 2001). The *P. aeruginosa* T3SS is encoded by 36 genes found in five operons that are clustered together into the exoenzyme S regulon (Frank, 1997). This regulon is divided into 5 parts: needle complex, translocated secreted proteins, regulated proteins, chaperone proteins, and effector proteins (Fig. 1-1) (Hauser, 2009). The T3SS of *P. aeruginosa* has been shown to enhance disease severity in an acute pneumonia model (Lee et al., 2005), bacteremia (Vance et al., 2005), keratitis (Lee et al., 2003), burn infections (Holder et al., 2001) and ventilator-associated pneumonia (Hauser et al., 2002).
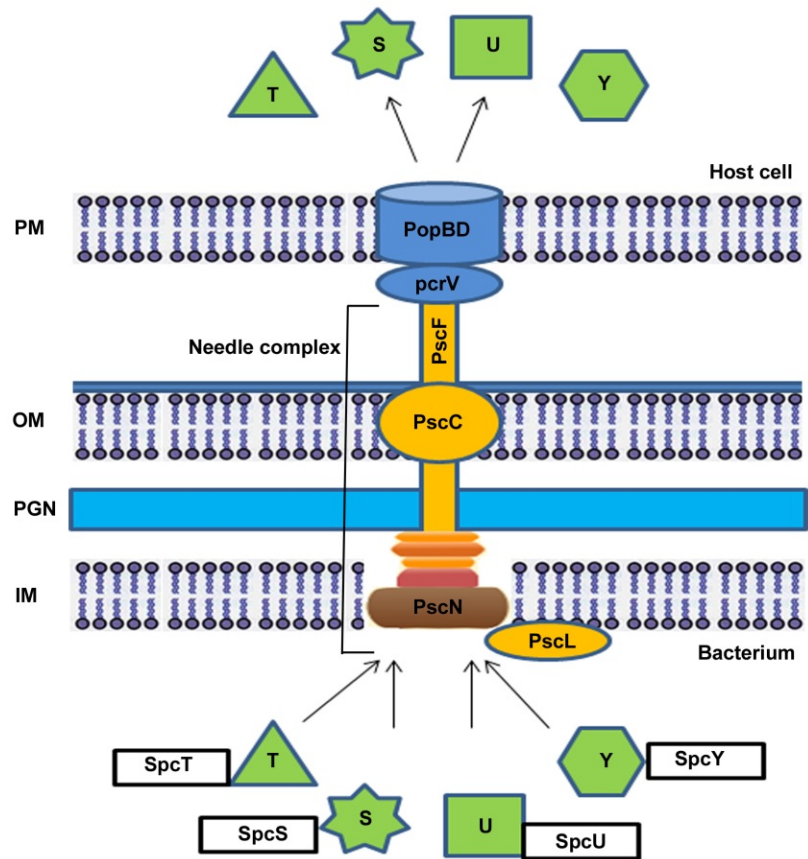
Figure 1.1; *Pseudomonas aeruginosa* **T3SS**

 The components of T3SS are: the needle complex (Yellow, Brown), translocation apparatus (Blue), the effector proteins (Green), chaperon (White), and regulatory proteins (not presented in this figure). PM, plasma membrane; OM, outer membrane; PGN, peptidoglycan layer; IM, inner membrane. T, ExoT; S,ExoS; Y,ExoY; U,ExoU. Figure adapted from (Hauser, 2009)

1.2 Autophagy

Autophagy, derived from the Greek words meaning "self-eating" was coined by Christian De Dove in 1963 (Klionsky, 2008). He used it to describe what had been called 'cytolysosomes', structures related to lysosome that contained a variety of cytoplasmic contents, including mitochondria, ER membranes, and ribosomes in an apparent state of decomposition. The essentials of an autophagocytic vacuole are the presence of diverse cytoplasmic contents contained within a double membrane vacuole (Fig. 1-2). Autophagy is an essential homeostatic process and the only system for the degradation of large cellular components and aggregates which cannot be degraded by the ubiquitin-proteasome pathway. This important lysosomal degradation pathway is activated as one of the adaptive responses to starvation, and subsequent studies have shown that it is a process found in virtually all eukaryotic cells that is essential for survival. 34 autophagy related (ATG) genes have been identified in yeast, with their orthologous well conserved throughout eukaryotes (Heath and Xavier, 2009b). It is also a pathway used to degrade microorganisms i.e. viruses, bacteria and protozoa that invade intracellularly (Deretic and Levine, 2009), (Virgin and Levine, 2009), . A large number of studies have shown that the Atg genes play an important role, not just in the response to nutrient deprivation, but also in inflammatory diseases, neurodegenerative disorders and cancer (Heath and Xavier, 2009a).

Three different forms of autophagy have been described; macroautophagy, microautophagy and chaperone-mediated autophagy. Macroautophagy is the main pathway, which encloses cytoplasmic contents

in a double membrane structure, after which it is combined with a lysosome (Cesen et al., 2012). In Microautophagy, a lysosome directly surrounds the degraded structures (Cesen et al., 2012). In the chaperone mediated autophagy (CMA), proteins with a KFERQ-like motif of Hsp70 chaperones are recognized and led to the lysosome, where they pass through the lysosomal membrane-associated protein 2 (LAMP-2A) into the lysosome and are degraded (Bandyopadhyay et al., 2008).

1.2.1 Autophagy pathway

1.2.1.1 Induction

The molecular mechanisms of autophagy were first described in yeast cells; these seem well conserved throughout higher eukaryotes. Autophagy induced by nutrient starvation is mediated by a protein kinase called target of rapamycin (Tor). Tor is a negative regulator of autophagy with two main effects: firstly it controls both general transcription and translation machinery; secondly it specifically acts to produce hyperphosphoryation of the Atg13 protein which results in this protein having a much lower affinity for the Atg1 kinase that results in inhibition of autophagy. Rapamycin, through inhibiting Tor, relieves this inhibition and is thus a potent inducer of autophagy.

The subsequent steps of the process can be broken down into selection of cargo and packaging, nucleation of the autophagocytic vesicle, expansion and closure of the vesicle, retrieval of targeting proteins, targeting, docking and fusion with lysosomes, and finally vesicle breakdown. This is an extremely complex series of processes with many proteins being

involved at each step. A large number of these proteins have homologues with very similar functions in higher eukaryotes. I will highlight here some of the more important proteins involved. Atg8 is an ubiquitin-like protein which has essential role in the formation of the autophagocytic vacuole. It undergoes a complex processing pathway analogous to the ubiquitin conjugation system pathway. This pathway transfer ubiquitin initially to an ubiquitin-activating enzyme (E1). In turn the ubiquitin is then transferred to an ubiquitin carrier enzyme (E2). Finally, the action of an ubiquitin ligase (E3) binds to the E2-ubiquitin complex and transfers the ubiquitin to its target. The mechanism is as follows:

1. Initially the C terminus of Atg8 is proteolytically cleaved by the Atg4 to reveal a terminal glycine.

2. This glycine is conjugated to the E1-like enzyme Atg7.

3. The Atg8 is then transferred from Atg7 and conjugated to the E2-like enzyme Atg3.

4. A complex of covalently joined Atg5-Atg12 together with Atg16 acts as an E3-like ligase, covalently linking the Atg8 to the lipid phosphatidylethanolamine.

This lipid modification targets the Atg8 molecule to the autophagocytic vacuole membrane. Importantly, Atg8 is not retrieved from the membrane. Thus, the detection of lipid-modified Atg8 and its localization to the autophagocytic membrane are very useful markers of the autophagocytic process. Importantly, the proteins involved in this lipid

modification are highly conserved in higher eukaryotes. In mammals, the Atg8 gene family has expanded into three sub-families (Slobodkin and Elazar, 2013), of which microtubule-associated protein light chain 3 (MAPLC3) is the functional analogue of Atg8 in yeast. Specifically, MAPLC3 B (usually abbreviated LC3B) shows the closest functional relationship to yeast Atg8 and is a reliable marker of autophagosome in mammalian cells when lipidated. Levels of the Atg8 mRNA and protein are usually markedly upregulated in yeast following induction of autophagy (Kirisako et al., 1999). Mammalian LC3B also show transcriptional and translational upregulation following induction of autophagy (Polager et al., 2008).

1.2.1.2 Autophagosome formation

There are several potential interconnections between the protein complexes involved in autophagosomal membrane formation which could be a potential source for membrane formation (Behrends et al., 2010). According to some studies membranes of mitochondria, ER, plasma membrane and the nuclear membrane could be sources for autophagosome membrane formation (Hailey et al., 2010, Ravikumar et al., 2010) but the absence of specific protein markers for these structures on the autophagosomal membrane does not agree with the assumption that these membrane could be the source of autophagosome membrane.

1.2.1.3 Docking and fusion with the lysosome

The mechanism of closure of the autophagosome and fusion with the lysosome are not as clear as the mechanisms of the early stages of autophagosome formation (Noda et al., 2009). As LC3 does not dissociate

from the autophagosome like the Atg16 complex, it may play an important role in the closure of autophagosome (Fujita et al., 2008). After closure, the autophagosome is trafficked to the peri-nuclear region of the cell for fusion with lysosomes with the help of microtubules and dynein (Kimura et al., 2008). Upon closure, the Atg16 complex rapidly dissociates from the autophagosome while the modified LC3 remains attached. Dynein may be recruited to the phagosome through an interaction with LC3 after the dissociation of the Atg16 complex (Noda et al., 2009). The final step is maturation of the autophagosome in which there is fusion of the outer autophagic membrane with the lysosomal membrane resulting in the formation of the autolysosome (Fig. 1-2).
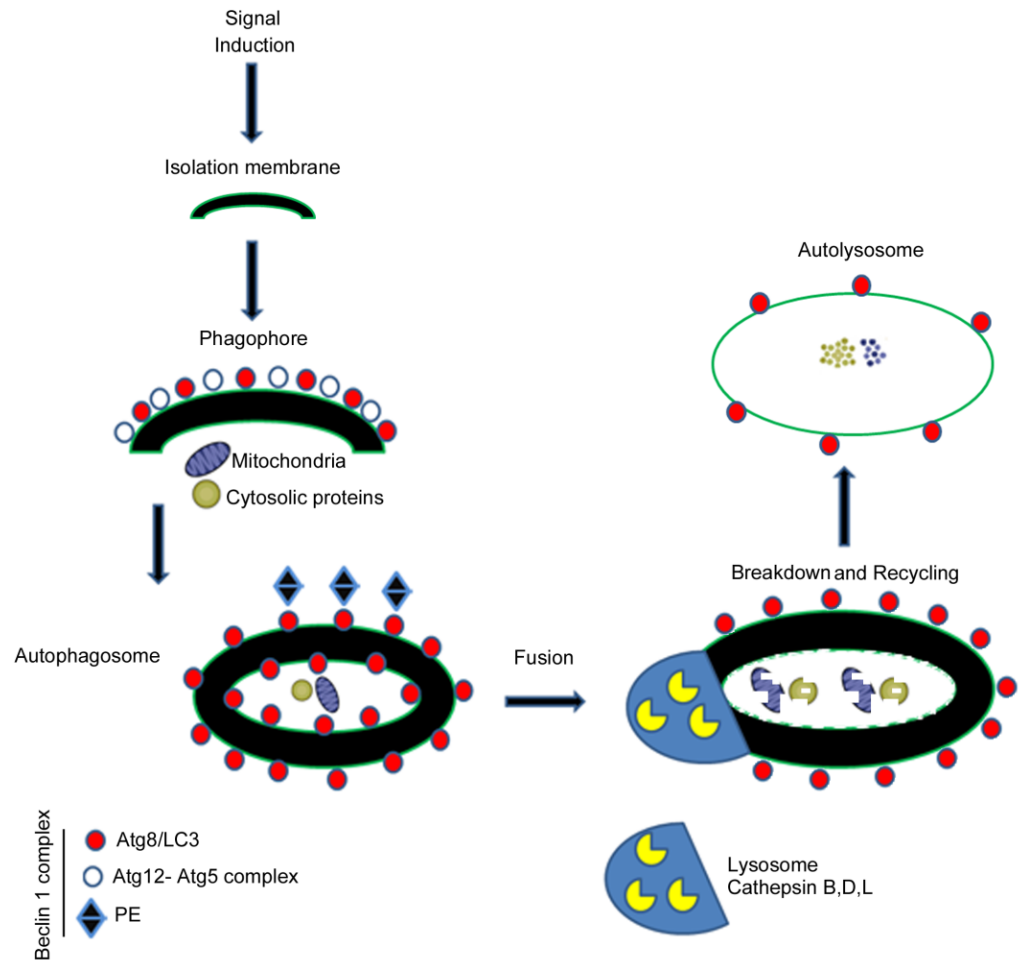
Figure 1.2; Autophagy pathway.

Schematic representation of Autophagy pathway steps; Induction, Autophagosome formation, Autophagosome fusion, and Autophagosome breakdown.

1.2.2 Mitophagy

The autophagocytic process may also target specific organelles within the cell. One important organelle targeted in this fashion is the mitochondria, which I explore in some detail in the experimental work carried out in this thesis; this process is termed mitophagy (Kim et al., 2007). Mitochondria are removed by this process in cells such as reticulocytes as part of a developmental program (Zhang et al., 2009). However, mitochondria are also removed as part of a quality control process when they become depolarized (Wu et al., 2009). This process has increasingly been recognized as important in the pathophysiology of a number of important disease states. Genetic studies of familial forms of Parkinson's diseases revealed two genes linked to the development of disease termed Parkin and PINK1. The protein products of these genes are now understood to be on the same pathway and linked to the mechanism whereby defective mitochondria are removed by mitophagy (Jin and Youle, 2012). PINK1 has a mitochondrial-targeting signal that results in the protein being located within the inner mitochondrial membrane. Here it is processed from its full length 64 kDs form to a truncated 52 kDs fragment. This shorter PINK1 fragment is then degraded by a protease, keeping steady state levels of PINK1 low. However, on mitochondrial damage and depolarization, the import and processing of PINK1 are inhibited, leading to an accumulation of mature full-length PINK1 in the outer mitochondrial membrane. This then acts to recruit Parkin to the damaged mitochondrion. Parkin is an E3 ubiquitin ligase, producing ubiquitinylation of numerous mitochondrial proteins that lead to the initiation of mitophagy. The

accumulation of defective mitochondria in patients with mutations in parkin is thought to underlie the onset Parkinson's diseases in these families.

More recent work has linked mitochondrial damage to the activation of the inflammasome, and this is considered in more detail below.

1.2.3 Role of autophagy in host defence

Autophagy participates in nearly all aspects of immunity, affecting both innate and adaptive immunity processes (Deretic, 2011) (Fig. 1-3). The autophagy pathway and autophagy proteins play a major part in controlling immunity in multicellular organisms. This has possibly evolved as a stress response to allow eukaryotic organisms to survive in unfavourable conditions, probably by regulating energy homeostasis and quality control of proteins and organelles (Kroemer et al., 2010). There are direct interactions between autophagy proteins and immune signalling molecules (Saitoh and Akira, 2010).

Type-I autophagy

(Specialized roles)

Type-II autophagy

(Cellular homeostatic roles)

Cell-autonomus pathogen elimination

SLR sequestasome like receptors autophagic adaptors

PAMP-PRRs (TLR, NLR, RLR) Regulator/effector

DAMP/ IL-1 HMGB1

Immunity related GTPases (IRG)

Innate immunity

Autophagy in immunity

Adaptive immunity

Thymic selection naive T-cell repertoires

T-cell maturation

T-cell polarization (effector function)

T and B cell homeostasis

Antigen procesing and presentation MHC-I, MHC-II

Figure 1.3; Autophagy in immunity.

Schematic representation role of autophagy in immunity. Figure adapted from (Deretic, 2011)

The role of autophagy proteins in adaptive immunity, includes the development and homeostasis of the immune system and in antigen presentation. The knockout of different autophagy genes in specific lymphocyte populations in mice has shown a crucial role for autophagy proteins in the maintenance of a number of cell lineages of importance in the immune response, including B1a B cells, CD4+ T cells, CD8+ T cells and fetal haematopoietic stem cells (Heath and Xavier, 2009b). In T cells, in which mitochondrial numbers are developmentally regulated during the transition from thymocyte to mature circulating T cell, the developmental defect in autophagy-deficient cells may be related to the defective clearance of mitochondria (Noda et al., 2009). Autophagy plays a role in the elimination of autoreactive T cells in the thymus (Noda et al., 2009). Within thymic epithelial cells, in which autophagy participates in the delivery of self-antigens to MHC class II loading compartments. This is important as genetic disruption of *Atg5* in thymic epithelial cells leads to the altered selection of certain MHC class II restricted T-cell specificities and autoimmunity (Meissner et al., 2010).

Initially, autophagy was considered as a non-selective bulk degradation process, but now it has become quite clear that this process can degrade substrates in a selective manner as well (Kraft et al., 2010). For example, intracellular pathogens can be degraded by autophagy, a process called xenophagy. The precise mechanism of xenophagy and its membrane dynamics is still not clearly understood. The vacuoles of engulfed bacteria are similar to the autophagosomes and their formation requires the core autophagy machinery. The diameter of the vacuoles containing bacteria are typically bigger than the autophagosomes which are

generated by the RAB7 dependent fusion of small isolation membranes (Yamaguchi et al., 2009). There are four pathways assumed to be used for ATG protein dependent targeting of bacteria to the lysosome(Levine et al., 2011):

1. Autophagy proteins may induce bacteria- containing phagosomes to fuse with lysosomes for degradation.

2. Autophagosomal membranes may engulf bacterial phagosomes/endosomes.

3. Fusion of bacteria containing phagosomes/ endosomes with autophagosomes, or

4. Xenophobic capture of bacteria that are within the cytoplasm, but the precise route for several bacteria is still unclear.

A microbial sensor SLAM, the self-ligand and cell-surface receptor, recruits complex of beclin-1 class-III PI(3)K kinase to the bacteria containing phagosome. This facilitates phago-lysosomal fusion and activation of NADPH oxidase (NOX2) complex (Berger et al., 2010). In addition the engagement of TLR or Fcγ receptors during phagocytosis recruits LC3 to the phagosome through NOX2-dependent generation of reactive oxygen species (Huang et al., 2009a). In bacterial infections, this process may thus contribute to removal of intracellular bacteria. Impaired recruitment of autophagy proteins to the phagosome may contribute to the pathogenesis of chronic granulomatous disease, a genetic disorder caused by mutations in the *NOX2* (*CYBB*) gene and characterized by recurrent bacterial and fungal infections and inflammatory complications.

Autophagy proteins can also destroy pathogens independent of triggering autophagy, as seen in interferon-γ (IFN-γ) treated macrophages

infected with the parasite *Toxoplasma gondii*. A parasite derived membranous vacuole undergoes destruction through a mechanism that involves ATG5 dependent recruitment of the immunity-related GTPase proteins to the parasitophorous vacuole leading to parasite death inside the infected cell (Zhao et al., 2008, Zhao et al., 2009). The mechanisms that cells use to target intracellular bacteria to autophagosomal compartments are similar to the selective autophagy of endogenous cargo. Cellular cargo is commonly targeted to autophagosomes by interactions between a molecular tag and LC3 in the autophagosome membrane. Examples of such molecules are the polyubiquitin adaptor proteins i.e. p62 (SQSTM1 or sequestome-1) and NBR1 (which recognize these tags and contain an LC3-interacting region (LIR) characterized by a WXXL or WXXI motif) (Kraft et al., 2010). After escape into the cytoplasm or in vacuolar membrane compartments damaged by type-III secretion system (T3SS) effectors, bacteria-containing compartments may become coated with ubiquitin and associate with p62 and nascent LC3-positive isolation membranes. *Salmonella targeting* also requires a cellular factor, NDP52 (nuclear dot protein-52), an autophagy adaptor protein that, like p62, contains an LIR and ubiquitin-binding domains restricting intracellular bacterial replication (Shahnazari et al., 2010) .

These different molecular strategies may be used to target microbes inside the cytoplasm to the autophagosome, which will facilitate their destruction following fusion with lysosomes. In addation, autophagic targeting of pathogen-damaged membranes could help to control detrimental downstream inflammatory signalling during bacterial invasion in to host cell.

1.3 Inflammation

Inflammation is a localized nonspecific response of the body to injury. It is characterized by five cardinal signs which are pain, redness, heat, swelling, and loss of function. These signs reflect increased blood flow, elevated cellular metabolism, vasodilation, release of soluble mediators, extravasation of fluids and cellular influx. Inflammation usually is a self-limiting process that protects the host against a variety of invading pathogens or injury. Inflammation can occur and dissipate over a short time frame (acute inflammation) or can persist for a much longer periods (chronic inflammation) (Ferrero-Miliani et al., 2007). Inflammation utilizes a great amount of metabolic energy and can result in damage and destruction of the tissue. Therefore, controls over the termination of inflammation are required, to limit any possible damage caused (Barton, 2008).

1.3.1 Innate immune response

Immunity is defined as the body's resistance against infectious agents. There are two types of immunity: innate (natural) and acquired. Innate immunity is the type of immunity which is genetically pre-programmed and is not specific to a particular pathogen. As a result, it is able to recognize diverse microorganisms such as bacteria, viruses, and fungi. Pattern recognition receptors (PRRs) allow the innate immune system to recognise specific molecular feature of microbes. Recognition of these lead to activation of various inflammatory pathway that contribute to host defence. Increasingly, it has been realized that PRRs not only recognize invading pathogens but also the damage they cause. .

PRRs are expressed by several cell types such as monocytes, macrophages, dendritic cells (DCs), neutrophils and epithelial cells (Martinon et al., 2009). PRRs include: soluble pentaxin receptors, membrane –bound receptors: Toll like receptors (TLRs) (Akira et al., 2006) C-type lectin receptors (CLRs) (Brown, 2006), as well as cytosolic Nod-like receptors (NLRs) (Martinon et al., 2009), RIG-like helicase, RLRs (Nakhaei et al., 2009) and DNA sensors (Hornung et al., 2009) (Fig. 1-4).
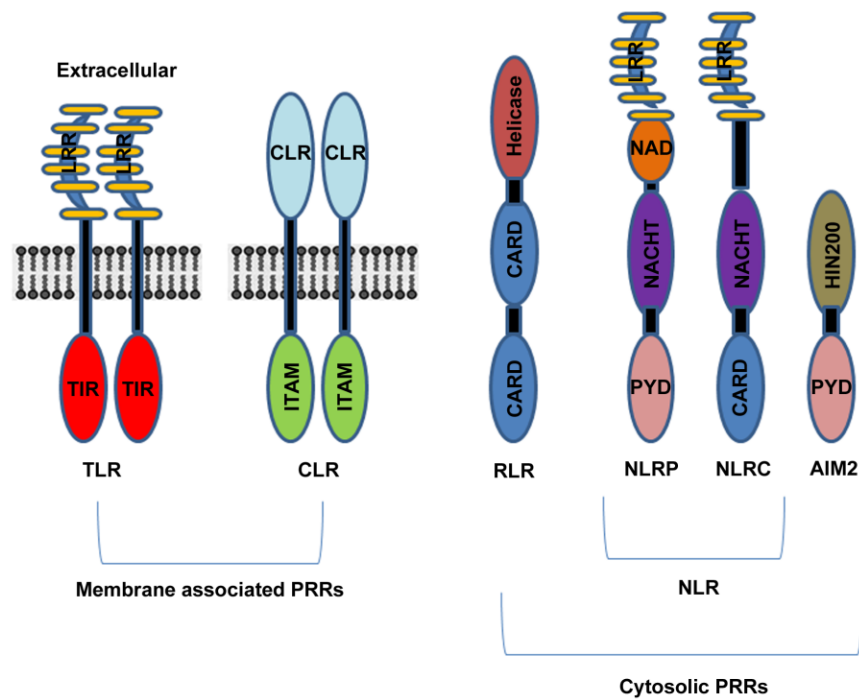
Figure 1.4; Structure of different PRRs

Schematic representation of PRRs. Abbreviation; TLR; Toll-like receptor, CLR; C-type lectin receptor, RLR; RIG-1-like receptor; NLR; NOD-like receptor, NLRP and NLRC; major subfamilies in NLR-protein family, Aim2; absence in melanoma 2 (DNA sensor), LRR; leucine-richrepeats, TIR;Toll-interleukin-1 receptor interacting domain, ITAM; immunoreceptor tyrosine-based activationmotif, NAD; NACHT associated domain, NACHT; nucleotide binding and oligomerization domain, PYD; pyrin domain, CARD; Caspase recruitment domain and HIN200, HIN200 domain. Figure adapted from (Bryant and Fitzgerald, 2009).

1.3.2 Inflammasome

The inflammasome is a multi-protein complex that leads to activation of the 17KDa pro-inflammatory cytokine IL-1β, from its 31kDa precursor, pro-IL-1β, via caspase 1. This process also leads to activation of the IL-1 family member IL-18. (Ghayur et al., 1997) IL-33 is another IL-1 family member, but it is not clear if caspase-1 is necessary for its activation *in vivo* (Carriere et al., 2007), although activation via caspase-1 has been demonstrated *in vitro* (Schmitz et al., 2005). Activation of the inflammasome is also associated with the onset of a form of cell death termed pyroptosis (Fernandes-Alnemri et al., 2007). The name inflammasome comes from the word inflammation, which reflects the function of the complex, and "some", which is from the Greek word for body, soma. The name also reflects similarities with the apoptosome, which triggers apoptosis (Zou et al., 1999). The production of IL-1β and IL-18 by the inflammasome is one of the first lines of defence against tissue damage and pathogen invasion.

1.3.2.1 IL-1β and IL-18

Interleukin-1β (IL-1β) also known as catabolin, is a member of the interleukin 1 cytokine family of ligands, which include, IL-1α, IL-18 and IL-33(Dinarello, 2009). IL-1β is related to IL-18 and IL-33 and all of these cytokines result in the intiation of a Myd88-depending signaling pathway, similar to the pathway intiated by TLR4 signalling. Inflammasome activation therefore leads to the activation of a TLR-like receptor such as IL-1R and IL-18R. IL-1β is a pleiotropic cytokine. It is involved in the inflammatory response, cell growth, and tissue repair in the cortex. It is a proinflammatory cytokine, which plays an important role as a mediator of inflammation

(Dinarello, 2009). It is produced by blood monocytes but also by macrophage, dendritic cells and a variety of other cells in the body (Ferrero-Miliani et al., 2007). IL-1β participates in the generation of systemic and local responses to infection and injury by generating fever, activating lymphocytes and by promoting leukocyte infiltration at sites of infection or injury. IL-18 induces IFN-γ production and contributes to T-helper 1 (Th1) cell polarization. IL-1β is believed to be the major mediator of inflammation in the periodic fever syndromes caused by mutations in the NLRP family genes. It has been shown that treatment of the patients with an inhibitor of IL-1(IL-1Ra) can improve their symptoms (Hawkins et al., 2003). IL-1Ra has also been shown to help patients with rheumatoid arthritis (Dinarello, 2009).

The inflammasome is able of recognizing a diverse range of threats, both from endogenous and exogenous sources. Endogenous signals that are known to activate the inflammasome include uric acid, ATP, potassium efflux (Kahlenberg and Dubyak, 2004) from the cell and a newly identified endogenous peptide, acALY18. External stressors include pathogen-associated molecular patterns derived from a diverse range of conserved molecular motifs that are unique to bacteria, viruses and parasites, from exogenous chemicals or ultraviolet light. The mechanism by which these signals are detected has yet to be fully elucidated for the majority of inflammasomes.

The core structure of all inflammasomes is of course caspase-1, variety of other proteins co-assemble with procaspase-1 to bring about its activation. Many, but not at all inflammasomes, have a member of the neucleotide-binding domin and leucine-rich repeat containing (NLR) gene

family (Ting et al., 2008). Protiens encoded by this gene family have a tripartite domain structure: a central nucleotide-binding oligomerization domain; a C terminal leucine-rich repeat containing domain; and an N terminal domain from four recognizable families. These N terminal domains are used to classify the NLR proteins into subfamilies, denoted by a letter appended to the NLR designation: an acidic transactivation domain (A); a pyrin domain (P); a caspase recruitment domain (CARD) (C); and a baculoviral inhibitory repeat-like (BIR) domain (B). Finally, for NLR proteins with an N terminal domain that has no recognizable homology to other NLR family members are denoted by appending X. Different members of the subfamilies are denoted by sequential numbers. More recently, inflammasome without a member of the NLR family have been recognized and these are considered further below.

Another protein of central importance in controlling Inflammasome activation is apoptosis speck-like protein containing a caspase activation and recruitment domain (ASC), which contains PYRIN domains but lacks a CARD domain. It also plays an important role in inflammasomes containing an NLR protein with CARD domains (Broz et al., 2010). Only one ASC speck is formed in a cell following infection (Huang et al., 2009b)

Thus, the inflammasome contains a variety of proteins that following activation results in the recruitment of pro-caspase-1 in to the complex that is then proteolytically processed to active caspase-1 via an auto-catalytic pathway. Once caspase-1 is activated, it is then able to cleave and active a number of key pro-inflammatory cytokines, such as pro-IL-1β and pro-IL-18

(Fig. 1-5). In general, pro-IL-1β is present at very low level in resting cells, and requires activation of its gene to produce protein expression. This is typically achieved by inflammatory signalling through Toll-like receptor or other innate immune signalling pathways. Conversely, pro-IL-18 is present in resting cells and an induction stimulus is not required.
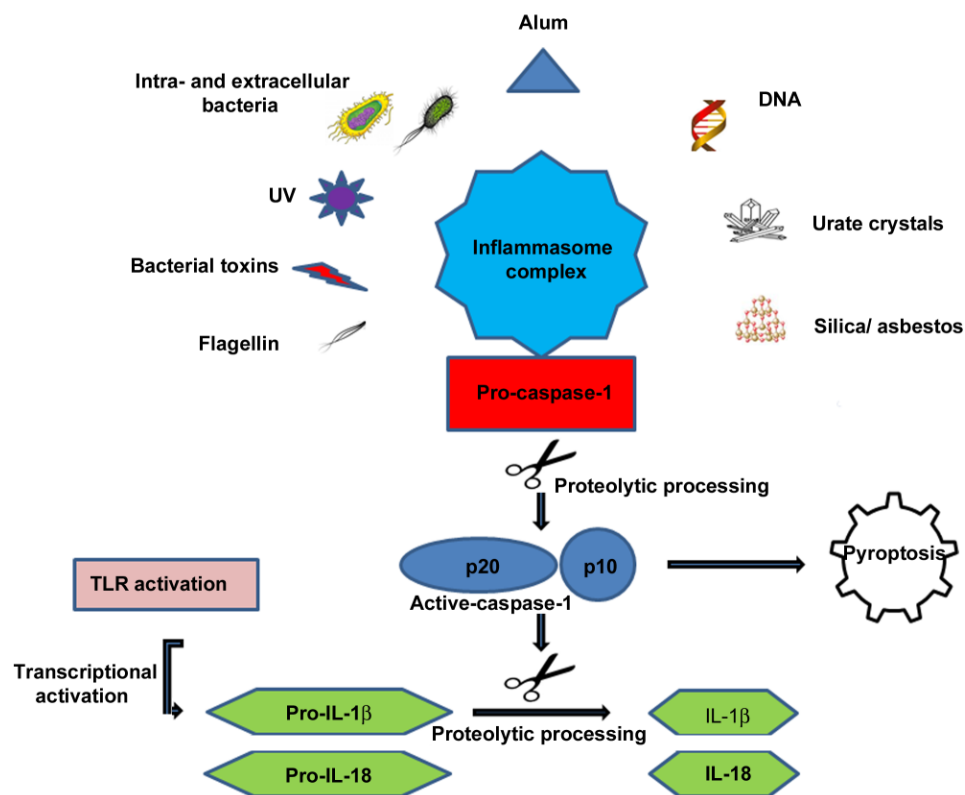
Figure 1.5; Caspase-1 activation .

Schematic representation of the activation of the inflammasome complex by a wide range of stimuli. Figure adapted from (Evans, 2009).

A number of inflammasome complexes have been identified, of which we will consider four in more details; NLRP1, NLRP3, NLRC4 and Aim2. In addition, several NLRP proteins might be involved as scaffolding proteins of the inflammasome complex (Martinon et al., 2007) (Fig.1-6).
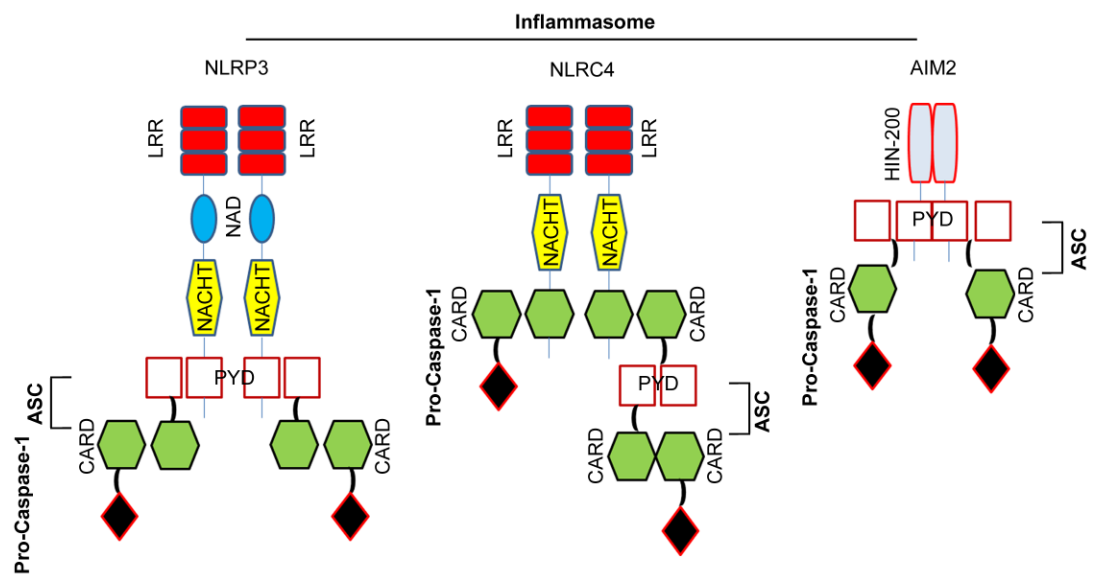
Figure 1.6; The inflammasome structure.

The inflammasomes are assembled by self-oligomerizing proteins. The NLRP3 inflammasome consists of NLRP3, ASC and caspase-1. NLRC4 directly binds with procaspase-1 but NLRC4 activation may require ASC. The AIM2 inflammasome is composed of AIM2, ASC and caspase-1. The PYD domain of AIM2 interacts with PYD of ASC through homotypic PYD-PYD interaction, so that the ASC CARD domain can recruit procaspase to the compex. Figure adapted from (Eitel et al., 2010) .

1.3.2.2 NLRP1

The first inflammasome identified was the NLRP1 inflammasome by (Martinon et al., 2002). The NLRP1 inflammasome has been shown to be activated following exposure to anthrax lethal toxin. Anthrax is caused by *Bacillus anthracis* through the action of its secreted toxins. One of these toxins is anthrax lethal toxin. It has been shown that a polymorphism in the NLRP1 gene results in impaired caspase-1 activation (Boyden and Dietrich, 2006). The proteolytic activity of LeTx appears to be responsible for NLRP1 activation by causing cleavage of NLRP1B; this was sufficient for activation (Chavarria-Smith and Vance, 2013). NLRP1 is also activated following exposure to muramyl dipeptide (MDP) moiety of peptidoglycans (Faustin et al., 2007) .

1.3.2.3 NLRP3

The NLRP3 inflammasome consists of the NLR protein, NLRP3 the ASC adaptor, and caspase-1. The NLRP3 inflammasome is triggered upon exposure to pathogens, as well as numbers of structurally diverse and environmental irritants (Gross et al., 2011).

NLRP3 is the best studied of all inflammasomes but it still remains unclear how such a wide array of stimuli elicit a response from a single sensor (Gross et al., 2011). One feature that many NLRP3 activators share is the ability to cause loss of intracellular potassium, first describe by Petrili (Petrilli et al., 2007). The activation of the NLRP3 inflammasome by reduction in intracellular potassium provided an explanation as to how so many different stimuli could all lead to NLRP3 activation. Thus, extracellular

ATP acts on the P2X7 receptor which acts as an ATP-gated potassium channel (Di Virgilio, 2007), while lytic toxins such as pneumolycin also cause potassium efflux from cells by forming non-selective pores in the cell membrane (Witzenrath et al., 2011).

However, other intermediates also play a role in NLRP3 activation. Production of reactive oxygen species (ROS) is important (Cruz et al., 2007). Although ROS production is often associated with a drop in intracellular potassium concentration, the exact relationship between ROS production and reduction in intracellular potassium remains unclear.

Another report suggests that crystals formed within lysosomes cause disruptions and a release of active cathepsin-B which may act as an upstream activator of NLRP3 (Hornung et al., 2008). Once activated, NLRP3 interacts with ASC and procaspase-1 enzymes (Agostini et al., 2004) to cause the cleavage and activation of Caspase-1, which in turn cleaves and activates IL-1β and IL-18 cytokines.

Recently, an important role for mitochondria in NLRP3 activation has been suggested (Zhou et al., 2011) . That ROS from damaged mitochondria activated NLRP3 also linked with earlier work showing that autophagy down-regulated NLRP3 activation (Saitoh et al., 2008a). Selective mitophagy of damaged mitochondria would thus act to down-regulate NLRP3 activation. Several papers suggest that mitochondria are the main source of ROS and oxidized DNA necessary to activate NLRP3 (Nakahira et al., 2011, Shimada et al., 2012) while others suggest that ROS production is sufficient to prime the NLRP3 response but not activate it

(Bauernfeind et al., 2011). Intriguingly, the studies of Nakahira et al and Shimada et al suggested it was the release of DNA from damaged mitochondria that was responsible for NLRP3 activation. Oxidation of this DNA was thought to potentiate its NLRP3 activating ability (Shimada et al., 2012). However, this remains controversial since another study found no role for mitochondrial damage in NLRP3 activation, just loss of intracellular potassium (Munoz-Planillo et al., 2013).

A number of accessory proteins are known to modify NLRP3 activation (Latz et al., 2013). The role of these protiens is in many cases not entirely clear. For example, Guanylate binding protein 5 (GBP5) has been found to promote NLRP3 activation (Shenoy et al., 2012); however, GBP5 seems to have no involvement in mitochondrial recruitment or other stimuli thought to active NLRP3.

Although the basic mechanisms of the NLRP3 inflammasome activation is remain unclear, its role within signalling in disease is better appreciated. Several autoimmune conditions are brought about by mutations which cause a gain of function which can be ameliorated by the neutralisation of IL-1β (Goldbach-Mansky and Kastner, 2009). Furthermore the NLRP3 inflammasome has been linked to the production of excess inflammation in response to host cell damage in the absence of infection (Duewell et al., 2010). Such cases are thought to increase the severity of tissue damage in sterile injury.

1.3.2.4 NLRC4

In contrast to NLRP3, the inflammasome based on the NLR protein NLRC4 has been shown to respond to bacterial derived products delivered via secretion systems. Activation of the NLRC4 inflammasome has been shown to be important in host defence for a number of pathogens. The first pathogen described to active the inflammasome in a NLRC4-dependent manner was *Salmonella typhimurium* (Mariathasan et al., 2004). Despite this NLRC4-dificient mice did not have enhanced susceptibility to infection with *Salmonella typhimurium* but caspase-1 deficient mice did (Lara-Tejero et al., 2006). This indicates that additional pathways are involved in the caspase-1 activation by *Salmonella. L.pneumophila* also activates the inflammasome in a NLRC4-dependent manner (Zamboni et al., 2006). *Pseudomonas aeruginosa* has been shown to active the inflammasome in a NLRC4-dependent manner. Additionally it has been shown that NLRC4-deficient mice are more susceptible to infection by *Pseudomonas aeruginosa* in a pulmonary and peritoneal *in vivo* infection model (Franchi et al., 2007) (Sutterwala et al., 2007). However, another study found that activation of the NLRC4 inflammasome increases bacterial burden in a model of *P. aeruginosa pneumonia* (Cohen and Prince, 2013). NLRC4 inflammasome activation is critical in host defence against *Klebsiella pneumonia* (Cai et al., 2012).

In contrast to the NLRP3 inflammasome, the molecular mechanisms underlying NLRC4 activation are much better understood. Specific bacterial ligands are known to trigger the activation. The first of these to be described was bacterial flagellin (Miao et al., 2006, Franchi et al., 2006, Amer et al.,

2006). The flagellin was introduced into the cell via a type III or type IV secretory system.

However, certain aspects of this activation were not easily explained. Flagellin deficient mutants of *P. aeruginosa* were efficient activators of the NLRC4 inflammasome (Sutterwala et al., 2007, Arlehamn et al., 2010). Additionally, no direct interaction between NLRC4 and flagellin had been demonstrated. Further work has clarified the nature of the activation of NLRC4 by flagellin. Additonal proteins belonging to the NLR apoptosis-inhibitory protein (NAIP) family, specifically NAIP5, has been shown to sense flagellin directly and to activate NLRC4 (Lightfield et al., 2008, Kofoed and Vance, 2011). Morever, further work identified a conserved protein called PrgJ in *Salmonella spp*. That is part of the T3SS rod apparatus as an additional activator of the NLRC4 inflammasome (Miao et al., 2010). This activation also required a NAIP family member, in this case NAIP2 (Zhao et al., 2011). More recently, it has been proposed that multiple needle proteins of the T3SS can also activate the NLRC4 inflammasome, requiring NAIP1 as an accessory protein (Yang et al., 2013).

Additional signals also regulate NLRC4 activation. Phosphorylation of NLRC4 has been shown to be essential for its activation (Qu et al., 2012). How this relates to the interactions between bacterial proteins and NAIP family members is not clear.

1.3.2.5 AIM2

Aim2 is a member of the pyrin and HIN domain-containing protein (PYHIN) family. Double- stranded DNA triggers Aim2 oligomerization, which results in Aim2 inflammasome formation together with ASC and caspase-

1(Fernandes-Alnemri et al., 2009). Aim2 was recently identified as the key sensor for cytoplasmic dsDNA (Burckstummer et al., 2009) (Hornung et al., 2009). Not surprisingly, Aim2 plays an important role in host defence against viruses such as CMV and vaccinia (Rathinam et al., 2010). However, it is also important in defence against a range of bacterial pathogens, including *Francisella tularensis, Listeria monocytogenes,* and *Legionella pneumophila* (Rathinam et al., 2010) (Kim et al., 2010) (Ge et al., 2012)*.* Release of bacterial DNA into the cytoplasm during infection would appear to be the trigger in these infections. Aim2 is also recently reported to be important in inflammasome activation during infection with *Streptococcus pneumonia* (Fang et al., 2014)*.*

1.3.2.6 Caspase-11

Genetically engineerd mice lacking Caspase-1 have been widely used to determine the role that this protein plays in infection and immunity. However, the mouse strain in which the *Caspase-1* gene was detected were generated using 129 ES cells which harbour a 5 bp detection encompassing the *Cap11* exon 7 splice acceptor junction (Kayagaki et al., 2011). Consequently, these mice have a non-functional *Caspase-11* gene and do not produce functional *Caspase-11*. *Caspase-1* and *Caspase-11* are tightly linked, hence separation of the alleles by backcrossing is very rare and thus the *Casp1* knockout mice are also *Casp*11 null as well. This led to a re-evaluation of the relative roles in of Caspase-1 and Caspase-11 in inflammasome function. Caspase-11 has been shown to be important in host defence against *Salmonella typhimurium* (Broz et al., 2012) and a

variety of Gram-negative and other bacteria that escape into the host cytosol (Rathinam et al., 2012) (Aachoui et al., 2013).

1.3.3 Role of Autophagy in inflammatory and autoimmune diseases

There are clear links between the genes controlling autophagy and control of immune response. For example, a study by (Barrett et al., 2008), identified a number of genes involved in the pathogenesis of Crohn's disease, that induced genes involved in the autophagy pathway such as *ATG16L1* also described by (Saitoh et al., 2008a). Dendritic cells from patients with the Crohn's disease associated *ATG16L1 mutation* (*T300A*) risk variant are defective in presenting bacterial antigen to CD4+ T cells (Cooney et al., 2010). However, it is not yet known how the T300A mutation affects the function of the mammalian ATG16L1 protein. This mutation resides in the carboxy-terminal WD-repeat domain that is absent in yeast Atg16 and is dispensable for autophagy. It remains controversial whether the increased risk versus protective alleles of *ATG16L1* has differences in stability or antibacterial autophagic activity (Fujita et al., 2009).

The study of (Saitoh et al., 2008a), shows that loss of *Atg16L1* function in mice results in enhanced TLR agonist induced pro-inflammatory cytokine production by macrophages. Other studies also suggest that changes in the autophagy pathway may also result in inflammatory autoimmune disease. Genome-wide association studies have linked several single nucleotide polymorphisms (SNPs) in *ATG5* to SLE susceptibility (Han et al., 2009) . *Atg5* has an important role in negative selection in the thymus during T cell development: this may underline the autoimmunity and multi-organ inflammation in mice lacking *Atg5* (Nedjic et al., 2008).

1.4 Reciprocal Interaction between inflammasome activation and autophagy

Several studies have now shown strong cross-talk between autophagocytic pathways and inflammasome activation. Studies reveal that treatment with LPS, a potent TLR4 agonist, is not sufficient to induce inflammasome activation in wild type macrophages. However, Atg16L1$^{-/-}$ and Atg7$^{-/-}$ macrophages which lack specific autophagy receptors can undergo LPS-dependent inflammasome activation, implying that in wild type macrophages autophagy normally counters this activation with LPS (Saitoh et al., 2008b). Although the specific mechanisms were not identified in this study, LPS-dependent inflammasome activation in Atg16L1 knockout animals is dependent on K+ efflux and generation of reactive oxygen species, which suggests the involvement of NLRP3. It has been suggested that autophagosomes may target the inflammasome for degradation (Harris et al., 2011). However, given the dependency of NLRP3 activation on ROS generation and the suppressive effect ROS blockade has on NLRP3 activation (Saitoh et al., 2008b, Bensaad et al., 2009, Dupont et al., 2009) an inhibition of the inflammasome through indirect suppression of ROS generation cannot be ruled out. Furthermore, autophagy appears to downregulate pyroptosis (Suzuki and Nunez, 2008) and ROS derived from both NADPH oxidases and the mitochondrial electron transport chain up-regulate autophagocytosis (Chen et al., 2009, Huang et al., 2009a). Therefore, the regulation of autophagy through ROS may represent a negative feedback system which acts to limit ROS modulated caspase-1 activation while also removing organelles which have been damages by ROS. Another report by Suzuki et al. (2007) which implicates that the

inflammasome down-regulates autophagy further complicates the situation. This study found that Caspase-1 deficiency increases autophagy in cells infected with *S. flexneri*, an IPAF agonist. There is a considerable need for further research in order to fully understand the complexity of this relationship.

1.5 Hypothesis and aims

Autophagy not only degrades unwanted organelles, but also helps in controlling immunity and inflammation. As outlined above, there is considerable evidence showing that autophagy can downregulate NLRP3 inflammasome activation. This is little current information regarding any possible involvement of autophagy in controlling inflammasome activation by NLRC4. Moreover, there are no studies that have addressed the possible influence of inflammasome activation on autophagy. The specialised bacterial virulence mechanism, the Type III secretion system (T3SS) is able to activate the inflammasome producing IL-1β production. The relationship between this process and induction of autophagy is not clear.

The central hypothesis underlying this study is that induction of autophagy by infection will inhibit NLRC4 inflammasome activation in macrophages, limiting the inflammatory response and promoting cell survival. We also propose that other pro-inflammatory pathways will be similarly down-regulated. We studied the microbe *Pseudomonas aeruginosa* an extra-cellular bacterium which possesses a T3SS that can activate the inflammasome. Our aims are:

1. To determine the role of the T3SS in the induction of autophagy within macrophages following infection.

2. To investigate the effects of autophagy on activation of the NLRC4 inflammasome by these bacteria.

3. To investigate the effects of autophagy on the activation of other pro-inflammatory pathways following infection with these bacteria.

4. To investigate the effects of inflammasome activation on the induction and progression of autophagy.

2   Materials and methods

2.1 Tissue culture

2.1.1 Cell line

2.1.1.1 THP-1 cells

THP-1 cells are a human monocytic cell line (gift of Dr. Damo Xu, University of Glasgow). Cells are derived from an acute monocytic leukemic patient. Cells were grown in RPMI-1640 media (Sigma. Cat.No.R8758, USA) supplemented with 2mM L-glutamine (Invitrogen. Cat.No.25030, USA), 10% heat inactivated fetal calf serum (Invitrogen. Cat. No.15561020, USA), 100 µg/ml Streptomycin, 100 IU/ml Penicillin (Sigma. Cat. No. P0781 UAS), and 1 mM Hepes solution (Sigma. Cat. No. H0887, USA). To maintain cell culture, cells were split at approximately 85% confluence. 2hr before infection cells were washed twice with sterile PBS (Invitrogen. Cat.No.14190-094, USA) and complete media without Penicillin and Streptomycin was added.

2.1.1.2 J774A.1 cells

The murine macrophage cell line J774A.1 was grown in RPMI -1640 medium as described for THP-1 cells. Cell culture was maintained at 37°C in 5% CO2. Cell were cultured at a concentration 1×10^6 cell/ml. 24 hr before infection, cells were seeded in complete RPMI-1640 media in 6, and 12 well tissue culture plates (Costar. Cat.No.3513, USA). 2hr before infection cells were washed twice with sterile PBS and complete media without Penicillin and Streptomycin was added.

39

2.1.1.3 RAW264.7 cells

The murine macrophage cell line RAW264.7 was grown as described for THP-1 cells.

2.1.1.4 L929 cells

The murine cell line L929 produce M-CSF in cell culture. They were cultured in RPMI-1640 media supplemented with 2mM L-glutamine, 10% heat inactivated fetal calf serum, 100 µg/ml Streptomycin, 100 IU/ml Penicillin. When cells were around 85% confluent they were treated with 0.05% Trypsin with EDTA (Sigma. Cat.No.T3924, USA) to cover the cells. The culture flask was incubated for 5-10 min at 37°C until cells had detached. Complete RPMI-1640 media was added to stop the Trypsin. Cells were resuspended in fresh media. When culturing to obtain M-CSF, cells were split in to large tissue culture flask (Corning. Cat.No.430824, USA) and cultured for 7 days following full confluency. Cells supernatant was taken off, sterile filtered and then stored at -20°C until used for culturing of BMDMs.

2.1.1.5 HEK 293 cells

HEK 293 cells were grown in DMEM with 4.5gm/L D-Glucose and 1mM Sodium pyruvate (Gibco. Cat. No. 21969-035, UK) supplemented with 10% heat inactivated fetal calf serum, 100 µg/ml Streptomycin, 100 IU/ml Penicillin. When cells were around 85% confluent they were transfected with N-terminal FLAG-tagged WT and D281E D289E TRIF constructs.

2.1.2 Primary cell preparations

2.1.2.1 Bone –marrow derived macrophages

Mice were maintained according to Institutional and National (UK Home Office) guidelines. C57/BL6 mice were obtained from Harlan UK. Primary bone-marrow macrophages BMDMs were isolated as described from C57/BL6 mice (Celada et al., 1984). Briefly, mice were sacrificed by cervical dislocation and femurs and tibias were dissected out. Femurs and tibias were flushed with media using a 25G needle (BD. Cat.No.300600, USA) to obtain bone marrow mononuclear phagocytic precursor cells. To remove tissues and debris cell suspension was passed through a Nitex mesh (Cadisch Sons, London, UK). Cells were cultured in RPMI-1640 supplemented with 10% heat inactivated FCS, Streptomycin (100 µg/ml), Penicillin (100 IU/ml), L-glutamine (2mM) and 1 mM Hepes solution(Sigma.Cat.No. H0887, USA) pH 7.3 on 9 cm plastic Petri dishes (Sterlin. Cat.No.24998, UK) at a concentration of 3×10^6 cells/plate. Macrophages were selected by addition of M-CSF 10ng/ml (Peprotech. Cat.No.315-02, UK) or by using the supernatant of L929 cells at a final concentration of 30%. Cells were cultured at 37˚C, 5% CO_2 and allowed to grow for between 6 – 9 days before use. Under these conditions, the resultant cell population was > 95% macrophages as judged by staining with the macrophage marker F4/80 (Fig 2-1).

2.1.2.2 Generation of bone-marrow derived dendritic cells

Bone marrow derived dendritic cells was generated and grown as described for BMDMs but, instead of M-CSF, cells were cultured in complete RPMI-1640 media supplemented with 20ng/ml GM-CSF

(Peprotech. Cat. No. 315-03, UK). Under these conditions, the resultant cell population was > 95% dendritic cell as judged by staining with the D.cells marker CD11c (Fig 2-2).
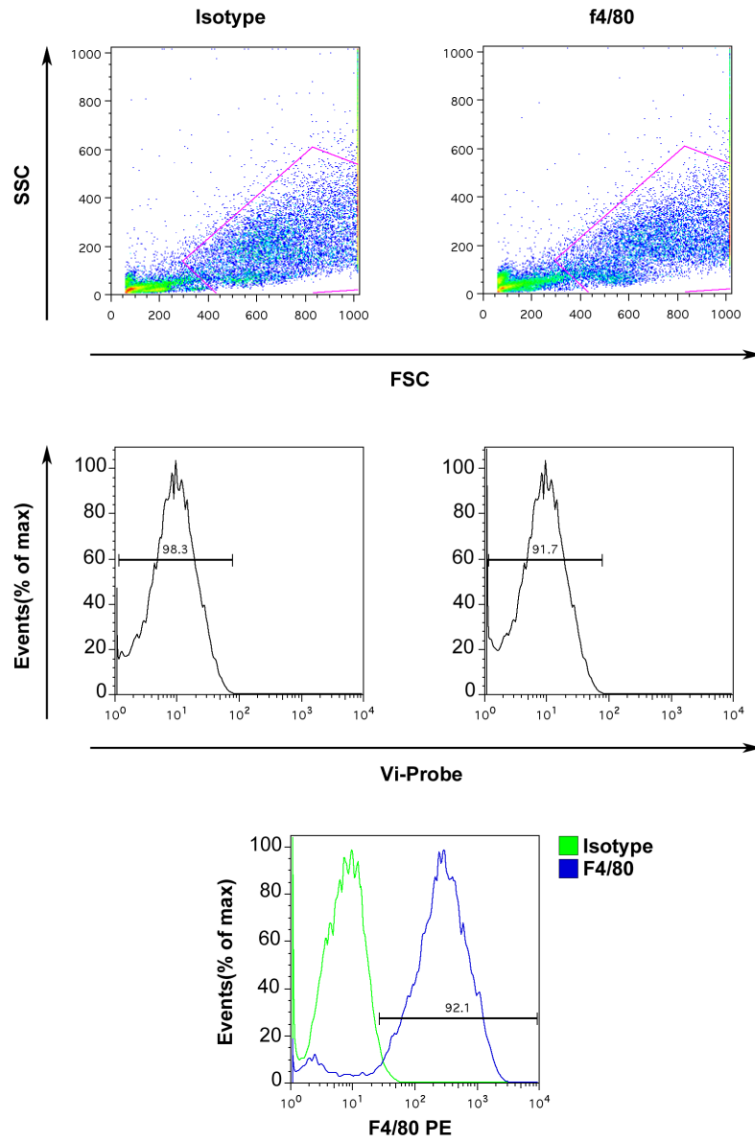
Figure 2.1; F4/80 staining of BMDMs.

BMDMs cells were isolated from WT mice and analysed for F4/80. F4/80 staining compared to isotype. Cells were gated based on forward and side scatter (top panels, 65.6% for isotype, and 64.1% for F4/80), these events were then gated based on 7-AAD (middle panel). Alive cells were gated based on F4/80 staining (bottom panel, 2.2% isotype, and 92.1% F4/80).
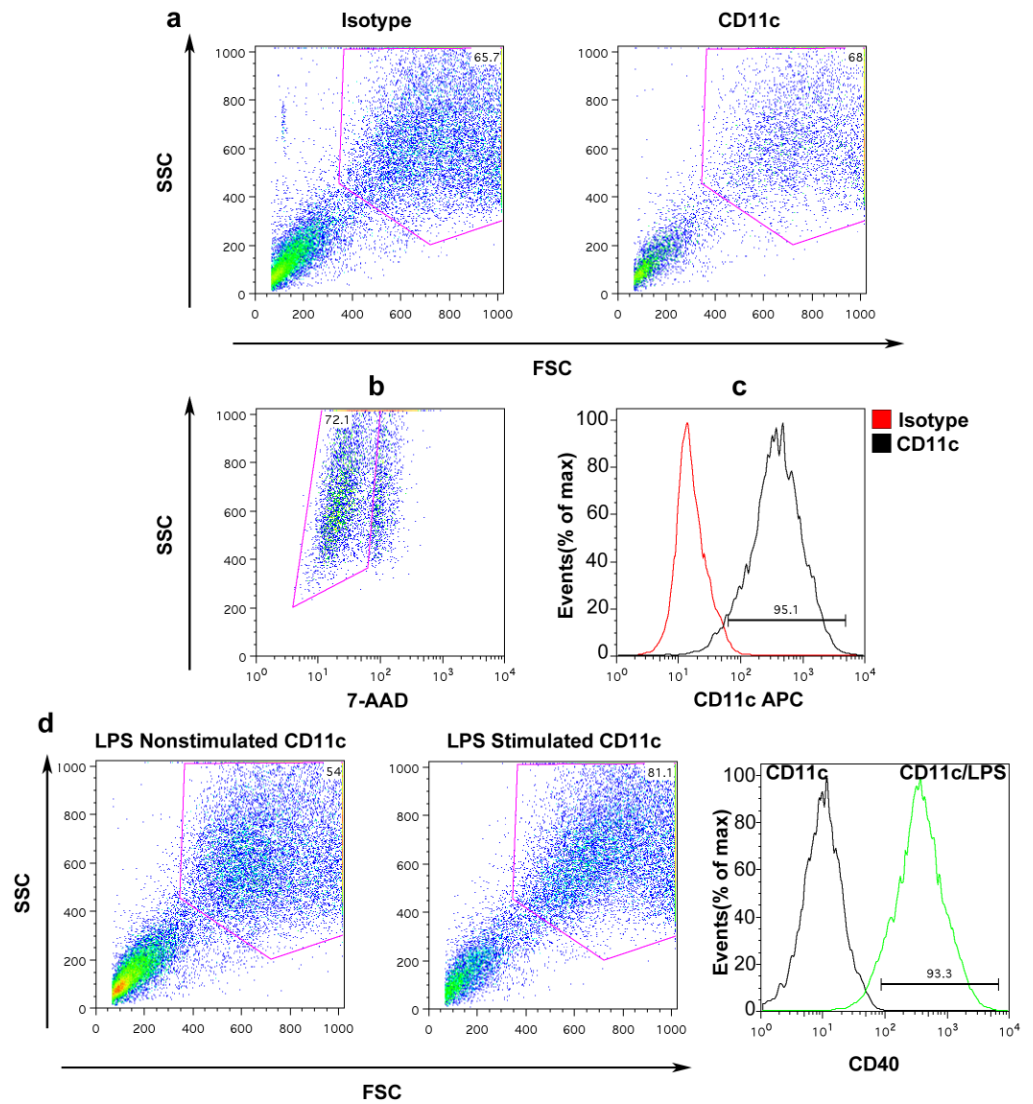
Figure 2.2; LPS CD11c staining of dendritic cells.

a, Dendritic cells were isolated from WT mice and analysed for CD11c. CD11c staining compared to isotype. Cells were gated based on forward and side scatter (65.7% for isotype, and 68% for CD11c). **b**, events were then gated based on 7-AAD, 7-AAD negative are live cells. **c**, Alive cells were gated based on CD11c staining. **d**, CD11c were treated with 1µg/ml LPS for 18 hrs for the expression of CD40.

2.2 Methods

2.2.1 Cell viability assay

Cell viability was determined by exclusion of trypan blue. 50µl of the cells were incubated at room temperature for 3 minutes with 50µl of 0.04% (w/v) trypan blue (Sigma. Cat. No. T8154, USA) in PBS and viable cells excluding trypan blue counted in a hemocytometer (Superior. Germany). Cell viability in all assays was >85%. In addition, the viability of the cells remained comparable throughout all time points used in this study.

2.2.2 Bacterial cultures

P. aeruginosa PA103ΔUΔT and PA103pcrV⁻ were kindly provided by Dara Frank. Bacterial strains were cultured in LB broth (Invitrogen. Cat. No.12780-052, USA) to mid-log phase (OD 0.4-0.6) immediately prior to use. The bacteria were then centrifuged at 3500 ×g for 15 minutes at 4˚C, the pellet was washed twice in sterile PBS and then resuspended in the same PenStrep -free media as the cells being infected to a concentration of approximately 1×10^6 cfu/µl = (O.D.600/0.4) ×1.8 ml. (1×10^6 cell/ml) were then infected at indicated multiplicity of infection (MOI) and time.

2.2.3 Immunofluorescence Microscopy

For immunofluorescence, cells were seeded onto Lab-tek 2 well chamber slides (Thermoscientific.Cat.No.177399, USA). Following experimental treatments, cells were washed 3 times with sterile PBS then fixed in 2% paraformaldehyde (VWR, UK) in PBS for 30 minutes at room temperature. Fixed cells were washed 3 times with PBS and then

permeabilized in 0.2% Triton X-100 (Sigma-Aldrich. Cat. No .9002-93-1, USA) in PBS for 20 minutes at room temperature. Permeabilized cells were washed 3 times in PBS and blocked with 10% normal goat serum (Sigma-Aldrich. Cat No.G9023, USA) in PBS for 1 hour. Cells were then incubated overnight at 4°C with1.25 µg/ml rabbit polyclonal LC3 (Abgent. Cat. No. AP1802a, USA), or with 1µg/ml mouse mab to ATPase inhibitory factor-1 antibody (abcam. Cat.No.ab110277, UK) in 10% NGS in PBS. Cells were then washed three times with 1ml sterile PBS for 5 minutes and incubated with 1µg/ml Alexa Fluor 488-conjugated goat anti-rabbit IgG (Invitrogen. Cat. No. A11034, USA), or with 1µg/ml Alexa Fluor 568-conjugated goat anti-mouse IgG (Invitrogen. Cat.No.A11031, USA)   in 10% NGS in PBS for 1 hour at room temperature. Following washing as before, cells were mounted in Vectashield with DAPI (Vector. Cat.No.H-1500, USA), and viewed using a Zeiss Axiovert S100 microscope using Open Lab software (PerkinElmer) or a LSM 510 Meta Confocal microscope (Carl Zeiss) using Meta 510 software.

For quantification of LC3 puncta, image analysis was performed using Image J (NIH, Maryland, USA). All results show values of mean number of puncta per cell; for each analysis at least 50 cells were analysed.

2.2.4 Western blot

Western blot was done according to manufacturer's standard protocol (abcam). Cells were infected, or stimulated as indicated. The cell samples were washed in ice- cold PBS 3 times and lysed in cold lysis buffer (20 mM Tris–HCl, pH 7.4, 150 mM NaCl, 1% SDS, and 1 mM EDTA) in the presence of protease inhibitors (Roche. Cat.No.04693159001, Germany) for 30 min on ice. Cells were harvested using a cell scraper (Greinor Bio-

One. Cat.No.541070, Germany) and cell lysate was collected. The protein concentrations were determined with Micro BCA protein detection kit (Pierce. Cat.No.23235, USA) and adjusted to equal concentrations across different samples. Lysates were diluted using LDS sample buffer (Invitrogen. Cat.No.NP0007, USA) and sample reducing agent (Invitrogen. Cat.No.NP0004, USA). Samples were heated at 70°C for 15 minutes and loaded on to NU-PAGE Bis-Tris gels (Invitrogen Cat.No.NP0322, NP0341, USA). 25µg of each sample was used. The gel was run at 100V, 125 mA until the dye reached the base of the gel. The samples were transferred on to Hybond-P polyvinylidene difluoride PVDF membrane (GE Healthcare Cat.No.RPN303F, UK) using a Hoefer TE 22 tank transfer unit (Amersham Bioscience. Cat. No. 80-6204-26, USA) and NuPAGE transfer buffer (Novex. Cat.No.NP0006-1, USA) supplemented with 20% methanol (Fisher chemicals. Cat.No.M/4000/PC17, UK) at 30v, 125mA for 2 hrs at room temperature. Transfer was checked by Ponceau's solution (Sigma-Aldrich. Cat.No.P7170, USA). The membranes were blocked with 5% dried skimmed milk (Marvel. Cat.No.92962, Ireland) in PBS 1% for 1 hr and then incubated overnight at 4°C with primary antibodies as shown in table (2-2). The unbound primary antibodies were washed away three times in PBS - Tween then the membranes were incubated with secondary antibodies table (2-2) for 1 hr in room temperature. The unbound secondary antibodies were washed off as above. Bound antibodies were detected using enhanced chemiluminescence ECL kit (GE Healthcare. Cat.No.RPN2209, UK) and visualized by exposure to X ray film. For reprobing blots they were rinsed in DD.W then Washed 3 times for 5 minutes in PBS/Tween. Stripping buffer (100m M 2-Mercaptoethanol, 2%SDS, 62.5 mM Tris-Hcl pH, 6.7) was

added to the blots, and incubated for 30 minutes at 50°C with occasional agitatation. Blots were then washed 3 times for 10 minutes in PBS/Tween before re-blocking in 5% dried skimmed milk for one hour at room temperature and then incubated overnight at 4°C with monoclonal Anti β-tubulin antibody (Sigma-Aldrich. Cat.No.T8328, USA). The unbound primary antibody was washed away three times in PBS /Tween then the membranes were incubated with Anti-mouse IgG HRP linked antibody (Cell signalling technology. Cat.No.7076, UK) for 1 hr in room temperature .The unbound secondary antibody was washed off as above. Bound antibodies were visualised as above.

2.2.5 ELISA

The cytokine concentration (IL-1β) in cell culture supernatants was measured by ELISA kit according to manufacturer's standard protocol (R and D systems Cat No. DY401, USA). ELISA flat bottom 96 well plates (Corning Costar. Cat. No.9018, USA) were coated with 50 μl capture antibody at a concentration of 4 μg/ml diluted in PBS, sealed and incubated overnight at room temperature. The wells were washed five times with wash buffer (PBS, 0.05% Tween 20) and blocked with 1 % BSA (Sigma. Cat. No. A7030-50, USA) in PBS at room temperature for 1 hour. After five washes in wash buffer, the samples and standards (50μl) were added with a top standard of 1000 pg/ml serially diluted 1:2 10 times. After 2 hours incubation at room temperature and five washes, detection antibody was added at a concentration of 2.5 μg/ml diluted in reagent diluent (0.1% BSA, 0.05% Tween 20 in Tris-buffered saline pH 7.4) and incubated 2hr at room temperature. After five washes, streptavidin-HRP was added at a dilution

1:200 in reagent diluent for 20 minutes at room temperature in the dark. After final five washes, TMB Micro well Peroxidase substrate solution (KPL, Cat.No. 52-00-00, USA) was added for 20 minutes at room temperature in the dark. Development was stopped by the addition 25µl of TMB stop solution (KPL, Cat.No.52-58-04, USA) and plates were read at 570 nm on a Tecan sunrise plate reader using Magellan software.

The cytokine concentration (TNF-α), in cell culture supernatants was measured by ELISA kit according to manufacturer's standard protocol (eBioscience Cat No. 88-7324-22, USA).

For human IL-1β, the protocol was as above for TNF-α assay except using coating buffer (Cat.No.00-0044-59), capture antibody (Cat.No.14-7018-68, USA), standard (Cat.No.39-8016-60, USA), and detection antibody (Cat.No.33-7016-68, USA).

2.2.6 Transmission electron microscopy

BMDM cells infected by *Pseudomonas aeruginosa* for 4 h were harvested by scraping the cells followed by centrifugation at 500 g for 10 min. The pellets were washed with Sorensen's Phosphate buffer and pre-fixed with 2% glutaraldehyde, followed by post-fixation with 1% OsO_4 in 6.6 mM Sorensen's phosphate buffer. All pellets were dehydrated stepwise in a graded series of ethanol and embedded in araldite CY212. The blocks were sectioned on Reichert–JunG ultra-cut microtome. Ultra-thin sections were double stained with uranyl acetate and lead citrate (all stains from Agar scientific). Sections were examined using a Tecnai transmission electron microscope (Model No. 943205018411, FEI Company, Czech republic)

equipped with Olympus digital camera (VELETA) at the Department of Pathology, Western Infirmary, Glasgow.

2.2.7   Flow cytometry

Blocking of non-specific Fc-mediated binding of antibodies to Fc receptors was performed using 1ug/ml of a rat anti-mouse CD16/CD32 antibody (BD Biosciences. Cat. No. 553141, USA) for 15 minute at 4°C. Intracellular LC3B II was detected as follows, following the method described by (Eng et al., 2010). Cells were fixed and permeabilized using fixation/permeabilization solution which contains 0.1% saponin (BD Bioscience, Cat. No. 51-2090KZ, USA) and resuspended in permeabilization wash buffer (BD Bioscience. Cat. No. 00-8333-56, USA). Cells were then incubated for 1hr at 4°C with 2 µg/ml rabbit polyclonal LC3 (Novus biological. Cat.No.NB100-2220, UK) in 1X permeabilization /wash buffer. After washing, cells were then incubated with 1µg/ml Alexa Fluor 488-conjugated goat anti-rabbit IgG (Invitrogen. Cat.No.A11034, USA) in 1X permeabilization/wash buffer for 1 h at 4°C. Cells were then washed and resuspended in phosphate buffered saline supplemented with 2.5% fetal calf serum for analysis.

Bacterial uptake was measured in cells using 1mg/ml pHrodo *E.coli* Bio Particles for 2hrs at 37°C (Invitrogen. Cat. No. P35366, USA) prior to analysis by flow cytometry. Reactive oxygen intermediates were assayed using CellRox deep red reagent at 5µM for 30 min at 37°C (Invitrogen. Cat. No. C10422, USA) and flow cytometry.

Mitochondrial ROS were measured in cells after infection as indicated by using MitoSox staining (Invitrogen. Cat. No. M36008, USA) at 2.5 µM for 30 min at 37˚C. For measurement of mitochondrial mass, cells were stained for 30 min at 37˚C with 50 nM MitoTracker Green FM (Invitrogen. Cat. No. M7514, USA), and 50 nM MitoTracker Red FM (Invitrogen. Cat. No. M22426, USA). Cells were then washed and resuspended in phosphate buffered saline supplemented with 2.5% fetal calf serum for analysis.

Cells were analysed using a CyAn ADP (Beckman Coulter) or Facscalibur flow cytometer (BD). Flow cytometry data was analysed with Flowjo Software (Tree Star Inc.).

2.2.8 RT-PCR

Total cellular RNA was isolated with an RNeasy Mini kit (Qiagen. Cat. No. 74104, UK) according to the manufacturer's instructions. cDNA was synthesised from DNase I treated RNA using Superscript II reverse transcriptase (Invitrogen. Cat. No. 18064-071, USA) according to the manufacturer's instructions. Quantitative reverse transcription PCR (q RT-PCR) was performed using fast SYBR Green PCR master mix (Applied Biosystems. Cat. No. 4385612, UK) using the 7900HT fast system (Applied Biosystems). The following primers were used for RT- PCR:

Ifn-β: sense, 5'-CCGAGCAGAGATCTTCAGGAA-3';

antisense, 5'-GCAACCACCACTCATTCT-3'.

Lc3b : sense, 5'-ACAAAGAGTGGAAGATGTCCG-3' ; antisense, 5'-CCCCTTGTATCGCTCTATATTCAC-3'.

Gene expression levels were normalised to TATA binding protein (TBP): sense, 5'-TTCACCATGACTCCTATGACC-3';

antisense, 5'-CAAGTTTACAGCCAAGATTCACG-3' .

The mean relative gene expression was calculated using Livak's method (Livak and Schmittgen, 2001). All determinations were performed in triplicate.

2.2.9 Measuring Cytoplasmic mitochondrial DNA

For measuring cytoplasmic mtDNA, 1×10^7 cells infected as indicated were homogenized with a Dounce homogenizer in 100 mM NaOH solution, pH 7.4, containing 0.25 M Sucrose, 1 mM EDTA, and protease inhibitors, then centrifuged at 800*g* for 12 min at 4 °C. The protein concentrations were determined with Micro BCA protein detection kit (Pierce. Cat.No.23235, USA) and adjusted to equal concentrations across different samples, followed by centrifugation at 12,000*g* for 30 min at 4 °C for the production of a supernatant corresponding to the cytosolic fraction. Total DNA was isolated from 200 µl of the cytosolic fraction with a DNeasy blood and tissue kit (Qiagen. Cat. No. 69504, UK).

2.2.10 Quantitative real-time PCR

Quantitative PCR was used for measurement of cytoplasmic mitochondrial DNA mtDNA using fast SYPR Green PCR master mix

(Applied Biosystems. Cat. No. 4385612, UK). The copy number of cytoplasmic mtDNA was normalized to that of nuclear DNA as the ratio of DNA encoding *cytochrome c oxidase* I to nuclear DNA encoding 18S ribosomal RNA (Tal et al., 2009). The following primers were used for q-PCR:

18S sense, 5′-TAGAGGGACAAGTGGCGTTC-3′,

 anti-sense, 5′-CGCTGAGCCAGTCAGTGT-3′;

 Mouse cytochrome *c* oxidase I sense, 5′-GCCCCAGATATAGCATTCCC-3′,

anti-sense, 5′-GTTCATCCTGTTCCTGCTCC-3′.

The copy number of DNA encoding *cytochrome c oxidase* I was measured by quantitative real-time PCR with same volume of the DNA solution.

2.2.11 Isolation of mitochondrial DNA

Mouse mitochondrial DNA (mtDNA) was isolated from 40×10^6 J774A.1cell with a mitochondrial DNA isolation kit (Thermo scientific Cat.No.89874, USA) according to the manufacturer's instructions. Mitochondrial DNA was isolated from the pellet with a DNeasy blood and tissue kit (Qiagen Cat. No. 69504, UK) according to the manufacturer's instructions. To generate oxidized mtDNA, the material was incubated with 100 µM hydrogen peroxide for 30 min at 37C.

2.2.12 Transfection of mtDNA

BMDMs were transfected for 6 hr with 2µg/ml isolated mtDNA, and oxidized mtDNA through the use of 3µl Attractene (Qiagen. Cat.No.301005, UK) according to the manufacturer's instructions.

2.2.13 Protein transfection

Protein transfection was performed using Polyplus reagent according to the manufacturer's standard protocol (Polyplus transfection. Cat. No. PPLU501-01, USA). Cells were incubated with the protein/transfection reagent complex for 5 hr at 37°C in a 5% CO2 incubator. After removing the media, cells were washed 2 times with sterile PBS, cells were incubated in complete growth media without antibiotic, and then infected with PA103ΔUΔT for 4 hr (MOI 1:25).

2.2.14 siRNA and transfection

Control siRNA and siRNAs to the indicated genes were all from Dharmacon RNAi Technologies UK (On Target plus SMART pool siRNA) Table (2-1). Silencing constructs were introduced into cells using HiPerfect transfection reagent (Qiagen. Cat.No.301704, UK), according to the Manufacturer's instructions. Transfection of BMDMs was optimised using SiGLO Green transfection indicator (Dharmacon RNAi Technologies. Cat. No. D-001630-01-05, UK) and flow cytometry. Cells were plated at a density of 0.5 x 10^6 cells per well of a 12-well plate in 500 µl of RPMI1640 culture medium. siRNA was added at a concentration of 40 nM together with 9 µl of transfection reagent. This routinely gave transfection efficiencies

greater than 90% Fig (2-3). For efficient knock down, cells were cultured for 24 – 48 h.

Table 2.1 siRNA used in this study

siRNA	Target sequences	Cat. No.
Lc3b	5´- ACUAUGGUGCGAUCAGUAA-3´ 5´- CAUCCUAAGUUGCCAAUAA-3´ 5´- GGAUAUAGCUCUAAGCCGG-3´ 5´- CUAAUAAAGGCACAACGAA-3´	L-040989-01-0005
Atg5	5´- GCAUAAAAGUCAAGUGAUC-3´ 5´- CCAAUUGGUUUACUAUUUG-3´ 5´- CGAAUUCCAACUUGCUUUA-3´ 5´- UUAGUGAGAUAUGGUUUGA-3´	L-064838-0005
Caspase-1	5´- GAAUACAACCACUCGUACA-3´ 5´- GCCAAAUCUUUAUCACUUA-3´ 5´- GGUAUACCGUGAAAGUGAA-3´ 5´- GCAUUAAGAAGGCCCAUAU-3´	L-048913-00-0005
Caspase-11	5´-GAUGUGCUACAGUAUGAUA-3´ 5´-CGAAAGGCUCUUAUCAUAU-3´ 5´-AAGCUAAUCUGGAAAUGGA-3´ 5´-GUGCAACAAUCAUUUGAAA-3´	L-042432-00-0005
TRIF	5´-GAUCGGUGCAGUUCAGAAUA-3´ 5´-GAACAGCCUUACACAGUCU-3´ 5´-GGAAAGCAGUGGCCUAUUA-3´ 5´-GAGAUAAGCUGGCCUCCAU-3´	L-055987-00-0005
Tlr4	5´- UGACGAACCUAGUACAUGU-3´ 5´- GGAAUUGUAUCGCCUUCUU-3´ 5´- GAGUUCAGGUUAACAUAUA-3´ 5´- GCAUAGAGGUAGUUCCUAA-3´	L-047487-00-0005
Nlrc4	5´- UCGAAACACUGUACGAUCA-3´ 5´- GAACAUCCCUGACUAUUUA-3´ 5´- CAAUAGGGCUCCUCUGUAA-3´ 5´- GCGAUGACCUCUUUGCAUU-3´	L-055000-00-0005
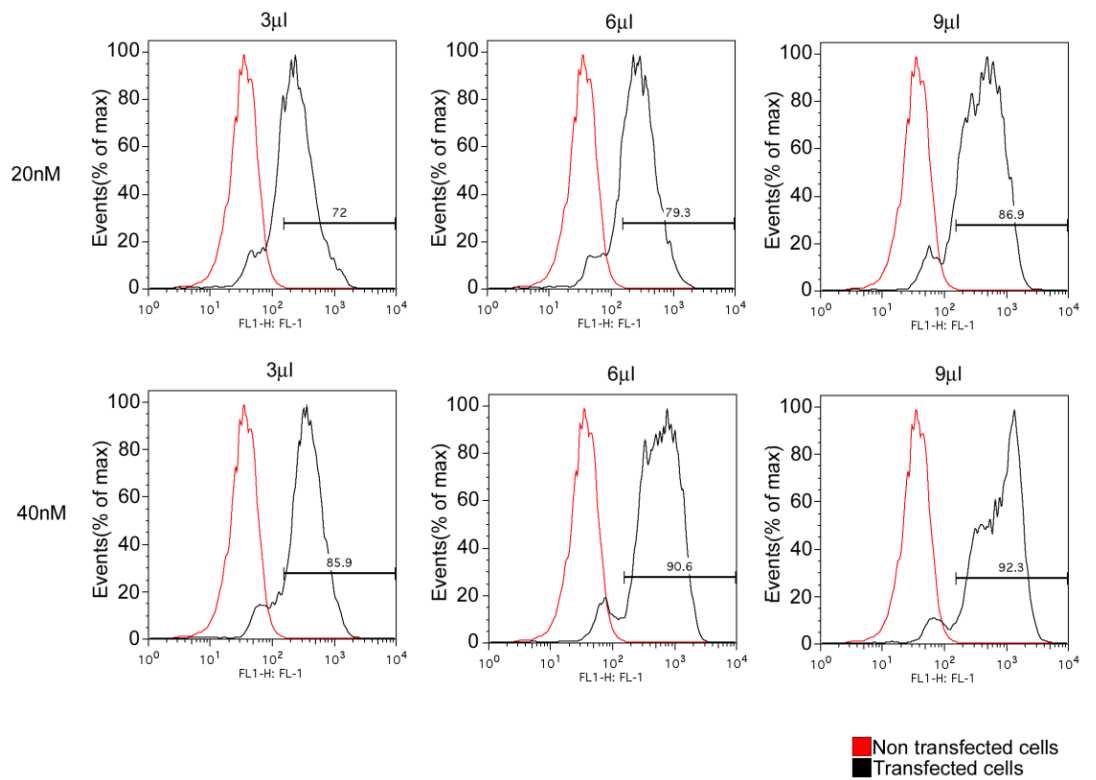
Figure 2.3; siRNA transfection optimization

 BMDMs were transfected using SiGLO Green transfection indicator at a concentration of (20, and 40 nM) with (3, 6, and 9 µl) of HiPerfect transfection reagent for 24 hr and then analysed using flow cytometry.

2.2.15 Transfection of electrocompetent *E.coli* (EC100)

TransforMax EC100 electrocompetent *E.coli* (Cambio bioscience .Cat.No.EC10005, UK) were transformed according to manufacturer's protocol. Briefly, electroporation cuvettes GenePluser cuvettes 0.1 cm (Life Technologies.Cat.No.P410-50, USA) were chilled on ice and 50µl electrocompetent cells were defrosted on ice. TRIF FLAG WT and D281E D289E Plasmids were added and mixed gently with the bacteria. Immediately following this cells were transferred to an electroporation cuvette and pulsed on a Gene Pluser X cell system (BioRad.Cat.No.165-2660, UAS) using a program for *E.coli* (1800 V, 25µF, 200 Ω, 4 seconds time constant). 950µl super optimal broth with catabolite repression (SOC) medium (Life technologies .Cat.No.15544-034, USA) at room temperature was then added and cells placed in a shaking incubator (Stuart scientific, UK) (250 RPM) at 37˚C for 1.5 hour to allow expression of any antibiotic resistance marker. 200 µl of bacteria were then plated on to appropriate LB-Agar plates with 75µg/ml Ampicillin (Sigma .Cat.No.A9518.USA) and allowed to grow at 37˚C overnight.

2.2.16 TRIF- FLAG plasmids purification

Plasmids were purified using plasmid maxi kit (Qiagen. Cat. No. 12162, UK) according to manufacturer's instructions.

2.2.17 Plasmid transfection

N-terminal FLAG-tagged WT and D281E D289E TRIF constructs (Lei et al., 2011) in pcDNA3.1 were kindly provided by Dr. Lei, (China). Plasmids were transfected into cells using Attractene (Qiagen. Cat. No.

301005, UK), or using Lipofectamine 2000 (Invitrogen, Cat. No.11668-027, USA), according to the manufacturer's instructions. Cells were harvested at 24 h after transfection.

2.2.18 Construction of plasmids

Restriction enzyme XbaI (New England BioLab. Cat. No. R0145S, UK), and BstXI (Promega. Cat. No. R6471, USA), all were used according to manufacturer's instructions in suitable buffers provided with enzyme.

C-terminal and N-terminal of WT FLAG plasmid were amplified using the following primers

TRIF C- Terminal sense,

5′-CACCATGCCCGCAGCTCCAGAAACCAGCA-3′,

anti-sense, 5′-TTCTGCCTCCTGCGTCTTGTC-3′;

TRIF N-Terminal sense,

5′-CACCATGGCCTGCACAGGCCCATCACTTC-3′,

anti-sense, 5′-ATCTGGGGCCACTTCGGGAAGCCC-3′;

The resulting product was cloned in to pcDNA3.1D/V5-His-Topo vector (Invitrogen. Cat. No. 45-0158, USA), according to manufacturer's instructions.

2.2.19 Agarose gel electrophoresis

PCR products, plasmid preparations and restriction enzyme digests were resolved using agarose gel electrophoresis and a Horizon 58 life

technologies horizontal gel electrophoresis apparatus (Serial No. 00239825, USA). 2% agarose (BIO-RAD, Cat. No. 161-3101, USA) was dissolved in 1x Tris/Borate/EDTA (TBE) buffer and 1x SYBR safe gel DNA stain (Invitrogen. Cat. No. S33102, USA). Gels were viewed and photographed using Gel Logic 200 imaging system (KODAK).

2.2.20 Generation of mtDNA deficient ρ^0 cells

J774A.1 macrophages were grown in RPMI 1640 media supplemented with 10% heat inactivated FCS, 100 µg/ml Streptomycin, 100IU/ml Penicillin, 1mM Hepes solution, and Uridine 25µg/ml . EtBr (500 ng/ml) (Sigma- Aldrich. Cat. No. 1510, USA) was added to the medium for 15 day (Hashiguchi and Zhang-Akiyama, 2009). Depletion of mitochondrial DNA was evaluated by quantitative PCR for the mitochondrial gene *cytochrome c oxidase* I and compared to nuclear DNA encoding 18S ribosomal RNA.

2.2.21 Immunoprecipitation

BMDMs were preloaded with BrdU (10 mM) (Sigma. Cat.No.B5002, USA) for 48 hr and then seeded into 6 well plates (Costar. Cat. No. 3516, USA) at 2.5 ×10^6 cell/ml RPMI 1640 media and then infected with PA103ΔUΔT (2, 4 hr) at (MOI 25). After infection cells were washed twice with ice-cold PBS and then lysed in 500µl RIPA lysis buffer (Thermo scientific. Cat.No.89900, USA) for 30 minutes. Cells were collected by cell scraper and the lysate centrifuged at 13,000 g at 4° C for 20 minutes. Lysates were pre-cleared by addition of 50 µl of anti-rabbit IgG beads (eBioscience. Cat.No.00-8800-25, USA) on ice for 50 minutes with gentle agitation and then spun at 11,000 x g for at 4° C for 3 minutes. 5µg of rabbit

anti-NLRC4 (Novus Biologicals. Cat. No. NBP1-78979SS, UK) antibody or 5 µg of negative control rabbit IgG (Dakocytomation. Cat.No.X0936, Denmark) were added to 250 µl aliquots of the lysate and incubated on ice for 1.5 hr. 50µl of anti-rabbit IgG beads was added and the samples were further incubated at 4°C for 1 hr. Immune complexes were then washed 3 times with ice-cold RIPA lysis buffer and bound material eluted with distilled water at 100°C for 10 minutes. A 20µl aliquot was analysed on a standard Western blot for NLRC4 protein. DNA in the remaining 80 µl aliquot was denatured by addition of 8 µl of 4M NaOH and 1.6µl of 0.5 M EDTA and incubated at 100°C for 5 minutes. The sample was cooled on ice and neutralized by addition of 110µl of ice-cold 2M Ammonium acetate pH 7 before transferring to nitrocellulose membranes using a Bio-Dot microfiltration apparatus (Bio-Rad Cat.No.170-6542, Germany). Membranes were rinsed in 2X SSC and cross-linked to the nitrocellulose using UV irradiation. Membranes were then blocked with 5% dried skimmed milk for 1 hr and incubated overnight at 4°C with primary antibodies to BrdU mAb (1.5µg/ml; Sigma. Cat.No.BU33, USA) or mouse anti-8OH-dG mAb (1µg/ml; Santa Cruz biotechnology. Cat.No.SC-66036, U.K.). Following washing and incubation with horseradish peroxidase conjugated secondary antibody, bound antibody was detected using enhanced a chemiluminescence ECL kit (Fisher scientific. Cat.No.RPN2209, UK).

2.2.22 Gentamicin protection assay

Viable intracellular bacterial counts were determined by a gentamicin protection assay as described (Lindestam Arlehamn et al., 2010).

2.2.23 LDH Release

Cells were incubated in media lacking Phenol red. Lactate dehydrogenase release determinations were performed using the Cytotox 96 cytotoxicity assay kit (Promega. Cat. No. G1781, USA).

2.2.24 Animal models

Model 1

Female C57/BL6 mice aged 8 weeks were obtained from Harlan UK. Mice were randomly divided into to three groups, n=3 per group. Control groups were injected intraperitoneally (ip) with sterile PBS. Experimental groups were injected (ip) with PA103ΔUΔT (10^7 cfu) alone or with caspase inhibitor Z-YVAD-FMK 0.1mg/kg. 6 hours after infection, animals were sacrificed and blood and peritoneal fluid collected for analysis as indicated.

Model 2

Peritoneal macrophages were depleted using clodronate liposomes (Foundation Clodronate Liposomes, Amsterdam). 200 μl clodronate liposomes were injected 96 hours and 24 hours prior to infection. Depletion was confirmed by performing peritoneal lavage on animals injected with clodronate liposomes or PBS liposome controls and performing total cell counts and Romanowski staining after cytocentrifugation. Bone marrow derived macrophages were stained with eFluor 450 proliferation dye (eBioscience, Cat. No. 65-0842, UK) at a concentration of 10 μM according to the manufacturer's instructions. Mice were injected intra-peritoneally with 5 x 10^6 of eFluor 450 stained macrophages. 1 hour later mice were injected with 10^7 cfu of PA103ΔUΔT or PBS. After 6 hours mice were culled by

inhalation of CO2. Peritoneal fluid was collected by injection and subsequent aspiration of 5ml of cold PBS.

Neutrophils were enumerated by performing total cell counts and Romanowski staining after cytocentrifugation or peritoneal lavage fluid. Cells were then stained with Alexa Fluor 700 anti-CD11b (M1/70, Biolegend), PE anti-F4/80 (BM8, Biolegend), Alexa Fluor 647 anti-Ly-6G (1A8, Biolegend) or appropriate isotype controls. Following fixation and permeabilisation cells were then stained for LC3 as already described. Macrophages were selected on the basis of being CD11b+F4/80+Ly-6G- and extrinsic macrophages were then identified on the basis of staining with eFluor 450.

Model 3

Female C57/BL6 mice aged 8 weeks were obtained from Harlan UK. Mice were randomly divided in to six groups (n=3 per group). Three control groups were injected intraperitonial (ip) with sterile PBS, rapamycin (1.5 gm/kg) (Harris et al., 2011), or 3-MA (30mg/kg) (Kim et al., 2012). Experimental groups were injected (ip) with PA103ΔUΔT (10^7 cfu) alone, or with rapamycin or with 3-MA. Blood and peritoneal fluid was taken after 6 hrs for analysis of IL-1β and TNF secretion by ELISA and for protein concentration.

Table 2.2 Antibodies used in this study

Antibody description	Manufacturer	Cat. No.	Applications	Working concentration
Purified rabbit polyclonal antibody Pab, Autophagy LC3 antibody (AP G8B) (N-term).	Abgent (USA)	AP 1802a	IF	1.25µg/ml
Alex flour 488 goat anti-rabbit IgG (H+L).	Invitrogen (USA)	A11034	IF FACS	1µg/ml
Alex flour 568 goat anti-mouse IgG (H+L).	Invitrogen (USA)	A11031	IF	1µg/ml
Negative control , Rabbit immunoglobulin fraction (sold-phase absorbed)	DakoCytomation (Denmark)	X0936	IF FACS IP	1.25µg/ml 5µg/ml
8-OHdG Mouse monoclonal IgG2b	Santa cruz biotechnology (UK)	Sc-66036	IP	1µg/ml
Mouse monoclonal Anti-BrdU	Sigma-Aldrich (USA)	B8434	IP	2µg/ml
Anti-rabbit IgG HRP- linked antibody.	Cell signaling technology (UK)	7074	WB	1:2000
LC3 Antibody LC3 B	Novus Biological (UK)	NB100-2220	WB FACS	1µg/ml
Anti-Mouse IgG HRP- linked antibody.	Cell signaling technology (UK)	7076	WB	1:2000
Monoclonal Anti-β-Tubulin antibody produced in mouse	Sigma-Aldrich (USA)	T8328	WB	1µg/ml
Capture Antibody.	R and D	80134	ELISA	4µg/ml

	system (USA)			
Detection Antibody.	R and D system (USA)	80135	ELISA	600ηg/ml
Caspase -1 p10 (M-20) Antibody.	Santa cruz biotechnology (UK)	sc-514	WB	1µg/ml
Caspase -1 (A-19) Antibody.	Santa cruz biotechnology (UK)	sc-622	WB	1µg/ml
Capase-11 Antibody	Abcam (UK)	ab22684	WB	1/5000
Rabbit polyclonal to IL-1 β.	Abcam (UK)	ab9722	WB	1µg/ml
Rabbit polyclonal to TRIF.	abcam (UK)	ab13810	WB	1 µg/ml
NLRC4 Antibody.	Novus Biologicals	NBP1-78979SS	WB IP	2µg/ml 5µg/ml
Monoclonal ANTI-FLAG, M2, Clone M2.	Sigma (USA)	F1804	WB	1µg/ml
Mouse Anti-rabbit IgG .mAb (HRP conjugate).	Cell signaling technology (UK)	5127	WB	1:2000
Anti-AIM2 Purified.	eBioscience (UK)	14-6008	WB	1. 5µg/ml
Capture Ab purified anti-mouse TNF –α.	eBioscience (UK)	14-7423-67A	ELISA	1:250
Detection Ab Biotin-conjugate anti-mouse TNF –α polyclonal.	eBioscience (UK)	13-7341-67A	ELISA	1:250
Capture Ab	eBioscience	14-7018-	ELISA	1:250

purified anti-human IL-1β.	(UK)	68		
Detection Ab Biotin-conjugate anti-human IL-1 β –α polyclonal	eBioscience (UK)	33-7016-68	ELISA	1:250
Anti-Atg5 Antibody.	Novus Biologicals (UK)	NB110-53818SS	WB	0.5µg/ml
Ms mab to ATPase inhibitory factor 1.	abcam (UK)	ab110277	WB IF	1µg/ml
Mouse TLR4 Ab	Abcam(UK)	Ab22048	WB	2µg/ml
Anti- rabbit IgG IP beads	eBioscience (UK)	00-8800-25	IP	1:10
Rabbit polyclonal anti-PINK1 Antibody	Novus Biological	BC100-494	W.B.	1µg/ml
Mouse anti- V5 tag	Invitrogen	377500	W.B.	1µg/ml

Table 3.3 Knockout mice used in this study

KO Mice	Source
Tlr4	Prof. Tim Mitchell University of Glasgow (UK)
Nlrc4	Prof. Clare Bryant University of Cambridge (UK)
Trif	Prof. Clare Bryant University of Cambridge (UK)
Aim2	Prof. Katherine Fitzgerald University of Massachusetts (USA)
Atg7	Prof. Anna Katharina Simon University of Oxford (UK)
Myd88	Prof. David Gray University of Edinburgh (UK)

2.3 Solutions and buffers used in this study

- Phosphate buffer saline (8.0 gm Nacl+0.45gm NaH_2Po_4+2.3gm Na_2HPo4+ 0.2 gm KCl) in 1liter of distilled water, PH=7.4.

- Trypan blue stain. (Sigma-Aldrich. Cat No.T8154, USA).

- 10% Normal goat serum in PBS. (Sigma-Aldrich. Cat No.G9023, USA).

- Fetal calf serum. (Invitrogen .Cat No.15561020, USA).

- Vectashield with DAPI. (Vector. Cat No.H-1500, USA).

- Micro BCA Reagent A (MA), 240 ml (in Product No. 23235), containing sodium carbonate, sodium bicarbonate, bicinchoninic acid and sodium tartrate in 0.2 M sodium hydroxide (Pierce. Cat.No.23231, USA).

- MicroBCA Reagent B (MB), 240 ml, containing 4% bicinchoninic acid in water (Pierce. Cat.No.23232, USA).

- MicroBCA Reagent C (MC), 12 ml, containing 4% cupric sulphate, pentahydrate in water (Pierce. Cat.No.23234, USA).

- Albumin Standard Ampules, 2 mg/ml, 10 × 1 ml ampoules, containing bovine serum albumin (BSA) at 2.0 mg/ml in 0.9% saline and 0.05% sodium azide (Pierce. Cat.No.23209, USA).

- Lysis buffer (1mM EDTA, 150 mM NaCl, 20 mM Tris-Cl, PH7.5, and 1% SDS in DW.

- LDS (Loading) buffer 4X. (Invitrogen. Cat.No.NP0007, USA).

- Sample reducing agent 10X. (Invitrogen. Cat.No.NP0004, USA).

- MES SDS Running buffer 20X. (Invitrogen. Cat.No.NP0002, USA).

- Transfer buffer 20X. (Invitrogen. Cat.No.NP0006-1, USA).

- Ponceau's solution 0.1% PonceauS. (w/v) in 5% (v/v) acetic acid. (Sigma-Aldrich. Cat.No.P7170, USA).

- HRP- Streptavidin Horseradish Peroxidase Conjugate. (Invitrogen. Cat No.43-4323, USA).

- ECL kit (Lumigen P5-3 detection reagent solution A, Cat. No. RPN 2132 V1 and Lumigen P5-3 detection reagent solution B, Cat. No. RPN 2132 V2, GE healthcare (UK).

- 5% dried skimmed milk (Marvel. Cat.No.92962, Ireland) in PBS.

- Stripping buffer (100m M 2-Mercaptoethanol, 2%SDS, 62.5m M Tris-Hcl. pH 6.7).

- (2S,3S)-Trans-Epoxysuccinyl-L-leucylamido-3-methylbutane ethyl ester, EST. (Sigma-Aldrich. Cat. No. E8640, USA).

- Pepstatin A. (Sigma-Aldrich Cat.No.P5318, USA).

- Bafilomycin A (Sigma. Cat. No. B1793, USA).

- 1% BSA (Sigma. Cat. No. A7030-50, USA) in PBS.

- ELISA Reagent diluent (0 .1% BSA, 0.05% Tween 20 in Trise-buffered saline (20 mM Trizma base, 150m M NaCl) PH 7.2-7.4, 0.2 μm filtered.

- ELISA Substrate Solution (1:1 mixture of colour reagent A H_2O_2 and colour reagent B Tetramethylbenzidine. (Rand D system. Cat. No. DY 999, USA).

- ELISA Stop Solution 2N H_2SO_4. (R and D system. Cat. No. DY 994 USA).

- Triton X-100. (Sigma-Aldrich. Cat. No .9002-93-1, USA).

- Low- potassium buffer (140 mM NaCl, 5 mM KCl, 10 mM Hepes solution, 1.3 mM $CaCl_2$, 0.5 mM $MgCl_2$, 0.36 mM K_2HPO_4, 0.44 mM KH_2PO_4, 5.5 mM D-glucose, and 4.2mM $NaHCO_3$). Autoclaved and filtered then supplemented with 1X MEM vitamin solution (Cat.No.M6895), 2 mM L-glutamine (Cat.No.G7513), 1X MEM amino acids solution (Cat.No.M1567), and 100 μM /ml Sodium Pyruvate (Cat. No. S 8636) all from (Sigma-Aldrich, USA).

- High- Potassium buffer (5 mM NaCl, 140 mM KCl, 10 mM Hepes solution, 1.3 mM $CaCl_2$, 0.5 mM $MgCl_2$, 0.36 mM K_2HPO_4, 0.44 mM KH_2PO_4, 5.5 mM D-glucose, and 4.2mM $NaHCO_3$). Autoclaved and filtered then supplemented with 1X MEM vitamin solution (Cat.No.M6895), 2 mM L-glutamine (Cat.No.G7513), 1X MEM amino acids solution (Cat.No.M1567), and 100 μM /ml Sodium Pyruvate (Cat. No. S 8636) all from (Sigma-Aldrich, USA).

- 2% PFA (Alfa Aesas. Cat. No. 43368, USA).

- Tween 20. (Sigma-Aldrich. Cat.No.P2287, USA).

- LDH Assay buffer. (Promega. Cat. No. G 180, USA). Substrate mix (Promega. Cat. No. G 179, USA).

- Stop solution. (Promega. Cat. No. G 183, USA).

- 5X siRNA buffer (Dharmacon. Cat. No. B-002000-UB-100, UK) containing (300 mM KCl, 30mM Hepes solution pH 7.5, and 1.0mM $MgCl_2$).

- 1X siRNA buffer four volumes of sterile RNase-free water- (Dharmacon. Cat. No. B-002000-WB-100, UK) with one volume of 5X siRNA buffer.

- TE buffer 10 mM Tris pH 8.0 and 1 mM EDTA.

- SOC medium (Invitrogen. Cat.No.15544-034, USA).

- Mitochondrial isolation buffer (100 mM trise base, pH7.4 containing 0.25 M Sucrose, 1mM EDTA and protease inhibitor).

- 20 X SSC (3M NaCl +0.3M Trisodium citrate). Dissolve 175.0 gm NaCl and 88.2gm Trisodium citrate in D.W. Adjust volume to 1 L with D.W.

- RNase free water. (Qiagen. Cat. No. 74104, UK).

- Mitochondrial isolation reagent A. (Thermo scientific. Cat. No. 1859692, USA).

- Mitochondrial isolation reagent B. (Thermo scientific, Cat. No. 1859693, USA).

- Mitochondrial isolation reagent C. (Thermo scientific, Cat. No. 1859694, USA).

- AW1. (Cat. No. 69504), AW2. (Cat. No. 69504), ATL. (Cat. No. 69504), AE. (Cat. No. 69504), and AL. (Cat. No. 69504) (all from Qiagen, UK).

- Buffer P1. (Cat. No. 12162), Buffer P2. (Cat. No. 12162), Buffer P3. (Cat. No. 12162), Buffer QF. (Cat. No. 12162), Buffer QBT. (Cat. No. 12162), and Buffer QC. (Cat. No. 12162) (all from Qiagen, UK).

- FACS buffer 2%FCS in PBS, and 0.05% Sodium azide.

- Live imaging solution 1X pH 7.4 (Hepes buffered physiological saline) (Invitrogen. Cat.No.A1429IDJ, USA).

- TBE buffer (54g Tris base, 27.5g of Boric acid, and 20ml of 0.5 M EDTA in 1L DW).

2.4 Statistics

Comparison between groups at one time point was made using unpaired t test. A p value of < 0.05 was considered significant.

3 Role of T3SS in autophagy following *Pseudomonas aeruginosa* infection

3.1 Introduction

Autophagy is a cellular process whereby cytosolic components are incorporated into a double membrane-bound compartment that is then targeted for lysosomal delivery and ultimate degradation. It was originally described as a process occurring in response to starvation that allowed degradation of cellular organelles and proteins to supply new materials for continued cell survival. It is a process found in virtually all eukaryotic cells and the basic machinery that regulates autophagy is evolutionarily highly conserved (Kundu and Thompson, 2008). Increasingly, autophagy is recognised as playing a part in many human diseases ranging from cancer to atherosclerosis. In infectious disease, autophagy is important in removing intracellular microbes, as well as producing and delivering ligands that trigger innate immune signalling (Deretic and Levine, 2009).

Pseudomonas aeruginosa is an important gram negative organism and accounts for about 25% of all gram negative infections isolated from hospital environments. *P. aeruginosa* commonly infects immunodeficient people and those with Tuberculosis, cystic fibrosis and cancer could be potential victims of this pathogen (Yuan et al., 2012). *P. aeruginosa* has been classified as an extracellular pathogen with a spectrum of virulence factors, which help prevent it from clearance by the host innate immunity (Sadikot et al., 2005). *P. aeruginosa* can produce resistant strains and traditional antibiotic therapies fail to protect against these resistant strains (Chastre and Fagon, 2002). To study the relationship between macrophages and microorganisms is important to clear the picture of host

defence and might help finding some new therapies for the control of these pathogens (Wang et al., 2010) (Yuan et al., 2012)

Bacteria use many mechanisms to subvert cellular processes to their benefit. One such mechanism is the Gram-negative type III secretion system (T3SS), a nanomachine that directly introduces bacterial toxins into animal cells and is widely distributed amongst pathogenic Gram-negative organisms. In addition to delivering bacterial toxins, the T3SS has been implicated in delivering other pathogen-derived molecules that can activate the inflammasome, such as flagellin (Miao et al., 2006).

The classical intracellular autophagic pathway consist of a signalling mechanism which relies mainly on two Ubiquitin-like conjugation systems involving autophagy-related genes (Atg), Atg7-Atg12-Atg5 or Atg4-Atg7-Atg8 (called LC3 in mammals).These two systems rely on Atg6 (beclin-1 in mammals) which is crucial in early complex formation containing class III phosphoinositide3-kinase (PI3K, also known as VPS4), and eventually forming the autophagosome (Ohsumi and Mizushima, 2004). Another system involving Atg-8 (LC3) is cleaved by another autophagy related protein Atg-4 to expose its C terminal Glycine residue. This system is also similar to the first system in which LC3 is activated by Atg7 and then transferred to Atg3 (a ubiquitin 2 like protein) The activated LC3 then forms complex with PE which is present abundantly in the membrane phospholipids of the cells (Ichimura et al., 2000)

Recent research has demonstrated an essential role of autophagy in immune response against pathogens in many diseases including viral and

bacterial infections (Ogawa et al., 2005, Colombo, 2007). Virus and bacteria once engulfed by macrophages are capable of escaping from phagosome but they are taken up by autophagosome again for further survival and replication (Dorn et al., 2002, Campoy and Colombo, 2009). Autophagy potentially captures pathogens that have escaped from phagosome into the cytoplasm and thereby deliver it to autophagosomes and then to autolysosomes, where they are destroyed by the lysosomal enzymes (Campoy and Colombo, 2009).

According to some authors, the outcome of autophagy is specific for different types of bacteria and there are different mechanisms of autophagy for destruction of different bacteria (Colombo, 2007, Ogawa et al., 2005), i.e. Mycobacterium and group A Streptococci also induce autophagy where they benefit from the host defence (Songane et al., 2012). Until now most of the studies demonstrated autophagy in the intracellular pathogens (Burdette et al., 2008, Ogawa et al., 2009, Songane et al., 2012) and very little is known about the autophagy induction in extracellular pathogens (Yuan et al., 2012).

The inflammasome is a multi-subunit platform for the activation of caspase-1, resulting in processing of IL-1β and IL-18 from inactive precursors to their active secreted forms (Franchi et al., 2009, Martinon et al., 2009, Yu and Finlay, 2008). The inflammasome also triggers a form of cell death termed pyroptosis, itself also important in host defence (Miao et al., 2011). Although autophagy and inflammasome activation both play significant roles in host defence against microbial infection, they do have some clear opposing effects. Thus, autophagy can promote cell survival

(Baehrecke, 2005) while inflammasome activation will lead to cell death by pyroptosis (Bergsbaken et al., 2009). Additionally, autophagy can act to down-regulate inflammasome activation by the sequestration of defective mitochondria (Saitoh et al., 2008). This results in inhibiting the release of mitochondrial reactive oxygen intermediates and mitochondrial DNA that can activate the NLRP3 inflammasome (Martinon, 2012, Shimada et al., 2012, Nakahira et al., 2011). The effects of inflammasome activation on autophagy are not known.

We hypothesized that inflammasome activation would lead to a reciprocal inhibition of autophagy. To test this hypothesis, we used a model system of infection of macrophages with the Gram-negative pathogen *P. aeruginosa.* This microbe is a common cause of pneumonia in immunocompromised and hospitalized patients, as well as cystic fibrosis (Pier and Ramphal, 2005). It activates the NLRC4 inflammasome through a type III secretion dependent pathway (Miao et al., 2008, Sutterwala et al., 2007, Franchi et al., 2007). We demonstrate here that *P. aeruginosa* activates autophagy in macrophages following infection via the classical autophagy pathway. We show by multiple independent methods that inhibition of inflammasome and caspase-1 activation augments the autophagocytic response.

To know whether autophagy is induced by *P. aeruginosa*, we studied this degradative mechanism in mammalian cells such as mice BMDMs, dendritic cells, RAW264.7 cells, J774A.1 cells, and human cell line THP-1 cells. Our study revealed that autophagy is induced by *P. aeruginosa* in BMDMs through different pathways including Atg8 (LC3), Atg5 and Atg7.

Our observation could provide useful potential information for understanding this important mechanism in innate immune cells during infection with *P. aeruginosa*.

3.2 Results

3.2.1 *Pseudomonas aeruginosa* induces autophagy that is enhanced in the absence of T3SS.

P. aeruginosa PAO1 has been shown to induce autophagy (Yuan et al., 2012). We set out to determine the influence of the T3SS upon this process. We used a strain of *P. aeruginosa*, PA103ΔUΔT that has a functional T3SS but does not translocate any exotoxins, and an isogenic strain, PA103pcrV⁻, that lacks a functional T3SS (Frank et al., 2002, Vallis et al., 1999). Recent studies have demonstrated that inflammasome activation following infection is entirely dependent on a functional T3SS in both PAO1 and PA103ΔUΔT (Arlehamn and Evans, 2011, Sutterwala et al., 2007). We used a number of different methods to quantify and confirm the presence of autophagy. Firstly, we followed the conversion of the protein LC3 to its lipidated form (LC3 II) by Western blot (Fig. 3-1), a modification that is produced following incorporation of LC3 into the autophagocytic vacuole (Mizushima et al., 2010). This clearly demonstrated a marked increase in the absolute amount of LC3 II relative to β-tubulin following infection, to levels in excess of those seen using the positive control of rapamycin, a classic inducer of autophagy. Moreover, the ratio of LC3 II to β-tubulin following infection with *P. aeruginosa* was consistently significantly greater with an otherwise isogenic strain that lacked PcrV, an essential component of the T3SS (Fig. 3-1, a, b and c).

We confirmed these observations using a number of different approaches. The localization of endogenous LC3 to autophagocytic vacuoles was visualized using immunofluorescence. Following infection

with *P. aeruginosa*, we observed a marked increase in the numbers of LC3 containing vacuoles within BMDMs that was consistently significantly higher in the T3SS defective mutant (Fig. 3-2, a and b), and to a level comparable to that seen with rapamycin. Both in these experiments following LC3 by immunofluorescence and in those using Western blotting, we noticed that the apparent expression level of LC3 also increased. We quantified this using RT-PCR and found that *P. aeruginosa* infection increased the expression of *Lc3b* as has been described in the induction of autophagy in other systems, notably in yeast (Stromhaug and Klionsky, 2001). The increase in *Lc3b* expression was higher in the T3SS mutant (Fig. 3-2, c), consistent with the results obtained by Western blotting and immunofluorescence.

Finally, we used a validated flow cytometric method to quantify intracellular LC3 II staining following cell permeabilization (Eng et al., 2010) . This was in agreement with our other results showing that the level of autophagy was increased in the absence of a functional T3SS (Fig. 3-2, d). Examination of infected cells by transmission electron microscopy confirmed the presence of autophagosomes containing cytoplasmic contents (Fig. 3-3) (Fig. 3-4). In these panels, the double membrane structure of the autophagosome is arrowed and surrounds another membrane bound organelle, probably degraded mitochondria as well as other cytoplasmic structures. During the time and dose course experiments we observed that *P. aeruginosa* induced autophagy which could be detected at 1hr with different MOI (5, 25) (Fig. 3-5).

We confirmed that the increase in LC3 II reflected a real increase in flux through the autophagocytic pathway by repeating the experiment in the presence of inhibitors of lysosomal degradation (Fig. 3-6). This increased still further the amounts of LC3 II following infection, showing that the increased levels observed were due to greater flux of LC3 through the autophagocytic pathway and not inhibition of LC3 processing. Our data showed that conversion of LC3-I to LC3-II was increased when cells pre-treated with lysosomes inhibitors such as Pepstatin A, E64d, and Bafilomycin A, which prevent loss of LC3-II during lysosomal degradation and recycling of the lipid conjugation form LC3-II to the cytosolic form LC3-I after fusion between autophagosome with lysosomes. Therefore these inhibitors increase the autophagy markers via blocking autophagy flux (Mizushima and Yoshimori, 2007). Importantly, under the conditions of these experiments, we did not observe a significant increase in cell death, as measured by the release of LDH (Fig. 3-7).
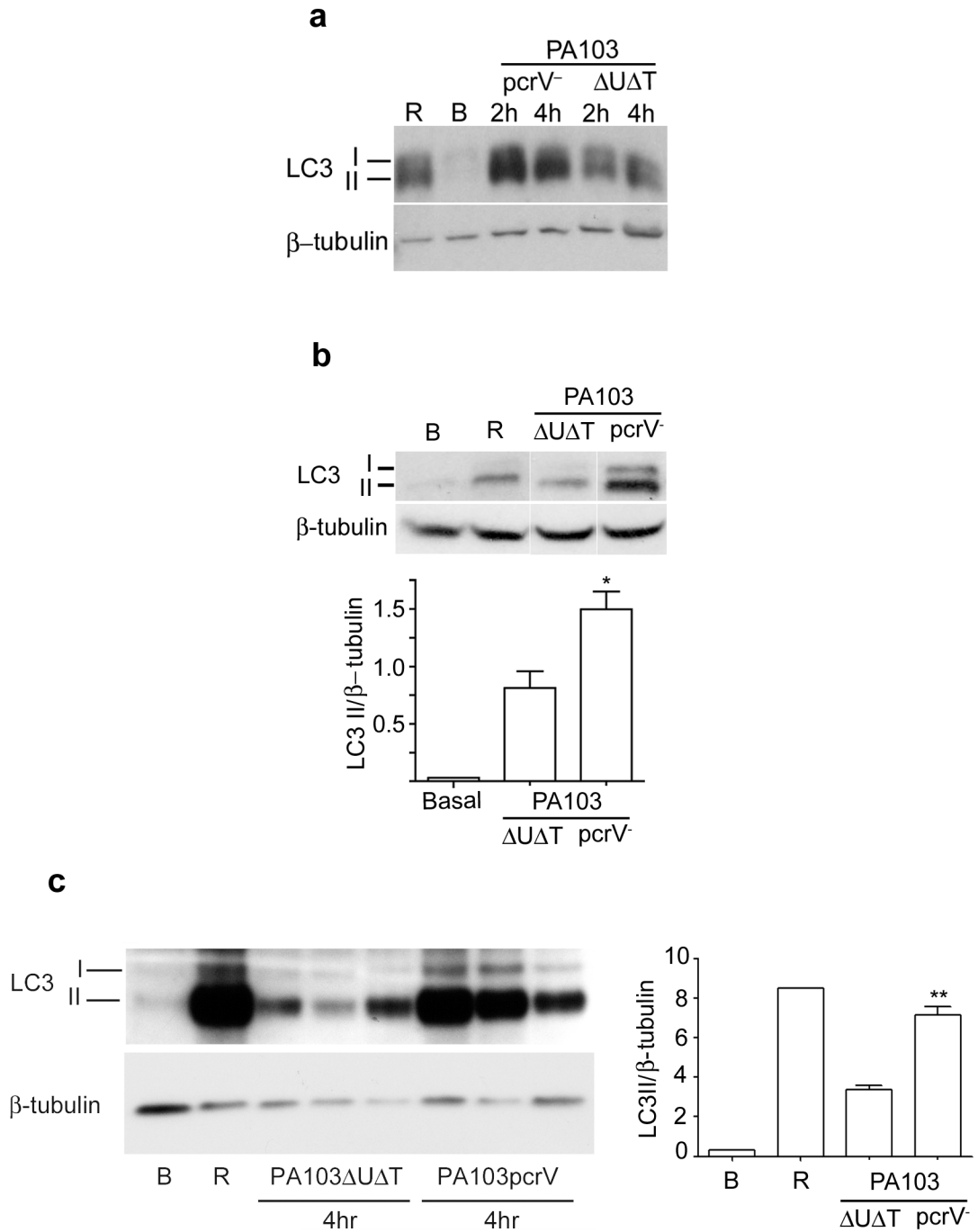
Figure 3.1; Assessment of LC3 I and II levels in BMDMs cells infected with *Pseudomonas aeruginosa.*

a, Western blot analysis of LC3-I and LC3-II protein levels in BMDM left untreated (B), infected with PA103ΔUΔT or PA103pcrV⁻ strains of *P. aeruginosa* for 2,and 4 hrs (MOI 5), or treated with rapamycin (50μg/ml) for 4 h. Blot was stripped and reprobed for β-tubulin. **b,** BMDM left untreated (B), infected with PA103ΔUΔT or PA103pcrV⁻ strains of *P. aeruginosa* for 3 hrs (MOI 10), or treated with rapamycin (50μg/ml) for 4 hrs. Graph shows densitometric measurement of the ratio of LC3-II/ β-tubulin. * Statistically different from PA103ΔUΔT, p< 0.05. **c,** BMDM left untreated (B), infected with PA103ΔUΔT or PA103pcrV⁻ strains of *P. aeruginosa* for 4 h (MOI 25), or treated with rapamycin (50μg/ml) for 4 hrs. Graph shows densitometric measurement of the ratio of LC3-II/ β-tubulin in 3 independent experiments. ** statistically different from PA103ΔUΔT, p < 0.01 (repeated in 3 independent experiments).
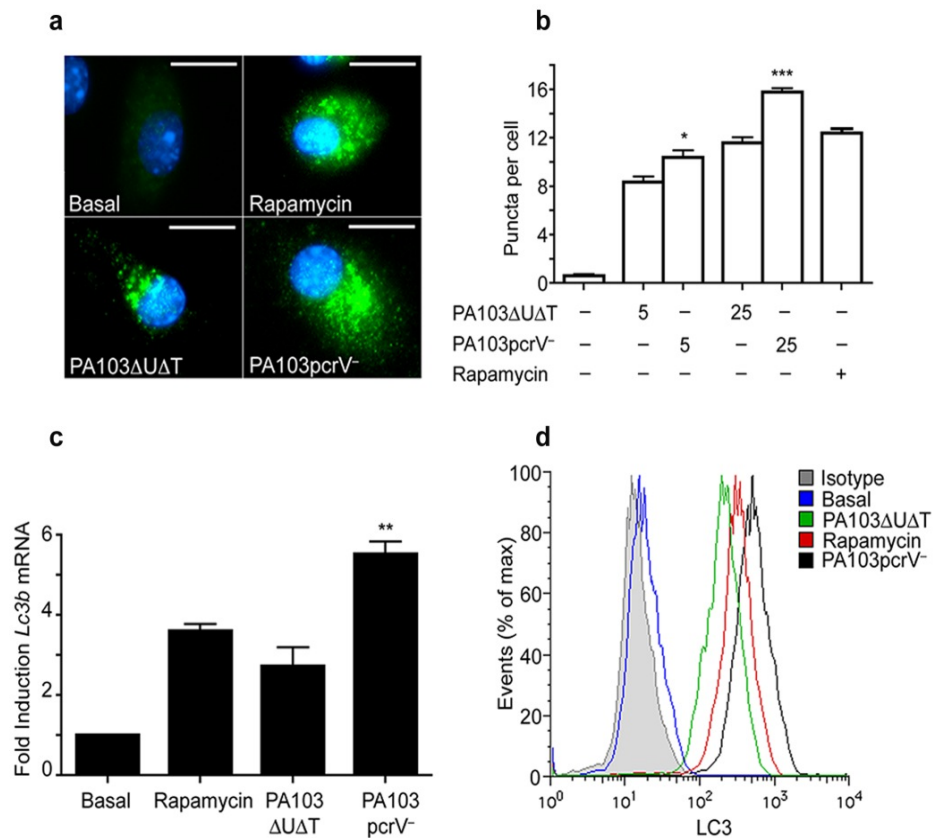
Figure 3.2; *P. aeruginosa* **induces autophagy in BMDMs that is enhanced in the absence of a functional T3SS.**

a , Representative immunofluorescence images of LC3 in BMDM left uninfected (Basal), treated with rapamycin, or infected with PA103ΔUΔT or PA103pcrV⁻ strains for 4hrs at a MOI of 25. Cells were stained with DAPI to visualize nuclei (blue), and LC3 staining is shown as green. Scale bar 10 μm (5 independent experiments). **b**, Number of LC3 puncta in BMDM cells following infection (at specified MOI) or rapamycin treatment as indicated cells were quantified using Image J software . Asterisks indicate statistically different from PA103ΔUΔT at the same MOI, * $p < 0.05$, *** $p < 0.001$. **c**, qRT-PCR of *Lc3b* mRNA following infection as indicated at a MOI of 25 for 4hr (3 independent experiments). ** Statistically different from PA103ΔUΔT, $p < 0.01$. **d**, FACS analysis for LC3 protein following infection with the strains indicated (MOI 25 for 4h) or treatment with rapamycin (3 independent experiments).
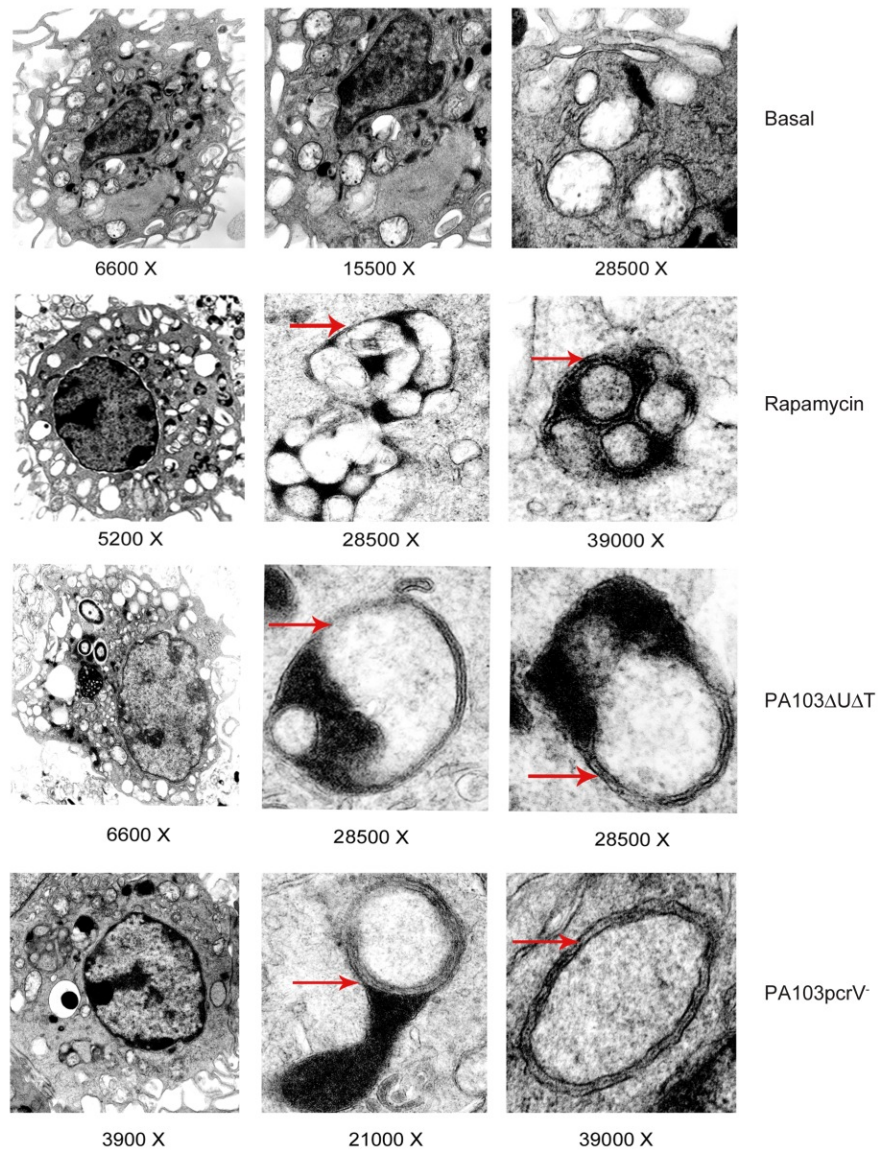
Figure 3.3; TEM observation of autophagosome in BMDMs infected with
P. aeruginosa.

Electron micrographs of autophagosomes in BMDM infected with PA103ΔUΔT
or PA103pcrV⁻ for 4hr, at (MOI 25). BMDM left uninfected (Basal), or treated
with rapamycin 50μg/ml as a positive control. Arrows indicate autophagosomes
in different stages. Scale bar 200 nm.
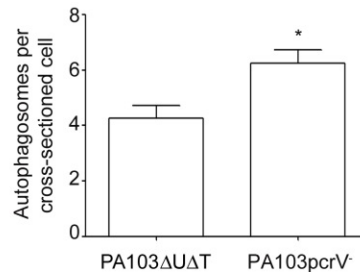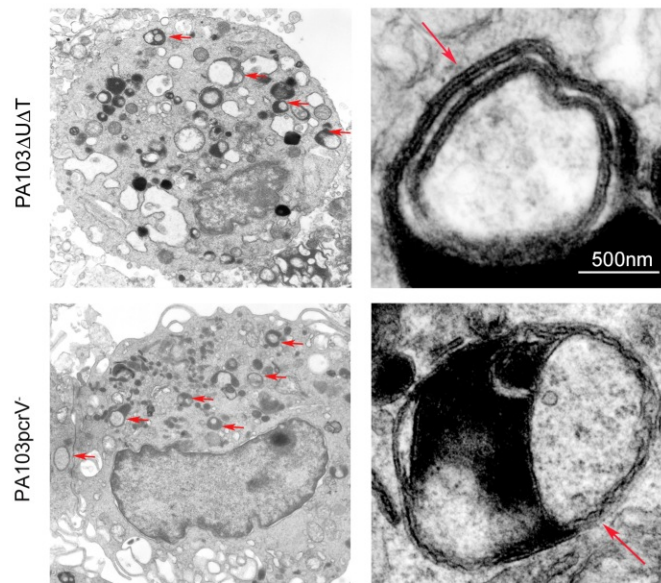
Figure 3.4; Ultrastructural analysis of *Pseudomonas aeruginosa* induced autophagy by TEM.

Electron micrographs of autophagosomes in BMDM infected with PA103ΔUΔT or PA103pcrV⁻ for 4hr, at (MOI 25). Arrows indicate autophagosomes in different stages.Graph represents quantitation of the number of autophagosomes per-cross sectioned cell.* Statistically different from PA103ΔUΔT, $p < 0.05$.
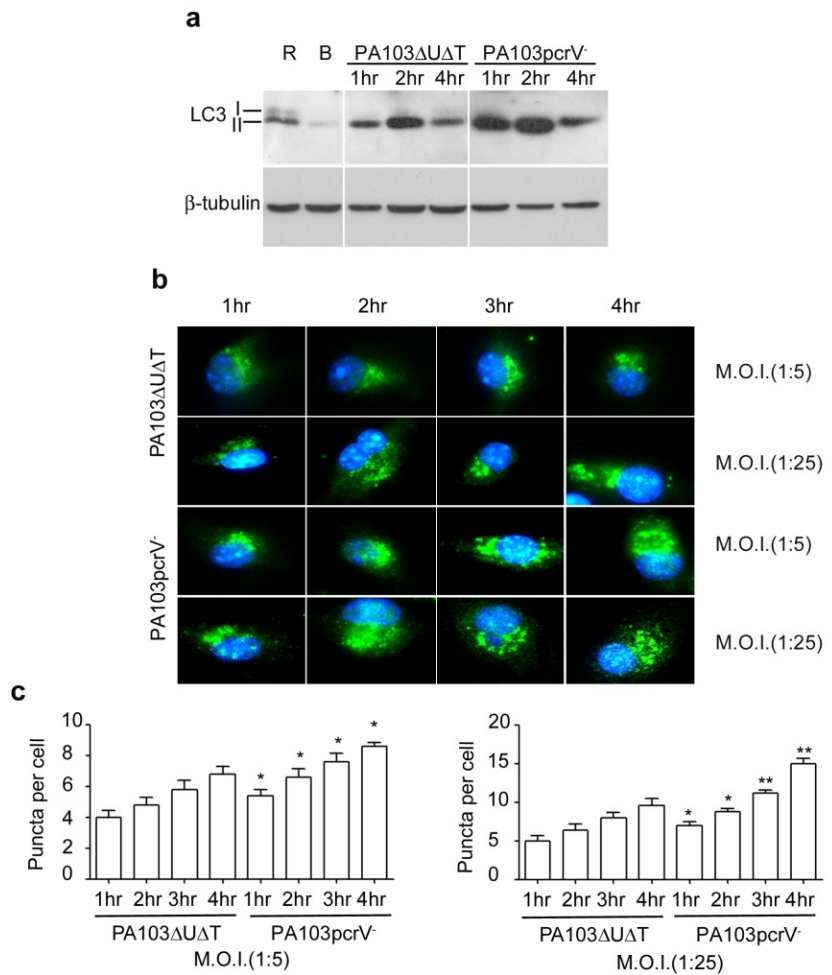
Figure 3.5; *P. aeruginosa* **induced autophagy in a dose and time dependent manner.**

a ,Western blot analysis of LC3-I and LC3-II protein levels in BMDMs infected with PA103ΔUΔT or PA103pcrV⁻ for 1, 2, and 4hr,at (MOI 25). BMDM left uninfected (Basal), treated with rapamycin 50μg/ml for 4hrs as a positive control. **b**, Representative immunofluorescence images of LC3 in BMDMs were infected with PA103ΔUΔT or PA103pcrV⁻ strains for indicated time at (MOI 5, 25). Cells were stained with DAPI to visualize nuclei (blue), and LC3 staining is shown as green. Scale bar 10 μm (5 independent experiments). **c**, Number of LC3 puncta in BMDM cells following infection (at specified MOI) . Asterisks indicate statistically different from PA103ΔUΔT at the same MOI. Columns are mean of five independent determinations; error bars are SEM. * $p < 0.05$, ** $p < 0.01$. (5 independent experiments).
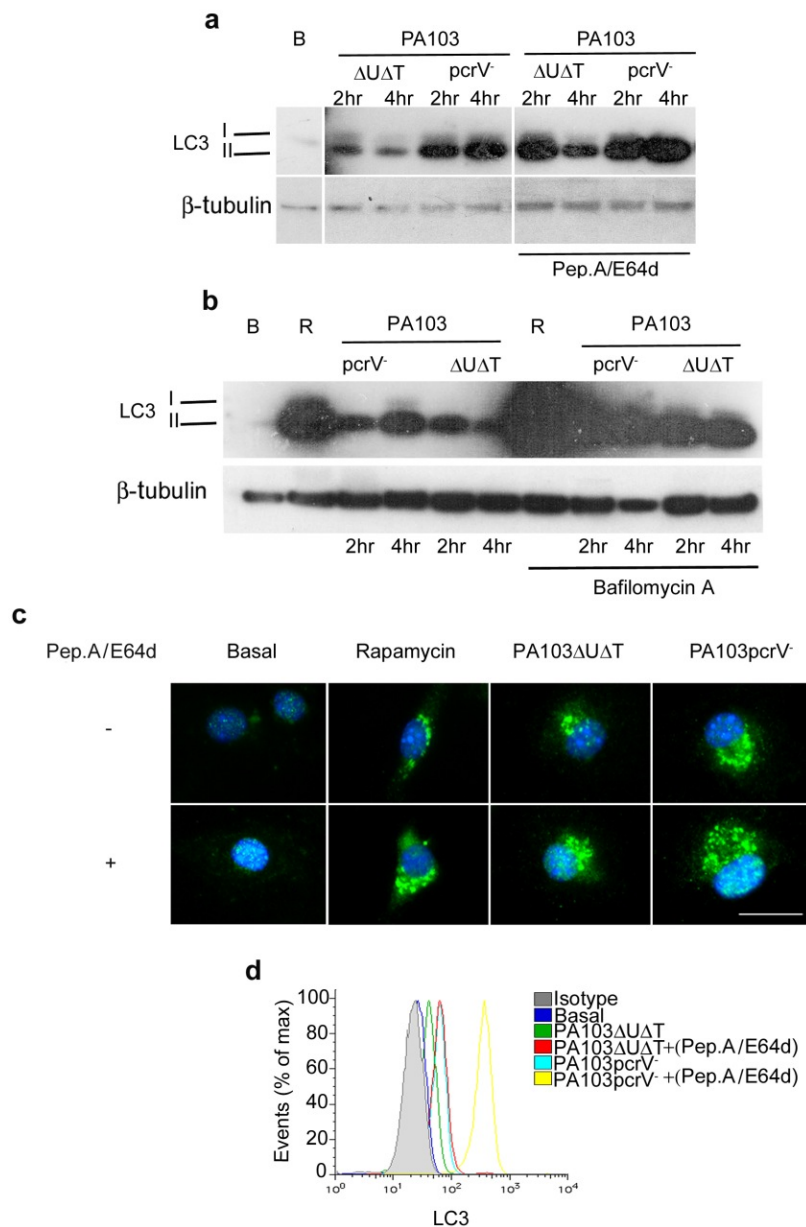
Figure 3.6; Lysosomes inhibitors increase autophagy flux .

a ,**b**, Western blot analysis of LC3-I and LC3-II protein levels in BMDMs were infected with PA103ΔUΔT or PA103pcrV¯ for and 4hr in the presence (+) or absence(-) of 10μg/ml Pepstatin A , E64d (a) and 50nM/ml Bafilomycin A (b) ,at (MOI 25). BMDM left uninfected (Basal), treated with rapamycin 50μg/ml for 4hrs as a positive control. **c**, Representative immunofluorescence images of LC3 in BMDMs were infected with PA103ΔUΔT or PA103pcrV¯ strains for 4hrs at (MOI 25). Cells were stained with DAPI to visualize nuclei (blue), and LC3 staining is shown as green. Scale bar 10 μm .**d**, FACS analysis for LC3-II protein following infection with the strains indicated (MOI 25 for 4h) (3 independent experiments).
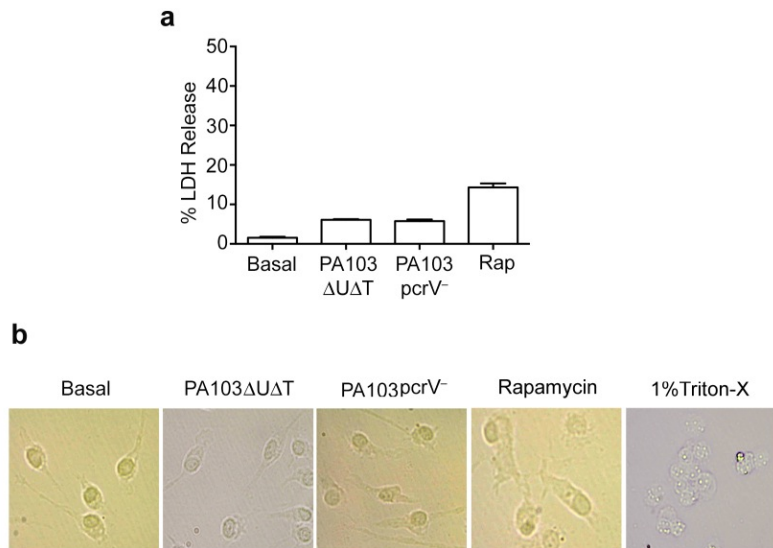
Figure 3.7; LDH release caused by _P. aeruginosa_ in BMDMs.

a, BMDMs were infected with PA103ΔUΔT or PA103pcrV⁻ for 2hrs (MOI 5) . Supernatants were analysed for cytotoxicity caused by measurement of LDH release. **b**, Light microscope observation of BMDMs infected as indicated, or treated with 1% Triton-x as a positive control, or left without treatment (basal). Scale bar 10µm. (3 independent experiments).

3.2.2 Autophagy is induced by *P. aeruginosa* in several mammalian cells.

In order to investigate whether *P. aeruginosa* is able to induce autophagy in other mammalian cells, dendritic cells, J774A.1, RAW264.7 cells, and THP-1 cells were infected with PA103ΔUΔT and PA103pcrV⁻ as indicated. We used a number of different methods to quantify and confirm the presence of autophagy. Firstly, we followed the conversion of the protein LC3 to its lipidated form (LC3 II) by Western blot analysis and the localization of endogenous LC3 to autophagocytic vacuoles was visualized using immunofluorescence. Following infection with *P. aeruginosa*, we observed a marked increase in the number of LC3 containing vacuoles within cells that was consistently significantly higher in the T3SS defective mutant, to a level comparable to that seen with rapamycin. Both in these experiments following LC3 by immunofluorescence and in those using Western blotting, we noticed that the apparent expression level of LC3 also increased. We quantified this using RT-PCR and found that *P. aeruginosa* infection increased the expression of *Lc3b* as has been described in the induction of autophagy in other systems, notably in yeast following incorporation of LC3 into the autophagocytic, Finally, we used a validated flow cytometric method to quantify intracellular LC3 II staining following cell permeabilization. Our results showed PA induces autophagy. Since both strains induce autophagy, a functional T3SS does not seem to be required for this process (Figures (3-8), (3-9), (3-10), and (3-11) respectively).
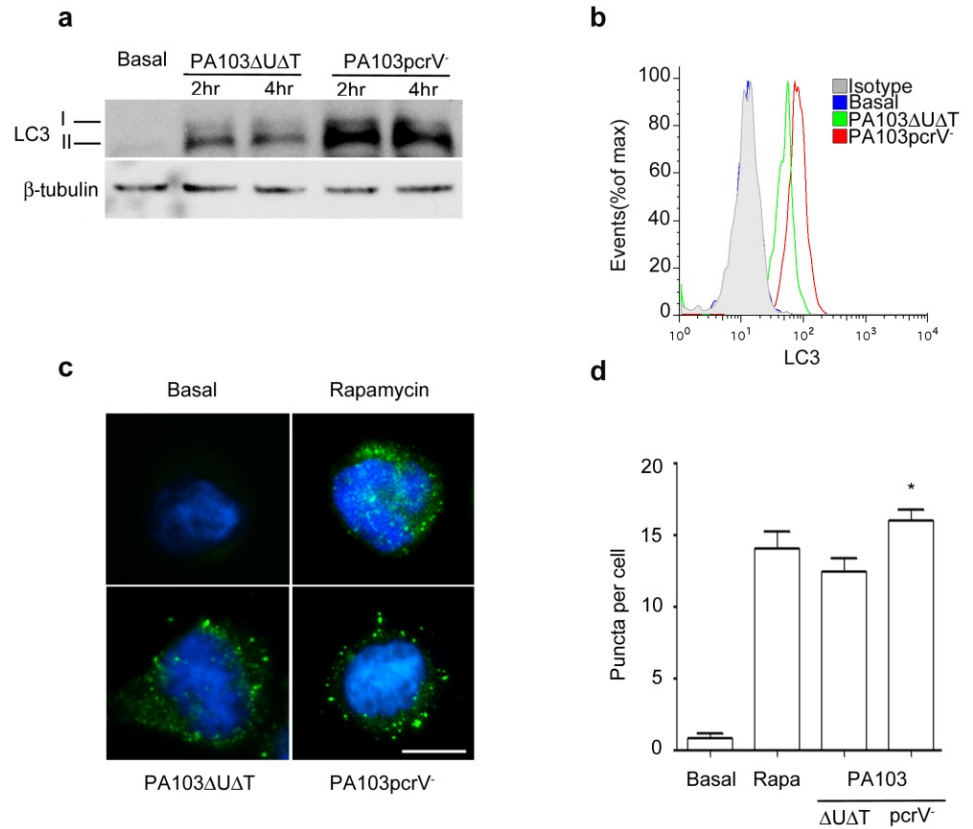
Figure 3.8; Induction of autophagy in THP-1 cells by *P. aeruginosa*.

a ,Western blot analysis of LC3-I and LC3-II protein levels in THP-1 cells infected with PA103ΔUΔT or PA103pcrV⁻ for 2, and 4hr,at (MOI 25) or left uninfected (Basal). **b**, FACS analysis for LC3-II protein following infection with the strains indicated (MOI 25 for 4h) . **c**, Representative immunofluorescence images of LC3 in THP-1 left uninfected (Basal), treated with rapamycin as a positive control, or infected with PA103ΔUΔT or PA103pcrV⁻ strains for 4hrs at a MOI of 25. Cells were stained with DAPI to visualize nuclei (blue), and LC3 staining is shown as green. Scale bar 10 μm. **d**, Number of LC3 puncta in THP-1 cells following infection (at 25 MOI) or rapamycin treatment as indicated. Staining was quantified using Image J software. Asterisks indicate statistically different from PA103ΔUΔT at the same MOI. error bars are SEM. * $p < 0.05$. (3 independent experiments).
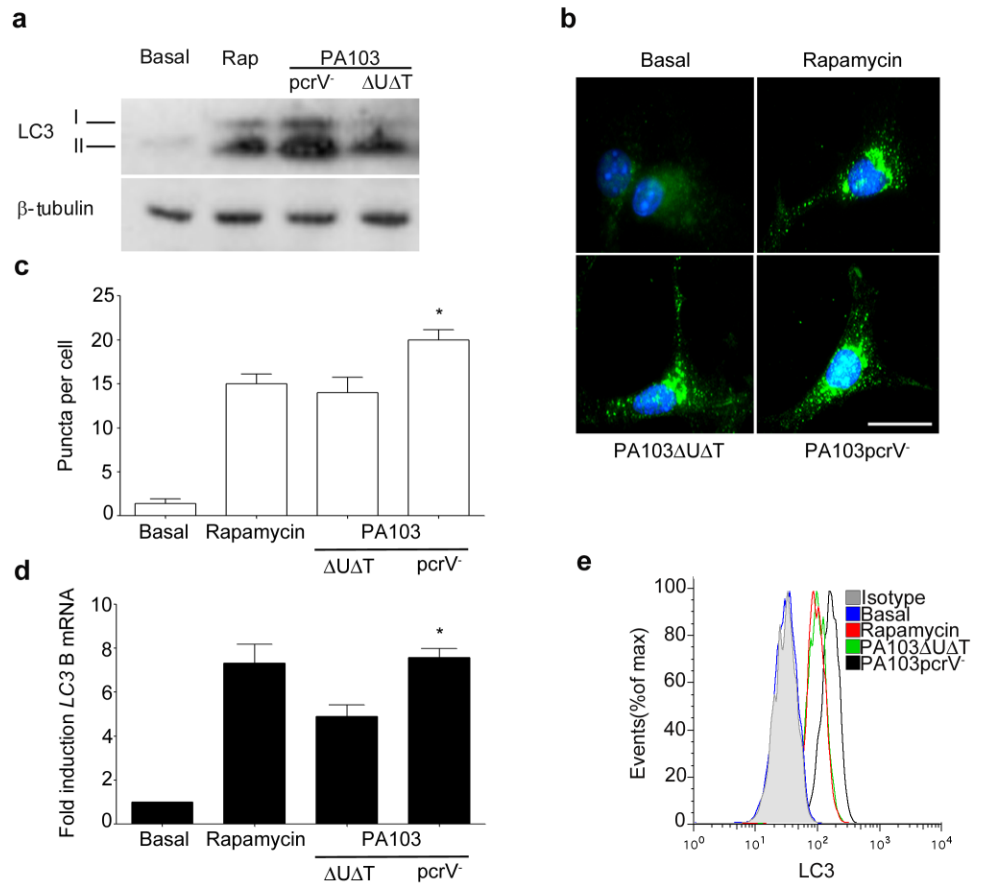
Figure 3.9; Induction of autophagy in D.cells by *P. aeruginosa*.

a ,Western blot analysis of LC3-I and LC3-II protein levels in D.Cs infected with PA103ΔUΔT or PA103pcrV⁻ for 4hrs,at (MOI 25). D.Cs left uninfected (Basal) or treated with rapamycin as a positive control. **b**, Representative immunofluorescence images of LC3 in D.Cs left uninfected (Basal), treated with rapamycin as a positive control, or infected with PA103ΔUΔT or PA103pcrV⁻ strains for 4hrs at a (MOI of 25). Cells were stained with DAPI to visualize nuclei (blue), and LC3 staining is shown as green. Scale bar 10 μm. **c**, Number of LC3 puncta in D.Cs cells following infection (at 25 MOI) or rapamycin treatment as indicated. Staining was quantified using Image J software. Asterisks indicate statistically different from PA103ΔUΔT at the same MOI, * $p < 0.05$. **d**, qRT-PCR of *Lc3b* mRNA following infection as indicated at a MOI of 25 for 4hr (3 independent experiments). * Statistically different from PA103ΔUΔT, $p < 0.05$. **e**, FACS analysis for LC3-II protein following infection with the strains indicated (MOI 25 for 4h) or treatment with rapamycin (3 independent experiments).
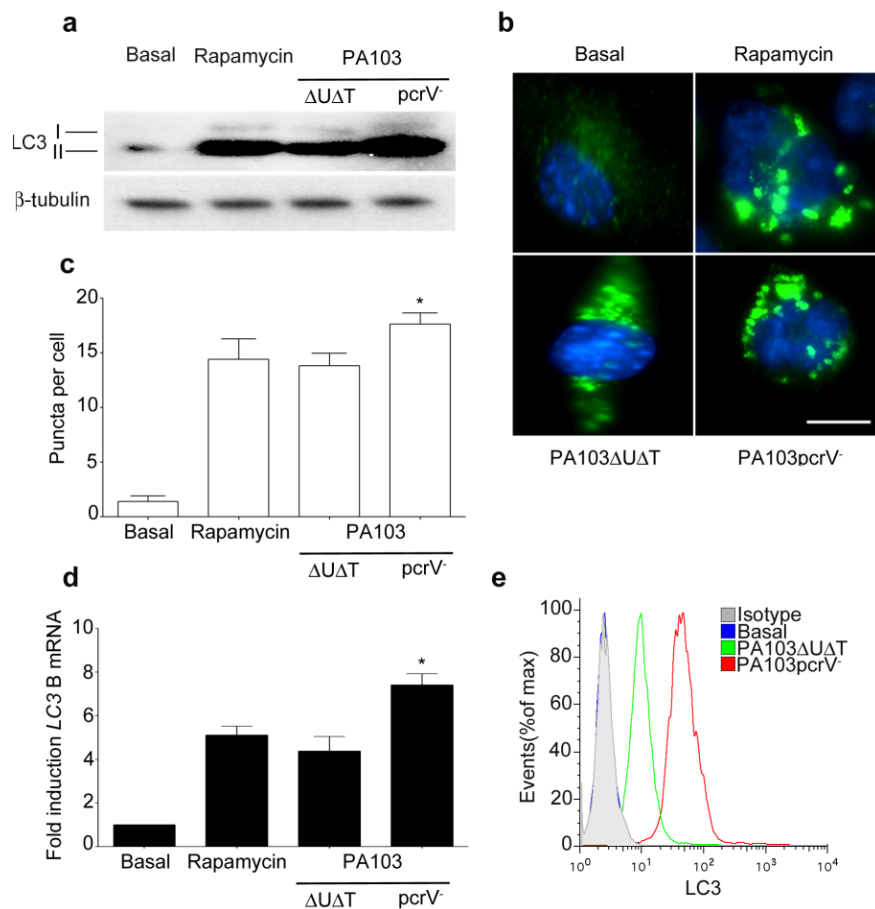
Figure 3.10; Induction of autophagy in J774A.1 cells by *P. aeruginosa*.

a, Western blot analysis of LC3-I and LC3-II protein levels in J774A.1 cells infected with PA103ΔUΔT or PA103pcrV⁻ for 4hrs,at (MOI 25) or left uninfected (Basal) or treated with rapamycin as a positive control. **b**, Representative immunofluorescence images of LC3 in J774A.1 left uninfected (Basal), treated with rapamycin as a positive control, or infected with PA103ΔUΔT or PA103pcrV⁻ strains for 4hrs at a MOI of 25. Cells were stained with DAPI to visualize nuclei (blue), and LC3 staining is shown as green. Scale bar 10 μm. **c**, Number of LC3 puncta in J774A.1 cells following infection (at 25 MOI) or rapamycin treatment as indicated. Staining was quantified using Image J software. Asterisks indicate statistically different from PA103ΔUΔT at the same MOI, * $p < 0.05$.**d**, qRT-PCR of *Lc3b* mRNA following infection as indicated at a MOI of 25 for 4hr.* Statistically different from PA103ΔUΔT, $p < 0.05$. **e**, FACS analysis for LC3-II protein following infection with the strains indicated (MOI 25 for 4h) or cells left untreated(Basal) (3 independent experiments).

90
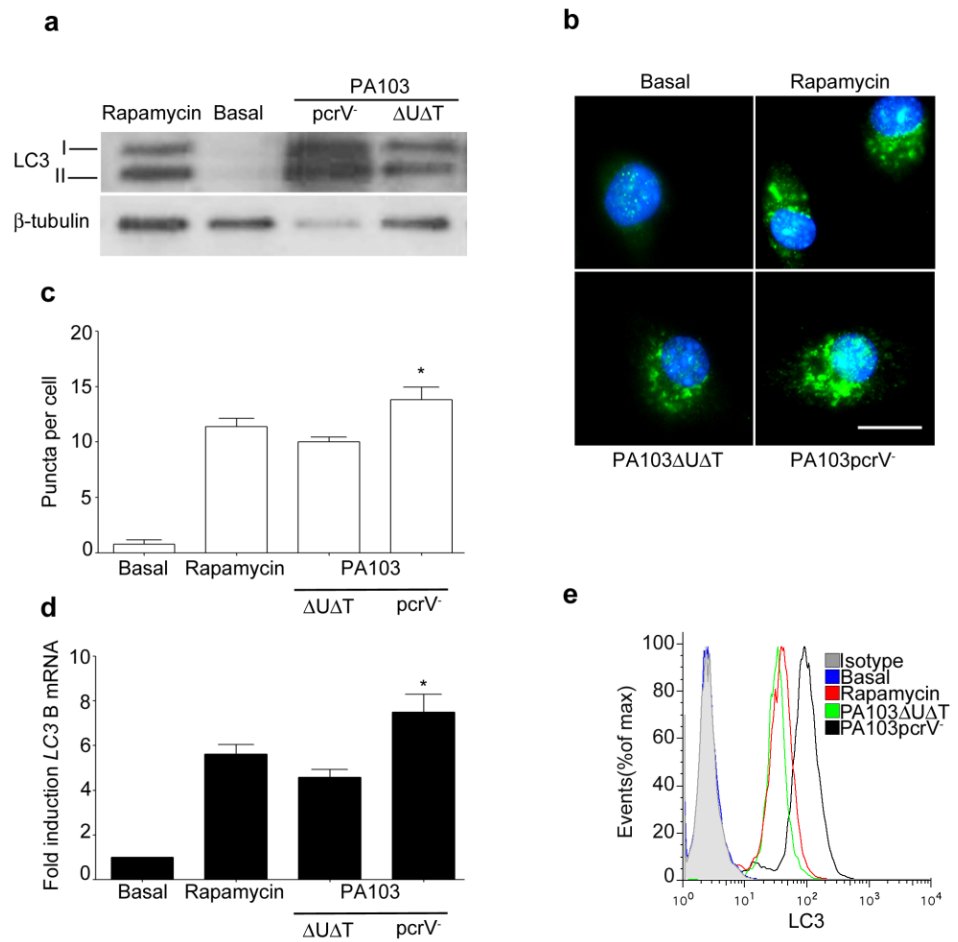
Figure 3.11; Induction of autophagy in RAW264.7 cells by *P. aeruginosa*.

a, Western blot analysis of LC3-I and LC3-II protein levels in RAW264.7 cells infected with PA103ΔUΔT or PA103pcrV⁻ for 4hrs,at (MOI 25) or left uninfected (Basal) or treated with rapamycin as a positive control. **b**, Representative immunofluorescence images of LC3 in RAW264.7 left uninfected (Basal), treated with rapamycin as a positive control, or infected with PA103ΔUΔT or PA103pcrV⁻ strains for 4hrs at a MOI of 25. Cells were stained with DAPI to visualize nuclei (blue), and LC3 staining is shown as green. Scale bar 10 μm. **c**, Number of LC3 puncta in RAW264.7 cells following infection (at 25 MOI) or rapamycin treatment as indicated. Staining was quantified using Image J software. Asterisks indicate statistically different from PA103ΔUΔT at the same MOI, * $p < 0.05$.**d**, qRT-PCR of *Lc3b* mRNA following infection as indicated at a MOI of 25 for 4hr (3 independent experiments). * Statistically different from PA103ΔUΔT, $p < 0.05$. **e**, FACS analysis for LC3-II protein following infection with the strains indicated (MOI 25 for 4h) or treatment with rapamycin (3 independent experiments).

3.2.3 *Pseudomonas aeruginosa* induced autophagy in BMDMs cells via classical autophagy pathway

We tested the role of the genes involved in the classical autophagocytic pathway. Knockdown of *Lc3b* confirmed that the signals used to quantify autophagy by analysis of LC3 by Western blot, enumeration of puncta, RT-PCR and flow cytometry were indeed specific for this gene and protein (Fig. 3-12). In a similar fashion, we tested the dependence of autophagy following *P. aeruginosa* infection on the genes *Atg7* and *Atg5*. Infection of BMDMs from mice with a conditional KO of *Atg7* in bone marrow precursors (Mortensen et al., 2010) compared to control BMDMs showed a large significant reduction in the processing of LC3 to its lipidated form as well as the accumulation of LC3 in autophagocytic vacuoles,and RT-PCR (Fig. 3-13). Finally, using siRNA to knockdown *Atg5*, we showed that, as with *Atg7*, this resulted in a reduction in LC3 lipidation, accumulation of autophagocytic puncta and increased detection of intracellular LC3 as assayed by flow cytometry (Fig. 3-14). Using the same assays, we also showed the autophagy following infection was inhibited by 3-methyladenine (Fig. 3-15), and (Fig. 3-16) respectively.
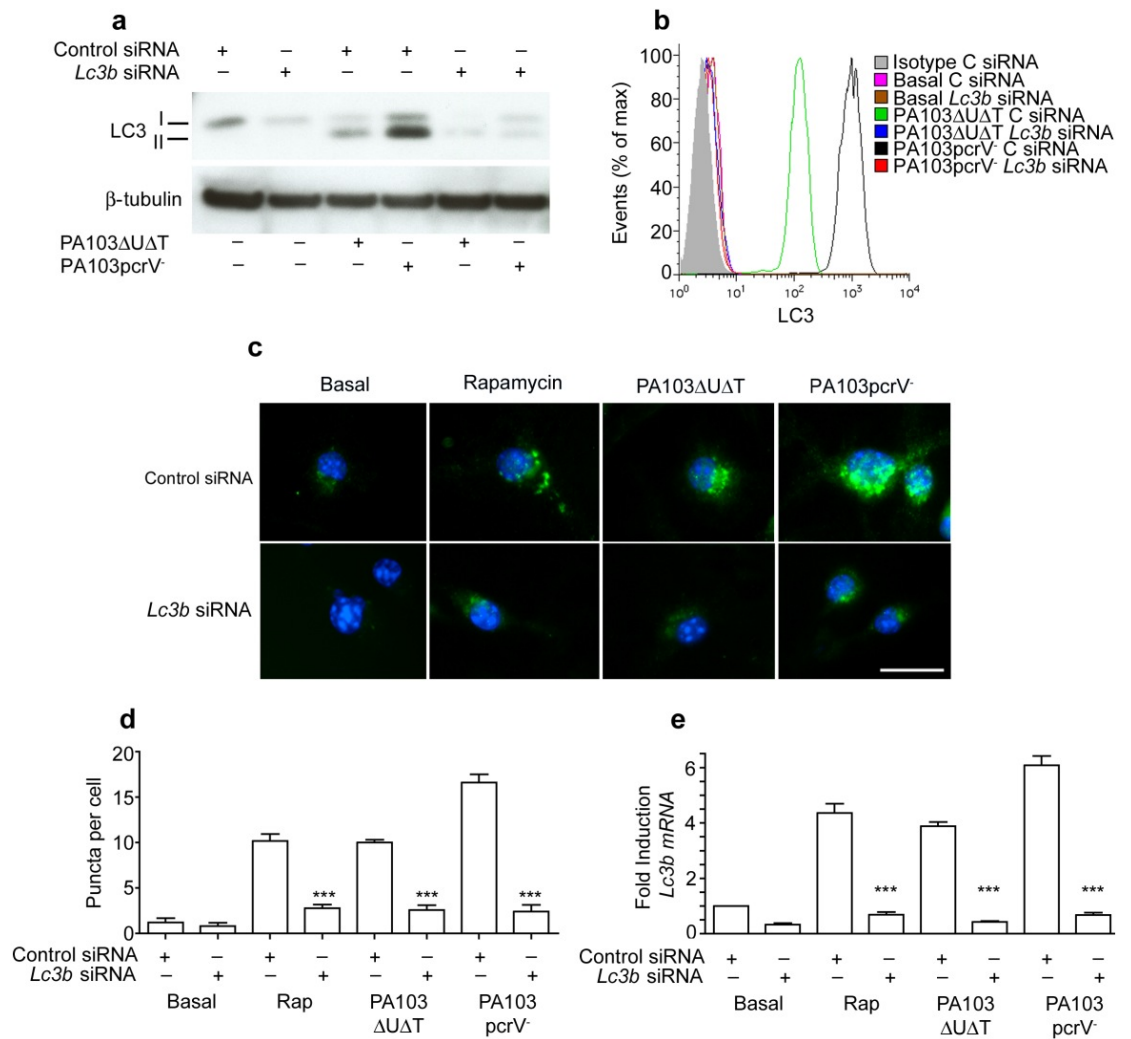
Figure 3.12; *P. aeruginosa* induced autophagy is dependent on *Lc3b*.

a, Western blot analysis of LC3-I and LC3-II protein levels in BMDMs. Cells transfected with siRNA against *Lc3b* then infected with PA103ΔUΔT or PA103pcrV⁻ for 4hrs,at (MOI 25) or left uninfected (Basal). **b**, Levels of intracellular LC3-II assayed by flow cytometry following treatments as indicated. **c**, Representative immunofluorescence images of LC3 in BMDMs left uninfected (Basal), treated with rapamycin as a positive control, or infected with PA103ΔUΔT or PA103pcrV⁻ strains for 4hrs at a MOI of 25. Cells were stained with DAPI to visualize nuclei (blue), and LC3 staining is shown as green. Scale bar 10 μm. **d**, Quantification of LC3 puncta present per cell following treatments and infections as indicated. *** denotes significant difference between control and *Lc3b* siRNA, p < 0.001. **e**, qRT-PCR of *Lc3b* mRNA levels following treatments as shown; *** significant difference between control and *Lc3b*, p < 0.001 . (3 independent experiments).
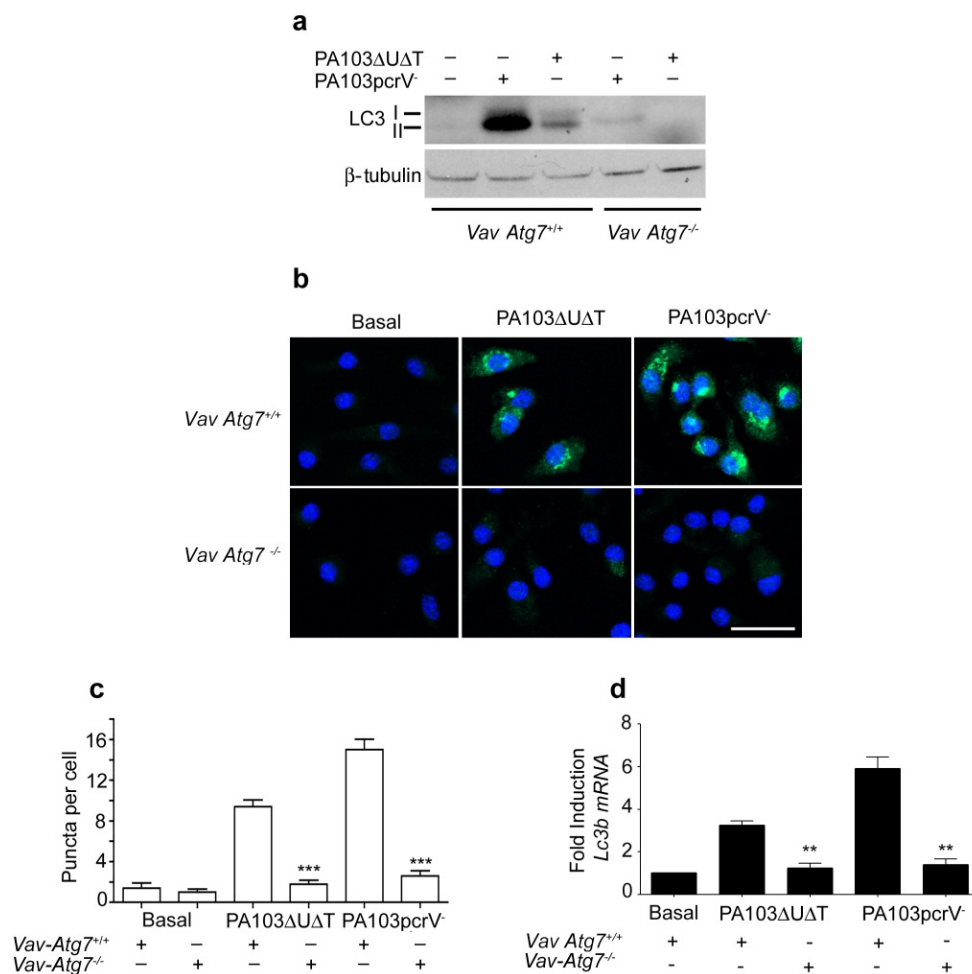
Figure 3.13; *P. aeruginosa* induced autophagy is dependent on *Atg7*.

a, Western blot analysis of LC3-I and LC3-II protein levels in BMDMs lacking *Atg7* (*Vav-Atg$^{-/-}$*) vs WT BMDMs *Vav-Atg7$^{+/+}$* . Cells were infected with PA103ΔUΔT or PA103pcrV$^-$ for 4hrs,at (MOI 25) or left uninfected (Basal). **b**, Representative immunofluorescence images of BMDMs lacking *Atg7* (*Vav-Atg$^{-/-}$*) vs WT. Cells left uninfected (Basal), or infected with PA103ΔUΔT or PA103pcrV$^-$ strains for 4hrs at a MOI of 25. Cells were stained with DAPI to visualize nuclei (blue), and LC3 staining is shown as green. Scale bar 10 µm. **c**, Quantification of LC3 puncta present per cell following treatments and infections as indicated. *** denotes significant difference between BMDMs WT and *Vav-Atg7$^{-/-}$*, p < 0.001. **d**, qRT-PCR of *Lc3b* mRNA levels following treatments as shown; ** significant difference between BMDMs WT and *Vav-Atg7$^{-/-}$*, p < 0. 01. (3 independent experiments).
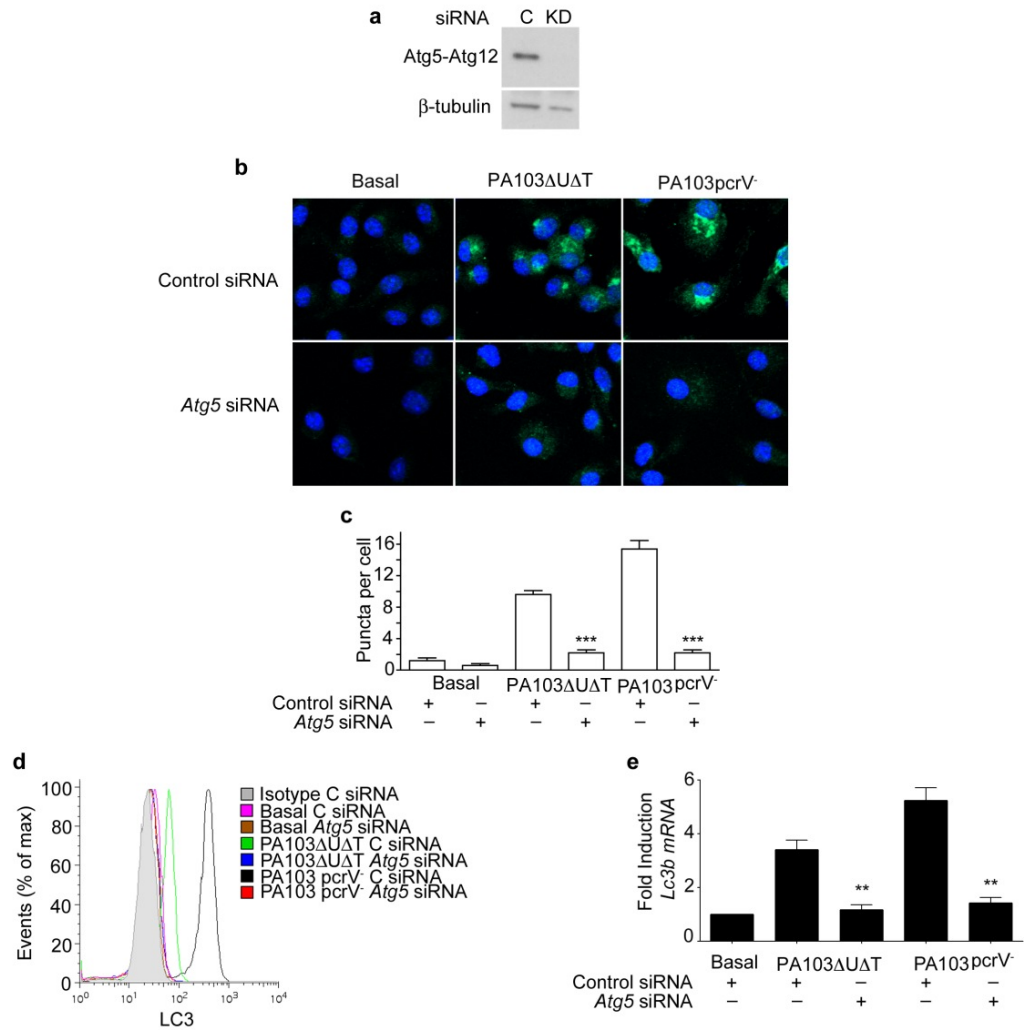
Figure 3.14; *P. aeruginosa* **induced autophagy is dependent on** *Atg5*.

a, Western blot of *Atg5* was performed to show the successful reduction in *Atg5*. β-tubulin was probed as a loading control. **b**, Representative immunofluorescence images of LC3 in BMDMs left uninfected (Basal) or infected with PA103ΔUΔT or PA103pcrV⁻ strains for 4hrs at a MOI of 25. Cells were stained with DAPI to visualize nuclei (blue), and LC3 staining is shown as green. Scale bar 10 µm. **c**, Quantification of LC3 puncta present per cell following treatments and infections as indicated. *** denotes significant difference between control and *Atg5* siRNA, p < 0.001. **d**, Levels of intracellular LC3-II assayed by flow cytometry following treatments as indicated. **e**, qRT-PCR of *Lc3b* mRNA levels following treatments as shown; ** significant difference between control and *Atg5*, p < 0.01 . (3 independent experiments).
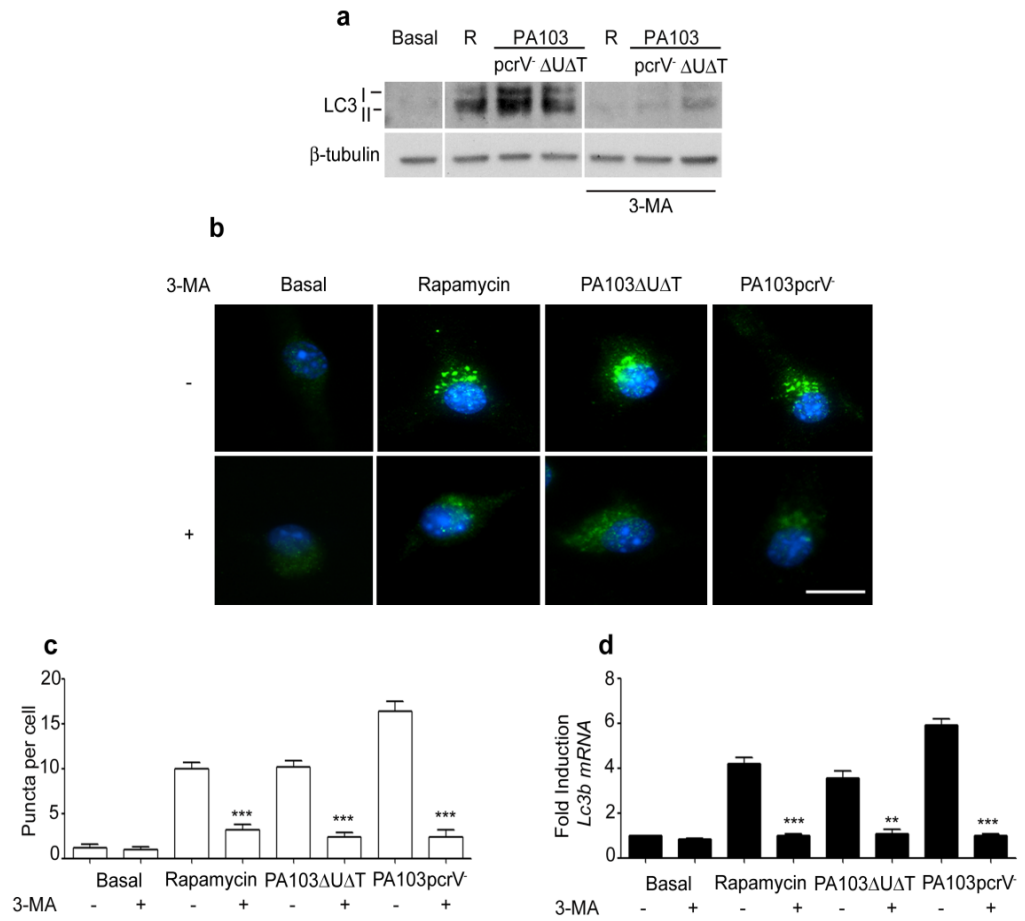
Figure 3.15; 3-MA inhibits autophagy following *P.aeruginosa* infection in BMDMs.

BMDMs were infected with *P.aeruginosa* at (MOI 25) for the indicated time in hours in the presence (+) or absence (–) of 3-MA (10 mM). **a**, Western blot analysis of LC3-I and LC3-II protein levels in BMDMs cells infected with PA103ΔUΔT or PA103pcrV⁻ for 4hrs,at (MOI 25) or left uninfected (Basal) or treated with rapamycin as a positive control. **b**, Representative immunofluorescence images of LC3 in BMDMs left uninfected (Basal) or infected with PA103ΔUΔT or PA103pcrV⁻ strains for 4hrs at a MOI of 25. Cells were stained with DAPI to visualize nuclei (blue), and LC3 staining is shown as green. Scale bar 10 μm. **c**, Quantification of LC3 puncta present per cell following treatments and infections as indicated. *** significant difference between infected BMDMs±3-MA, p < 0.001.**d**, qRT-PCR of *Lc3b* mRNA levels following treatments as shown; *** significant difference between infected BMDMs ±3-MA, p < 0.001 . (3 independent experiments).

.
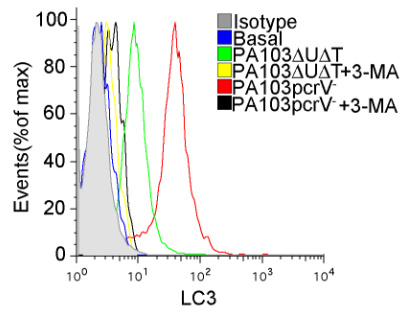
Figure 3.16; 3-MA inhibits autophagy following *P.aeruginosa* infection in THP-1 cells.

THP-1 were infected with PA103ΔUΔT (MOI 25) for the indicated time in hours in the presence (+) or absence (–) of 3-MA (10 mM). Levels of intracellular LC3-II assayed by flow cytometry following treatments as indicated. Cells left uninfected (Basal), or infected with PA103ΔUΔT, and PA103pcrV⁻ strain for 4hrs at a MOI of 25.

3.2.4 Caspase-1 activation by the inflammasome down regulates autophagy.

The reduction in autophagy following infection with *P. aeruginosa* in a strain with a functional as compared to a non-functional T3SS suggested that this might be due to the effects of caspase-1 activation by the inflammasome that is induced by the T3SS. We thus tested the effect of Z-YVAD-FMK, a selective caspase-1 inhibitor, on autophagy following PA103ΔUΔT infection. This drug produced the expected reduction in caspase-1 processing and secretion of IL-1β as shown in (Fig. 3-17). Inhibition of caspase-1 with this drug increased autophagy following infection as evidenced by enhanced levels of LC3- II as detected by Western blotting and a marked increase in the number of LC3 containing vacuoles. Additionally, level of *lc3b* mRNA increased as shown by RT-PCR, and increased intracellular staining of LC3-II as assayed by flow cytometry (Fig. 3-18). We repeated this experiment using different mammalian cells. Again, in the presence of caspase-1 inhibitor, we observed a marked increase in the level of LC3II as detected by western blotting, and increased intracellular staining of LC3-II assayed by flow cytometry (Fig. 3-19).

To confirm the role of caspase-1 in inhibiting autophagy, we measured levels of LC3 II following infection of BMDMs derived from mice lacking *capase-1*. This showed an increase in the conversion of LC3 I to LC3 II following infection in the absence of caspase-1 (Fig. 3-20). However, *caspase*-1 knockout animals also lack a functional caspase-11, which has been shown to be important in inflammasome activation with various bacteria, but not *P. aeruginosa* possessing a functional T3SS that we are using in our experiments (Rathinam et al., 2012, Kayagaki et al., 2011). We

tested specifically for a role of caspase-1 by knocking down the gene using siRNA (Fig. 3-21a). Knockdown of *caspase-1* increased LC3 lipidation and formation of autophagocytic puncta, increased expression of *lc3b* mRNA, and increased intracellular staining of LC3-II as assayed by flow cytometry (Fig. 3-21c, d, e, and f) respectively. We tested for involvement of caspase-11 by knocking down the protein using siRNA (Fig. 3-22a). This had no effect on induction of autophagy or production of IL-1β following infection (Fig. 3-22b-e).Taken together, these results demonstrate that activated casapse-1 inhibits the process of autophagy following infection with *P. aeruginosa* and that caspase-11 is not involved.
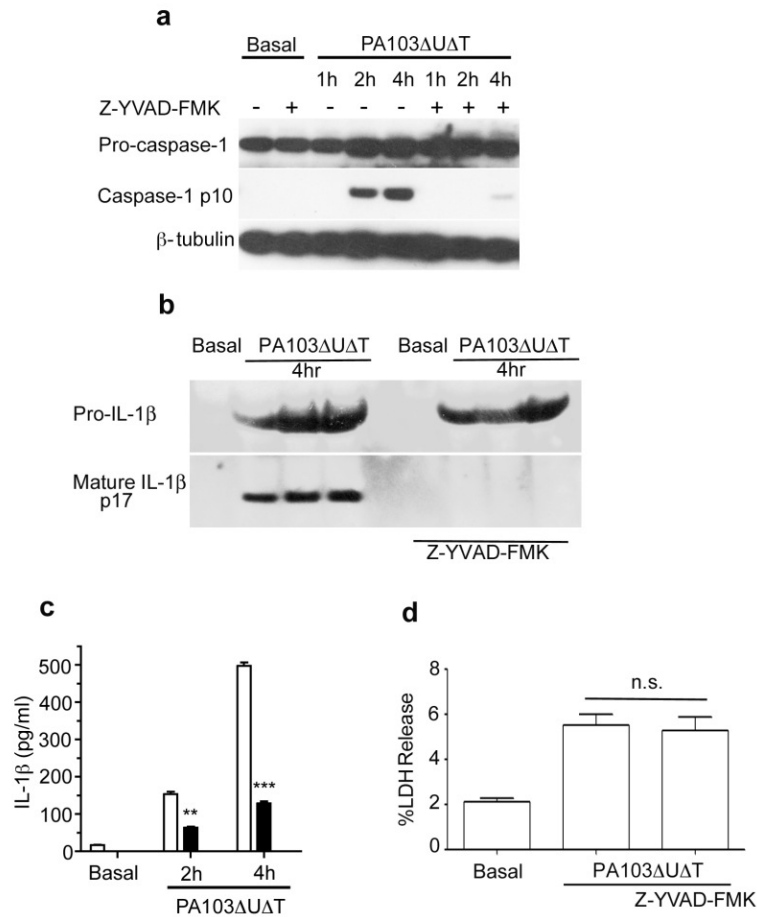
Figure 3.17; Inflammasome activation by *P.aeruginosa* is inhibited by caspase-1 inhibitor Z-YVAD-FMK.

a, BMDMs were infected with PA103ΔUΔT (MOI 25) for the indicated time in hours in the presence (+) or absence (–) of the capsase-1 inhibitor Z-YVAD-FMK (10µM/ml). The panels show Western blot of pro-caspase-1, the caspase-1 p10 subunit, and β-tubulin as a loading control. **b**, Western blot analysis of Pro-IL-1β and mature IL-1β in cell supernatants form BMDMs infected as indicated in the presence(+) or absence(-) of the caspase-1 inhibitor Z-YVAD-FMK(10µM/ml). **c,** IL-1β levels following infection as indicated in the absence (open bars) or presence (filled bars) of Z-YVAD-FMK. Column shows the mean; error bars are SEM. ** and *** indicate significant differences between the levels in the presence and absence of the inhibitor, $p < 0.01$ and < 0.001 respectively. **d**, percent cytotoxicity in supernatant were measured using LDH release. (3 independent experiments).
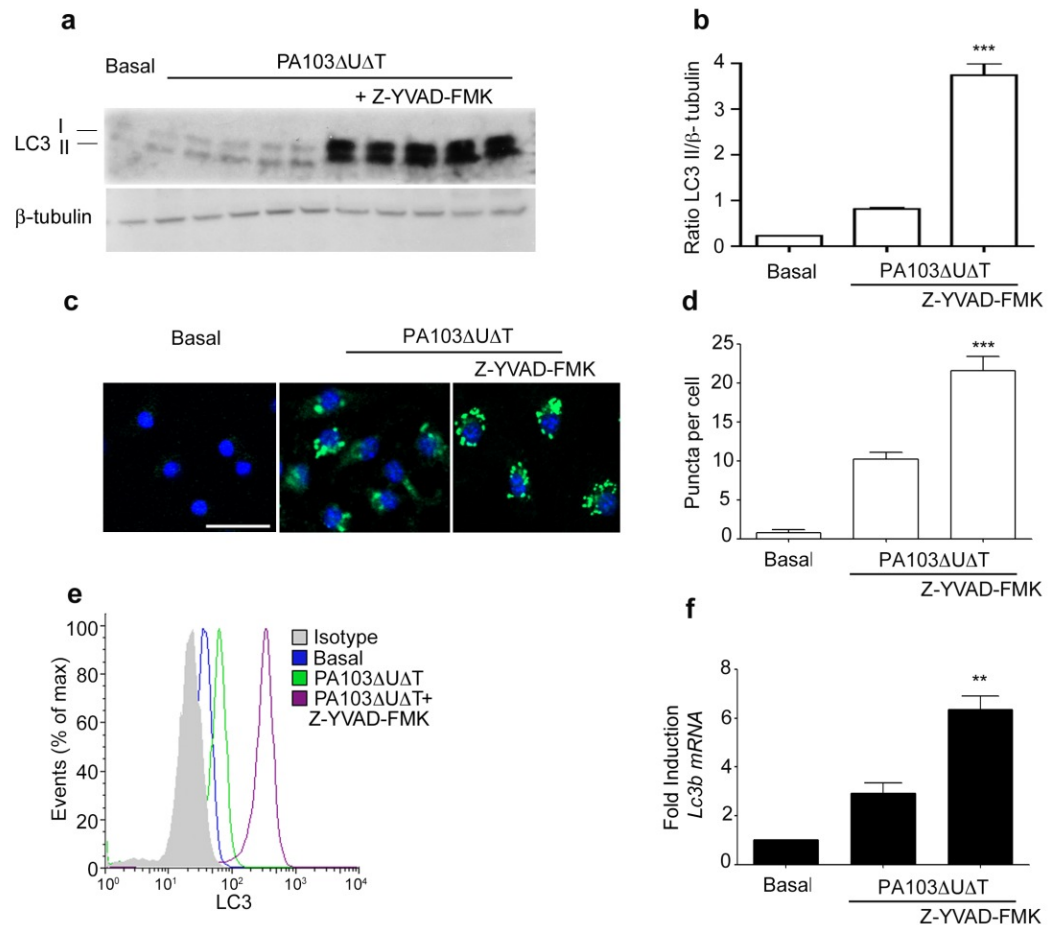
**Figure 3.18; Caspase-1 inhibitor Z-YVAD-FMK Up-regulates autophagy following
P.aeruginosa infection.**

a, BMDMs were infected with PA103ΔUΔT (MOI 25) for the indicated time in hours in the presence (+) or absence (−) of the capsase-1 inhibitor Z-YVAD-FMK (10µM/ml). The panels show Western blot analysis of LC3-I and LC3-II protein levels, and β-tubulin as a loading control. **b**, densitometric ratio of LC3-II to β-tubulin for 5 independent experiments; each column shows the mean; error bar is SEM. ***, significantly different between untreated and treated cells, p < 0.001.**c**, Representative immunofluorescence images of LC3 in BMDMs left uninfected (Basal) , or infected with PA103ΔUΔT for 4hrs at a MOI of 25 in the presence (+) or absence (−) of the capsase-1 inhibitor Z-YVAD-FMK (10µM/ml) . Cells were stained with DAPI to visualize nuclei (blue), and LC3 staining is shown as green. Scale bar 10 µm. **d**, Quantification of LC3 puncta present per cell following treatments and infections as indicated. *** significant difference between infected BMDMs± Z-YVAD-FMK, p < 0.001. **e**, Levels of intracellular LC3-II assayed by flow cytometry following treatments as indicated. **f**, qRT-PCR of *Lc3b* mRNA levels following treatments as shown; ** significant difference between BMDMs ± Z-YVAD-FMK, p < 0.01 . (3 independent experiments).
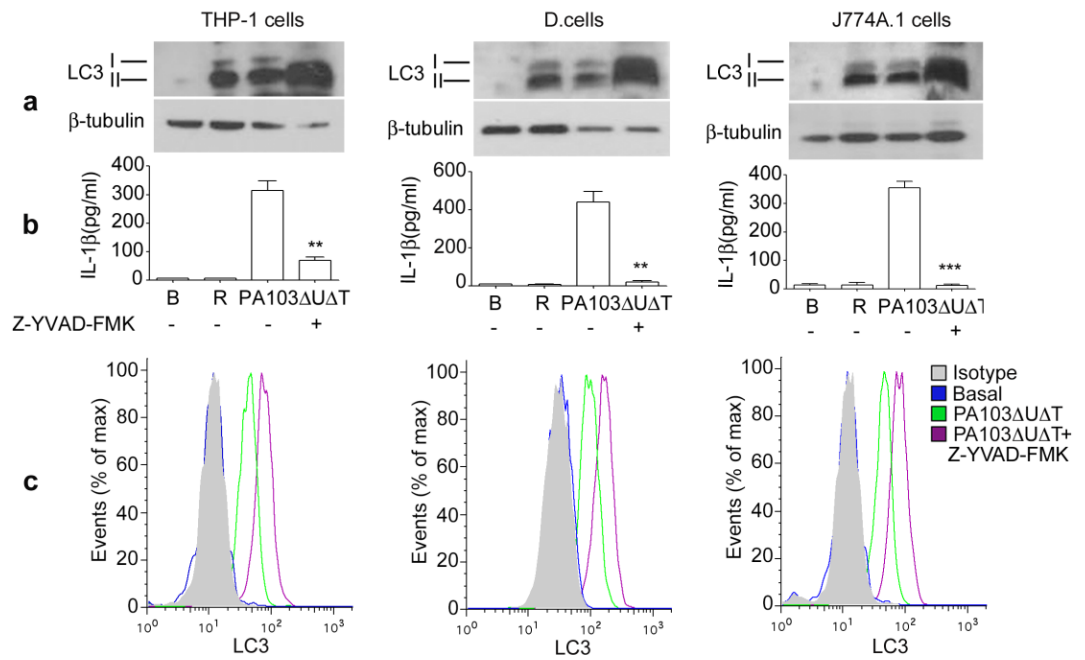
Figure 3.19; Caspase-1 inhibitor Z-YVAD-FMK Up-regulates autophagy following *P.aeruginosa* infection in mammalian cells.

a, Cells were infected with PA103ΔUΔT (MOI 25) for 4hrs in the presence (+) or absence (–) of the capsase-1 inhibitor Z-YVAD-FMK (10μM/ml). The panels show Western blot analysis of LC3-I and LC3-II protein levels, and β-tubulin as a loading control. **b**, Secreated IL-1β released during infection as indicated in the absence or presence of Z-YVAD-FMK a measured by ELISA. ** and *** indicate significant differences between the levels in the presence and absence of the inhibitor, $p < 0.01$ and < 0.001 respectively. **c**, Levels of intracellular LC3-II assayed by flow cytometry following treatments as indicated . (2 independent experiments).

.
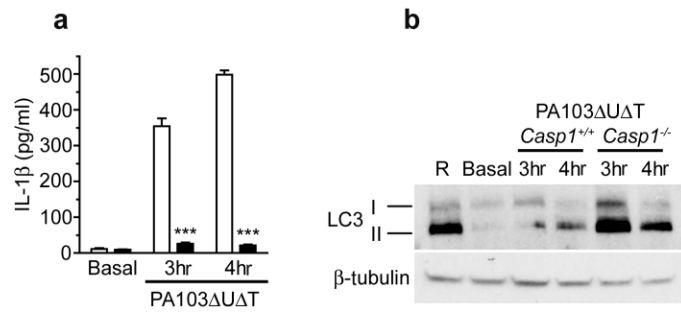
Figure 3.20; Caspase-1 Knockout BMDMs Up-regulate autophagy following *P.aeruginosa* infection.

a, IL-1β levels in supernatants of BMDMs treated as shown (MOI of 25) in WT (open bars) and *Casp1⁻/* animals (filled bars). Bars are mean of triplicate determinations; error bars are SEM. *** significant difference between animal groups, p < 0.001. **b**, Western blot of LC3 I and II isoforms in cells left uninfected (Basal), treated with rapamycin (R), or infected with PA103ΔUΔT (MOI 25) for the indicated time in hours in WT (*Casp1⁺/⁺*) mice or in animals lacking Caspase-1 (*Casp1⁻/⁻*). Experiment repeated with the same results.

.
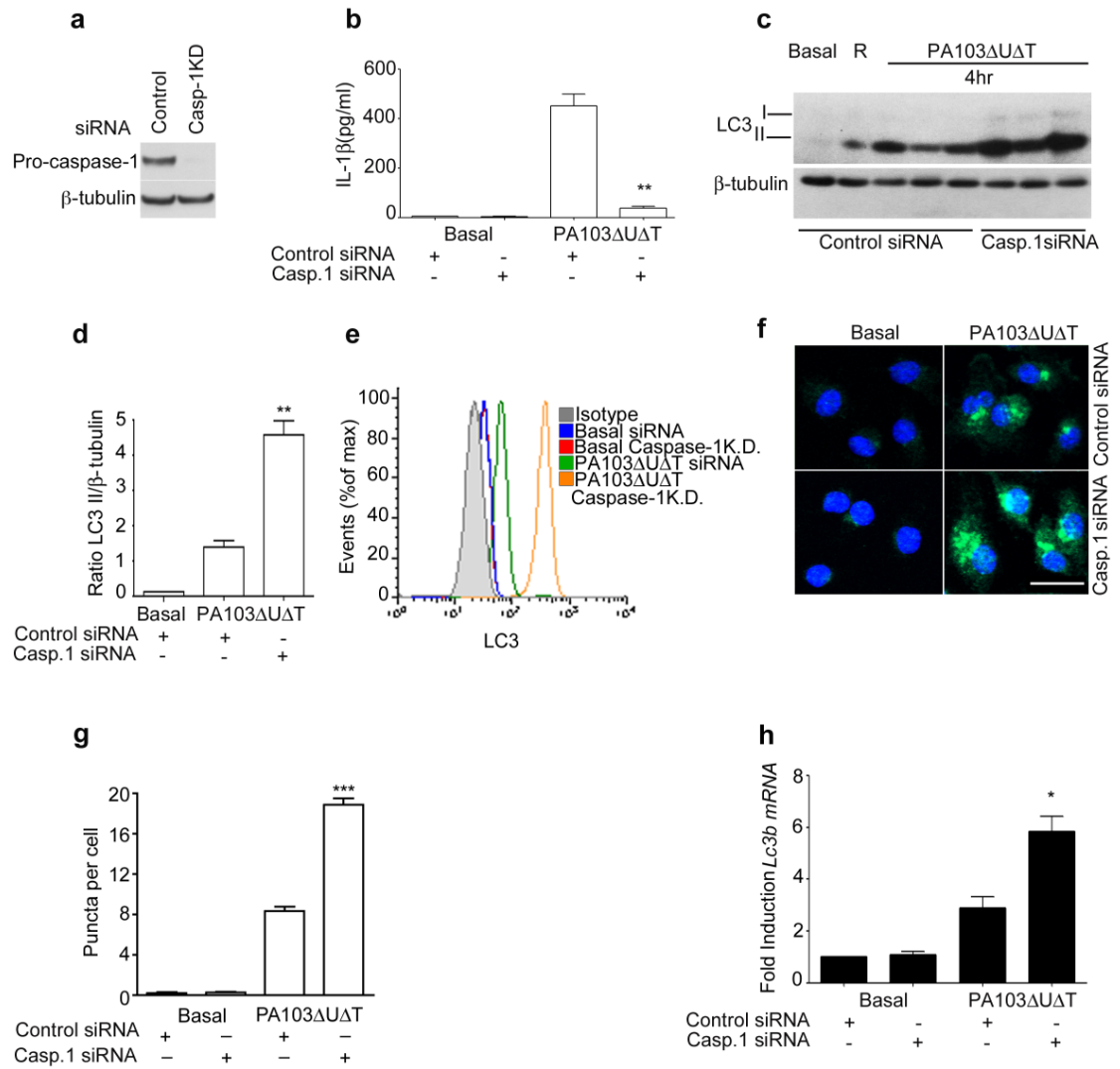
Figure 3.21; Caspase-1 Knock -down Up-regulated autophagy following
P.aeruginosa **infection.**

a, Western blot of caspase-1 was performed to show the successful reduction in levels after siRNA knockdown. β-tubulin was probed as a loading control. **b,** IL-1β levels in supernatants of BMDMs treated as shown (MOI of 25) in control siRNA against *Casp1* siRNA BMDMs. Bars are mean of triplicate determinations; error bars are SEM. ** significant difference between animal groups, p < 0.01. **c**, Western blot analysis of LC3 I and II levels following infection for 4h at MOI of 25 with PA103ΔUΔT as show in BMDMs transfected with control siRNA or siRNA specific for caspase-1 . **d**, shows the ratio of LC3 II/β-tubulin with indicated treatments for 3 independent experiments. Bars are means; error bars are SEM. **, significantly different from control siRNA. **e**, Levels of intracellular LC3 assayed by flow cytometry following treatments as indicated. **f**, Representative immunofluorescence images of LC3 in BMDMs left uninfected (Basal) or infected with PA103ΔUΔT for 4hrs at a MOI of 25. Cells were stained with DAPI to visualize nuclei (blue), and LC3 staining is shown as green. Scale bar 10 µm. **g**, Quantification of LC3

puncta present per cell following treatments and infections as indicated. *** denotes significant difference between control siRNA and *Casp.1* siRNA, p < 0.001. **h**, qRT-PCR of *Lc3b* mRNA levels following treatments as shown; * significant difference between control and caspase-1, p < 0.05. (3 independent experiments).

.
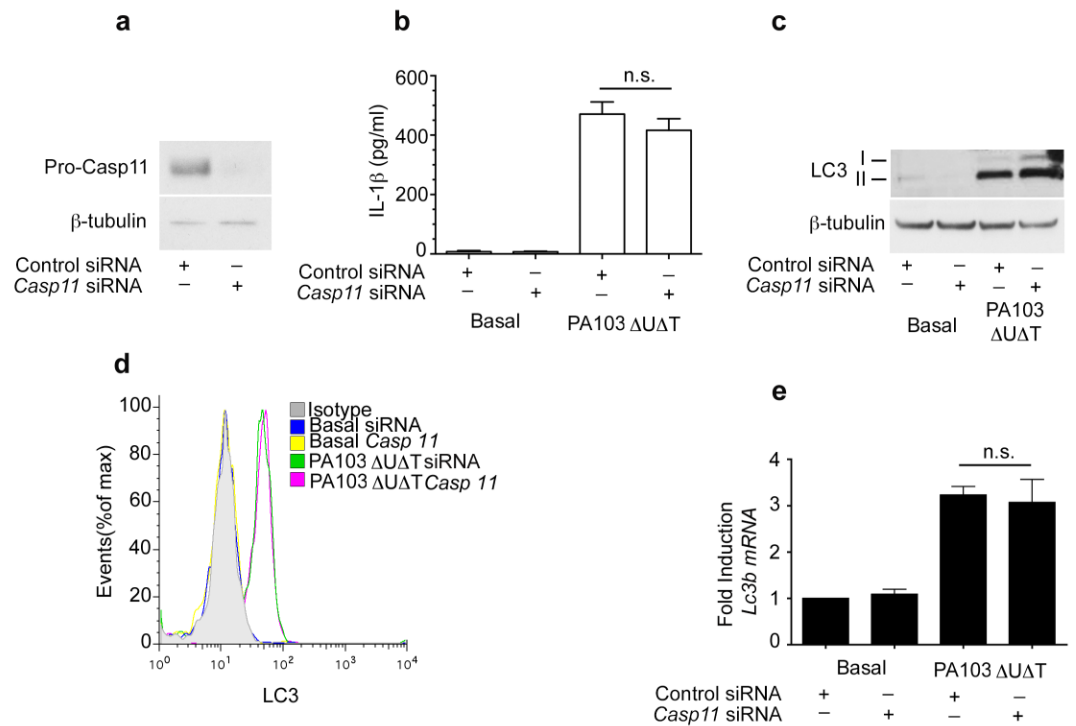
Figure 3.22; Caspase-11 does not influence autophagy following *P.aeruginosa* infection.

a, Western blot of caspase-11 was performed to show the successful reduction following siRNA knockdown. β-tubulin was probed as a loading control. **b**, IL-1β levels in supernatants of BMDMs treated as shown (MOI of 25) in control siRNA against caspase-11 siRNA BMDMs. Bars are mean of triplicate determinations; error bars are SEM. ns is non- significant difference between groups, p > 0.05. **c**, Western blot analysis of LC3 I and II levels following infection for 4h at MOI of 25 with PA103ΔUΔT as show in BMDMs transfected with control siRNA or siRNA specific for caspase-11. **d**, Levels of intracellular LC3-11 assayed by flow cytometry following treatments as indicated. **e**, qRT-PCR of *Lc3b* mRNA levels following treatments as shown; ns is non- significant difference between control and capase-11, p > 0.05 .

.

This inhibitory effect of caspase-1 on autophagy was most likely mediated by the activation of the NLRC4 inflammasome following *P. aeruginosa* infection. To confirm this supposition, we assayed the amount of autophagy observed following *P. aeruginosa* infection after inhibition of this inflammasome by various means. Previously, it has been shown that elevation of extracellular K^+ inhibits NLRC4 inflammasome activation by *P. aeruginosa* (Lindestam Arlehamn et al., 2010). We confirmed that BMDMs, THP-1 cells, dendritic cells, and J774A.1cells incubated in a high extracellular concentration of K^+ had a markedly attenuated production of caspase-1 p10 and IL-1β following infection (Fig. 3-23), while maintaining very similar levels of production of TNF-α (Fig. 3-23b). This inhibitory effect on inflammasome activation resulted in elevation of the levels of LC3 II, increased numbers of autophagocytic puncta, increased expression of *lc3b* mRNA, and increased intracellular staining of LC3-II as assayed by flow cytometry (Fig. 3-24) (Fig. 3-25). Similarly, in BMDMs derived from animals with a targeted gene deletion of *Nlrc4*, infection with *P. aeruginosa* resulted in increased conversion of LC3 to its lipidated form, and increased numbers of autophagocytic puncta (Fig. 3-26). Knockdown of *Nlrc4* mRNA with siRNA also increased autophagy following infection, as evidenced by an increase in the numbers of autophagocytic LC3 containing puncta per cell, and increased formation of LC3 II as well as intracellular LC3 and levels of *Lc3b* mRNA (Fig. 3-27). Taken together, these data demonstrate that activation of the NLRC4 inflammasome following *P. aeruginosa* infection leads to an inhibition of autophagy and that this is directly mediated by caspase-1.
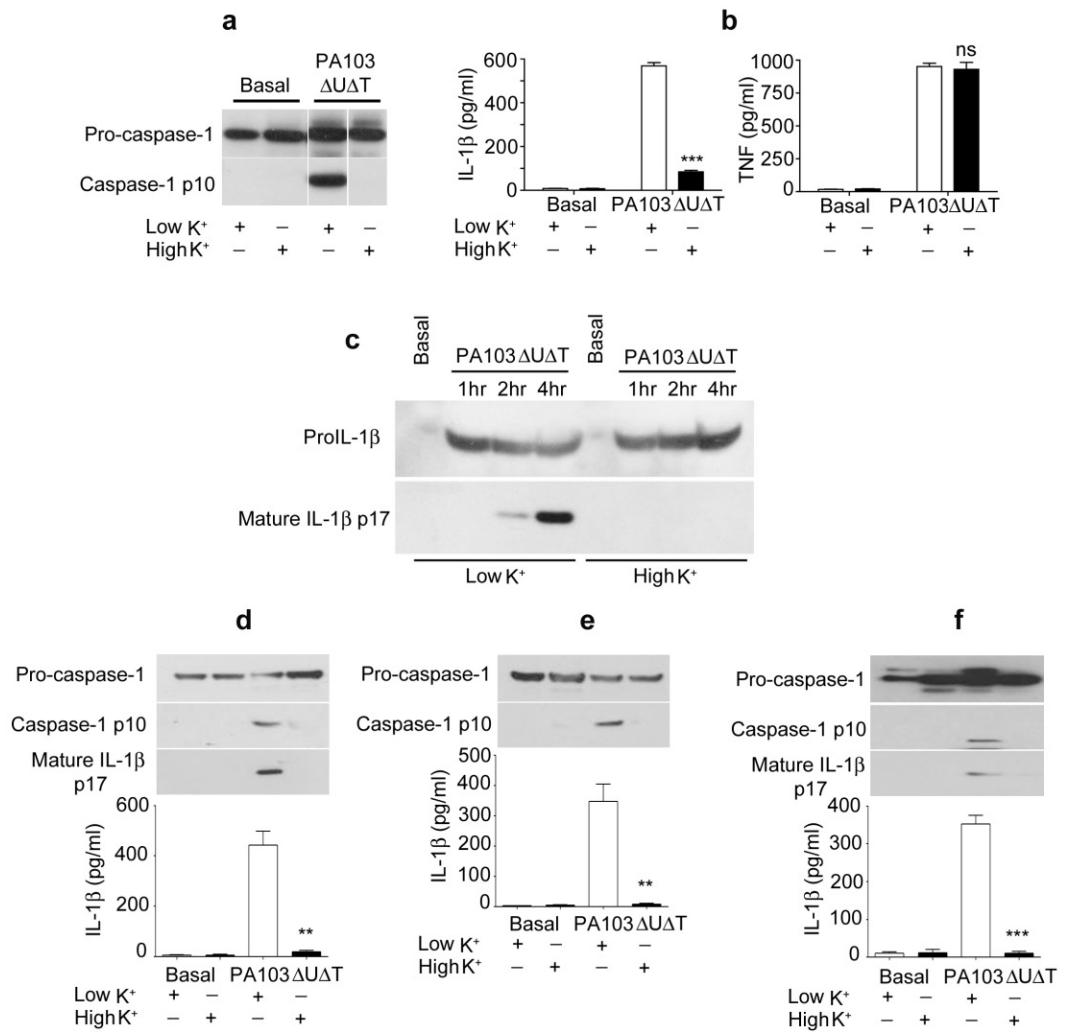
Figure 3.23; Inflammasome activation following *P.aeruginosa* infection is dependent on Potassium efflux.

BMDMs, THP-1cells, D.Cs, and J774A.1 cells were incubated in media with normal K$^+$ (5 mM; Low K$^+$) or high K$^+$ (140 mM) as indicated and infected with PA103ΔUΔT (4h, MOI of 25) and levels of processed caspase-1, and procaspase-1 (**a**), secreted IL-1β, and secreted TNF (**b**) determined as shown. Columns are means of triplicate determinations; error bars are SEM. Open bars are in low K$^+$, closed bars high K$^+$. ***, significantly different from levels seen with low K$^+$ (p < 0.001). **c**, Western blot analysis of Pro-IL-1β and mature IL-1β in cell supernatants form BMDMs infected as indicated in media with normal K$^+$ (5 mM; Low K$^+$) or high K$^+$ (140 mM) as indicated. **d** – **f**, shows Western blot analysis of pro-caspase- 1 , caspase-1, and mature IL-1β in cells lysates, and β-tubulin was probed as a loading control in DCs(**d**), THP-1 cells(**e**), or J774A.1 cells(**f**) . Graphs show IL-1β secretion was measured by ELISA. Columns are means of triplicate determinations; error bars are SEM. Open bars are in low K$^+$, closed bars high K$^+$. **, ***, significantly different from levels seen with low K$^+$ (p<0.01),(p < 0.001) respectively. (Experiments repeated three times).
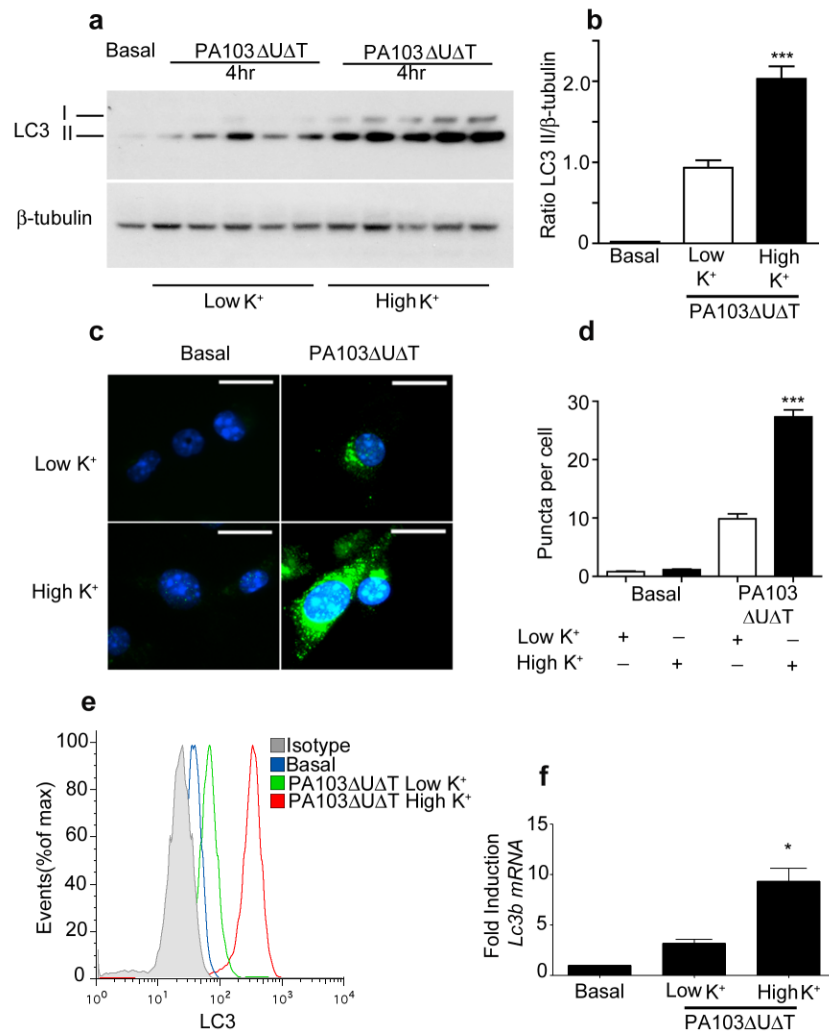
Figure 3.24; Blocking K⁺ efflux up-regulates level of autophagy following *P.aeruginosa* infection.

BMDMs were incubated in media with normal K⁺ (5 mM; Low K⁺) or high K⁺ (140 mM) as indicated and infected with PA103ΔUΔT (4h, MOI of 25). **a**, Western blot analysis of LC3 I and II levels following infection for 4h at MOI of 25 with PA103ΔUΔT. **b**, shows the ratio of LC3 II/β-tubulin with indicated treatments for 5 independent experiments. Bars are means; error bars are SEM. ***, significantly different between groups, (p < 0.001). **c**, Representative immunofluorescence images of LC3 in BMDMs left uninfected (Basal) or infected with PA103ΔUΔT for 4hrs at a MOI of 25. Cells were stained with DAPI to visualize nuclei (blue), and LC3 staining is shown as green. Scale bar 10 μm. **d**, Quantification of LC3 puncta present per cell following treatments and infections as indicated. *** significant difference between group, p < 0.001. **e**, Levels of intracellular LC3-II assayed by flow cytometry following treatments as indicated. **f**, qRT-PCR of *Lc3b* mRNA levels following treatments as shown; * significant difference between groups, p < 0.05 . (3 independent experiments).
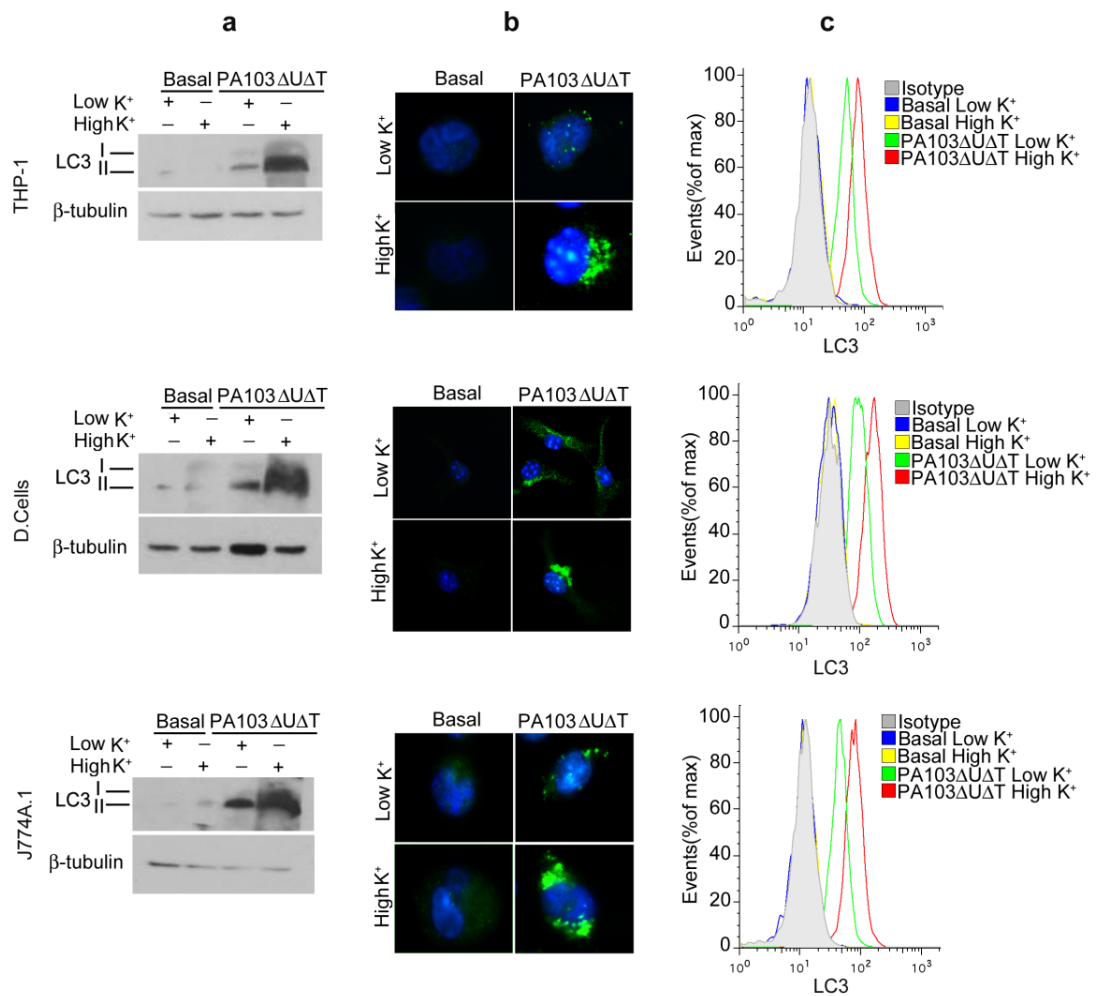
**Figure 3.25; Blocking Potassium efflux up-regulates level of autophagy following *P.aeruginosa* infection in different mammalin cells.**

THP-1cells, D.Cs, and J774A.1 cells were incubated in media with normal K^+ (5 mM; Low K^+) or high K^+ (140 mM) as indicated and infected with PA103ΔUΔT (4h, MOI of 25). **a**, Western blot analysis of LC3 I and II levels following infection for 4h at MOI of 25 with PA103ΔUΔT. **b**, Representative immunofluorescence images of LC3 in BMDMs left uninfected (Basal) , or infected with PA103ΔUΔT for 4hrs at a MOI of 25. Cells were stained with DAPI to visualize nuclei (blue), and LC3 staining is shown as green. Scale bar 10 µm. **c**, Levels of intracellular LC3-II assayed by flow cytometry following treatments as indicated. (Experiments repeated three times).

Figure 3.26; *Nlrc*4 influences level of autophagy following *P. aeruginosa* infection.

a, IL-1β levels in supernatants of BMDMs treated as shown (MOI of 25) in WT and *Nlrc4$^{-/-}$* animals. Bars are mean of triplicate determinations; error bars are SEM. *** significant difference between animal groups, p < 0.001. **b**, Western blot of LC3 I and II isoforms in cells left uninfected (Basal), or infected with PA103ΔUΔT (MOI 25) for 4hrs in WT (*Nlrc4$^{+/+}$*) mice or in animals lacking Nlrc4 (*Nlrc4$^{-/-}$*). **c**, Representative immunofluorescence images of LC3 in BMDMs left uninfected (Basal) or infected with PA103ΔUΔT for 4hrs at a MOI of 25. Cells were stained with DAPI to visualize nuclei (blue), and LC3 staining is shown as green. Scale bar 10 µm. Experiment repeated with the same results.

.
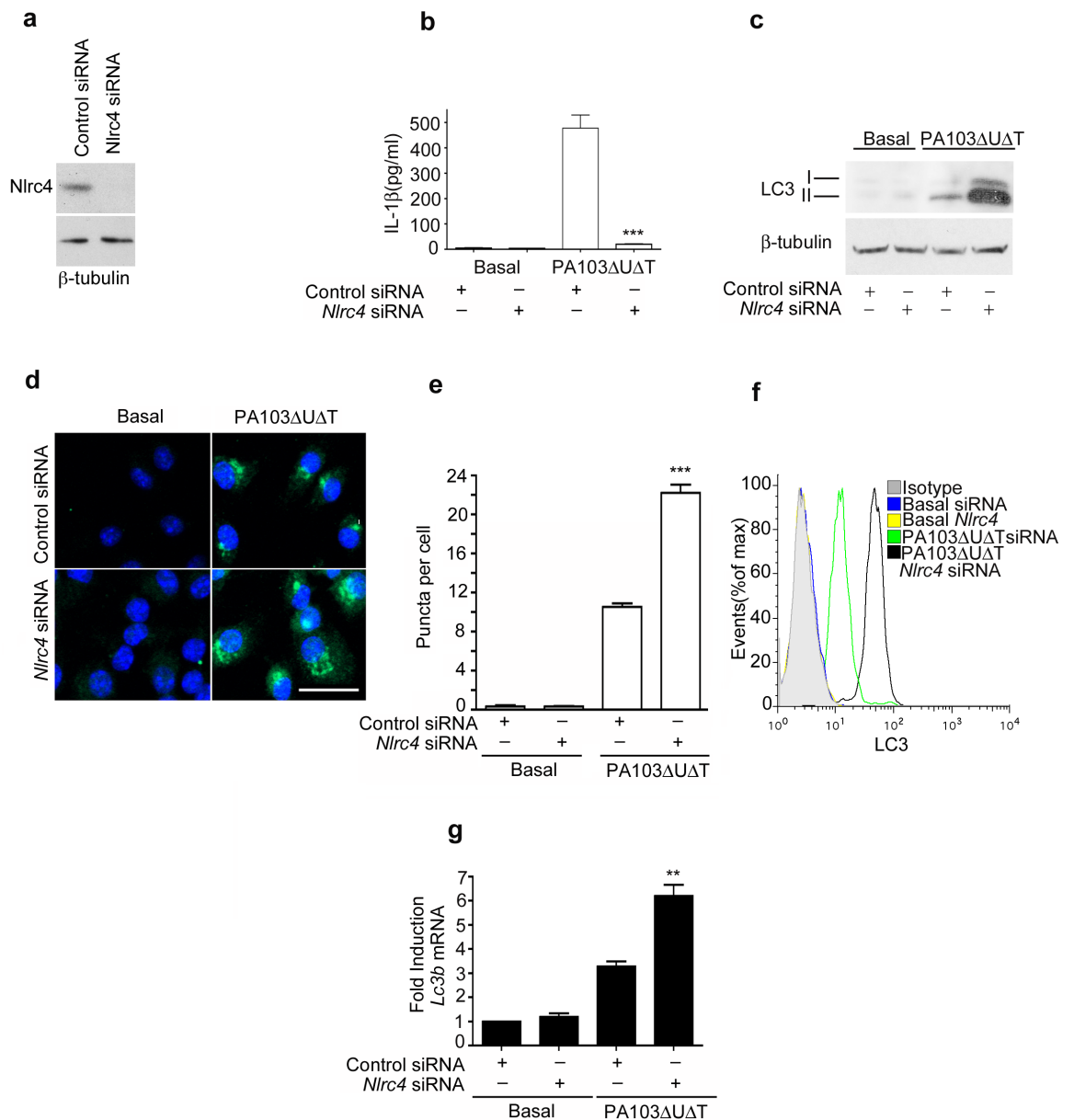
Figure 3.27; ***Nlrc*4 Knock-down up-regulates autophagy following *P. aeruginosa* infection.**

a, Western blot of *Nlrc4* was performed to show the successful reduction in *Nlrc4.* β-tubulin was probed as a loading control. **b,** IL-1β levels in supernatants of BMDMs treated as shown (MOI of 25) in control siRNA against *Nlrc4* siRNA treated BMDMs. Bars are mean of triplicate determinations; error bars are SEM. *** significant difference between groups, p < 0.001. **c,** Western blot analysis of LC3 I and II levels following infection for 4h at MOI of 25 with PA103ΔUΔT as show in BMDMs transfected with control siRNA or siRNA specific for *Nlrc4* . **d,** Representative immunofluorescence images of LC3 in BMDMs left uninfected (Basal) or infected with PA103ΔUΔT for 4hrs at a MOI of 25. Cells were stained with DAPI to visualize

nuclei (blue), and LC3 staining is shown as green. Scale bar 10 µm. **e**, Quantification of LC3 puncta present per cell following treatments and infections as indicated. *** Significant difference between control siRNA and *Nlrc4* siRNA, p < 0.001. **f**, Levels of intracellular LC3 assayed by flow cytometry following treatments as indicated. **g**, qRT-PCR of *Lc3b* mRNA levels following treatments as shown; ** significant difference between control and *Nlrc4*, p < 0.01 . (3 independent experiments).

3.3 Discussion

In our study, we found that *P. aeruginosa* infection induces autophagy in macrophages, D.Cs, J774A.1 and RAW264.7 cells, and the human cell line THP-1 cells. We observed that autophagy could be induced in macrophages through a classical pathway including Atg7 and Atg5. We also observed the involvement of LC3 (Atg-8) in the induction of autophagy through *P. aeruginosa*. Previous literature has shown the induction of autophagy with intracellular bacteria but the involved pathway, the impact and outcome of infection with these bacteria remained is different as compared to *P. aeruginosa.*

P. aeruginosa is considered as an extracellular bacterium and its virulence factors e.g. biofilms and type III secretion systems are crucial in its pathogenicity (Hoiby et al., 2011). These virulence factors could possibly be involved in the autophagic pathway.

As we know from the previous literature that new microtubule associated protein light chain-3 MAP-LC3 is produced in the cells and is processed at its C terminus through an autophagy related protein, Atg4. After processing LC3 is converted to LC3-I and is distributed in the cytoplasm. When there are some stressful conditions like starvation or infection, LC3-1 is converted to LC3-II by the conjugation of phosphatidyl ethanolamine (PE) (Ichimura et al., 2004). The conjugated form of LC3 is distributed to both outer and inner membranes of autophagosome, a double membrane vesicle inside the cells. The presence of LC3-II is used as a typical marker for the autophagy detection.

Rapamycin a widely used autophagy inducer was used as positive control and we found a similar strong signal in samples infected with *Pseudomonas aeruginosa* mutant strain pcrV⁻ and found that there is increase in the signal produced by the bacterial infection. When we compared our results using genetic methods such as *Atg*7 knock out animals , *Atg5* siRNA, and *Lc3b* siRNA, or with 3 Methyl adenine (3MA), we found that autophagy was inhibited and the production of LC3 positive markers decreased with 1 hour pre-treatment with 3-MA.

In our experimental work, we used some genetic methods to inhibit autophagy. Deletion of *Atg7* blocked autophagy induction by the bacterium *P. aeruginosa*. Similarly Atg5-siRNA transfection was also performed and found also resulted in autophagy inhibition. These experiments together indicated that *P. aeruginosa* induces autophagy and is dependent upon the classical pathway for autophagy.

Macrophages play an important role in innate and adaptive immunity during bacterial infection and the induction in these macrophages could impact infection with *P. aeruginosa*. To find whether autophagy only occurs in BMDMs, we also investigated *P. aeruginosa* infection in murine D.Cs, J774A.1 cells, RAW264.7 cells and the human cell line THP-1 cells. A similar pattern of autophagy induction was seen in these cells.

In conclusion, the results presented in this chapter demonstrate that the extracellular bacterium *P. aeruginosa* infection induced autophagy in BMDMs, DCs, J774A.1 cells, RAW264.7 cells, and THP-1 cells. We have studied this using the human pathogen *P. aeruginosa* and different cell type. To determine the role of the T3SS in this process, we utilised two bacterial

strains, both derivatives of the type strains, PA103ΔUΔT has a fully functional T3SS but does not translocate any bacterial exotoxins and PA103pcrV⁻ lacks a functional T3SS.Our results showed PA induces autophagy. Since both strains induce autophagy, a functional T3SS does not seem to be required for this process. PA also infection also strongly induced activation of the inflammasome which was absolutely dependent on a functional T3SS. We found that inhibition of inflammasome activation increased autophagy, suggesting that the inflammasome normally inhibits this process. Loss of type III secretion increased autophagy, which was due to NLRC4 activation and caspase-1 activity. We also addressed another important question: what specific role does autophagy play in the immune response?

4 TRIF –Dependent TLR4 signalling is required for *Pseudomonas aeruginosa* induced autophagy

4.1 Introduction

Microbial interactions with host immune cells can trigger a number of innate immune responses (Akira et al., 2006, Kumar et al., 2009, Diacovich and Gorvel, 2010). Two fundamental processes that can be initiated are those of macroautophagy (Orvedahl and Levine, 2009, Deretic and Levine, 2009) (hereafter termed autophagy) and activation of the inflammasome (Martinon et al., 2009, Franchi et al., 2012b). Autophagy is a process that results in sequestration of cytoplasmic contents within a membranous vacuole that then fuses with lysosomes, ultimately resulting in degradation and recycling of the vacuole contents (Kundu and Thompson, 2008). Autophagy has now been to occur found in almost all eukaryotic cells, with genes controlling the pathway being highly conserved from yeast to mammals (Stromhaug and Klionsky, 2001). Autophagy also occurs in response to microbial infection and has been shown to be important in host defence against a number of microbes, such as *Mycobacterium tuberculosis*, group A streptococcus, *Shigella flexneri*, *Salmonella enterica*, and *Listeria monocytogenes*, viruses such as herpes simplex virus type 1(HSV-1), and parasites such as *Toxoplasma gondii* (Songane et al., 2012, Birmingham et al., 2006, Py et al., 2007, Iwasaki, 2007, Andrade et al., 2006) as well as enhancing antigen presentation in adaptive immune response to a variety of pathogens (Patterson and Mintern, 2012).

TLR4 is the signalling receptor that mediates a robust inflammatory response to LPS, but it requires several co-receptors as well as adaptor molecules for signal transduction (Lu et al., 2008).Toll-like receptors (TLRs) are membrane-expressed signaling pattern recognition receptors (PRRs).

For example, TLR2, and TLR4, distributed on the cell surface, and TLR3/7/8/9, located within endosomal compartments, can recognize viral molecular determinants. With the exception of TLR3, all these TLRs recruit the adaptor MyD88 upon engagement. TLR4 recruits in addition the adaptor TRIF, which is also used by TLR3. MyD88 associates with a serine protease to transduce signals to activate nuclear factor-kappa B (NF-κB), a transcription factor that regulates the synthesis of inflammatory cytokines (Lebeis et al., 2009). TRIF relays signals leading to the activation of type I IFN regulatory transcription factors (IRF), for type I IFN synthesis. A MyD88-dependent signal may also trigger type I IFN production upon virus infection. Newly synthesized type I IFN are the major effector cytokines of the host immune response against viral infections. They bind to the type I IFN receptor (IFNAR) which transduces signals leading to the expression of hundreds of IFN stimulating genes (ISGs) that have a direct antiviral effect (Guo and Cheng, 2007).

We demonstrate in chapter three that *P. aeruginosa* activates autophagy in macrophages following infection via the classical autophagy pathway. We show by multiple independent methods that inhibition of inflammasome and caspase-1 activation augments the autophagocytic response. This inhibitory effect of caspase-1 on induction of autophagy is shown to result from caspase-1 mediated cleavage of the signalling intermediate TRIF, an essential part of the TLR4 mediated signalling pathway leading to promotion of autophagy (Xu et al., 2007). Moreover, we also found that caspase-1 cleavage of TRIF reduced the signalling required to induce type I IFNs. We show that these inhibitory effects of activated caspase-1 have important functional effects, reducing macrophage

phagocytosis and reactive oxygen generation. Additionally, the caspase-1 mediated down-regulation of autophagy results in a reduction of NLRP3 inflammasome activation by LPS+ATP.

4.2 Results

4.2.1 Autophagy following P. aeruginosa infection is mediated via TLR4 and TRIF.

LPS has been shown to induce autophagy through TLR4 signalling to the intermediate TRIF (Xu et al., 2007). We hypothesised that a similar pathway might operate to induce autophagy following *P. aeruginosa* infection. We tested this by measuring the amount of autophagy in BMDMs from mice with a targeted deletion of *Tlr4* compared to wild-type animals. Firstly, we confirmed that LPS induced autophagy in BMDMs by assaying for conversion of LC3 I to the lipidated LC3 II form. This conversion was significantly abrogated in BMDMs from *Tlr4* KO mice, reduced numbers of autophagocytic puncta, and reduced intracellular LC3 II as assayed by flow cytometry (Fig 4-1). We then followed the conversion of LC3 to its lipidated form over time following *P. aeruginosa* infection (Fig 4-2a). This showed clearly that the increase in autophagy following infection was largely abolished in the absence of TLR4, both for the PA103ΔUΔT and PA103pcrV⁻ strains. Autophagy induced by rapamycin was, as expected, not diminished in the absence of TLR4 (Fig 4-2a). To confirm these observations, we followed the accumulation of LC3 puncta following infection as a marker of autophagy. This also showed a virtual abolition of autophagy following infection in the absence of TLR4 (Fig 4-2a and b). Finally, using siRNA to knockdown *Tlr4*, our results showed reduced intracellular LC3 II as assayed by flow cytometry (Fig 4-2d).
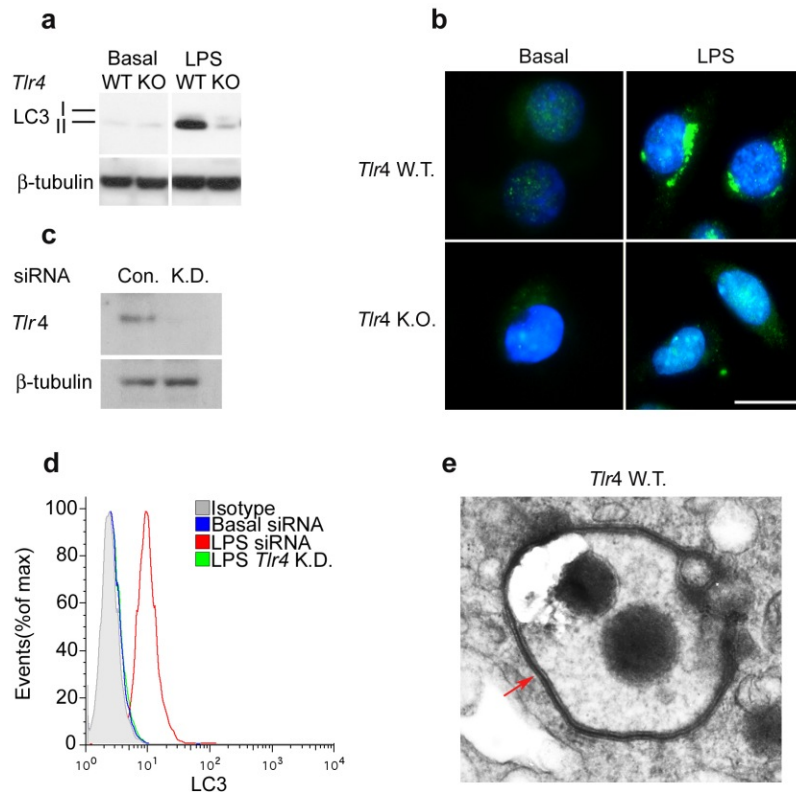
Figure 4.1; LPS induces autophagy via *Tlr*4 dependent signaling.

a, Western blot analysis of LC3 I and II levels. Cells were treated with LPS 500ng/ml for 4h. **b**, Representative immunofluorescence images of LC3 in BMDMs left untreated (Basal), or treated with LPS 500ng/ml for 4hrs. Cells were stained with DAPI to visualize nuclei (blue), and LC3 staining is shown as green. Scale bar 10 μm. **c**, Western blot of *Tlr*4 was performed to show the successful reduction in *Tlr*4. β-tubulin was probed as a loading control. **d**, levels of intracellular LC3 assayed by flow cytometry following treatments as indicated. **e**, electron micrographs of autophagosome in *Tlr*4 WT BMDMs after treated with 500ng/ml LPS for 4 hrs. Arrow indicated autophagosome. (Experiments repeated 2 times)
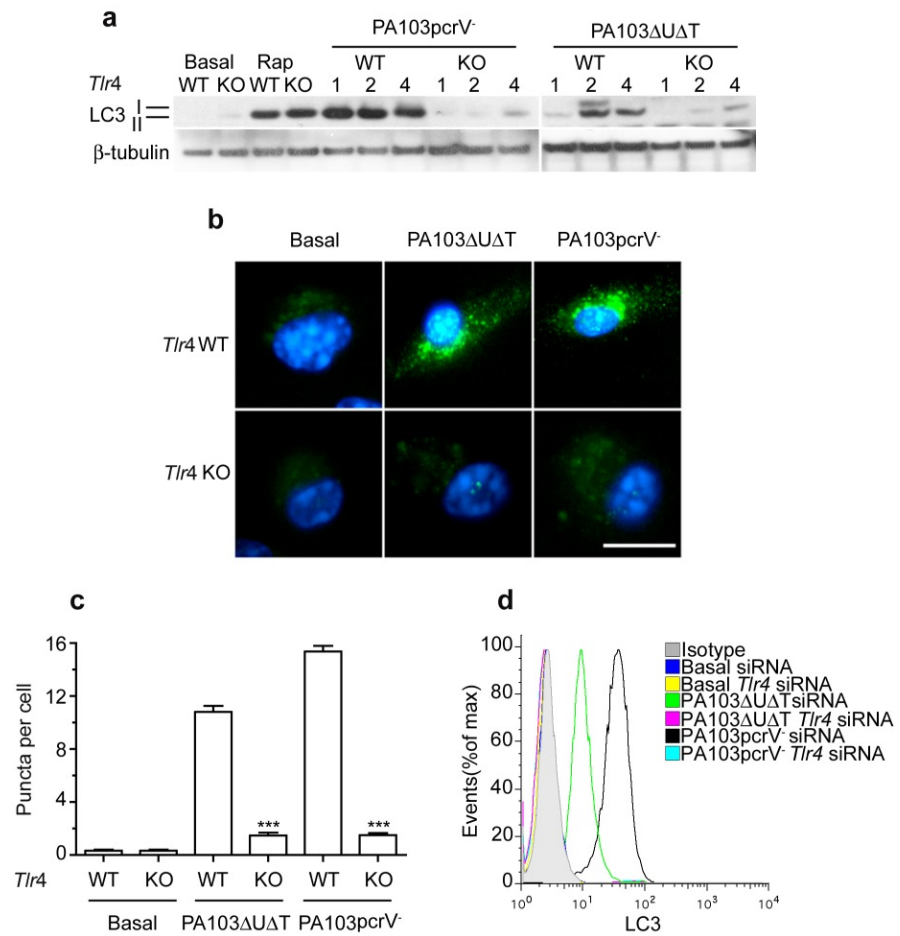
Figure 4.2; Autophagic signaling is induced by _Pseudomonas aeruginosa_ via _Tlr4_ dependent signaling.

a, LC3 I and II assayed by Western blotting in BMDMs from WT or _Tlr4_[-/-] mice (KO), uninfected (Basal), rapamycin (Rap) or infected with _P. aeruginosa_ strains as indicated (MOI 25) for 1, 2 or 4 h. **b**, Representative immunofluorescence images of LC3 in BMDMs left uninfected (Basal) , or infected with _P.aeruginosa_ strains as indicated(MOI 25) for 4hrs. Cells were stained with DAPI to visualize nuclei (blue), and LC3 staining is shown as green. Scale bar 10 μm. **c**, Number of puncta per cell in BMDMs infected as shown under the conditions in panel **b**. Bars are means of 3 independent counts for at least 50 cells; error bars are SEM. ***, significantly different from WT cells, p < 0.001.**d**, Levels of intracellular LC3 assayed by flow cytometry following treatments as indicated. (Experiments repeated 2 times)

We then determined the role of Myd88 and TRIF in the induction of autophagy following *P. aeruginosa* infection. In macrophages from mice with a deletion of *Myd88*, there was no reduction in autophagy following infection with the PA103 strains or the wild type PAO1 (Fig 4-3a). In macrophages from mice with deletion of *Trif*, we found that autophagy as measured by conversion of LC3 I to the LC3 II form was greatly reduced (Fig 4-3b) following infection with both PA103 strains and the wild type PAO1. Similarly, the accumulation of LC3 puncta was abrogated in the absence of TRIF (Fig 4-3c and d). Taken together, these data show that *P. aeruginosa* induces autophagy via signalling through TLR4 and the intermediate TRIF.
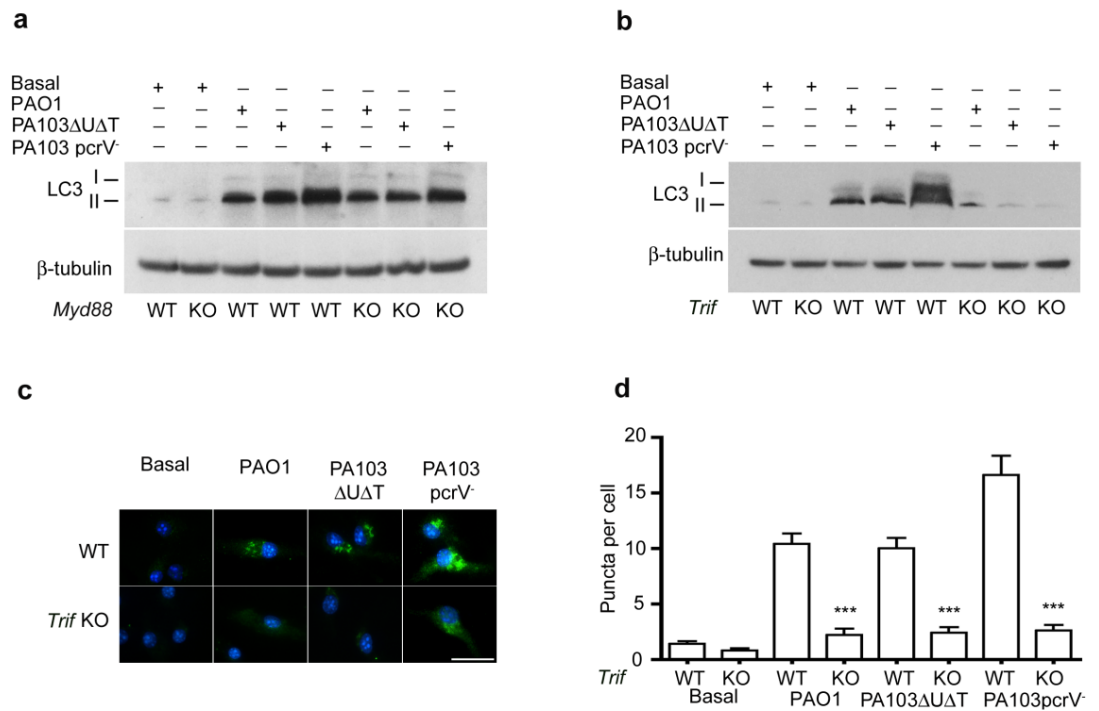
Figure 4.3; TRIF is required for *Pseudomonas aeruginosa* induced autophagy.

 a, **b**, Western blot analysis of LC3 I and II levels. Cells were infected with *P. aeruginosa* strains as indicated (MOI 25) for 4hr in wild type or *Myd88* and *Trif* deficient macrophages (KO). **c**, Representative immunofluorescence images of LC3 in BMDMs left uninfected (Basal) , or infected with *P.aeruginosa* strains as indicated (MOI 25) for 4hrs. Cells were stained with DAPI to visualize nuclei (blue), and LC3 staining is shown as green. Scale bar 10 μm. **d**, Number of puncta per cell in BMDMs infected as shown under the conditions in c. Bars are means of 3 independent counts for at least 50 cells; error bars are SEM. ***, significantly different between (WT) and (KO) *Trif* cells, $p < 0.001$. (Experiments repeated 3 times).

4.2.2 Caspase-1 Cleaves TRIF

Caspases have been proposed to cleave the signalling intermediates Cardif and TRIF (Rebsamen et al., 2008). We hypothesised that one mechanism that could explain why caspase-1 activation down-regulated autophagy was through proteolytic cleavage of TRIF. To test this hypothesis we examined cell lysates for endogenous TRIF fragments following infection of BMDMs with *P. aeruginosa.* After infection with the inflammasome activating strain PA103ΔUΔT, we observed immunoreactive TRIF fragments between 28 – 30 kDa at 4 hours after infection. These were not seen following infection with the T3SS inactive strain PA103pcrV⁻ which does not activate the inflammasome, and were also considerably reduced in the presence of ZYVAD-FMK, a caspase-1 inhibitor (Fig 4-4a). This was a highly reproducible finding, shown for four independent cell lysates in (Fig 4-4b), although the separation of the cleaved product into two bands of similar molecular weight varied depending on the exact conditions under which the proteins were separated by SDS PAGE. The antibody used in these immunoblots recognises a C terminal epitope, thus suggesting that the cleavage site lies in the middle portion of TRIF (molecular weight 74kDa), to generate the ~ 30kDa fragments seen in (Fig 4-4).

To confirm that the observed cleavage products were produced by caspase-1, we examined lysates from BMDMs from mice with targeted deletion of the *Caspase-1* gene as well as WT animals (Fig 4-5a). This showed that the cleavage products were absent following infection of BMDMs from the *Capsase-1* knock out animals. We obtained the same results with knockdown of *Caspase-1* (Fig 4-5b). Knockdown of caspase-11

had no effect on TRIF cleavage following infection (Fig 4-6a), which was also seen with the wild type PAO1 strain. In macrophages from NLRC4 knockout mice, no TRIF cleavage was seen, either with PA103ΔUΔT or the wild type PAO1 (Fig 4-6b). Similarly, infection of BMDMs in high extracellular potassium (which inhibits inflammasome activation), also inhibited the appearance of these cleaved products (Fig 4-7).

.
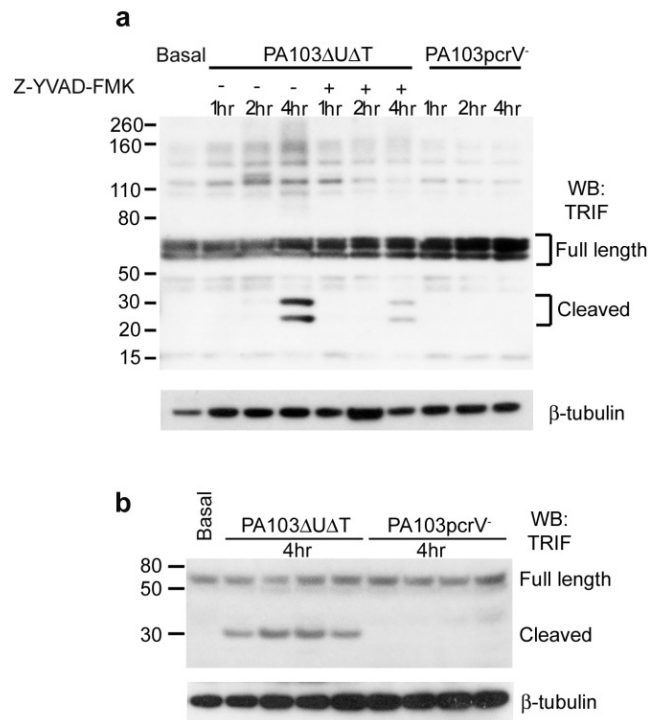
Figure 4.4; TRIF is cleaved following infection with *P. aeruginosa* PA103ΔUΔT strain.

a, Western blot using 12% acrylamide gel for TRIF in BMDMs lysates that were uninfected (Basal), or infected with the *P. aeruginosa* strains shown for 1, 2, and 4 hrs. Where shown, cells were treated with the caspase-1 inhibitor Z-YVAD-FMK. Full length and cleaved TRIF products are labelled. Molecular weight markers in kDa are shown to the left of the gel. The blot was re-probed for β-tubulin as a loading control (lower panel). Experiment repeated with the same results. **b** As **a,** but using 4-12% acrylamide gel; cells infected for 4h at MOI of 25. Each lane of infected samples represents an independent experiment.
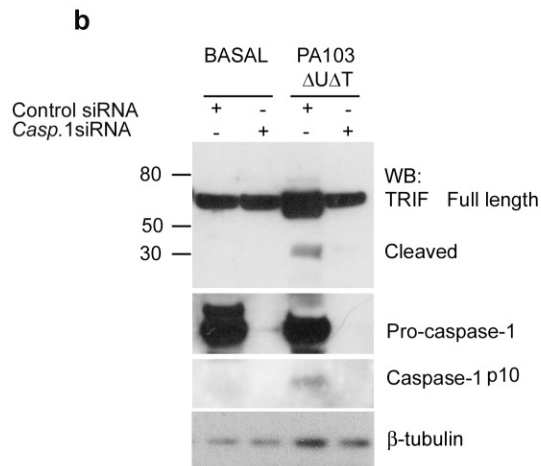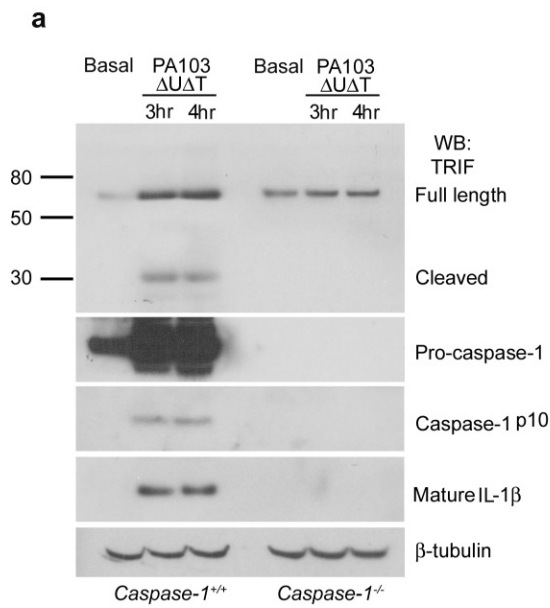
Figure 4.5; TRIF is cleaved by Caspase-1 following _P. aeruginosa_ activation of the inflammasome.

a, Western blot using 4-12% acrylamide gel for TRIF in BMDMs lysates from WT (_Casp1_$^{+/+}$) or _Casp1_ KO mice (_Casp1_$^{-/-}$) that were uninfected (Basal), or infected with the _P. aeruginosa_ strains shown (MOI 25) for 4 hrs. Full length and cleaved TRIF products are labelled. Molecular weight markers in kDa are shown to the left of the gel. The middle panels shown Pro-caspase-1, Caspase-1, and mature IL-1β. The blot was re-probed for β-tubulin as a loading control (lower panel). Experiment repeated with the same results. **b** As **a,** but using BMDMs from control siRNA against Caspase-1 siRNA. (Experiment repeated with the same results)
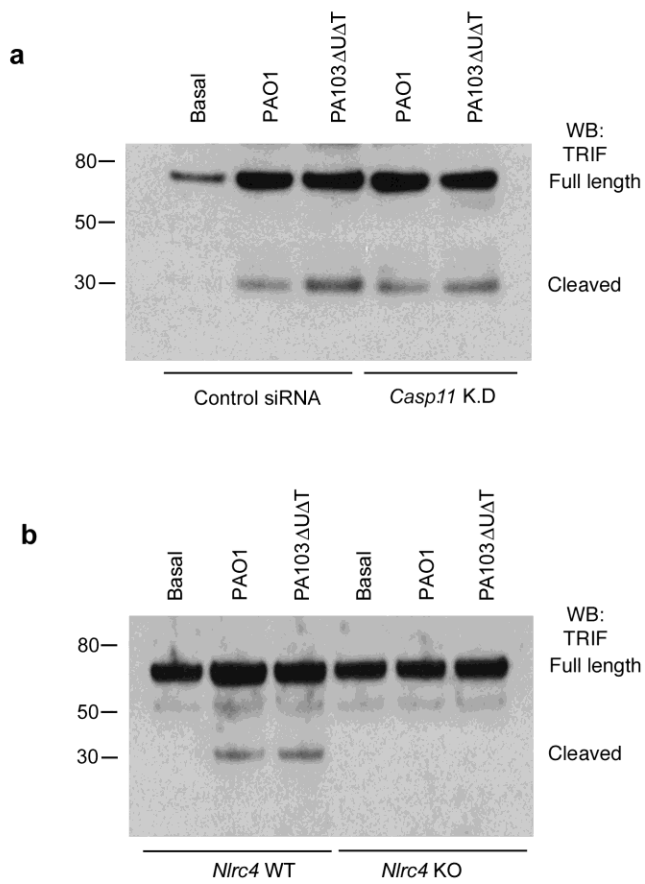
Figure 4.6; Role of Nlrc4 and Caspase-11 in TRIF cleavage following *P. aeruginosa* infection.

Western blot using 4-12% acrylamide gel for TRIF in BMDM lysates that were uninfected (Basal), or infected with the *P. aeruginosa* strains shown (MOI 25) for 4 hrs. Cells were transfected with Control siRNA or siRNA specific for *Caspase-11* (**a**) and in BMDMs from (WT) or *Nlrc4* (KO) mice (**b**). Full length and cleaved TRIF products are labelled. Molecular weight markers in kDa are shown to the left of the gel. Experiment repeated with the same results.
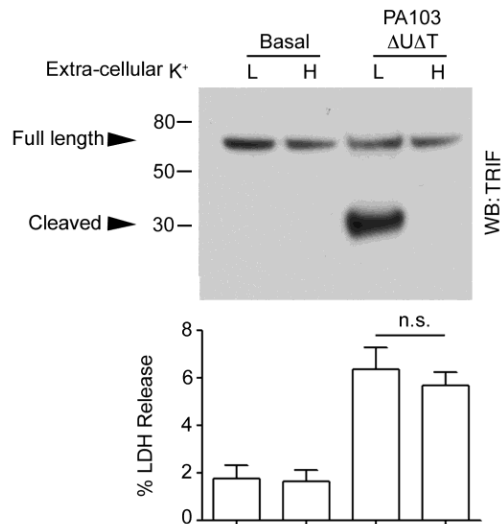
Figure 4.7; Role of extracellular Potassium in TRIF cleavage following *P. aeruginosa* infection.

BMDMs cells were incubated in media with normal K^+ (5 mM; Low K^+) or high K^+ (140 mM). Western blot using 4-12% acrylamide gel for TRIF in BMDM lysates that were uninfected (Basal), or infected with the *P. aeruginosa* strains shown for 4 hrs. Full length and cleaved TRIF products are labelled. Molecular weight markers in kDa are shown to the left of the gel. Graph shows cytotoxicity under the same conditions, measured by LDH release.

Although these data show that caspase-1 is required for the generation of TRIF cleavage products, it might be an indirect effect via activation of other caspases or proteases by caspase-1. To prove that caspase-1 directly cleaved TRIF, we purified recombinant TRIF expressed in HEK cells with the FLAG epitope tag. The previous report that suggested TRIF was a substrate for caspase cleavage identified the aspartic acid residues at positions 281 (VAP<u>D</u>A) and 289 (GLP<u>D</u>T) of the human sequence as essential for caspase-mediated cleavage (Rebsamen et al., 2008). Mutation of both of these residues to glutamic acid residues (D281E D289E) effectively abolished caspase cleavage. Murine TRIF has similar well conserved caspase-1 cleavage sites at positions 286 (ILP<u>D</u>A) and 292 (AAP<u>D</u>T). We thus additionally purified recombinant FLAG-tagged D281E D289E TRIF from HEK cells. The purified proteins were then incubated with recombinant activated human caspase-1. This cleaved the WT TRIF but not the D281E D289E mutant. Thus, caspase-1 directly cleaves TRIF (Fig 4-8).
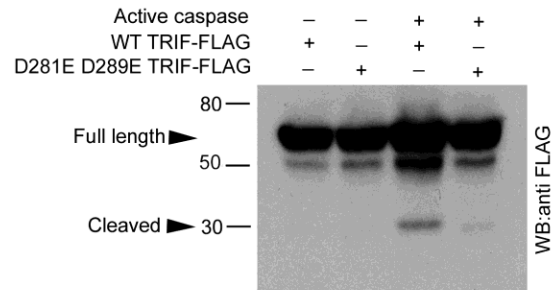
Figure 4.8; Caspase-1 is required for the generation TRIF cleavage products.

HEK cells were transfected with WT TRIF-FLAG, and D281E D289E TRIF-FLAG plasmids. Purified recombinant TRIF proteins as shown incubated with active caspase-1 as shown and analysed by Western blot for the FLAG epitope.

4.2.3 Prevention of TRIF Cleavage by Caspase-1 Augments Autophagy

To confirm that the cleavage products we observed in pervious figures were truly derived from TRIF, we expressed FLAG-tagged human TRIF within BMDMs. Following infection with PA103ΔUΔT, we again saw the appearance of a cleaved product of molecular weight ~ 30kDa (Fig 4-9). This was not seen following infection with the T3SS defective mutant strain PA103pcrV⁻ that does not activate the inflammasome. Moreover, mutation of the sites previously identified as essential to TRIF cleavage by caspases also inhibited the production of the cleaved products following infection (cells transfected with plasmid expressing D281E D289E TRIF-FLAG) (Fig 4-9) .

We noted in these experiments that although TRIF was cleaved, the levels of full-length TRIF were not significantly diminished. We hypothesised that cleavage of TRIF would generate products that could exert a dominant negative effect and thus inhibit TRIF function as previously described (Yamamoto et al., 2002). To test this hypothesis, we cloned the segments of TRIF encoding the N terminal (amino-acids 1 - 281) and C terminal (amino-acids 290 – 712) that are generated by caspase-1 cleavage and expressed these in BMDMs. Expression of both the N and C terminal fragments individually and together potently inhibited the induction of autophagy following infection (Fig 4-10), even at low levels of expression. The two fragments also inhibited the induction of *Ifnb* mRNA induction in BMDMs following treatment with the TLR3 agonist polyI:C (Fig 4-11). Thus, caspase-1 cleavage of TRIF generates products that inhibit TRIF induction of autophagy and *Ifnb* gene expression.

Proteolytic cleavage of TRIF prevents it functioning normally. Thus, cells expressing the D281E D289E TRIF-FLAG that is not cleaved by caspase-1 should have enhanced TRIF functions under conditions where caspase-1 is active compared to cells expressing the WT TRIF. To test this hypothesis, we transfected BMDMs with WT TRIF-FLAG or D281E D289E TRIF-FLAG and then followed the progress of autophagy within these cells after infection with the PA103ΔUΔT strain of *P. aeruginosa*. This strain will activate the inflammasome, leading to capsase-1 cleavage and inactivation of TRIF. Since TRIF is an essential intermediate in initiating autophagy following *P. aeruginosa* infection, prevention of its cleavage by caspase-1 should lead to increased autophagy. We tested this directly by infecting BMDMs transfected with either WT TRIF or the non-cleavable D281E D289E TRIF construct. When cells were transfected with the D281E D289E TRIF construct we observed an increase in the degree of autophagy, as assayed by increased amounts of LC3 II (Fig 4-12), increased number of LC3 containing puncta (Fig 4-13), increase in intracellular LC3 II staining on flow cytometry, and increase in the degree of induction of the *Lc3b* mRNA (Fig 4-14). This was under conditions where the expression level of the different TRIF proteins was identical (Fig 4-9).

Previous study of the TRIF fragments generated by caspase cleavage clearly demonstrated that the D281E D289E mutant TRIF had completely normal signal-transducing functions (Rebsamen et al., 2008). We tested the effects of expression of the D281E D289E mutant TRIF on *Ifnb* expression induced by PolyI:C (Fig 4-15). Expression of the mutant did not affect TLR3 signal transduction; additionally, no cleavage of TRIF was seen in response to PolyI:C which does not activate the inflammasome

when added extracellularly (Rajan et al., 2010). Thus, the effects of the mutant non-cleavable TRIF are not due to effects on over all TRIF function.

Similarly, infecting human THP-1 cells transfected with either WT TRIF or the non-cleavable D281E D289E TRIF construct. When cells were transfected with the D281E D289E TRIF construct we observed an increase in the degree of autophagy, as assayed by increased amounts of LC3 II (Fig 4-16). Thus, capsase-1 activation leads to TRIF cleavage, which partially inhibits the pathway leading to autophagy following infection.
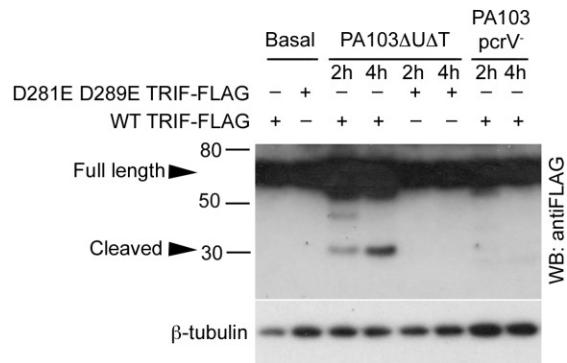
Figure 4.9; Effect of mutant Caspase-1 cleavage site on TRIF cleavage following *P. aeruginosa* infection.

Cells were transfected with plasmids encoding FLAG-tagged WT TRIF or with the indicated mutations, and then left uninfected (Basal), or infected for the indicated times with the *P. aeruginosa* strains as shown (MOI 25). Western blot was probed with anti-FLAG antibody. β -tubulin western blot is shown as loading control. (Experiment repeated three times).
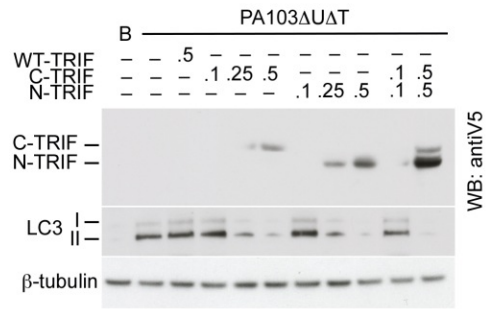
Figure 4.10; Dominant negative effect of TRIF cleavage inhibits autophagy following *P. aeruginosa* infection.

BMDMs transfected with indicated amounts of TRIF expression plasmids (µg) and left uninfected (B) or infected as shown. Panel shows cell lysates blotted for V5 (epitope tag for TRIF) and LC3; β-tubulin shown as loading control.
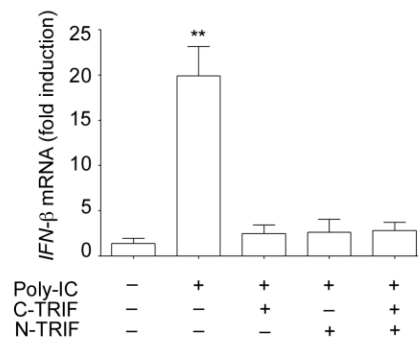
Figure 4.11; TRIF N and C fragments inhibit induction of *Ifnb* mRNA following treatment with TLR3 agonist PolyI:C.

Levels of *Ifnb* mRNA assayed by RT-PCR following PolyI:C treatment and transfection with TRIF constructs as shown. Columns are means of triplicates; error bars sem. ** significantly different from untreated (p<0.01).
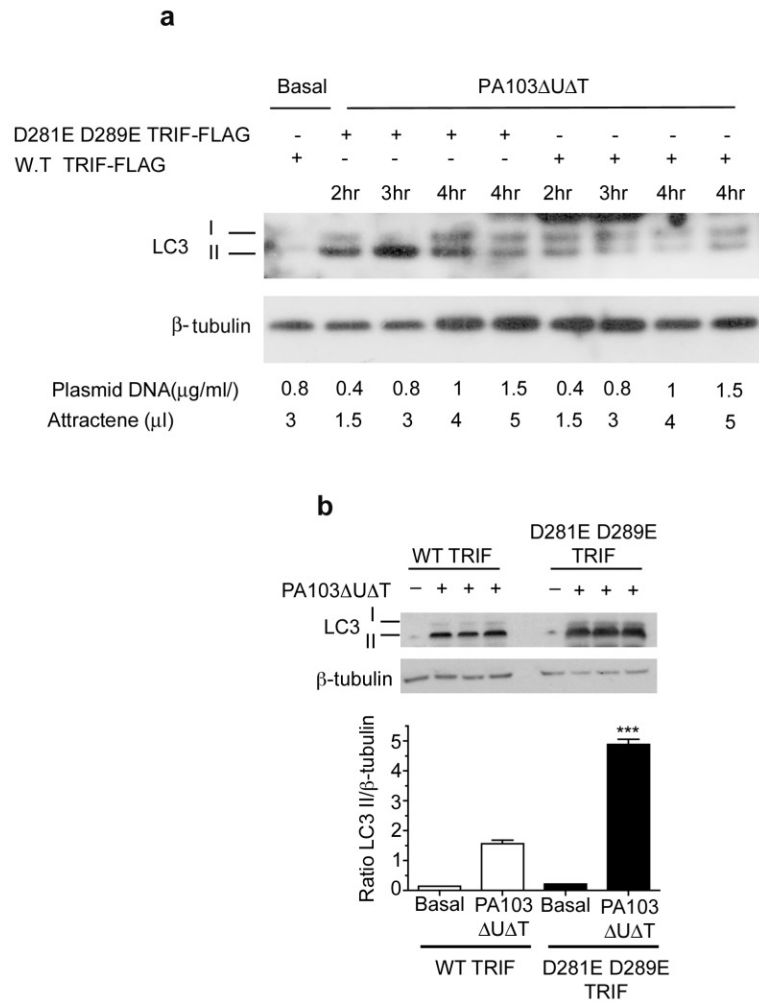
Figure 4.12; Effect of inhibiting TRIF cleavage on the level of LC3-II following *P. aeruginosa* infection.

a, Western blot analysis of LC3 I and II levels. BMDMs cells transfected with the indicated amounts of plasmids (in µg), using Attractene (in µl). Cells were left uninfected or infected with *P. aeruginosa* strain as indicated (MOI 25). b, BMDMs transfected with plasmids encoding FLAG-tagged WT TRIF or with the indicated mutations (0.8µg), using Attractene(3µl). Cells were infected as shown (4h, MOI 25) and assayed for LC3 I and II levels by Western blot (upper panel). Lower panel shows LC3/β-tubulin ratio for 3 independent experiments under the indicated conditions. Columns show means; error bar is SEM. ***, significantly different from infected cells transfected with WT TRIF, p < 0.001.
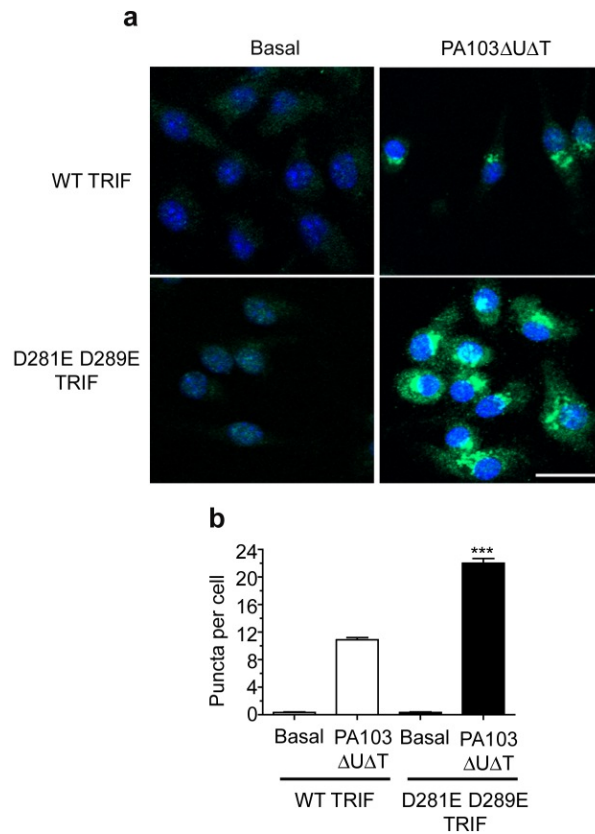
Figure 4.13; Inhibiting TRIF cleavage increases formation of autophagosomes following *P. aeruginosa* infection.

BMDMs transfected with plasmids encoding FLAG-tagged WT TRIF or with the indicated mutations. Cells were infected as indicated for 4 hrs. (MOI 25). **a**, Representative immunofluorescence images of LC3 in BMDMs left uninfected (Basal), or infected with *P .aeruginosa* strain PA103ΔUΔT . Cells were stained with DAPI to visualize nuclei (blue), and LC3 staining is shown as green. Scale bar 10 μm. **b**, LC3 puncta quantified in BMDMs transfected with indicated constructs and infected as shown (4hrs, MOI 25). ***, significantly different from infected cells transfected with WT TRIF, p < 0.001.
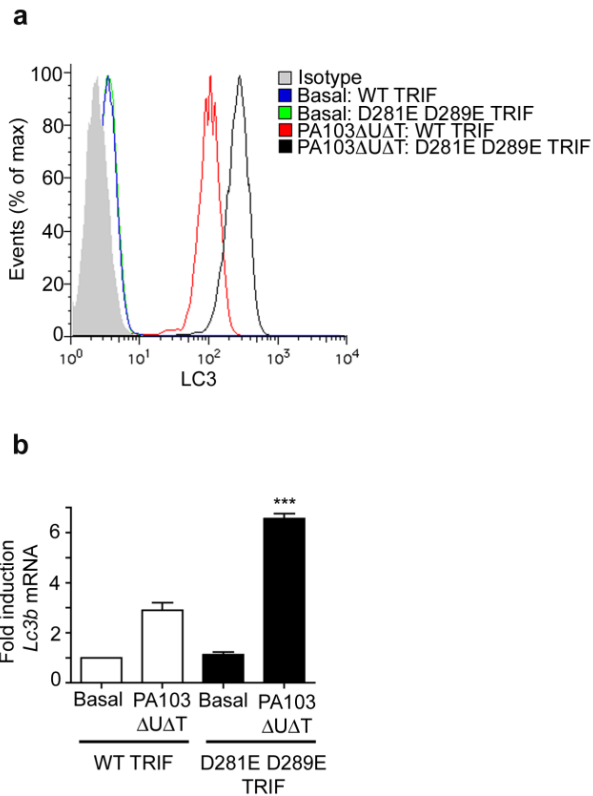
a, Intracellular LC3 II levels assayed by flow cytometry in cells transfected with indicated plasmids and left uninfected (Basal) or infected as indicted (4h, MOI 25)**b**, Levels of *Lc3b* mRNA with conditions as in **a** . ***, significantly different from infected cells transfected with WT TRIF, p < 0.001.
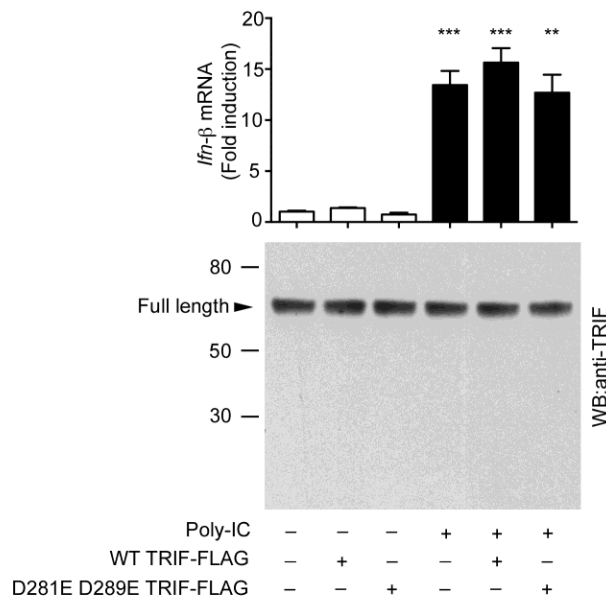
Figure 4.15; Non-cleavable TRIF mediated normal signal transduction after PolyI:C treatment.

BMDMs were treated with PolyI:C (1µg/ml for 5 hours) after transfection with TRIF constructs as shown. Levels of *Ifnb* mRNA were measured by RT-PCR; columns are means of triplicates; error bars are sem. *** and **, significant different from unstimulated cells, $p<0.001$ and 0.01 respectively. Differences between the results in the presence of PolyI:C were not significantly different from one another. Western blot shows TRIF following the same treatment as indicated.

a

PA103ΔUΔT

			4h	4h	4h	4h
WT TRIF-FLAG	0	.8	.4	.8	0	0
D281E D289E TRIF-FLAG	.8	0	0	0	.4	.8

WB: antiFLAG

Full length ► 80 — 50 —

Cleaved ► 30 —

β-tubulin

b

	Basal		PA103ΔUΔT	
WT TRIF-FLAG	+	-	+	-
D281E D289E TRIF-FLAG	-	+	-	+

LC3 I — II —

β-tubulin
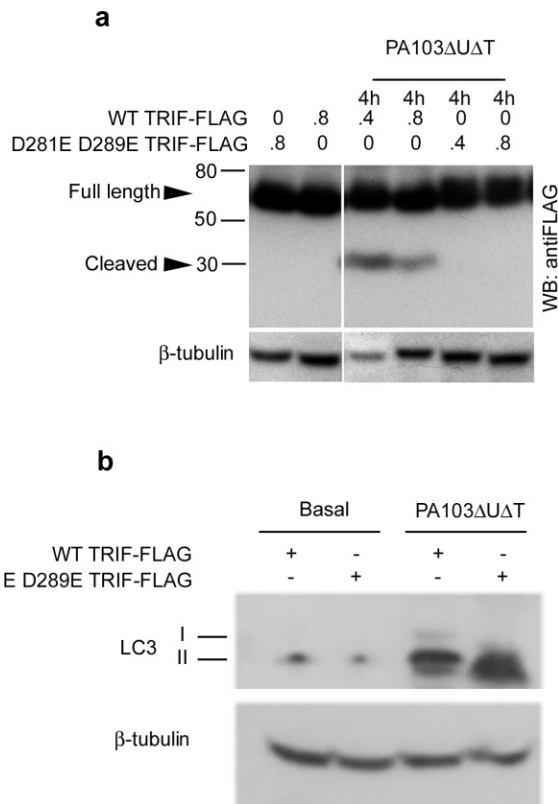
Figure 4.16; Inhibiting TRIF cleavge increases autophagy markers in human THP-1 cells.

a, Human THP-1 cells transfected with the indicated amounts of plasmids (in µg) were left uninfected or infected as shown (4h, MOI 25) and probed with antibody to FLAG. Experiment performed on two occasions with same results. **b**, THP-1 cells were transfected with plasmids encoding FLAG-tagged WT TRIF or with the indicated mutations (0.8µg), using Attractene(3µl). Cells were infected as shown (4h, MOI 25) and assayed for LC3 I and II levels by Western blot.

4.2.4 TRIF Cleavage by Capsase-1 Down-regulates Induction of Type I IFNs Following P. aeruginosa infection.

Next, we tested whether preventing TRIF cleavage by caspase-1 would lead to upregulation of other pathways mediated by TRIF following *P. aeruginosa* infection. Activation of TLR4 leads to induction of the type I IFNs via TRIF; type I IFN production plays a number of important roles in bacterial infection (Kelly-Scumpia et al., 2010). Firstly we showed that *P. aeruginosa* infection led to induction of IFN-β mRNA in BMDMs. Consistent with down-regulation of this pathway by caspase-1 activation, we found that the T3SS mutant PA103pcrV⁻ produced greater levels of *Ifnb1* mRNA compared to the T3SS competent PA103 ΔUΔT strain (Fig 4-17). In both cases, knockout of TRIF led to marked inhibition of *Ifnb1* mRNA induction, confirming that TRIF plays an essential role in the induction of type I IFNs following *P. aeruginosa* infection (Fig 4-17).
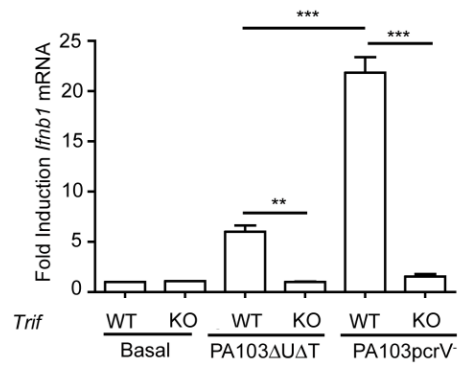
Figure 4.17; Role of TRIF in induction of type I IFNs following *P.aeruginosa* infection.

Quantitative RT-PCR levels of *Ifnb1* in BMDMs Cells from (WT) or *Trif* (KO) and left uninfected (Basal) or infected as shown (4h MOI 25). ***, shows significant difference between the pairs of values, p < 0.001.

We then investigated whether inhibition of caspase-1 activation following *P. aeruginosa* infection would lead to increased induction of *Ifnb1* mRNA. Inhibiting caspase-1 by chemical inhibition (Fig 4-18a) and by knock down of the caspase-1 gene by siRNA (Fig 4-18b) both led to a significant rise in the levels of *Ifnb1* mRNA following infection. Additionally, blocking inflammasome activation by raising extracellular K^+ concentration also led to increased *Ifnb1* mRNA induction (Fig 4-18c). These results support the conclusion that caspase-1 activation via the inflammasome leads to down-regulation of type I IFN induction by the proteolytic degradation of TRIF.

We confirmed this conclusion by comparing the degree of *Ifnb1* mRNA induction after infection in BMDMs transfected either with WT TRIF or the non-cleavable D281E D289E mutant TRIF. As shown in (Fig 4-19), in cells expressing the non-cleavable TRIF mutant, the levels of *Ifnb1* mRNA induced following infection were significantly increased. Thus, caspase-1 activation by the inflammasome leads to a reduction in TRIF activity and hence inhibition of the induction of type I IFNs.
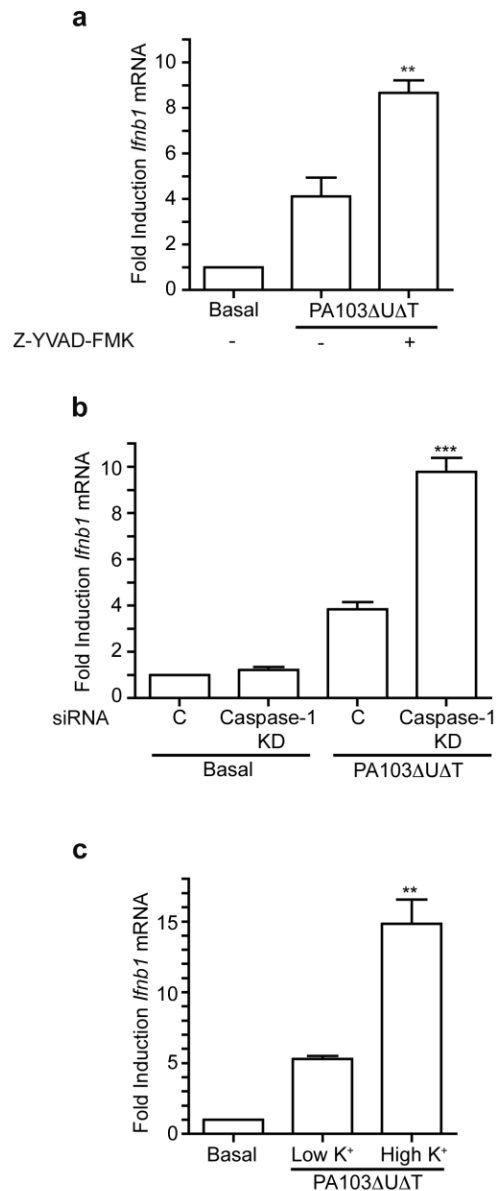
Figure 4.18; Inhibition of Caspase-1 increases induction of type I IFNs following _P.aeruginosa_ infection.

Quantitative RT-PCR levels of _Ifnb1_ in BMDMs **a,** cells infected as shown (4h MOI 25) in the absence (–) or presence (+CI) of the caspase-1 inhibitor Z-YVAD-FMK. **, significantly different from untreated, $p < 0.01$. **b,** cells transfected with control siRNA (C) or with siRNA specific for _Caspase-1_ and infected as in **a**. ***, significantly different from control siRNA, $p < 0.001$. **c,** cells infected as in **a** under conditions of low and high K^+. **, significantly different from low K^+, $p < 0.01$.
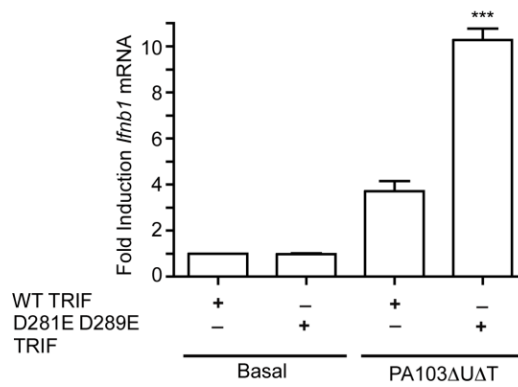
Figure 4.19; Inhibiting TRIF cleavge increases induction of type I IFNs following
***P.aeruginosa* infection.**

Quantitative RT-PCR levels of *ifnb1* mRNA in BMDMs cells transfected with the
constructs as shown and left uninfected (basal) or infected with PA103ΔUΔT (4h, MOI
25). ***, significantly different from WT TRIF, p < 0.001.

4.2.5 Functional Effects of TRIF Inactivation by Caspase-1 in BMDMs

Type I IFNs increase the phagocytic activity of macrophages as well as their production of reactive oxygen intermediates, both important in host defence against bacteria. We thus set out to determine whether the reduction in type I IFN induction resulting from caspase-1 cleavage of TRIF had such functional effects. We measured phagocytic activity of BMDMs by uptake of a tagged *E. coli* that only gave a fluorescent signal on trafficking to an acidic lysosomal compartment, and reactive oxygen production by another fluorescent probe, CellROX Deep Red. Firstly, we compared phagocytosis and production of reactive oxygen intermediates following infection of BMDMs with the T3SS competent strain of *P. aeruginosa* PA103ΔUΔT compared to the T3SS defective strain PA103pcrV⁻. This showed that PA103ΔUΔT led to less phagocytosis and lower production of reactive oxygen intermediates following infection compared to the PA103pcrV⁻ strain (Fig 4-20). This is consistent with the reduced levels of type I IFNs resulting from inflammasome activation by the T3SS competent strain and hence capsase-1 cleavage of TRIF. Importantly, adding β-IFN back to the BMDMs infected with the T3SS competent PA103ΔUΔT strain restored the level of phagocytosis and reactive oxygen production to the levels seen with the T3SS defective PA103pcrV⁻ strain (Fig 4-20). Thus, the defect in phagocytosis and production of reactive oxygen observed in the strain of *P. aeruginosa* that activates capsase-1 could be corrected by addition of a product normally produced via TRIF mediated signalling.
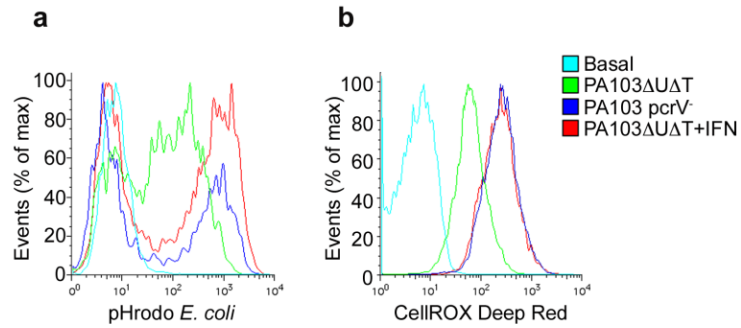
Figure 4.20; Type I IFNs is required for phagocytosis and intracellular killing of *P.aeruginosa* .

a, amount of phagocytosed *E. coli* particles (pHrodo *E. coli*; and **b** reactive oxygen (CellROX) Deep Red as assayed by Flow cytometry. BMDMs pre-treated with IFN (10ng/ml) and then infected as indicated (3h, MOI 25) or left uninfected (Basal).

To establish that the reduction in these macrophage functions was due to caspase-1 degradation of TRIF, we tested the effect of knocking down both TRIF and caspase-1 on phagocytosis and production of reactive oxygen. When TRIF levels were reduced by siRNA, the ability of BMDMs to perform these functions was markedly reduced (Fig 4-21a, and b). This inhibitory effect was reversed by the addition of β-IFN, demonstrating the importance of TRIF-mediated production of this cytokine in enhancing phagocytosis and production of reactive oxygen. Knock down of caspase-1 enhanced the ability of BMDMs to phagocytose and produce reactive oxygen following *P. aeruginosa* infection (Fig 4-21c, and d). This enhancement in these functions was similar to that seen following the addition of β-IFN to BMDMs infected with the inflammasome activating *P. aeruginosa* strain PA103ΔUΔT (Fig 4-21c, and d). Taken together, these results support the conclusion that caspase-1 mediated proteolysis of TRIF following *P. aeruginosa* infection of BMDMs leads to down regulation of IFN-β production and reduction in phagocytosis and reactive oxygen production.
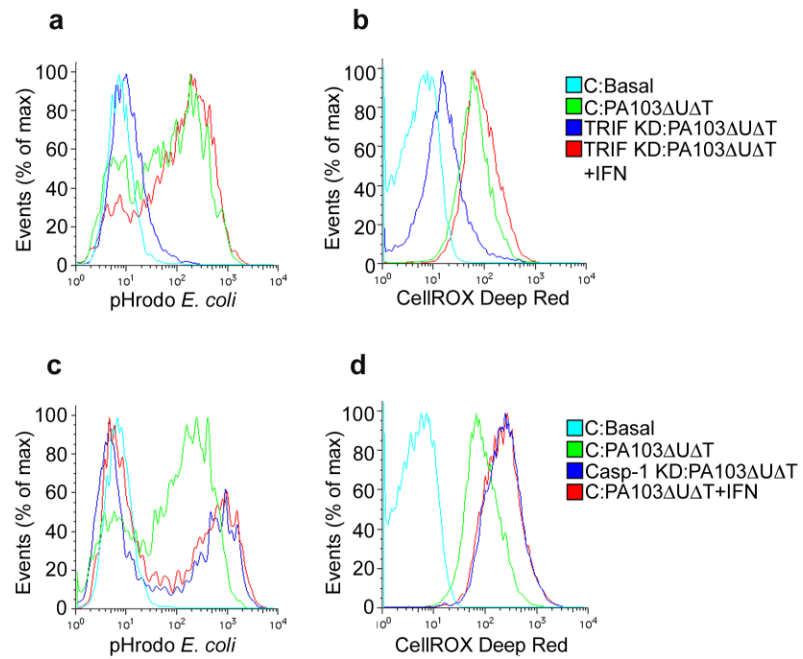
Figure 4.21; TRIF cleavage reduces type I IFN mediated increases in phagocytosis and generation of reactive oxygen intermediates.

a and **c** phagocytosed *E. coli* particles (pHrodo *E. coli* and **b** and **d** reactive oxygen (CellROX) Deep Red as assayed by Flow cytometry. Cells were treated with control (C) siRNA or specific siRNA as shown (KD). Where indicated, cells were pre-treated with IFN-β (IFN) (10ng/ml) and then infected as indicated (3h, MOI 25) or left uninfected (Basal).

To confirm that the cleavage of TRIF was responsible for the down-regulation of phagocytosis and reactive oxygen production following caspase-1 activation, we examined these functions in BMDMs transfected with wild-type and non-cleavable TRIF (D281E D289E TRIF). Compared to cells transfected with wild-type TRIF, BMDMs transfected with the D281E D289E TRIF had higher levels of phagocytosis and reactive oxygen production (Fig 4-22a, and b). Again, we could increase the lower levels seen in cells expressing wild-type TRIF by addition of β-IFN. Thus, by preventing TRIF cleavage by caspase-1, we could augment the ability of BMDMs to phagocytose *E. coli* particles and produce reactive oxygen intermediates through TRIF-mediated β-IFN production.
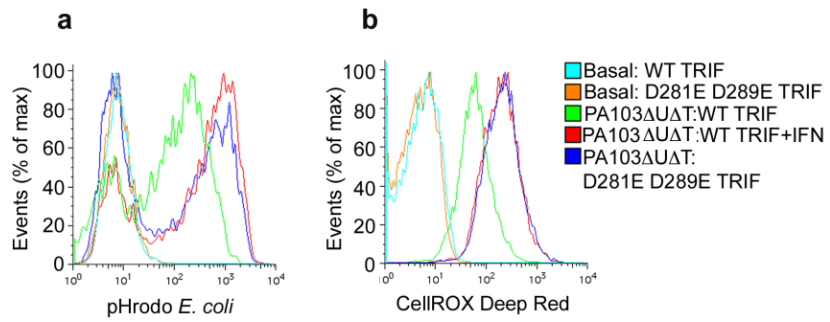
Figure 4.22; Inhibiting TRIF cleavge increases phagocytosis and intracellular killing of *P.aeruginosa* .

a, phagocytosed *E. coli* particles (pHrodo *E. coli* and **b** reactive oxygen (CellROX) Deep Red as assayed by Flow cytometry. Cells were transfected with plasmids encoding the TRIF constructs as shown. Cells were pre-treated with IFN-β (IFN) (10ng/ml) and then infected as indicated (3h, MOI 25) or left uninfected (Basal).

We determined the numbers of viable internalised *P. aeruginosa* in BMDMs following infection to gauge the net result of both phagocytosis and intracellular killing. Knock down of TRIF led to an increase in the numbers of viable intracellular PA103ΔUΔT; this could be reversed by the addition of β-IFN (Fig 4-23a). This suggests that under these conditions the reduction in reactive oxygen resulting from TRIF knock down is more significant than the reduction in phagocytosis, hence leading to an increase in the numbers of internalised viable bacteria. Inhibiting TRIF breakdown by adding inhibitors of caspase-1 or knock down by siRNA led to a reduction in the numbers of viable internalised bacteria (Fig 4-23b, and c). This was again consistent with the predominant effect of inhibiting TRIF function being to reduce the ability of BMDMs to kill intracellular bacteria. The reduction in viable intracellular bacteria consequent to inhibition or knock down of caspase-1 was reproduced by treating the BMDMs with β-IFN (Fig 4-23b, and c). Finally, we examined the numbers of viable intracellular bacteria recovered after infection in BMDMs transfected with expression vectors for either the WT or the non-cleavable D281E D289E TRIF. In the presence of the non-cleavable TRIF, fewer viable intracellular bacteria were recovered compared to cells expressing the WT TRIF protein (Fig 4-23d). This reduction in viable internalised bacteria could be reproduced in cells expressing WT TRIF by treatment with β-IFN. Thus, taken together, these data suggest that the caspase-1 mediated cleavage of TRIF leads to a reduction in β-IFN production that result in an increase in the numbers of viable *P. aeruginosa* following infection of BMDMs.
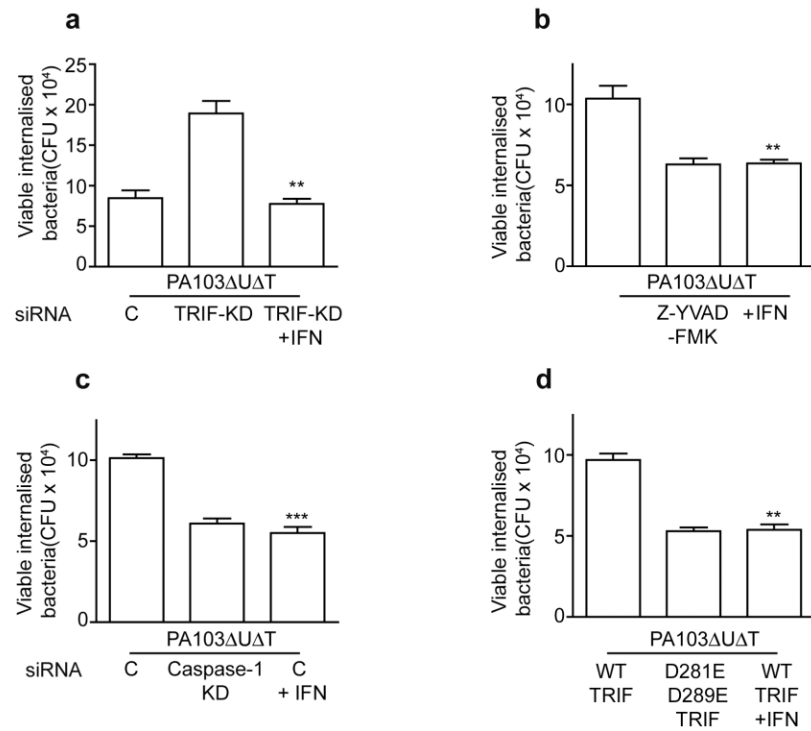
Figure 4.23; Bactericidal assay of infected BMDMs with *P.aeruginosa*.

Panels show numbers of viable internalized bacteria 3h after infection with PA103ΔUΔT (MOI 25) with the indicated treatments. Columns are means of triplicate determinations; error bars are SEM. Differences with IFN addition were significantly different, ** $p < 0.01$, *** $p < 0.001$.

4.2.6 Effect of caspase-1 TRIF cleavage on infection with P.aeruginosa in vivo

These data from macrophages in culture show important functional effects of TRIF cleavage but do not evaluate the total effect of this process on the cytokine responses and bacterial killing in an infectious process. Thus, we evaluated the effects of Caspase-1 TRIF cleavage on the cytokine responses and bacterial killing in an *in vivo* model of infection. We utilized an acute intraperitoneal model of *P. aeruginosa* infection in mice. Firstly, we evaluated the effects of inhibiting Caspase-1 activity in infection by intraperitoneal administration of ZYVAD-FMK. In this model, inhibition of caspase-1 led to reduced serum levels of IL-1β as expected with no reduction in TNF (Fig 4-24a). In cells harvested from the peritoneum 6 hours following infection (predominantly neutrophils), there was an increase in the level of lipidated LC3 in animals treated with the caspase-1 inhibitor (Fig 4-24a). The treated animals had a significant reduction in the numbers of viable bacteria recovered from the peritoneum (Fig 4-24a). These data suggest that the decreased IL-1β production and increased autophagy produced by caspase-1 inhibition results in increased bacterial clearance.

As a more direct test of the effect of preventing Caspase-1 mediated TRIF cleavage during infection, we set up the following animal model. We depleted intraperitoneal macrophages by instillation of liposomal clodronate (Fig 4-24b). We then re-introduced macrophages transfected with expression plasmids for either wild type TRIF or the D281E D289E mutant; these were loaded with a fluorescent dye to allow subsequent identification using flow cytometry. Animals were then infected with *P. aeruginosa* by the

intraperitoneal route. 6 hours following infection, we harvested serum and peritoneal contents. Autophagy within the introduced transfected macrophages was measured by flow cytometric measurement of intracellular LC3 II (Fig 4-24c and d). This showed that macrophage autophagy was increased following infection *in vivo,* and that macrophages expressing the non-cleavable TRIF mutant showed increased levels of autophagy compared to the wild type protein. Interestingly, animals populated with macrophages expressing the non-cleavable D281E D289E mutant TRIF had lower serum IL-1β levels compared to those populated with macrophages expressing wild type TRIF; TNF levels were the same (Fig 4-24d). Expression of the non-cleavable TRIF was also associated with significantly lower intraperitoneal protein concentrations and viable bacterial counts (Fig 4-24d). Thus, in this model, preventing TRIF cleavage results in increased autophagy following infection that is associated with reduced IL-1β production but decreased numbers of viable intraperitoneal bacteria. This suggests autophagy may well control NLRC4 inflammasome activation following *P. aeruginosa* infection as has been found for NLRP3 inflammasome activation (Saitoh et al., 2008).
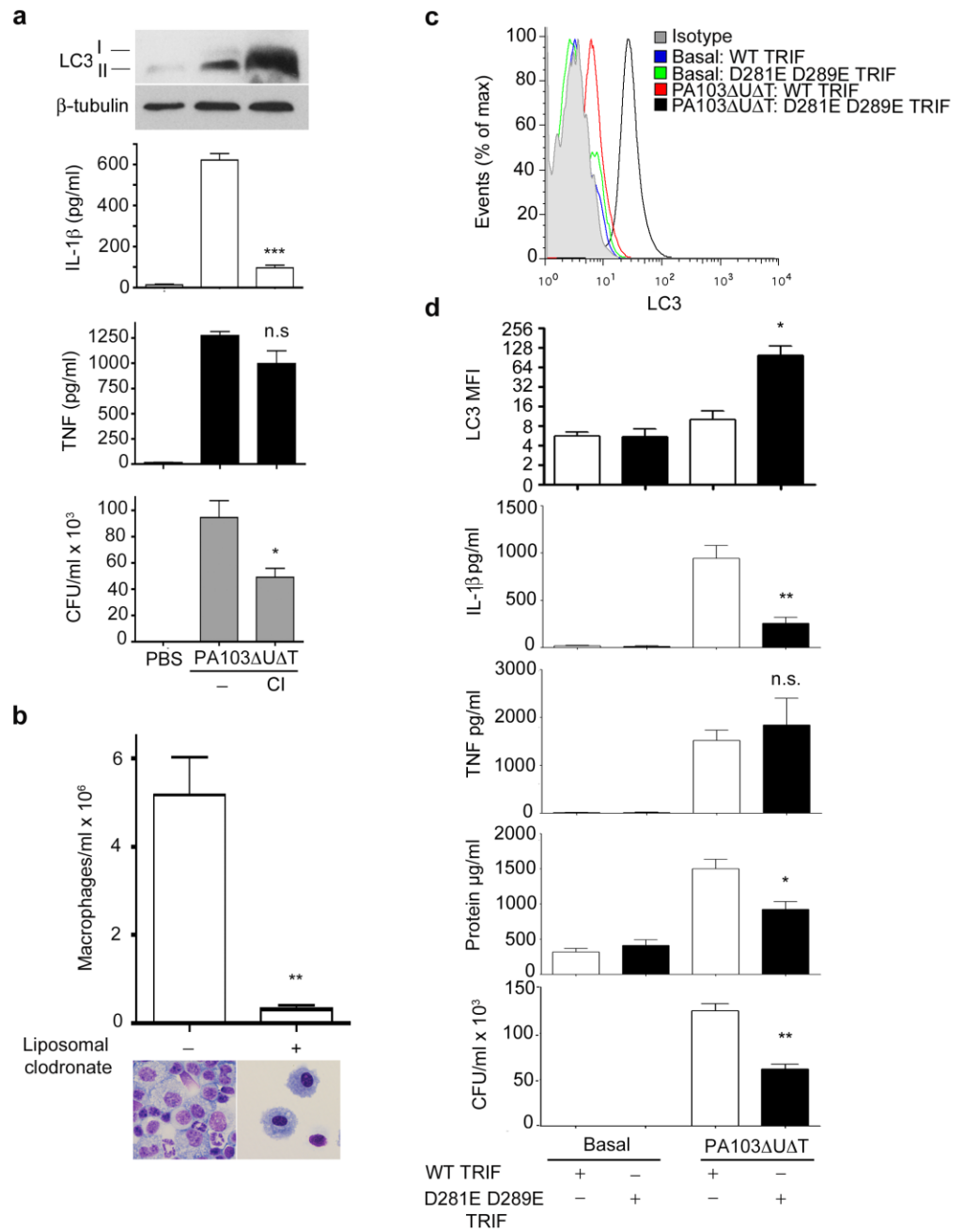
Figure 4.24; Role of TRIF cleavage by caspase-1 in an *vivo* infection model.

a, Mice were infected with *P. aeruginosa* ip or treated with PBS. Panels show LC3 immunoblot with loading control of total cell extract from one representative animal, mean levels of serum IL-1β and TNF (n = 3, error bars are SEM) and recovered viable bacteria

from the peritoneal cavity at 6h (n=3, error bars SEM). Animals were pre-treated with Z-YVAD-FMK (CI) as shown). * and *** are significant differences from untreated animals, p <0.05 and p < 0.001 respectively. **b,** Peritoneal macrophage population in animals treated with liposomal clodronate as shown. Columns are means of three determinations; error bars are SEM. **,** significantly different from control (p < 0.01). **c** and **d** show results from animals infected ip following depletion of intraperitoneal macrophages and reconstitution with macrophages transfected as shown. **c,** Levels of intracellular LC3 II assayed by flow cytometry, gated on introduced macrophage populations, transfected with constructs as shown. Representative plot from one animal. **d,** Panels show mean values of indicated measures from n=3 animals, error bars are SEM. Values are of LC3 II mean fluorescence intensity (LC3 MFI), serum IL-1β and TNF, peritoneal protein concentration, and recovered viable bacterial colonies (CFU/ml x 10^3). Peritoneal macrophages were transfected with constructs as shown before repopulation of the peritoneal cavity.

4.2.7 Effect of Caspase-1 TRIF Cleavage on Activation of the NLRP3 Inflammasome

We wished to extend our observations to other situations where TRIF cleavage by caspase-1 could have important effects. Recently, activation of the NLRP3 inflammasome has been shown to be triggered by mitochondrial damage (Nakahira et al., 2011). This activation is limited by autophagy of mitochondria – mitophagy – which by limiting release of mitochondrial DNA into the cytoplasm acts to inhibit NLRP3 inflammasome activation. We reasoned, therefore, that caspase-1 mediated inactivation of TRIF would limit mitophagy and thus could act to enhance NLRP3 activation, leading to greater capsase-1 activation and production of IL-1β. To test this hypothesis, we examined the effects of limiting TRIF cleavage by casapse-1 in BMDMs stimulated with LPS and ATP, which is a potent stimulus to NLRP3 inflammasome activation. We transfected BMDMs with expression vectors encoding either WT TRIF or the D281E D289E TRIF mutant that is resistant to caspase-1 cleavage. Following LPS/ATP stimulation, we observed increased levels of caspase-1 p10 and secreted IL-1β as expected in the BMDMs transfected with WT TRIF (Fig 4-25). This was associated with cleavage of TRIF as we have observed with inflammasome activation by *P. aeruginosa*. We also found that the LPS stimulus increased autophagy, as we have previously observed in these cells (Fig 4-1). In the cells transfected with the D281E D289E TRIF mutant that is resistant to caspase-1 cleavage, we observed an increase in levels of the LC3 II isoform following LPS/ATP stimulation, indicative of increased autophagy (Fig 4-25), a marked increase in the numbers of LC3 containing vacuoles, and increased intracellular staining of LC3 as assayed by flow

162

cytometry (Fig 4-26). We also observed a marked reduction in inflammasome activation and secretion of IL-1β (Fig 4-25), but not TNF. Thus, a highly significant effect of the caspase-1 induced cleavage of TRIF is to inhibit on going autophagy that otherwise would severely limit the degree of inflammasome activation and resultant IL-1β produced.
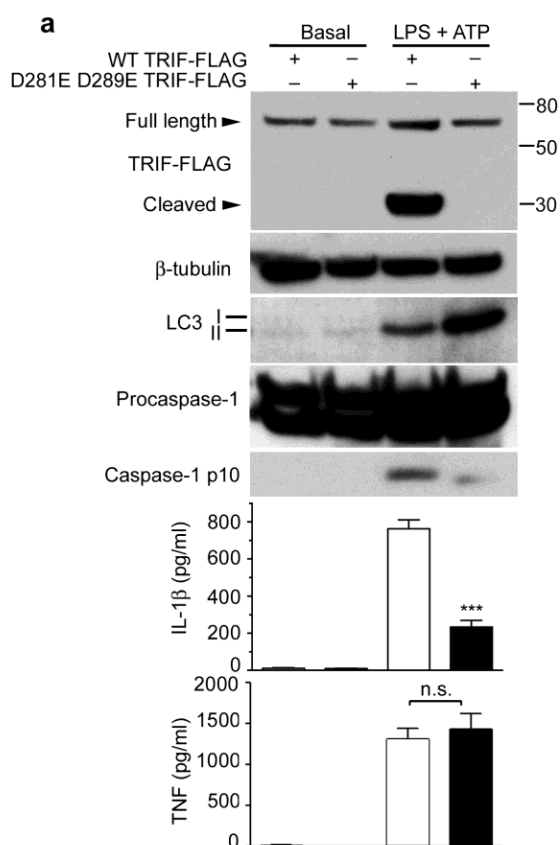
Figure 4.25; Effect of Inhibition of TRIF cleavge on NLRP3 activation following treatment with LPS+ATP.

BMDMs were transfected with plasmids expressing WT TRIF or the D281E D289E mutant as shown. Cells were left untreated (Basal) or LPS (500 ng/ml) was added for 4 hours followed by 5 mM ATP for 20 minutes where indicated (LPS + ATP). Western blot of the indicated proteins are shown. The bottom panel shows the levels of secreted Il-1β and TNF from the same cells as used in the Western blot with the treatments as indicated. Each column is mean of 3 determinations; error bars are SEM. Filled columns are results from cells transfected with the non-cleavable TRIF, open columns from WT TRIF. ***, significant from WT, $p < 0.001$.
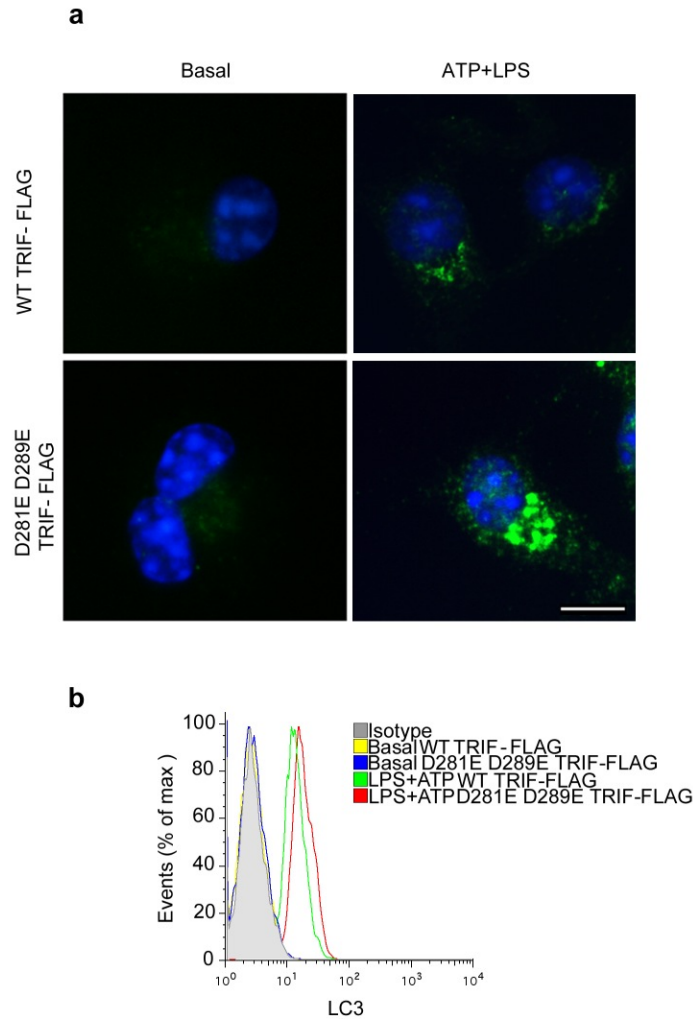
Figure 4.26; Inhibition of TRIF cleavage increases autophagy markers in BMDMs following treated with LPS+ATP.

BMDMs were transfected with plasmids expressing WT TRIF or the D281E D289E mutant as shown. Cells were left untreated (Basal) or LPS (500 ng/ml) was added for 4 hours followed by 5 mM ATP for 20 minutes where indicated (LPS + ATP). **a**, Representative immunofluorescence images of LC3 in BMDMs left untreated (Basal) , or treated with LPA+ATP. Cells were stained with DAPI to visualize nuclei (blue), and LC3 staining is shown as green. Scale bar 10 μm. **b**, Intracellular LC3 II levels assayed by flow cytometry in cells transfected with indicated plasmids and left uninfected (Basal).

We repeated this experiment but additionally down-regulated autophagy by knock down of *Lc3b* or *Atg5* expression using siRNA (Fig 4-27). In cells in which autophagy was inhibited, the amount of secreted IL-1β and caspase-1 activation in the presence of WT TRIF was significantly increased compared to cells transfected with control siRNA (Fig 4-27). This is consistent with autophagy down-regulating the signals required to trigger NLRP3 inflammasome activation and secretion of IL-1β in response to LPS + ATP. In cells expressing the D281E D289E mutant TRIF with inhibition of autophagy by *Lc3b* or *Atg5* knockdown, although there was a reduction in secreted IL1-β, this did not reach statistical significance compared to cells expressing WT TRIF (Fig 4-27). This is consistent with the conclusion that the reduction in secreted IL-β in the presence of TRIF that cannot be cleaved by caspase-1 is as a result of an increase in auto- and mitophagy that acts to attenuate the triggering of the NLRP3 inflammasome by LPS + ATP. Prevention of TRIF cleavage results in increased type I interferon production in infection; this has been shown to suppress NLRP3 inflammasome activation principally through an IL-10 mediated down-regulation of pro-IL-1β levels (Guarda et al., 2011) as well as an uncharacterised direct effect on the NLRP3 inflammasome that required at least 6 hours treatment. The suppressive effect of the non-cleavable TRIF is evident after 4 hours of LPS/ATP, and we did not observe any changes in pro-IL-1β or pro-caspase-1 levels in treated cells that had been transfected with the mutant D281E D289E non-cleavable TRIF (Fig 4-27). Thus, the observed effects of preventing TRIF cleavage on inhibiting NLRP3 activation by LPS/ATP would seem most likely mediated by the increased levels of autophagy rather than increased type I interferon production,

although some contribution of type I interferon directly inhibiting NLRP3

inflammasome activation cannot be ruled out entirely.
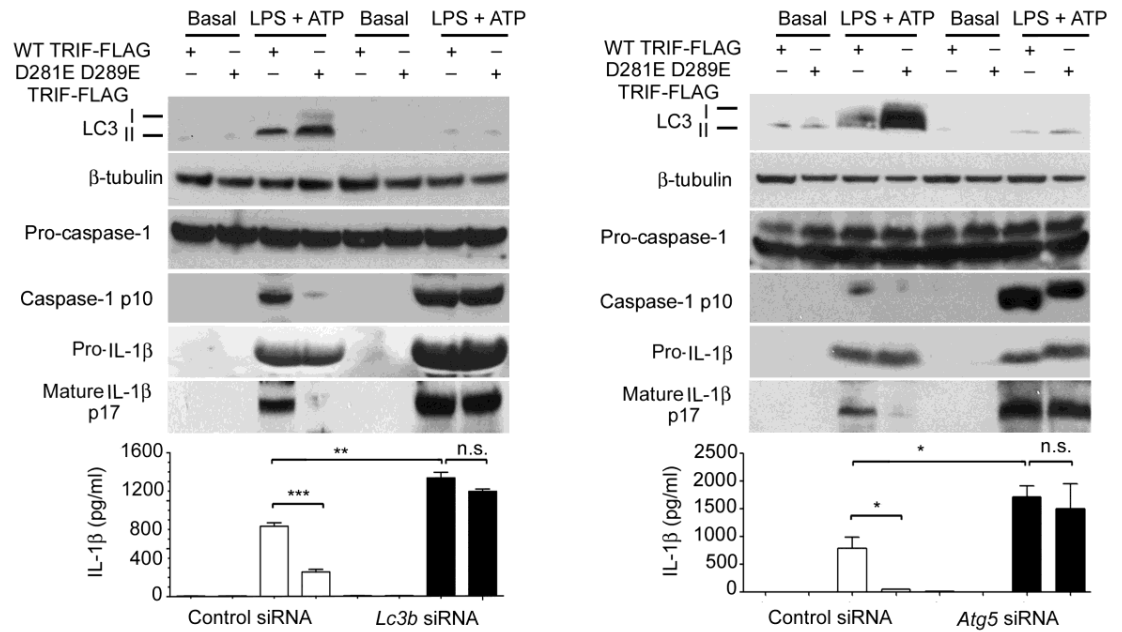
Figure 4.27; Prevention of TRIF cleavage attenuates NLRP3 mediated caspase 1 activation and production of mature IL-1β.

BMDMs were transfected with control siRNA or *lc3b* (left panel), or control or *Atg5* siRNA (right panel). Cells were left untreated (Basal) or LPS (500 ng/ml) was added for 4 hours followed by 5 mM ATP for 20 minutes where indicated (LPS + ATP). BMDMs were transfected with plasmids expressing WT TRIF or the D281E D289E mutant as shown. Western blot of the indicated proteins is shown. The bottom panel shows the levels of secreted IL-1β from the same cells as used in the immunoblotting with the treatments as indicated. Each column is mean of 3 determinations; error bars are SEM. Filled columns are results from cells transfected with the non-cleavable TRIF, open columns from WT TRIF. Statistical differences between bracketed columns are shown: *$p<0.05$, **, $p < 0.01$, *** $p < 0.001$. All experiments repeated 2 times.

Finally, we extended these observations using the human macrophage cell line THP-1 (Fig 4-28). In the presence of the mutant TRIF that cannot be cleaved by caspase-1, LPS + ATP produces less caspase-1 activation, less secreted IL-1β and a greater amount of autophagy as measured by conversion of LC3 to its lipidated type II isoform (Fig 4-28a). We also confirmed the increase in autophagy by measuring the numbers of LC3 puncta within the cells under the different conditions (Fig 4-28b).
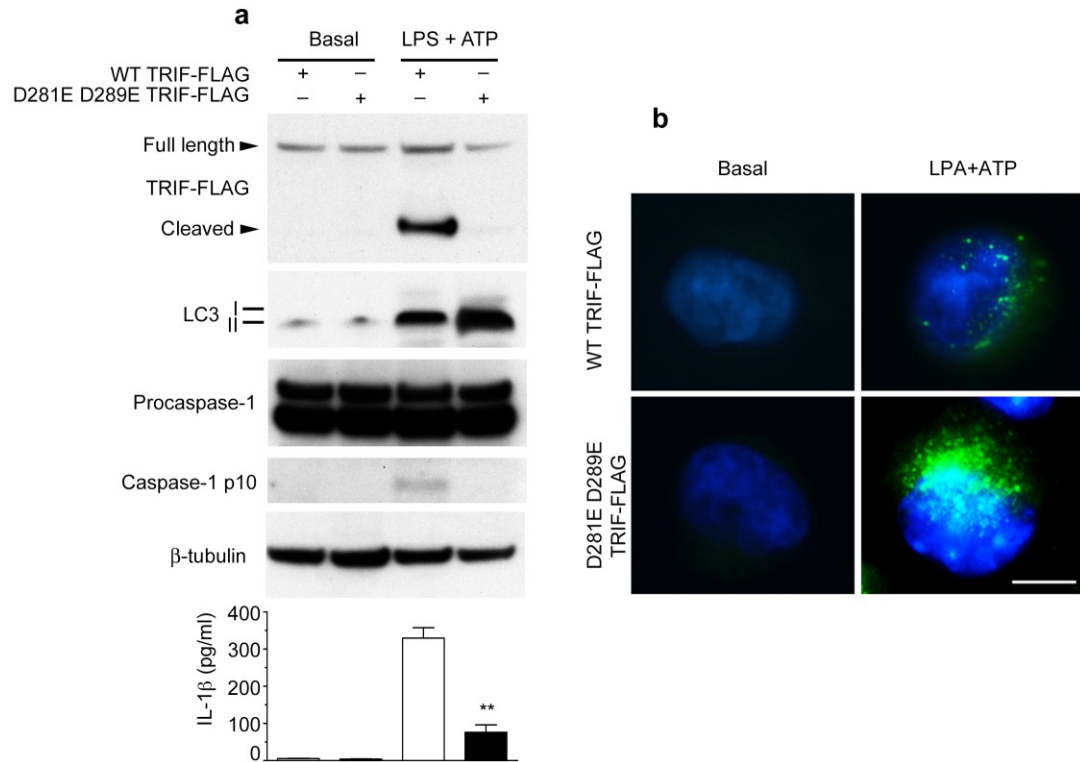
Figure 4.28; Prevention of TRIF cleavage attenuates NLRP3 mediated caspase-1 activation and production of mature IL-1β in THP-1 cells.

a, THP-1 cells were transfected with plasmids expressing WT TRIF or the D281E D289E mutant as shown. Cells were left untreated (Basal) or LPS (500 ng/ml) was added for 4 hours followed by 5 mM ATP for 20 minutes where indicated (LPS + ATP). Western blot of the indicated proteins are shown. The bottom panel shows the levels of secreted Il-1β from the same cells as used in the Western blot with the treatments as indicated. Each column is mean of 3 determinations; error bars are SEM. Filled columns are results from cells transfected with the non-cleavable TRIF, open columns from WT TRIF. **, significant from WT, p < 0.01. **b**, Representative immunofluorescence images of LC3 in THP-1 cells treated as in (**a**). Cells were stained with DAPI to visualize nuclei (blue), and LC3 staining is shown as green. Scale bar 10 µm.

4.3 Discussion

In this chapter, we have shown that activation of caspase-1 by either the NLRP3 or NLRC4 inflammasome leads to proteolytic cleavage of the signalling intermediate TRIF in both murine and human cells. TRIF plays a key role in mediating some of the effects of TLR4 signalling, including the induction of autophagy as well as the production of type I IFNs. By multiple independent methods, we demonstrate that TRIF cleavage leads to a down-regulation of autophagy following infection of BMDMs by *P. aeruginosa* or stimulation via LPS. Additionally, this cleavage of TRIF results in an inhibition of the production of type I IFN. We show that this results in a diminution in phagocytosis and production of reactive oxygen intermediates within BMDMs, and reduced the ability of macrophages to kill intracellular bacteria. In an *in vivo* model of *Pseudomonas aeruginosa* infection, preventing TRIF cleavage augmented bacterial clearance but reduced the production of IL-1β. One additional consequence of the inhibition of autophagy by caspase-1 is to prevent the limiting effect of autophagy on caspase-1 activation, hence leading to greater activation of this protein and increased IL-1β production. Thus, caspase-1 cleavage of TRIF results in multiple effects with significant impact on processes that are central to host defence and inflammation.

The results of TRIF cleavage by caspase-1 have a number of effects on immediate host defence to a pathogen such as *P. aeruginosa*. On the one hand, the reduction in production of type I IFNs results in a diminution in macrophage phagocytosis and production of reactive oxygen. However, we also found that following *in vivo* infection, there was a

reduction in production of IL-1β. This was associated with increased

bacterial clearance, as has been found by others (Cohen and Prince, 2013).

The reduction in IL-1β production following infection with *Pseudomonas*

aeruginosa under condition where TRIF cleavage is blocked, suggest that

autophagy restrains NLRC4 inflammasome activation in this infection, in

much the same way as has been shown for NLRP3 activation. We have

gone to explore this in depth and have found that autophagy does inhibit

NLRC4 inflammasome activation by *Pseudomonas aeruginosa* (chapter 5).

The reduction in auto- and mitophagy consequent to TRIF cleavage

prevents these processes inhibiting NLRP3 caspase-1 activation. If TRIF

were not cleaved in this way, the degree of activation of this inflammasome

would be much less and production of IL-1β significantly reduced. The

magnitude of this effect is large (Figs 4-26, 4-27, and 4-28) and thus we

speculate that this is the principal evolutionary selection pressure that has

maintained the cleavage site for caspase-1 within the TRIF protein. IL-1β is

a key cytokine in promoting host defence and without cleavage of TRIF by

caspase-1, the levels of active IL-1β following NLRP3 activation would be

much less. The overall effect of increased inflammasome activation

consequent to TRIF cleavage varies depending on the specific infection

involved. NLRC4 inflammasome activation is critical in host defence against

Klebseilla pneumoniae (Cai et al., 2012) and oral Salmonella infection in

Balb/c mice (Franchi et al., 2012a), but increases bacterial burden in model

of *Pseudomonas aeruginosa* pneumonia (Cohen and Prince, 2013).

Moreover, TRIF has been shown to be an important intermediate in

triggering autophagy not just from TLR4 but also from TLR3 stimulation

(Delgado et al., 2008). Thus, cleavage of TRIF may also play a role in

limiting autophagy and enhancing inflammasome activation in infections that signal via TLR3, such as influenza. Additionally, a previous study with *Shigella flexneri* infected macrophages suggested that caspase-1 activation limited autophagy (Suzuki et al., 2007). The data presented in the work described here suggest cleavage of TRIF would account for this effect.

TRIF has recently been shown to be an important intermediate in the induction of NLRP3 inflammasome activation by Gram-negative bacteria (Rathinam et al., 2012). Type I IFNs triggered by TLR4 via TRIF mediate the induction of capsase-11, a protease that can amplify caspase-1 activation by NLRP3. This has been shown to be of importance in infections caused by enterohemorrhagic *E.coli* and *Citrobacter rodentium* (Kayagaki et al., 2011), as well as other Gram-negative organisms (Broz et al., 2012, Aachoui et al., 2013). It does not seem to play a role in the activation of the NLRC4 inflammasome, the mechanism by which *P. aeruginosa* activates the inflammasome via its type III secretion apparatus. However, in organisms lacking a functional type III apparatus, the TLR4/TRIF/caspase-11 pathway can act to produce NLRP3 activation, albeit with much slower kinetics than the NLRC4 mediated effects (Rathinam et al., 2012). We show here by specific knockdown of Caspase-11 using siRNA that this protein does not play a role in the activation of the inflammasome by PA103ΔUΔT or in the cleavage of TRIF. From our results, we would predict that TRIF cleavage by caspase-1 would serve to down-regulate activation of caspase-11 by attenuating the continued production of type I IFNs. The overall influence of TRIF cleavage in an infection will thus be dependent on potentially complex interactions between caspase-11 dependent and independent pathways.

Although TRIF cleavage restricts autophagy and thus can augment NLRP3 activation and IL-1β secretion, it will also lead to down-regulation of type I IFN production. We show here that in isolated BMDMs these results in decreases in phagocytic ability and production of reactive oxygen intermediates. A number of studies have shown the importance of TRIF-mediated type I IFN production in a variety of enteric and pulmonary Gram-negative infections (Kelly-Scumpia et al., 2010). Again, the overall outcome will depend on the relative balance between effective IL-1β production and attenuation of type I IFN. This may be of greater significance in viral infections that trigger caspase-1 activation. In this setting, type I IFN production can be crucial in determining outcome.

The cleavage of TRIF by caspase-1 does reduce to some degree the levels of full-length TRIF, but not to an extent that could account for the inhibitory effects observed. We speculate, therefore, that one or more of the cleavage products of TRIF that are produced by caspase-1 is acting as a dominant-negative inhibitor. The central TIR domain of TRIF has been shown to be such an inhibitor (Yamamoto et al., 2002). Cleavage of TRIF at amino-acids 281 and 289 results in N- and C-terminal truncated products that have been shown to lack most TRIF activity (Rebsamen et al., 2008). Caspase-1 activation results in activation of caspase-7, which may cleave additional sites within the molecule (Lamkanfi et al., 2008). Moreover, initial cleavage may expose additional sites that can be cleaved by other cellular proteases. The detailed molecular mechanisms whereby TRIF cleavage results in inhibiting TRIF function requires further study. However, it is clear that in both human and murine cells, expression of mutated TRIF lacking

caspase-1 cleavage sites results in a molecule that augments autophagy and hence down-regulates the activation of the NLRP3 inflammasome.

Autophagy can down-regulate the activation of the NLRP3 inflammasome by removal of damaged mitochondria (Nakahira et al., 2011). We describe here a reciprocal process by which inflammasome activation of caspase-1 acts to down-regulate autophagy. This is achieved through the specific proteolysis of TRIF, the key signalling intermediate that triggers autophagy following TLR4 activation. We also show that this removal of TRIF activity acts to further enhance NLRP3 inflammasome activation, although it does limit TRIF-dependent induction of type I IFN responses. Modulation of autophagy is thus a possible therapeutic target – either to limit its negative effects on inflammasome activation to augment host defence or to augment its action to limit excessive inflammation by caspase-1 and to enhance TRIF-mediated responses.

In conclusion, we found that *Pseudomonas aeruginosa* induced autophagy through signalling via TLR4 and TRIF. Loss of type III secretion increased autophagy, which was due to NLRC4 activation and caspase-1 activity. We show that caspase-1 cleaved TRIF, resulting in a diminution of TRIF-mediated signalling, not only resulting in inhibition of autophagy but also in production of type I IFNs. Prevention of TRIF cleavage through mutation of the caspase-1 cleavage sites resulted in augmented autophagy, increased type I IFN production and enhanced phagocytosis and reactive oxygen production within macrophages. Expression of a mutated TRIF lacking caspase-1 cleavage sites enhanced autophagy and diminished NLRP3 inflammasome activation in both mouse and human cells, leading to

a marked reduction in IL-1β production. We have thus defined caspase-1 mediated TRIF cleavage as a key event in controlling both NLRP3 inflammasome activation and autophagy, with important functional consequences.

5 *Pseudomonas aeruginosa* activation of the NLRC4 inflammasome is dependent on release of Mitochondrial DNA and is inhibited by autophagy

5.1 Introduction

The innate immune response to infection is a key component in host defence that not only provides immediate protection but also shapes the nature of the subsequent adaptive immune response (Schenten and Medzhitov, 2011, Kumar et al., 2009). One of the main mediators of the innate response is the cytokine IL-1β, which has diverse roles, including induction of fever, production of pro-inflammatory chemokines and prostanoids, augmenting neutrophil, B cell and dendritic cell function, and acting as a co-factor in the differentiation of Th17 cells (Dinarello, 2009). IL-1β production is tightly regulated by a multi-subunit protein complex termed the inflammasome (Franchi et al., 2012, Brodsky and Monack, 2009, Martinon et al., 2009). At its core is caspase-1, which on activation will not only produce mature IL-1β from pro-IL1β but also release of active IL-18, a cytokine important in Th1 cell development (Smith, 2011). Understanding the mechanisms regulating inflammasome activation is thus of crucial importance in comprehending its role in innate immune response to infection as well as numerous inflammatory conditions.

Apart from caspase-1, a variety of other proteins can be present in the inflammasome and these determine the nature of the stimuli that will lead to inflammasome activation. One of the best understood inflammasomes is that based on the NOD-like receptor family protein NLRP3 (Franchi et al., 2012). The NLRP3 inflammasome can be activated by a wide variety of stimuli, including bacterial toxins (Chu et al., 2009), inert particles such as urate crystals (Martinon et al., 2006) and silica (Hornung et al., 2008), and ATP (Hogquist et al., 1991). The exact molecular

mechanisms by which these diverse stimuli activate the NLRP3 inflammasome are not clear. Another caspase, caspase-11 synergises with the assembled NLRP3 inflammasome and augments its activity (Aachoui et al., 2013, Rathinam et al., 2012, Kayagaki et al., 2011). Several groups have shown the importance of mitochondrial damage and sensing of released mitochondrial DNA in NLRP3 inflammasome activation (Nakahira et al., 2011, Shimada et al., 2012). Mitochondrial generation of reactive oxygen species has been implicated in the activation of the NLRP3 inflammasome, and removal of damaged mitochondria by selective autophagy (mitophagy) inhibits this activation. Nakahira et al showed that release of mitochondrial DNA following damage to this organelle was responsible for the NLRP3 activation (Nakahira et al., 2011). Shimada et al found that release and binding of oxidised mitochondrial DNA to the NLRP3 inflammasome was important in its activation (Shimada et al., 2012). However, a recent report found that lowering of intracellular K^+ levels was the only common factor in the diverse signals that can activate the NLRP3 inflammasome (Munoz-Planillo et al., 2013).

The inflammasome based on the NLR protein NLRC4 is activated by a number of bacterial pathogens (Franchi et al., 2012). The activation is dependent on bacterial products, notably flagellin (Miao et al., 2006, Franchi et al., 2006) and PrgJ (Miao et al., 2010, Zhao et al., 2011), one of the rod proteins found in the type III secretion system (T3SS) that are conserved in a number of Gram-negative organisms. These proteins in murine cells interact with the adaptors NAIP5 and NAIP2 respectively leading to NLRC4 inflammasome activation (Lightfield et al., 2008, Zhao et al., 2011). However, NAIP5 is dispensable for inflammasome activation by *Salmonella*

enterica, despite the flagellin of this organism binding to NAIP5 (Kofoed and Vance, 2011). T3SS needle proteins homologous to *Salmonella enterica* PrgI are also reported to activate NLRC4 via the adaptor NAIP1 (Yang et al., 2013).

Previous work demonstrated that activation of the NLRC4 inflammasome can be prevented by raising extracellular potassium ion concentration (Lindestam Arlehamn et al., 2010); similar findings have been reported for the NLRP1 (Fink et al., 2008) and AIM2 (Muruve et al., 2008) based inflammasomes. A previous study of inflammasome activation by the pathogen *Vibrio parahaemolyticus* suggested that a bacterial effector, Vop, inhibited NLRC4 inflammasome activation by inducing autophagy degradation, but the mechanism was not determined (Higa et al., 2013). This strongly suggests that additional mechanisms for activating these inflammasomes are operative. We set out therefore to examine in more details the nature of activation of the NLRC4 inflammasome using infection with the common human pathogen *Pseudomonas aeruginosa*, which produces a rapid activation of the inflammasome by a mechanism that is entirely dependent on its T3SS (Sutterwala et al., 2007, Miao et al., 2008, Franchi et al., 2007, Arlehamn and Evans, 2011). Infection with this bacterium also initiates autophagy (Yuan et al., 2012).

The NLRC4 inflammasome can be activated by pathogenic bacteria via products translocated through the microbial type III secretion apparatus (T3SS). Recent work has shown that activation of the NLRP3 inflammasome is down-regulated by autophagy, but the influence of autophagy on NLRC4 activation is unclear. We set out to determine how

autophagy might influence this process, using the bacterium *P. aeruginosa,* which actives the NLRC4 inflammasome via its T3SS. Infection resulted in T3SS-dependent mitochondrial damage with increased production of reactive oxygen intermediates and release of mitochondrial DNA. Inhibiting mitochondrial reactive oxygen release or degrading intracellular mitochondrial DNA abrogated NLRC4 inflammasome activation. Moreover, macrophages lacking mitochondria failed to activate NLRC4 following infection. Removal of damaged mitochondria by autophagy significantly attenuated NLRC4 inflammasome activation. Mitochondrial DNA bound specifically to NLRC4 immunoprecipitates and transfection of mitochondrial DNA directly activated the NLRC4 inflammasome; oxidation of the DNA enhanced this effect. We found that inhibition of autophagy upregulated inflammasome activation following *P. aeruginosa* infection. This was due to autophagy removing damaged mitochondria that released mitochondrial DNA following infection in a process dependent on production of reactive oxygen intermediates. Released mitochondrial DNA was found to bind and activate the NLRC4 inflammasome. Manipulation of autophagy altered the degree of inflammasome activation and inflammation in an *in vivo* model of *P. aeruginosa* infection. Our results reveal a novel mechanism for NLRC4 activation by *P. aeruginosa* via release of mitochondrial DNA triggered by the bacterial T3SS that is down-regulated by autophagy.

5.2 Results

5.2.1 Autophagy inhibits inflammasome activation following *P. aeruginosa*.

We have previously demonstrated that *P. aeruginosa* induces autophagy in BMDMs in a TLR4 dependent fashion (Jabir et al., 2014). We infected cells with *P. aeruginosa* PA103ΔUΔT which has a functional T3SS that activates the inflammasome via NLRC4. We set out to examine the effect of an absence of autophagy on the activation of the NLRC4 inflammasome by *P. aeruginosa* using BMDMs from mice with a targeted deletion of the essential autophagy gene *Atg7* in marrow precursors (*Vav-Atg7$^{-/-}$* mice) (Mortensen et al., 2011, Mortensen et al., 2010). We assayed for the induction of autophagy by measuring production of the lipidated form of LC3 (LC3 II) (Mizushima et al., 2010), and intracellular LC3 staining (Fig. 5-1a and b). In infected cells from the *Vav-Atg7$^{-/-}$* mice there was a virtually complete inhibition of autophagy compared to infected cells from wild type mice. We then compared inflammasome activation following infection in macrophages from wild type and *Vav-Atg7$^{-/-}$* mice. In the absence of autophagy, we found that inflammasome activation was markedly increased, as shown by enhanced conversion of caspase-1 to the active p10 form (Fig. 5-1c), and greater production of secreted IL-1β (Fig. 5-1d), but no significant change in secreted TNF (Fig. 5-1d). We used a different method to inhibit autophagy by knockdown of the essential autophagy gene *Atg5* (Fig. 5-2a). This also led to increased production of IL-1β, but not TNF and enhanced conversion of pro-caspase-1 and pro-IL-1β to the active p10 and secreted p17 IL-1 β forms respectively (Fig. 5-2b and c).

In a similar fashion, knock down of *Lc3b* with siRNA in BMDMs also increased production of activated caspase-1 (Fig. 5-3a) and IL-1β following infection (Fig. 5-3b) but not TNF (Fig. 5-3c).

To confirm these observations, we used 3-MA to inhibit autophagy following infection of BMDMs, murine J774A.1, and dendritic cells as well as the human macrophage cell line THP-1 (Fig. 5-4). 3-MA inhibited autophagy in all these cells, as assayed by conversion of LC3 to its lipidated form (Fig.5-4a), enumeration of LC3 containing puncta, and LC3 intracellular staining (Fig 5-4b and c). Inflammasome activation in these cells was determined by measurement of secreted IL-1β and conversion of caspase-1 to its active p10 subunit (Fig. 5-5 a and b). 3-MA enhanced production of the caspase-1 p10 subunit in BMDMs and increased the levels of IL-1β and did not affect TNF-α secretion (Fig. 5-5 c), and increased production of IL-1β in THP-1, J774 and dendritic cells (Fig. 5-5d). The *P. aeruginosa* PAO1 strain also induced autophagy in BMDMs. We verified this observation by assaying LC3 I conversion to LC3 II in these cells, which was prevented by 3-MA (Fig. 5-6). Taken together, these data show that in the absence of autophagy, there is an increase in the activation of the NLRC4 inflammasome following *P. aeruginosa* infection.
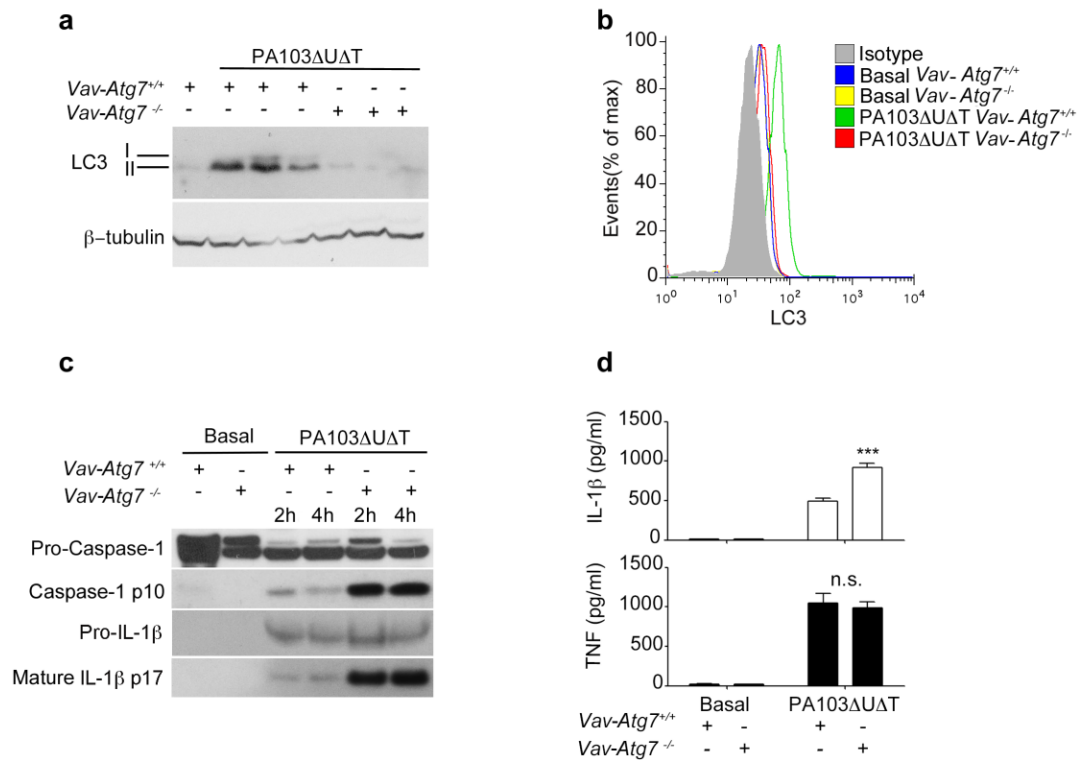
Figure 5.1; Absence of autophagic protein Atg7 increases Inflammasome activation following *P.aeruginosa* PA103ΔUΔT infection.

a – d, BMDMs from wild type mice (*Vav-Atg7*^{+/+}) or mice with a conditional deletion of *Atg7* in bone-marrow derived cells (*Vav-Atg7*^{-/-}) were infected with PA103ΔUΔT and autophagy quantified. **a**, Western blot of cell lysates infected as shown and immunostained for LC3. The unmodified (LC3 I) and lipidated isoform (LC3 II) are shown in three separate experiments. β-tubulin is shown as a loading control. **b,** Levels of intracellular LC3 assayed by flow cytometry following treatments as indicated. **c**, immunoblot for pro-caspase-1 and pro-IL-1β , and caspase-1 p10 fragment and mature IL-1β p17 (supernatants) of cells infected as shown. **d**, secretion of active IL-1β and TNF from basal and infected BMDMs as shown. Columns are means of 3 independent determinations; error bars are SEM. *** indicates a significant difference between the levels in BMDMs from WT or *Vav-Atg7*^{-/-} mice, p < 0.001.
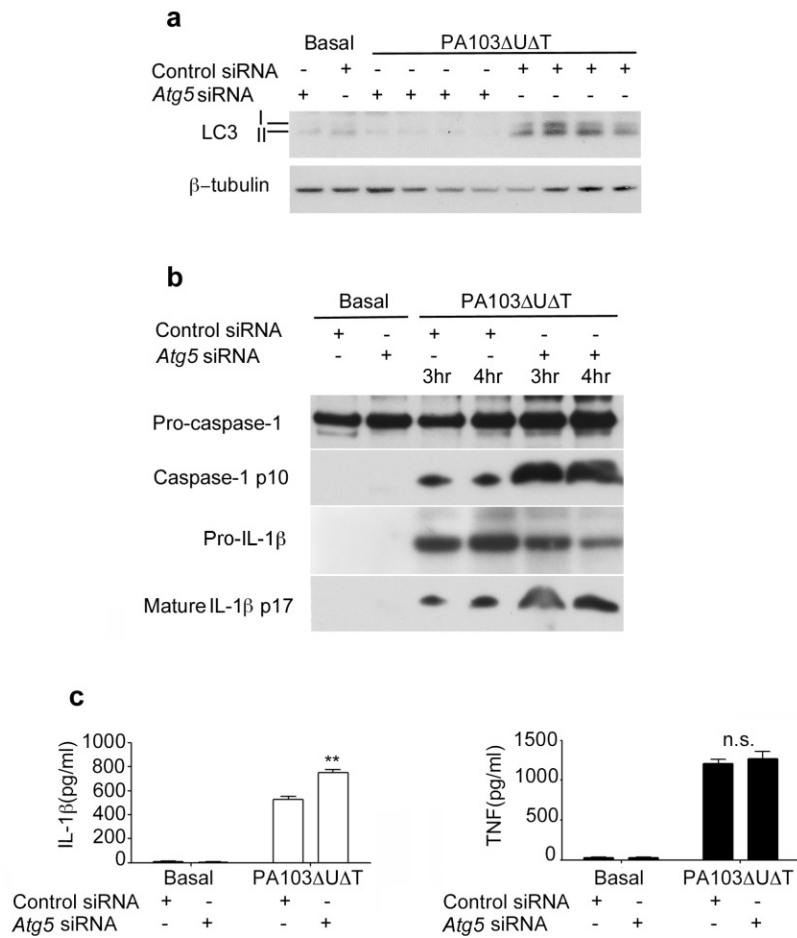
Figure 5.2; Absence of autophagic protein Atg5 increases Inflammasome activation following *P.aeruginosa* PA103ΔUΔT infection.

a, LC3 I and II assayed by Western blotting in BMDMs transfected with control siRNA or siRNA to *Atg5*, uninfected (Basal), or infected with *P. aeruginosa* strain as indicated (MOI 25) for 4 hr. Blot shows 4 independent experiments. **b**, immunoblot for pro-caspase-1 and pro-IL-1β , and caspase-1 p10 fragment and mature IL-1β p17 of cells infected as shown. **c**, ELISA of IL-1β and TNF secretion from cells treated as shown. Columns are means of triplicate independent experiments; error bars SEM. ** indicates significant difference between the levels in infected BMDMs transfected with siRNA to *Atg5*, compared to control siRNA, p < 0.01. n.s., not significant.
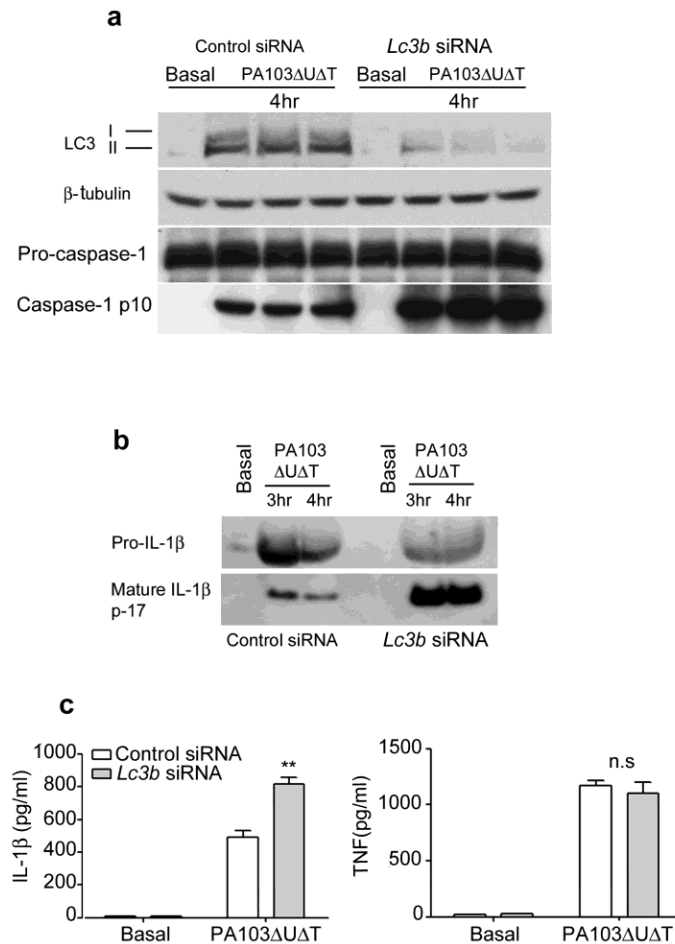
Figure 5.3; Gene silencing of *Lc3*b by siRNA increases Inflammasome activatation following *P. aeruginosa* PA103ΔUΔT infection.

a, immunoblot of cell lysates (LC3 and pro-caspase-1) and (capsase-1 p10) from cells infected and treated as shown. β-tubulin is shown as a loading control. **b**, Immunoblot of pro-IL-1 β and mature IL-1 β in cell supernatant after infections and treatments as indicated. **c**, ELISA of IL-1β and TNF secretion from cells treated as shown. Columns are means of triplicate independent determinations; error bars are SEM. ** indicates significant difference from control siRNA treated cells, p < 0.01. Data are representative of 3 independent experiments.
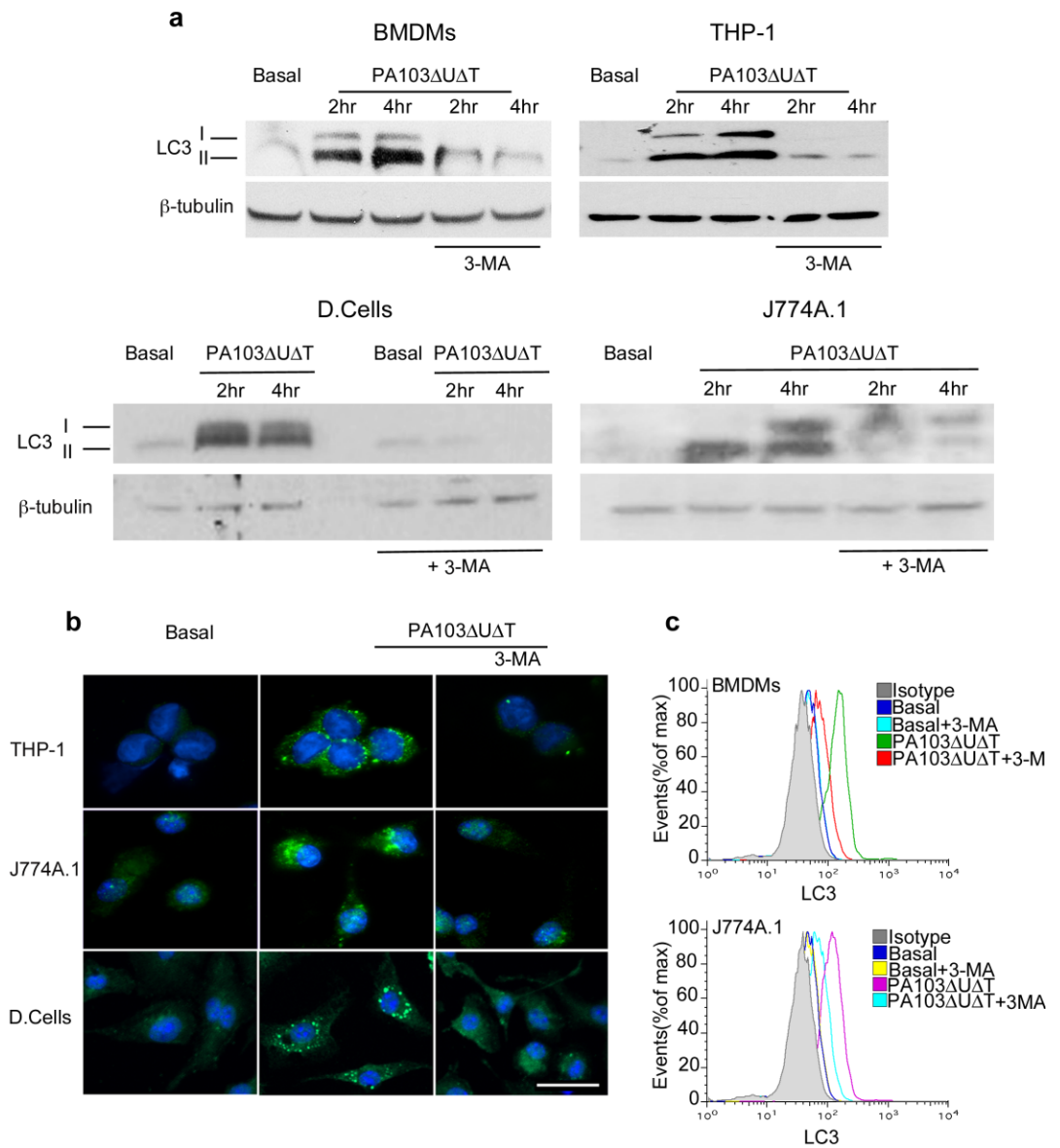
Figure 5.4; 3-MA inhibits autophagy following *P.aeruginosa* PA103ΔUΔT infection.

BMDMs, THP-1, dendritic cells, and J774A.1 cells were infected with PA103ΔUΔT (MOI 25) for the indicated time in hours in the presence (+) or absence (−) of 3-MA (10 mM). **a**, The panels show representative Western blot of LC3 isoforms and β-tubulin as a loading control. **b**, representative immunofluorescence images of cells as indicated; LC3 staining is green and nuclei are stained blue (DAPI). Scale bar is 10μm. **c**, Levels of intracellular LC3 assayed by flow cytometry following treatments as indicated.
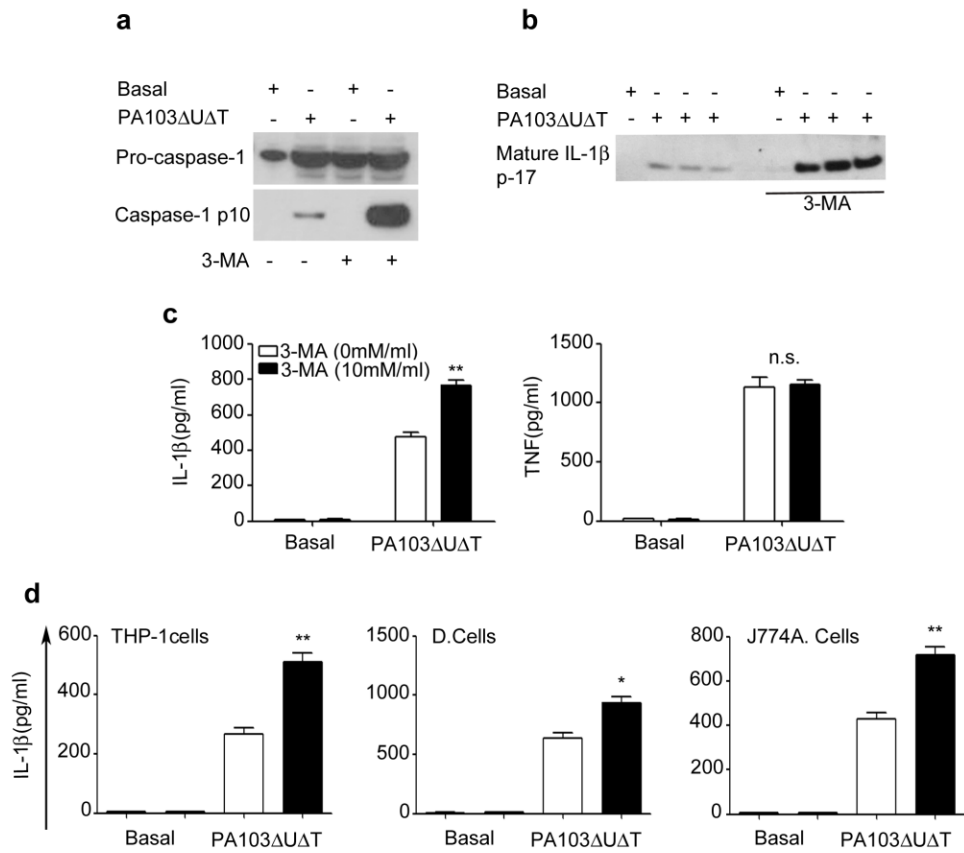
Figure 5.5; 3-MA increases Inflammasome activation following *P.aeruginosa* PA103ΔUΔT infection.

a, immunoblot of cell lysates of pro-caspase-1 and capsase-1 p10 subunit of cells infected and treated as shown. **b**, Immunoblot of mature IL-1 β in cell supernatant after infections and treatments as indicated. (3 independent experiment). **c**, **d**, ELISA of secreted IL-1β and TNF from cells as shown. Columns are means of triplicate independent determinations; error bars are SEM. * indicate significant differences between the levels in the presence and absence of 3-MA, p<0.05, and ** p < 0.01.
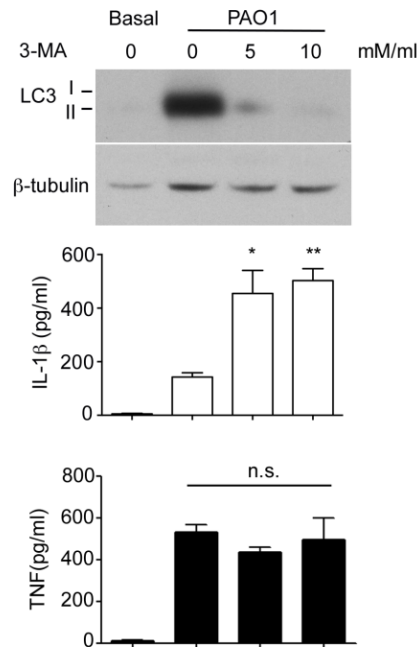
Figure 5.6; 3-MA increases Inflammasome activation following infection with
***P.aeruginosa* PAO1.**

BMDMs cells were infected with PAO1 (MOI 25) for 4 hours in the presence (+) or absence (–) of 3-MA (5,10 mM). The panels show representative Western blot of LC3 isoforms and β-tubulin as a loading control. ELISA of secreted IL-1β and TNF from cells supernatents as shown. Columns are means of triplicate independent determinations; error bars are SEM. * indicate significant differences between the levels in the presence and absence of 3-MA, p<0.05, and ** p < 0.01 respectively.

5.2.2 Mitochondrial Reactive Oxygen activates the inflammasome following *P. aeruginosa* infection.

Autophagy can removed damaged mitochondria by mitophagy. Thus, we hypothesized that the increase in inflammasome activation in *P. aeruginosa* infected cells after inhibition of autophagy was due to an increase in release of reactive oxygen intermediates from defective mitochondria that failed to be removed by mitophagy. To confirm that autophagy was indeed directly targeting mitochondria and removing them through mitophagy, we performed localization studies using immunofluorescent microscopy (Fig. 5-7). Mitochondria were visualised by staining with an antibody to the mitochondrial protein ATPase inhibitory factor. Following infection of BMDMs with PA103ΔUΔT, we found extensive co-localization of mitochondria with the LC3 protein that localizes on autophagocytic vacuoles. Transmission electron microscopy revealed the presence of mitochondria within double-membraned autophagocytic vacuoles (Fig. 5-8). The delivery of damaged mitochondria to autophagocytic vacuoles is controlled by the mitochondrial protein PINK-1(Narendra et al., 2012, Jin and Youle, 2012, Narendra et al., 2010). This normally undergoes proteolytic processing by healthy mitochondria, but following damage and depolarization, this processing is abrogated and full length PINK-1 accumulates on the surface of mitochondria. Full length PINK-1 then recruits Parkin to the mitochondrial surface and initiates mitophagy. Western blotting of BMDM lysates following infection with PA103ΔUΔT showed an accumulation of full length compared to cleaved PINK-1 (Fig. 5-9). This was partially reversed by Mito-TEMPO, a specific inhibitor of mitochondrial reactive oxygen production (Smith et al., 2011)

(Fig. 5-8). PA103 lacking a functional T3SS that does not activate the inflammasome, PA103pcrV⁻, did not prevent cleavage of PINK-1 (Fig. 5-9). These data show that mitochondria are damaged by the T3SS system in *P. aeruginosa* infection leading to inhibition of PINK-1 cleavage that then initiates mitophagy.
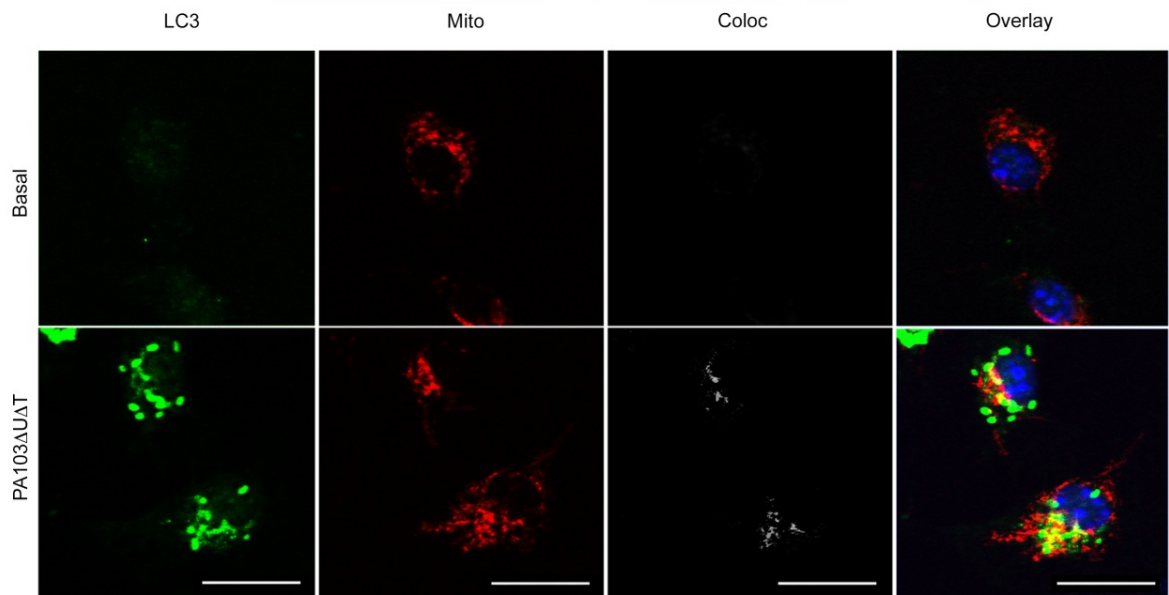
Figure 5.7; Mitochondria targeted by autophagosomes following *P.aeruginosa* infection.

Representative confocal images of BMDMs infected with PA103ΔUΔT (MOI 25 for 4h), fixed, permeabilized and stained for LC3 (green), and mitochondrial ATPIF1 (Mito, red); nuclei are stained blue with DAPI. Colo shows areas of colocalization of the mitochondrial and LC3 staining in grey. Overlay shows the merged LC3 and mitochondrial signals; co-localising areas shown as yellow. Scale bar is 0.5μm. Repeated three times.
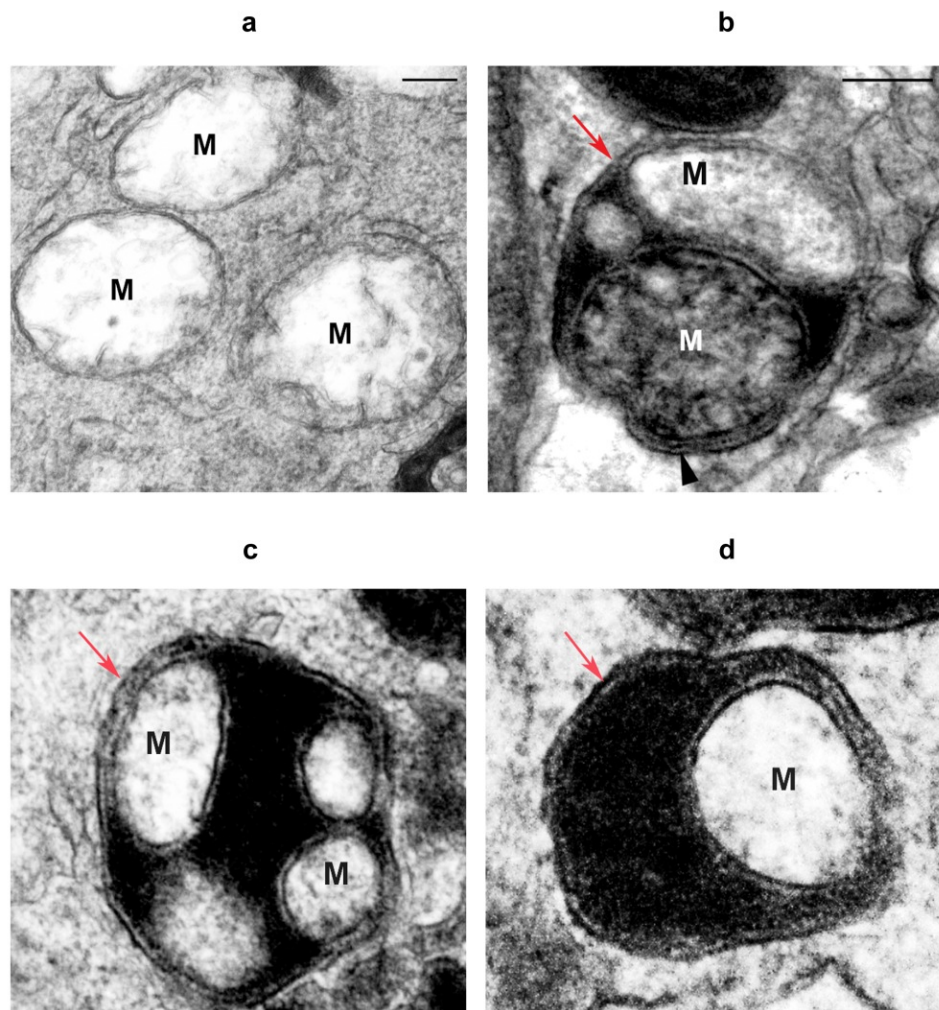
Figure 5.8; EM analysis of Mitochondria targeted by autophagosomes following *P.aeruginosa* infection.

Electron micrographs of **a** untreated BMDM (control) or **b**-**d** infected with PA103ΔUΔT (MOI 25) for 4 hrs. Arrow indicates autophagosome, M indicate mitochondria. Scale bar is 500 nm. Representative image from > 10 infected cells.
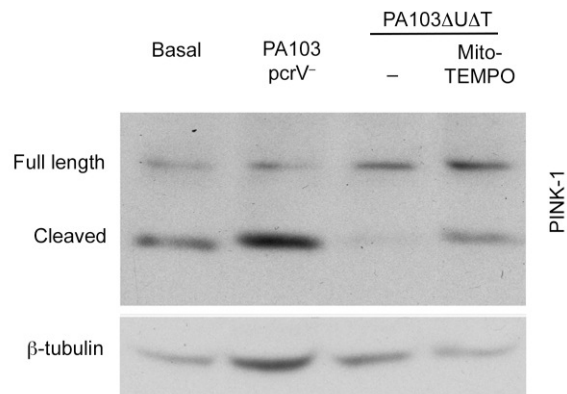
Figure 5.9; PINK-1 cleavage following *P.aeruginosa* infection.

Immunoblot of BMDMs infected at a MOI of 25 with PA103pcrV⁻ or PA103ΔUΔT± Mito-TEMPO (500µM) for 4 hours and probed for PINK-1. Full length and cleaved PINK-1 are labelled. The blot was re-probed for β-tubulin as a loading control. Representative of two independent experiments.

Next, we examined the production of reactive oxygen by mitochondria following infection with *P. aeruginosa* and the effect of this on inflammasome activation. We measured production of reactive oxygen intermediates from mitochondria using the selective fluorescent indicator MitoSox (Li et al., 2003). Following infection with the PA103ΔUΔT strain of *P. aeruginosa,* there was a marked increase in mitochondrial reactive oxygen production. However, following infection with the PA103pcrV⁻ mutant that does not have a functional T3SS and does not produce inflammasome activation, mitochondrial reactive oxygen was not increased (Fig. 5-10 a and b). To test the dependence of inflammasome activation following *P. aeruginosa* infection on production of mitochondrial reactive oxygen production, we used the general reactive oxygen inhibitor N-acetyl cysteine (NAC) as well as Mito-TEMPO, a specific inhibitor of mitochondrial reactive oxygen production. Following infection, both these inhibitors produced a dose-dependent reduction in capsase-1 activation and production of active IL-1β (Fig 5-11a), but with no effect on secreted TNF. Both inhibitors produced the expected reduction in mitochondrial production of reactive oxygen (Fig. 5-11b). PA103 lacks functional flagella, thus it activates NLRC4 via NAIP2 rather than NAIP5/6 (Zhao et al.2011; Kofoed and Vance, 2011). To determine if reactive oxygen production was important in infection with flagellated *P. aeruginosa* that can active NLRC4 via NAIP5/6, we utilised the strain PAO1. Infection of BMDMs with this strain activated the inflammasome with production of the p10 caspase-1 fragment and secreted IL-1β. Both NAC and Mito-TEMPO inhibited this activation (Fig 5-12a). Additionally, PAO1 infection produced an increase output of mitochondrial reactive oxygen that was inhibited by Mito-TEMPO

and NAC (Fig. 5-12b). Thus, *P. aeruginosa* signalling via either NAIP2 or NAIP5/6 produce mitochondrial reactive oxygen intermediates that are important in NLRC4 inflammasome activation.
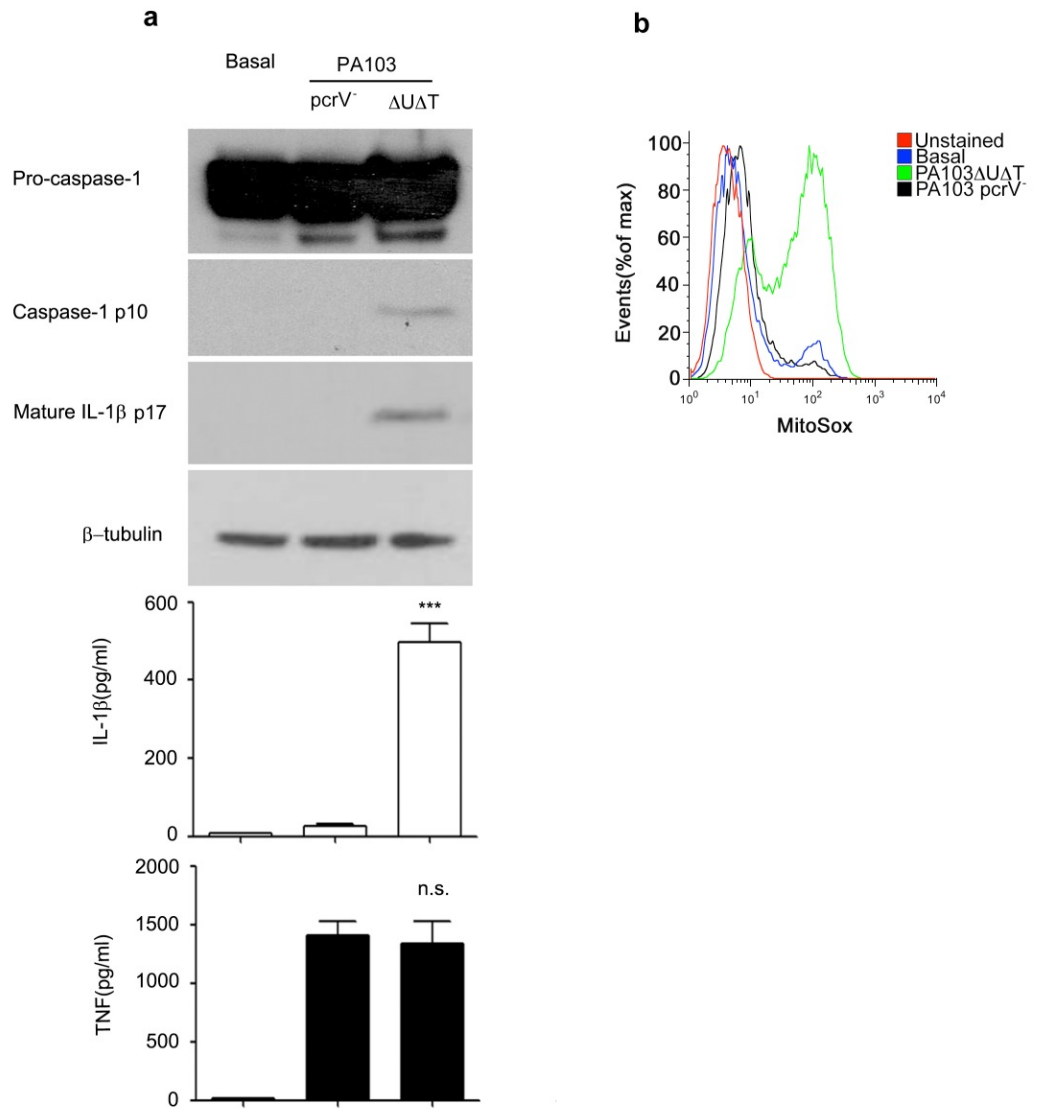
Figure 5.10; Mitochondrial ROS generation is dependent on inflammasome activation following Peudomonas aeruginosa infection.

a, Western blot analysis of Pro-caspase, caspase-1 p10 subunit, and mature IL-1β p17 (in cells supernatant) of BMDMs. Cells were left uninfected (basal) or infected with PA103pcrV⁻, and PA103ΔUΔT at (MOI of 25) for 4 hr. ELISA of secreted IL-1β and TNF from cells as shown. Columns are means of triplicate independent determinations; error bars are SEM. *** indicate significant differences. p<0. 001. **b**, Flow cytometry of untreated BMDMs (basal) or infected as indicate. Cells stained with MitoSox (2.5 µM for 30 min at 37˚C).
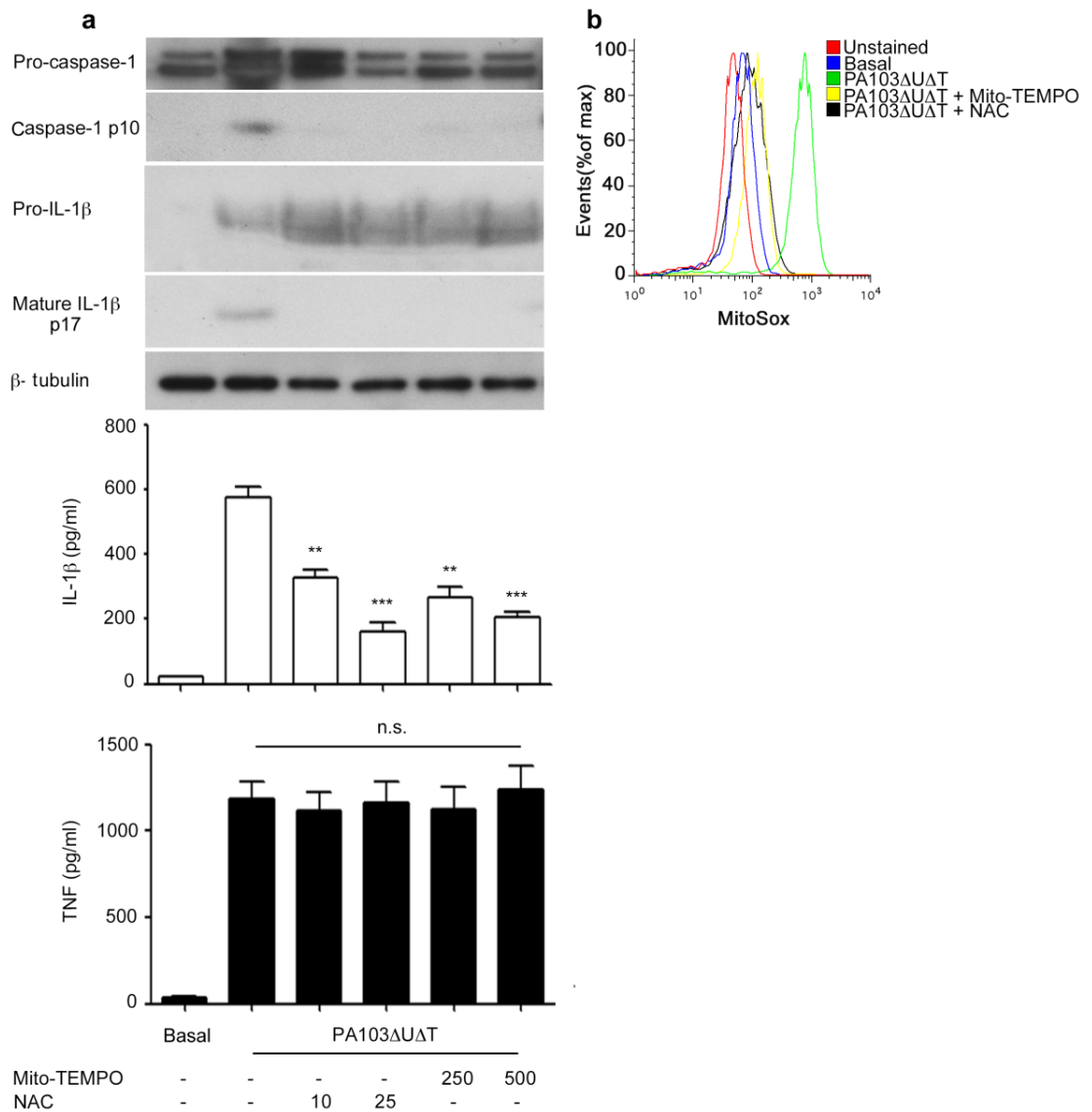
Figure 5.11; Mitochondrial inhibitors reduce inflammasome activation following *P.aeruginosa* PA103ΔUΔT infection.

a, Western blot analysis of Pro-caspase, caspase-1 p10 subunit, pro-IL1 β and mature IL-1β p17 of BMDMs. Cells were left uninfected(basal) or infected with PA103DUDT at a MOI of 25 for 4 hr ± Mito-TEMPO (μM), or ± NAC (mM). ELISA of IL-1β and TNF-α in BMDMs. Columns are means of triplicate independent determinations; error bars are SEM. **, and *** indicate significant differences between levels in the presence and absence of mitochondrial inhibitors. $p<0.01$, $p<0.001$ respectively. **b**, Flow cytometry of untreated BMDMs (basal) or infected as indicated. Cells stained with MitoSox (2.5 μM for 30 min at 37˚C).
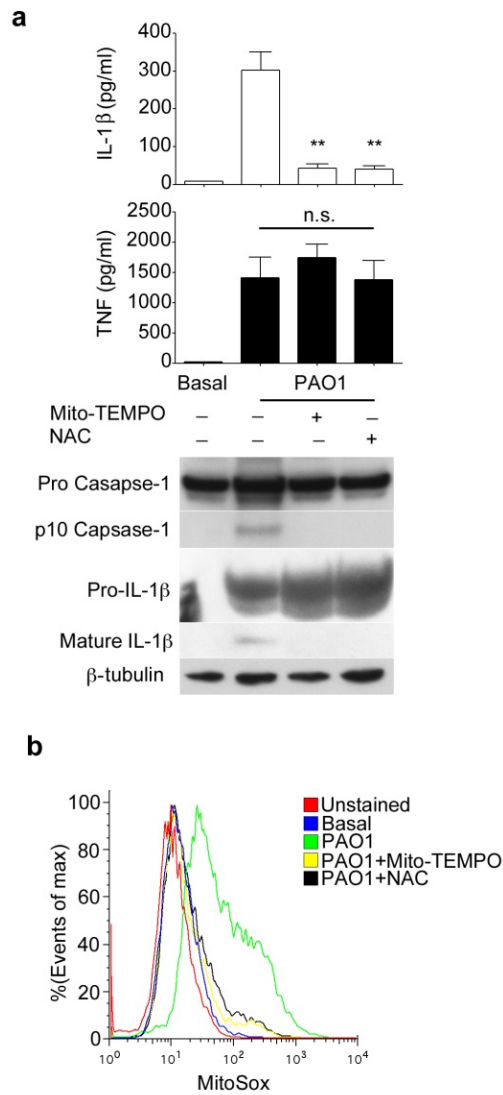
Figure 5.12; Inhibition of mitochondrial reactive oxygen production attenuates inflammasome activation by PAO1.

a, Western blot analysis of Pro-caspase, caspase-1 p10 subunit, pro-IL1 β and mature IL-1β p17 of BMDMs. Cells were left uninfected(basal) or infected with PAO1 at a MOI of 25 for 4 hr ± Mito-TEMPO (500µM), or ± NAC (25mM). ELISA of IL-1β and TNF-α in BMDMs. Columns are means of triplicate independent determinations; error bars are SEM. **, indicates significant differences between levels in the presence and absence of mitochondrial inhibitors. p<0.01. **b**, Flow cytometry of untreated BMDMs (basal) or infected as indicated. Cells stained with MitoSox (2.5 µM for 30 min at 37˚C).

Next, we tested the effect of inhibiting autophagy on the production of mitochondrial reactive oxygen intermediates and assessed the functional mitochondrial pool in cells following infection of BMDMs with *P. aeruginosa* PA103ΔUΔT. Production of mitochondrial reactive oxygen intermediates following infection was further increased when autophagy was inhibited with 3-MA (Fig. 5-13). Next, we attenuated autophagy by knockdown of the essential autophagy genes *Lc3b* and *Atg5* using siRNA. Using both these approaches, we observed a marked increase in the production of mitochondrial reactive oxygen intermediates following infection. Finally, in BMDMs from mice lacking the essential autophagy gene *Atg7* in bone-marrow cells (*Vav-Atg7*$^{-/-}$) there was an increase in the amount of mitochondrial reactive oxygen produced following infection compared to control wild type animals (Fig. 5-14), and (Fig. 5-15) . Taken together, these data show that autophagy reduced the levels of mitochondrial reactive oxygen produced following infection of BMDMs with *P. aeruginosa*.
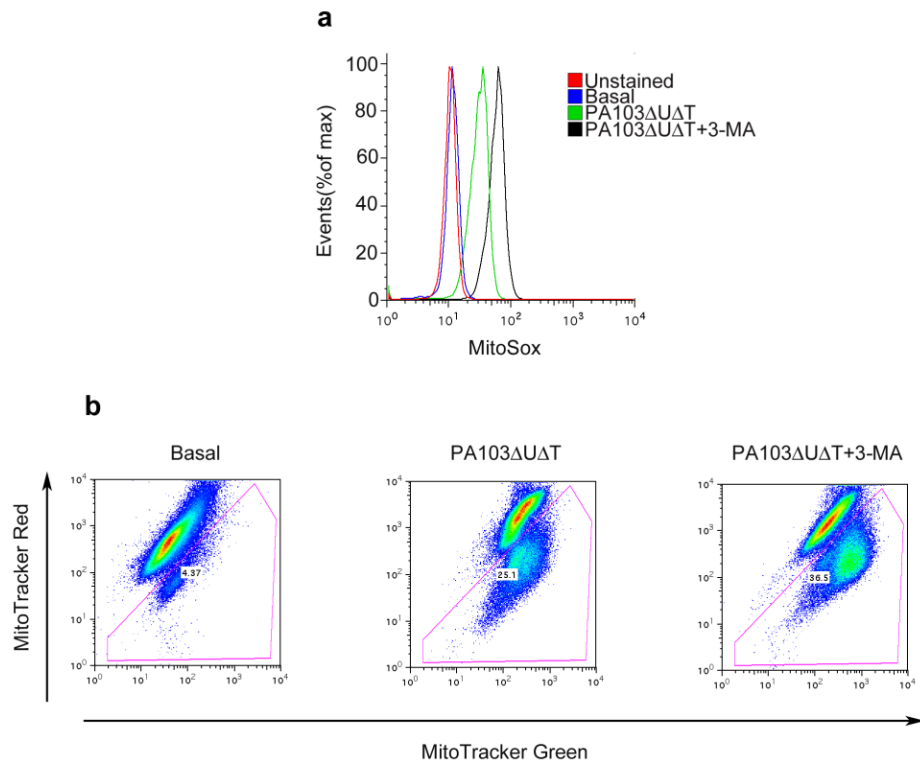
Figure 5.13; Inhibition of autophagy/mitophagy using 3-MA increases ROS generation and mitochondrial damage following *P.aeruginosa* PA103ΔUΔT infection.

a, Flow cytometry of untreated BMDMs (basal) or infected for 4h at MOI of 25 with PA103ΔUΔT. Cells stained with MitoSox(2.5 μM for 30 min at 37˚C) . **b**, Flow cytometry of BMDMs following treatments as in (**a**). Cells were stained with MitoTracker deep Red and MitoTracker Green (50 nM for 30 min at 37˚C). Numbers above indicate % cells with loss of mitochondrial membrane potential (damaged mitochondria). Representative of two independent experiments.
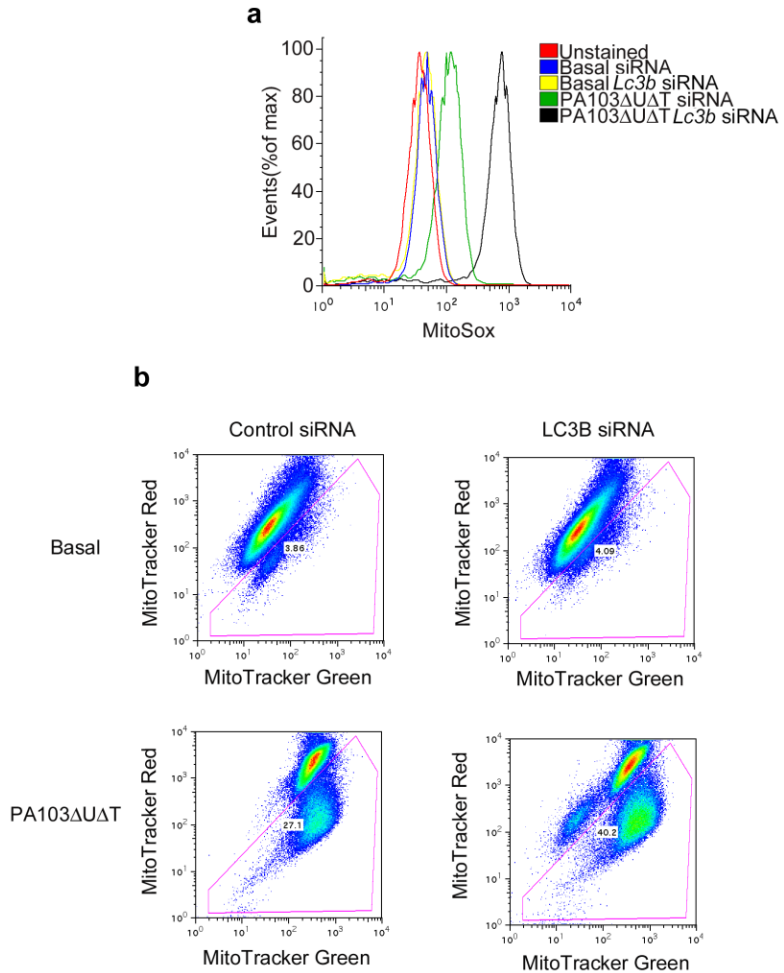
Figure 5.14; Gene silencing of Lc3b by siRNA increases ROS generation and mitochondrial damage following *P.aeruginosa* PA103ΔUΔT infection.

a, Flow cytometry of BMDMs transfected as shown and then left uninfected (basal) or infected for 4h at MOI of 25 with PA103ΔUΔT. Cells stained with MitoSox(2.5 µM for 30 min at 37°C) . **b**, Flow cytometry of BMDMs following treatments as in (**a**). Cells were stained with MitoTracker deep Red and MitoTracker Green (50 nM for 30 min at 37°C). Numbers above indicate % cells with loss of mitochondrial membrane potential (damaged mitochondria). Representative of three independent experiments.
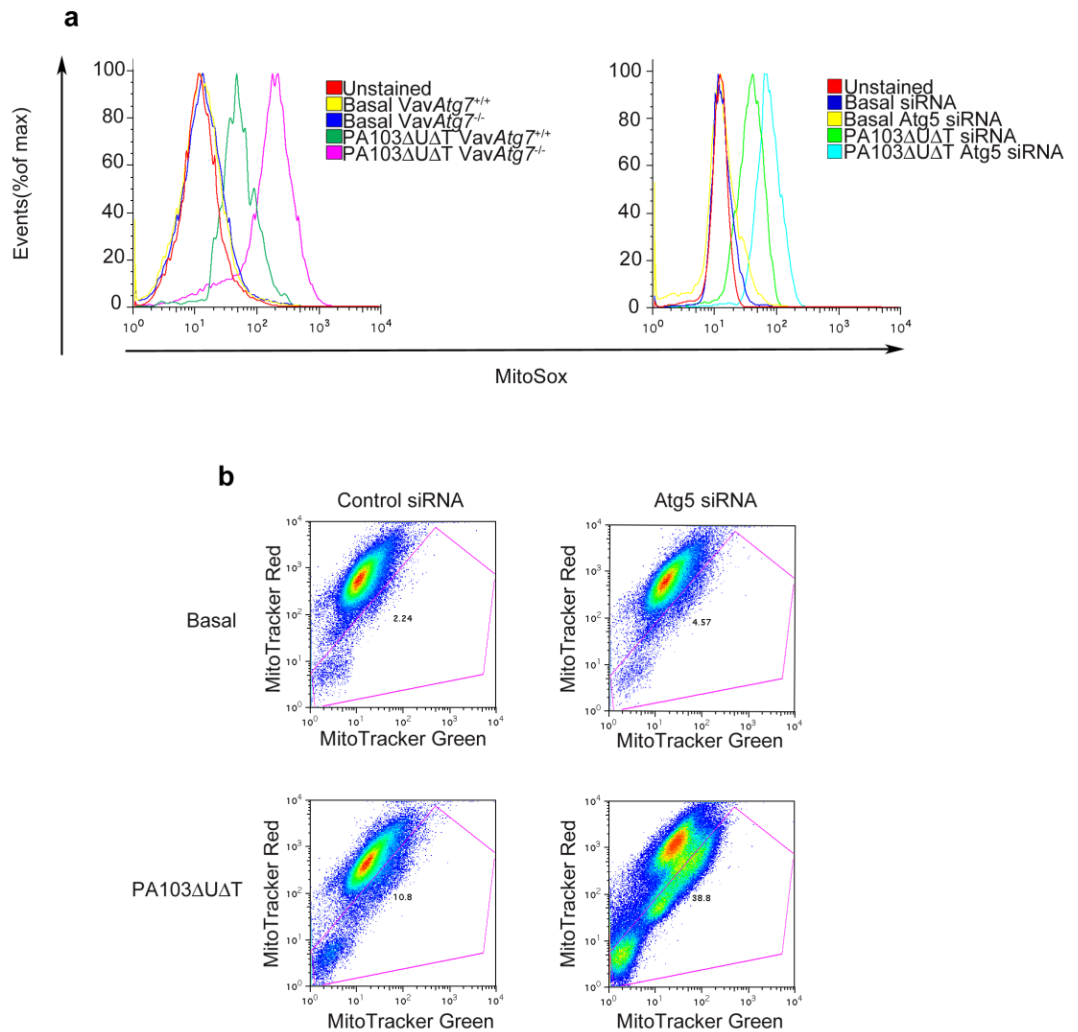
Figure 5.15; Depletion of autophagic proteins increases ROS generation and mitochondrial damage following *P.aeruginosa* PA103ΔUΔT infection.

a, Flow cytometry in BMDMs from WT or Vav-*Atg*7 $^{-/-}$ mice , and transfected with control siRNA or siRNA to *Atg5* as shown. Cells were left BMDMs (basal) or infected for 4h at MOI of 25 with PA103ΔUΔT. Cells stained with MitoSox (2.5 µM for 30 min at 37°C) . **b**, Flow cytometry of BMDMs transfected with control siRNA or siRNA to *Atg5.* Cells were left untreated (basal) or infected for 4h at MOI of 25 with PA103ΔUΔT. Cells were stained with MitoTracker deep Red and MitoTracker Green (50 nM for 30 min at 37°C). Numbers above indicate % cells with loss of mitochondrial membrane potential (damaged mitochondria). Representative of two independent experiments.

We then determined whether increased inflammasome activation following inhibition of autophagy in infected cells was due to increased mitochondrial reactive oxygen production. In BMDMs in which autophagy was inhibited by knock down of *Lc3b*, both NAC and mito-TEMPO prevented caspase-1 activation and production of mature IL-1β, without affecting TNF production (Fig. 5-16). In BMDMs in which autophagy was inhibited by 3MA, both NAC and mito-TEMPO prevented caspase-1 activation and production of mature IL-1β, without affecting TNF production (Fig. 5-17). Similarly, in infected cells from *Vav-Atg7*$^{-/-}$ mice, Mito-TEMPO reduced IL-1β but not TNF production and inhibited the production of activated caspase-1 (Fig. 5-18). Finally, we tested the effects of mito-TEMPO on inflammasome activation in infected BMDMs in which autophagy was inhibited by knockdown of *Atg5* with siRNA. Again, mito-TEMPO inhibited the increase in IL-1β production and generation of activated caspase-1 that was seen when autophagy was prevented (Fig. 5-19).
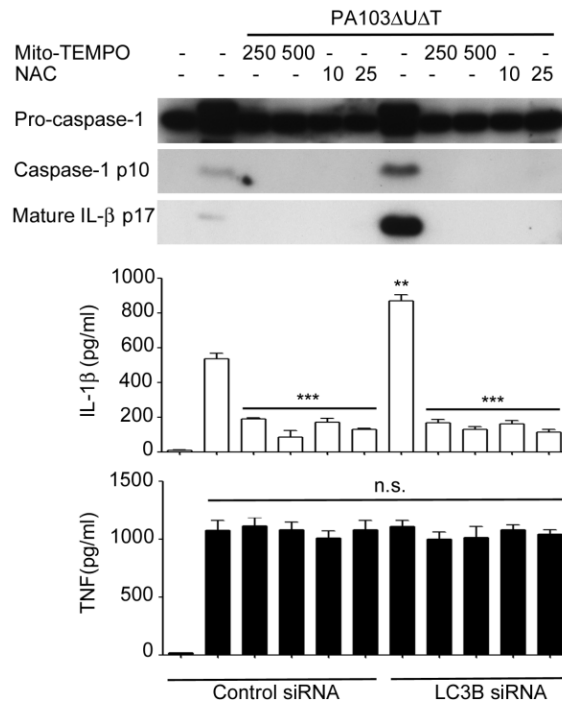
Figure 5.16; Increased inflammasome activation produced by gene silencing of Lc3b is dependent on ROS generation following *P.aeruginosa* PA103ΔUΔT infection.

BMDMs were transfected with control siRNA and siRNA to *Lc3b*. then infected with PA103ΔUΔT at MOI of 25 for 4 hr ± Mito-TEMPO (μM), or ± NAC (mM). Figure shows Western blot analysis of Pro-caspase-1, caspase-1 p10 subunit, and mature IL-1β and level of IL-1β and TNF-α secretion. Columns are means of triplicate independent determinations; error bars are SEM. *** indicates significant differences between the levels in the presence and absence of mitochondrial inhibitors, p<0.001. Representative of two independent experiments.
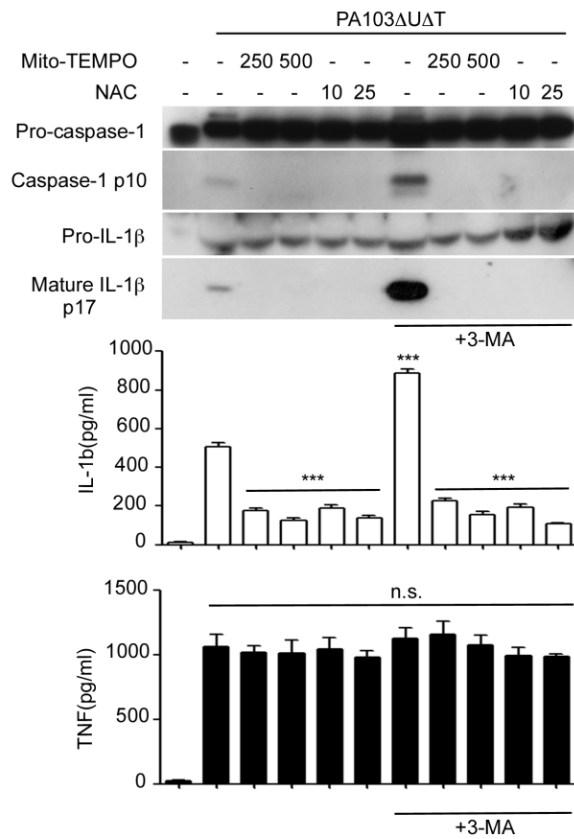
Figure 5.17; Increased inflammasome activation produced by autophagy inhibitor 3-MA is dependent on ROS following *P. aeruginosa* PA103ΔUΔT infection.

BMDMs cells were pre-treated in media with 3-MA (10 mM) then infected with PA103ΔUΔT at (MOI of 25) for 4 hr ± Mito-TEMPO (µM) ,or ± NAC (mM). Figure shows Western blot analysis of Pro-caspase-1, caspase-1 p10 subunit, Pro-IL-1β, mature IL-1β and level of IL-1β and TNF-α secretion. Columns are means of triplicate independent determinations; error bars are SEM. *** indicate significant differences between the levels in the presence and absence of mitochondrial inhibitors, and 3-MA (10 mM), p<0.001. Representative of two independent experiments.
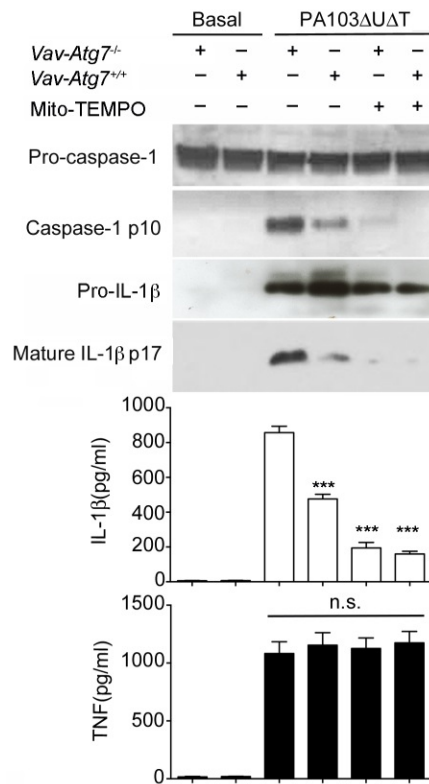
Figure 5.18; Increased inflammasome activation in the absence of autophagic protein Atg7 induced Inflammasome activation is dependent on ROS following *P.aeruginosa* PA103ΔUΔT infection.

Figure shows Western blot analysis of Pro-caspase, caspase-1 p10 subunit, mature IL-1β p17 ± Mito-TEMPO and levels of IL-1β and TNF-α in BMDMs from WT or Vav-*Atg7* [-/-] mice. Cells left uninfected (Basal), or infected with PA103ΔUΔT for 4hrs at a MOI of 25 ± Mito-TEMPO as indicated. Columns are means of triplicate independent determinations; error bars are SEM. *** indicate significant differences between WT animals and Vav-*Atg7* [-/-] mice ± Mito-TEMPO. p<0.001. n.s. not significant. Representative of two independent experiments.
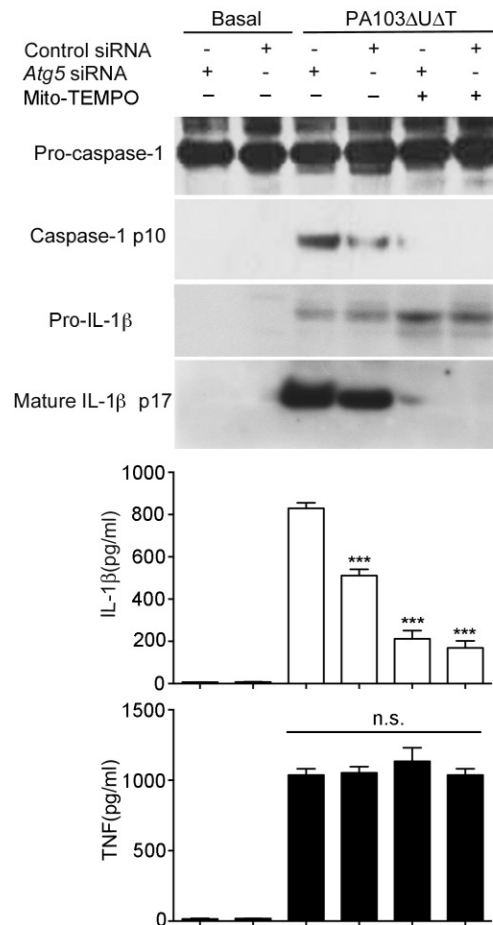
Figure 5.19; Increased inflammasome activation in the absence of autophagic protein Atg5 induced Inflammasome activation is dependent on ROS following *P.aeruginosa* PA103ΔUΔT infection.

Figure shows Western blot analysis of Pro-caspase, caspase-1 p10 subunit, Pro-IL-1 β, mature IL-1 β and levels of IL-1β and TNF-α secretion. Cells left uninfected (Basal), or infected with PA103ΔUΔT for 4hrs at a MOI of 25 ± Mito-TEMPO as indicated. Columns are means of triplicate independent determinations; error bars are SEM. **, and *** indicate significant differences between control siRNA and siRNA to *Atg*5 ± Mito-TEMPO. p<0.001. Representative of two independent experiments.

5.2.3 *P.aeruginosa* produces release of Mitochondrial DNA that is essential for activation of the NLRC4 inflammasome

One consequence of mitochondrial damage is release of mitochondrial DNA (Nakahira et al., 2011, Shimada et al., 2012). We hypothesised that the mitochondrial damage following *P. aeruginosa* infection would result in release of mitochondrial DNA that would be important in activating the NLRC4 inflammasome. First, we assayed for cytoplasmic mitochondrial DNA release following infection of BMDMs using quantitative PCR. Following infection with PA103ΔUΔT there was a marked increase in the relative amount of mitochondrial to nuclear cytoplasmic DNA (Fig. 5-20). This was further increased by inhibiting autophagy with 3-MA or by knockdown of *Lc3b* with siRNA (Fig. 5-20a). Inhibiting mitochondrial reactive oxygen production with Mito-TEMPO significantly inhibited mitochondrial DNA release (Fig. 5-20b).
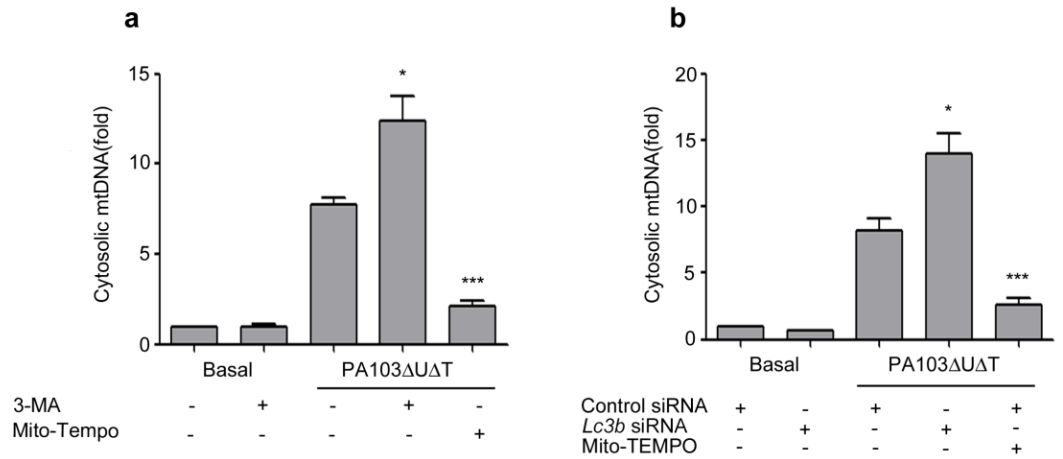
Figure 5.20; Mitochondrial DNA release following *P.aeruginosa* PA103ΔUΔT infection

qPCR analysis of cytosolic mitochondrial DNA (mtDNA) relative to nuclear DNA in macrophages pre-treated **a** with Mito-TEMPO (500 µM) or 3-MA(10 mM) or control or *Lc3b* siRNA (**b**) and infected with PA103ΔUΔT (MOI 25) for 4 hours or uninfected (Basal) as shown. Columns show means of three independent determinations; error bars are SEM. * and *** indicate significant differences between groups ± 3-MA, or Mito- TEMPO. p<0.05, p<0.001 respectively. Representative of two independent experiments.

Further to establish the importance of mitochondria in the activation of the NLRC4 inflammasome by *P. aeruginosa*, we grew J774A.1 murine macrophages in ethidium bromide to generate cells that lack mitochondria (Hashiguchi and Zhang-Akiyama, 2009) (ρ^0J774A.1). We confirmed that these cells had lost mitochondria by measuring cellular mitochondrial DNA content by quantitative PCR, Western blotting cell lysates for the mitochondrial protein ATPase inhibitory factor and flow cytometry of cells stained with the mitochondrial specific dye Mitotracker Green (Fig. 5-21a, b, and c). Infection of the ρ^0J774A.1 cells with PA103ΔUΔT gave no increase in mitochondrial reactive oxygen production (Fig. 5-22a). Moreover, when infected with PA103ΔUΔT the ρ^0J774A.1 cells lacking mitochondria failed to activate caspase-1 and produced significantly less IL-1β but similar amounts of TNF. Autophagy, as assayed by the formation of LC3 II and appearance of LC3 puncta, was maintained in ρ^0J774A.1 cells compared to J774A.1 cells (Fig. 5-22b, c, and d), showing that loss of mitochondria had not inhibited this process. Thus, mitochondria are essential for *P. aeruginosa* to activate the inflammasome.
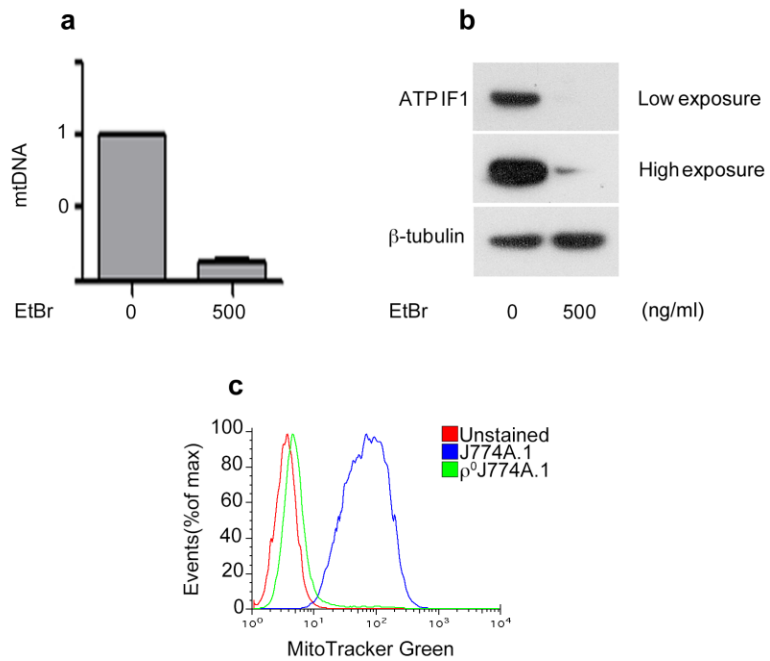
Figure 5.21; Depletion of Mitochondrial DNA following EtBr treatment

a, Mitochondrial content of J774A.1 cells exposed to EtBr at the indicated concentration (ng/ml) measured by qPCR (normalised to untreated cells) and **b** immunoblot for the mitochondrial protein ATPIF1 at low and high exposure time; β-tubulin is show as a loading control. **c**, mitochondrial content of control of ethidium bromide treated J774A.1 cells (ρJ774A.1) assayed by flow cytometry of MitoTracker stained cells. Representative of two independent experiments.
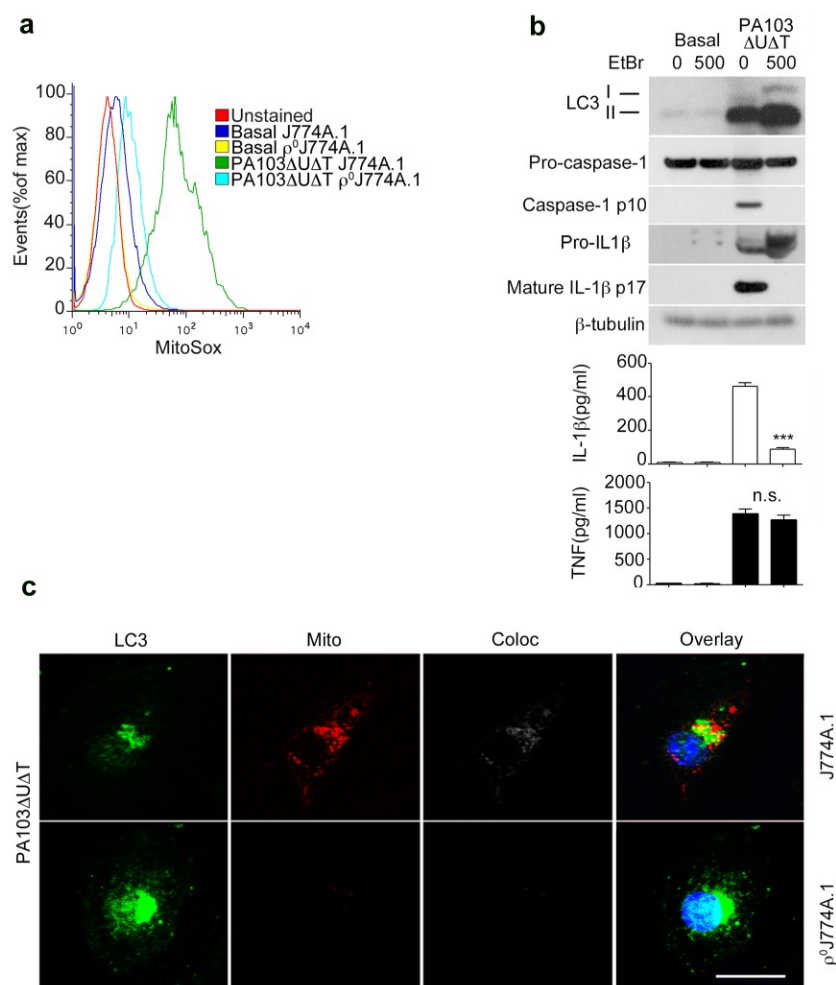
Figure 5.22; EtBr abolishes inflammasome activation following *P.aeruginosa* PA103ΔUΔT infection.

a, Flow cytometry of J774A.1 and ρ˚J774A.1 cells left uninfected (Basal) or infected with PA103ΔUΔT (MOI 25) for 4hr and stained with MitoSox (2.5µM for 30 min at 37˚C). **b,** J774A.1 and ρ˚J774A.1 cells left untreated (basal) or infected with PA103ΔUΔT(MOI 25) for 4 hrs. The panels show Western blot of LC3 II, pro-caspase-1, the caspase-1 p10 subunit, Pro-IL-1β, mature IL-1β and β-tubulin as a loading control. Graphs show IL-1β and TNF secretion. Columns show means of three independent determinations; error bars are SEM. *** indicate significant differences between the levels in the presence and absence of the EtBr (500ng/ml), p < 0.001. **c**, Immunofluorescent staining of cells following infection as in panel **b**, Panels show staining for LC3 (green), ATPIF1 (red; Mito), colocalized red and green signal (Coloc) and merged res and green channels together with nuclei stained blue (Overlay). Scale bar is 5µm. All data representative from 2-3 independent experiments.

5.2.4 Mitochondrial DNA directly activates the NLRC4 inflammasome

Next, we explored the role of cytoplasmic mitochondrial DNA in activating the NLRC4 inflammasome following *P. aeruginosa* infection. We transfected BMDMs with DNAse-1, or with a control protein LDH or heat-inactivated DNAse-1. We then determined the effect of these transfected proteins on the activation of the inflammasome. LDH or heat-inactivated DNAse-1 did not affect the production of activated capsase-1 or production of IL-1β following infection (Fig. 5-23). However, active DNAse-1 prevented caspase-1 activation and significantly reduced the production of mature IL-1β following infection without affecting production of TNF (Fig. 5-23). DNAse-1 treatment reduced the presence of cytosolic mitochondrial DNA as expected (Fig. 5-23). Transfection of active DNAse-1 also reduced the inflammasome activation produced by infection of BMDMs with PAO1 strain without affecting TNF (Fig. 5-24).
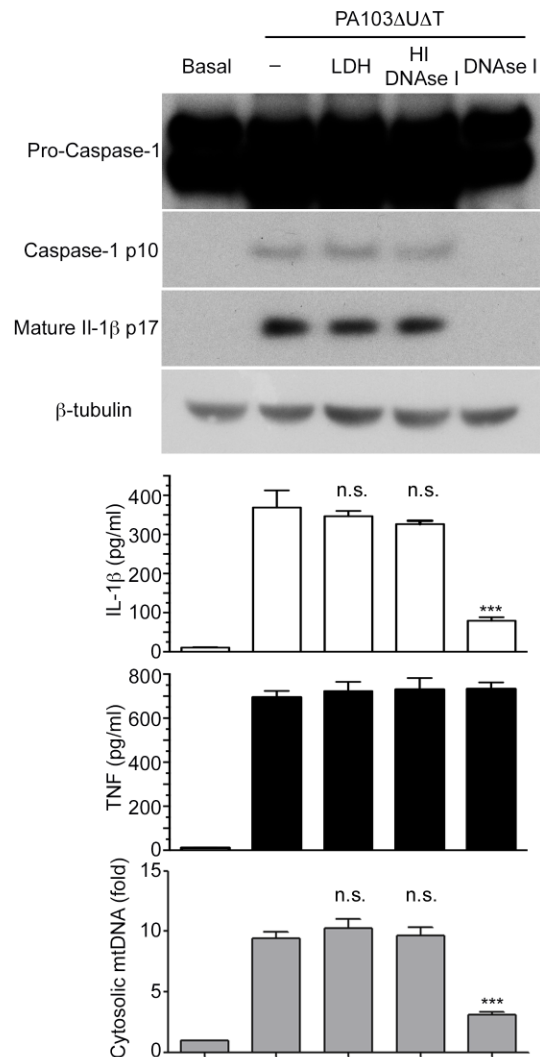
Figure 5.23; Cytosolic mtDNA is coactivator of NLRC4 inflammasome activation following *P. aeruginosa* PA103ΔUΔT infection

BMDMs were transfected with 3 µg DNAse-I, lactate dehydrogenase (LDH), or heat-inactivated (HI) DNAse-I as shown and then infected with PA103ΔUΔT (MOI 25) for 4 hrs. The panels show immunoblot of the indicated proteins and β-tubulin as a loading control. The graphs show IL-1β and TNF secretion and qPCR analysis of cytosolic mtDNA. Columns show means of three independent determinations; error bars are SEM. *** indicates significant difference from HI DNAse-I, $p < 0.001$. Representative of two independent experiments.
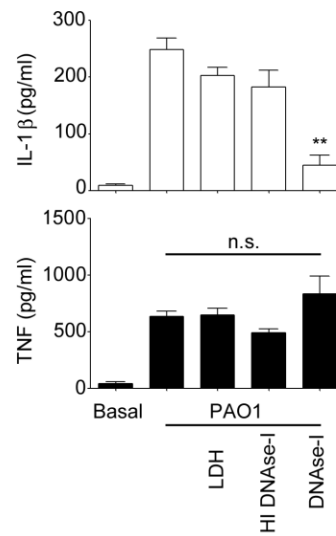
Figure 5.24; mtDNA is required for inflammasome activation following *P. aeruginosa* PAO1 infection.

BMDMs were transfected with 3 µg DNAse-I, lactate dehydrogenase (LDH), or heat-inactivated (HI) DNAse-I as shown and then infected with PAO1 (MOI 25) for 4 hrs. The panels show IL-1β and TNF secretion. Columns show means of three independent determinations; error bars are SEM. ** indicates significant difference from HI DNAse-I, p<0.01.

Mitochondrial DNA may undergo oxidation on release and oxidised mitochondrial DNA has been shown to be important in activating the NLRP3 inflammasome (Shimada et al., 2012). Thus, we set out to determine the role of native and oxidised mitochondrial DNA on activation of the NLRC4 inflammasome in *P. aeruginosa* infection. Firstly, we transfected native and oxidised mitochondrial DNA into LPS primed BMDMs and showed that this increased IL-1β but not TNF release (Fig. 5-25a) as has been shown previously. Oxidised mitochondrial DNA produced a significantly greater amount of IL-1β (Fig. 5-25 a). Digestion of the DNA with DNAse-1 abrogated the observed stimulation. We then repeated this experiment but infected the transfected BMDMs with PA103ΔUΔT. The transfected DNA significantly augmented the production of IL-1β in infected BMDMs without altering TNF secretion (Fig. 5-25 b). Again, oxidised DNA was more effective than native mitochondrial DNA. We repeated this experiment in BMDMs infected with PAO1 and found that transfection of mitochondrial DNA augmented inflammasome activation (Fig. 5-26). Taken together, these data support the conclusion that the release of mitochondrial DNA following infection with flagellated or non-flagellated *P. aeruginosa* is essential for subsequent activation of the NLRC4 inflammasome.
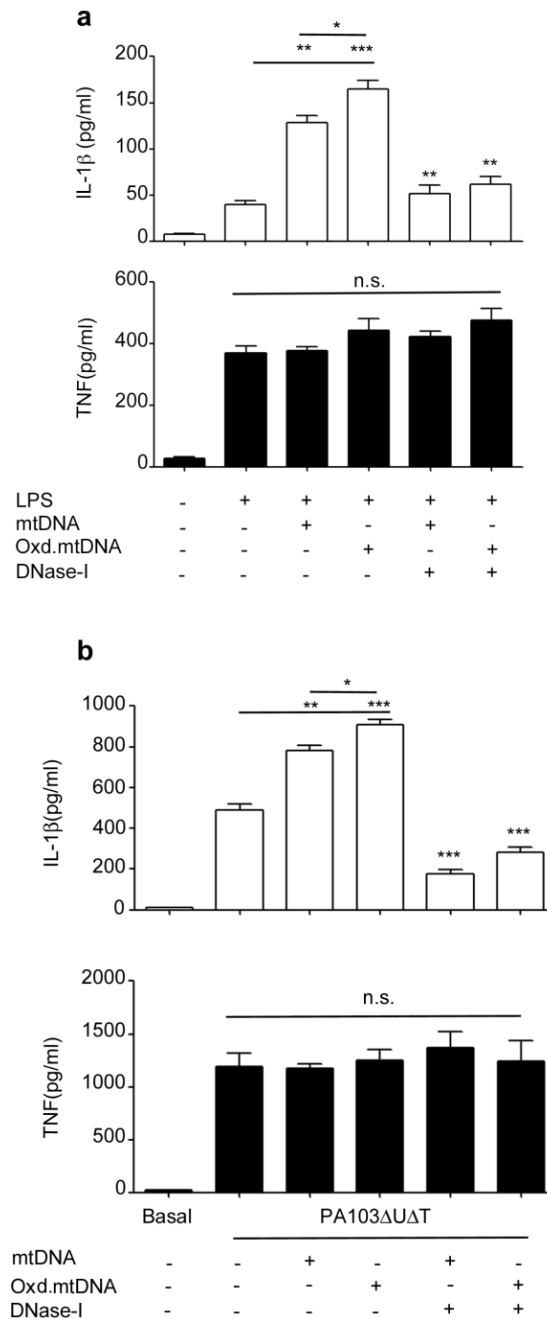
Figure 5.25; Cytosolic mtDNA is involved in NLRP3 and NLRC4 inflammasome activation

a, IL-1β and TNF secretion from LPS primed BMDMs transfected for 6 hr with 2 μg mtDNA, 2 μg oxidised mtDNA, or DNA predigested by DNAse-I.as shown. Columns are means of triplicate independent determinations; error bars are SEM. *, ** and *** indicate significant difference at a level of $p < 0.05$, 0.01 or 0.001 respectively for the indicted comparison or from the result with oxidised DNA + LPS. **b**, as panel **a** but in BMDMs infected with PA103ΔUΔT (MOI 25) for 4 hrs as shown. Representative of two independent experiments.
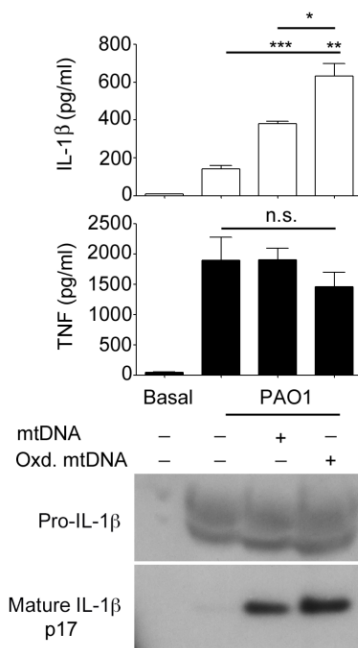
Figure 5.26; mtDNA is involved in NLRC4 inflammasome activation following *P.aeruginosa* PAO1 infection.

BMDMs were transfected with native or oxidised mDNA as shown and then infected with *P. aeruginosa* PAO1 (MOI: 25 for 4hrs). Upper panels show ELISA of IL-1β and TNF secretion. Columns are means of triplicate independent determinations; error bars are SEM. *, ** and *** indicate significant difference at a level of p < 0.05, 0.01 or 0.001 respectively for the indicted comparison or from the result with oxidised DNA. Lower panel shows western blot of pro-IL-1β and mature secreted IL-1β.

A number of cytoplasmic DNA sensors might be responsible for these observed effects, including AIM2 as well as NLRP3 as previously described. We thus examined the effect of transfected mitochondrial DNA on IL-1β production in BMDMs from mice with a knockout of the *Aim2* gene (Rathinam et al., 2010) (*Aim2*$^{-/-}$). Compared to wild type macrophages (*Aim2*$^{+/+}$), the transfected mitochondrial DNA produced less IL-1β in the *Aim2*$^{-/-}$ cells (Fig. 5-27). However, there was still a significant increase in IL-1β production following transfection of mitochondrial DNA into LPS primed *Aim2*$^{-/-}$ BMDMs (Fig. 5-27a). Oxidised DNA was more effective than native, and TNF levels were unaffected. Thus, there is an AIM2 independent production of IL-1β stimulated by mitochondrial DNA, as has been previously observed and attributed to NLRP3. Similarly, in cells infected with PA103ΔUΔT, there was a reduction in amounts of IL-1β produced in *Aim2* deficient cells, but this was still much greater than the output from uninfected cells (Fig. 5-27b). Again, even in the absence of AIM2, transfected mitochondrial DNA boosted IL-1β production in infected cells; oxidised DNA was more effective and TNF levels were unchanged (Fig. 5-27b).
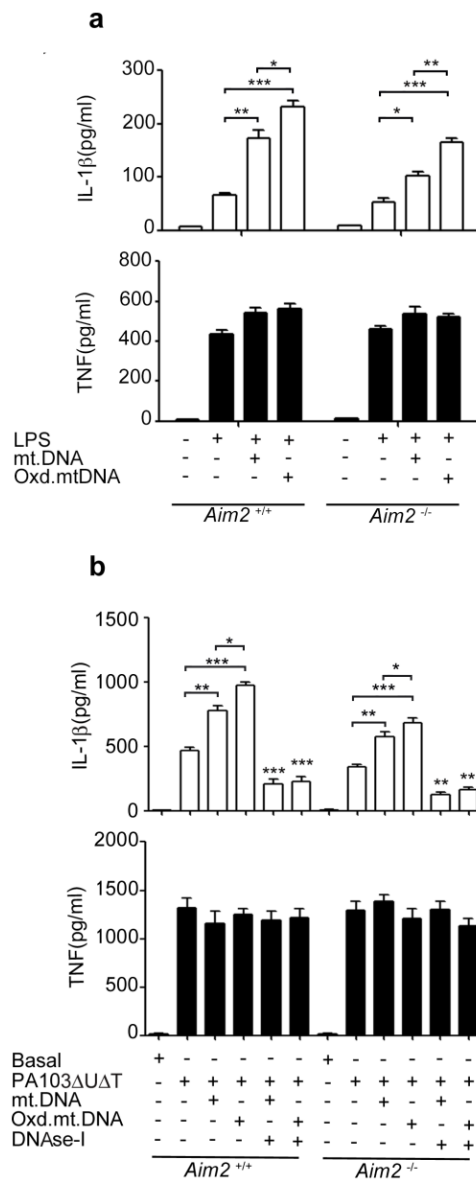
Figure 5.27; Mitochondrial DNA activates the inflammasome independently of Aim2.

a, **b**, IL-1β and TNF secretion from LPS primed BMDMs from *Aim2*^{+/+} and *Aim2*^{-/-} transfected for 6 hr with 2 μg mtDNA, 2 μg oxidised mtDNA, or DNA predigested by DNAse-I.as shown. Columns are means of triplicate independent determinations; error bars are SEM. *, ** and *** indicate significant difference at a level of p < 0.05, 0.01 or 0.001 respectively for the indicted comparison or from the result with oxidised DNA + LPS. **b**, as panel **a** but in BMDMs infected with PA103ΔUΔT (MOI 25) for 4 hrs as shown. Representative of two independent experiments.

Unequivocally to show a role for NLRC4 in the detection of mitochondrial DNA, we repeated these experiments using BMDMs from mice with a knockout of the *Nlrc4* gene (*Nlrc4*^{-/-}). LPS primed cells were then transfected with mitochondrial DNA and inflammasome activation determined. Compared to wild type BMDMs (*Nlrc4*^{+/+}), transfection of mitochondrial DNA into *Nlrc4* knockout cells produced significantly reduced amounts of IL-1β and activated caspase-1 (Fig. 5-28). There was still some residual response to mitochondrial DNA in the *Nlrc4*^{-/-} cells as would be expected from the remaining AIM2 and NLRP3, but it was substantially and significantly reduced. Therefore, NLRC4 independently can mediate activation of the inflammasome in response to transfected mitochondrial DNA. We then tested the effect of transfected DNA in infected cells from wild type and *Nlrc4* knockout animals. *Nlrc4*^{-/-} BMDMs showed no evidence of inflammasome activation following infection, as expected (Fig. 5-29). In *Nlrc4*^{-/-} BMDMs transfected with mitochondrial DNA there was some residual stimulation of inflammasome activation after infection, but much less than seen in the infected and DNA transfected wild-type cells (Fig. 5-29). Thus, there is a NLRC4 dependent response to mitochondrial DNA independent of other cytoplasmic DNA sensors.
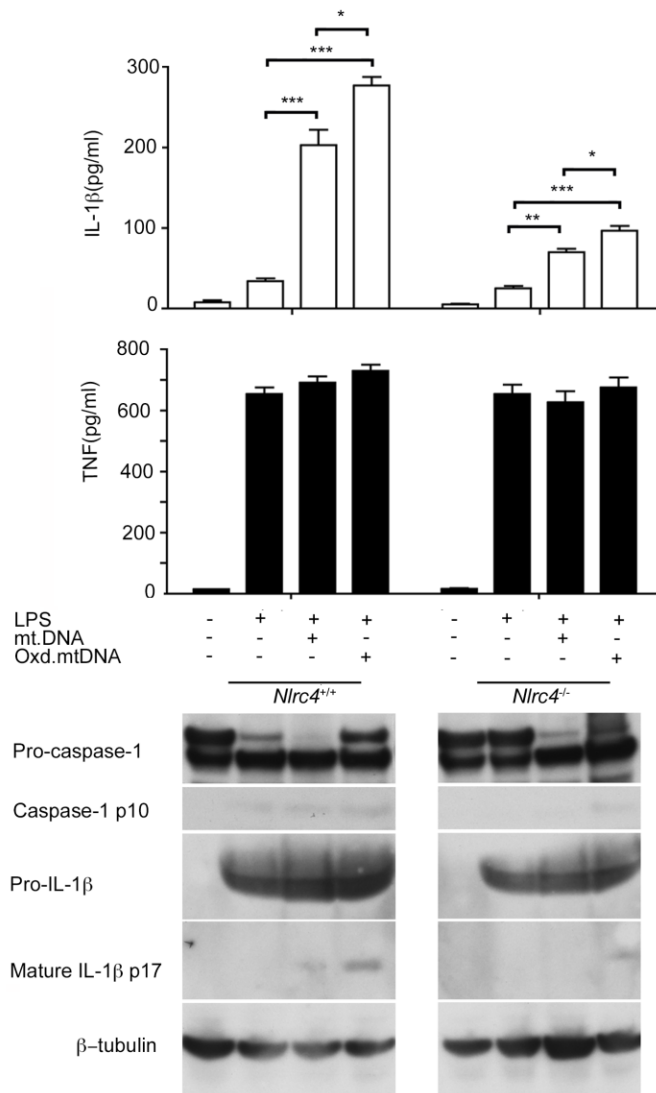
Figure 5.28; Role of NLRC4 in activation of the inflammasome by mediated mtDNA.

The panels show Western blot of pro-caspase-1, the caspase-1 p10 subunit, Pro-IL-1β, mature IL-1β in cells supernatant and β-tubulin as a loading control in LPS primed *Nlrc4⁺/⁺* and *Nlrc4⁻/⁻* BMDMs transfected for 6 hr with 2 μg mtDNA, or with 2 μg Oxd.mtDNA. Graphs show IL-1β and TNF secretion. Columns are means of triplicate independent determinations; error bars are SEM. *, ** and *** indicate significant difference at a level of p < 0.05, 0.01 or 0.001 respectively for the indicted comparison or from the result with oxidised DNA + LPS. Representative of two independent experiments.

IL-1β(pg/ml)

1000 —
750 —
500 —
250 —
0 —

*** , ** , *

TNF(pg/ml)

1500 —
1000 —
500 —
0 —

PA103ΔUΔT	-	+	+	+	-	+	+	+
mt.DNA	-	-	+	-	-	-	+	-
Oxd.mtDNA	-	-	-	+	-	-	-	+

Nlrc4$^{+/+}$ *Nlrc4*$^{-/-}$

Pro-caspase-1

Caspase-1 p10

Pro-IL-1β

Mature IL-1β p17

β–tubulin
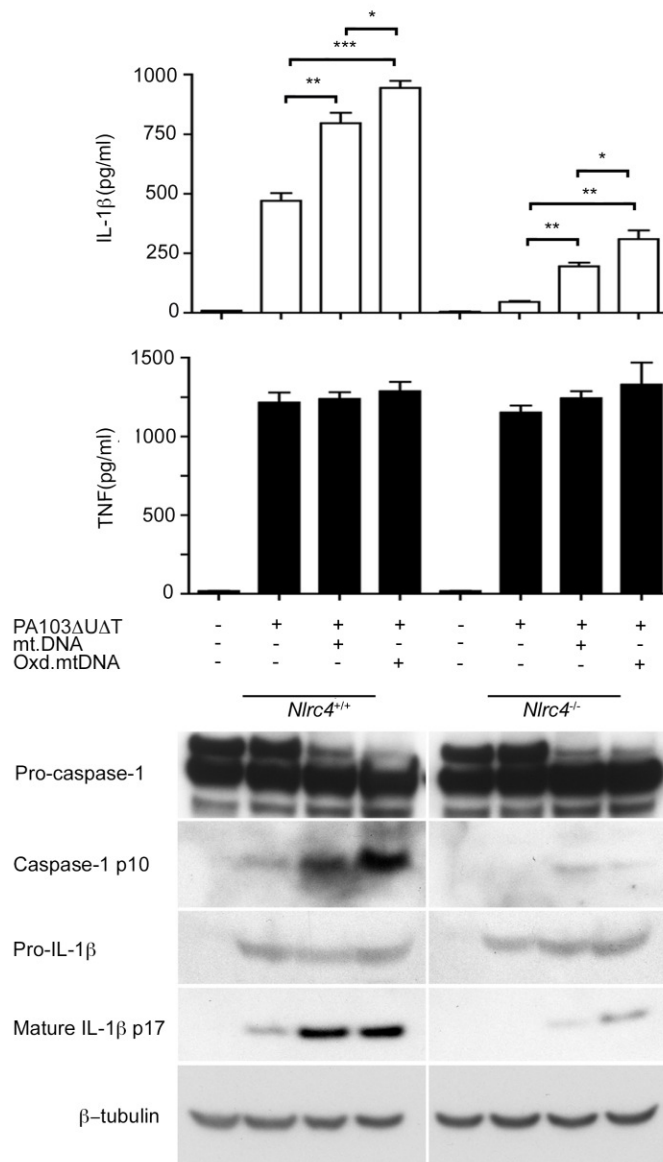
Figure 5.29; Role of NLRC4 in activation of the inflammasome by mtDNA following *P. aeruginosa* PA103ΔUΔT infection.

BMDMs from *Nlrc4*$^{+/+}$ and *Nlrc4*$^{-/-}$ were transfected for 6 hr with 2 μg mtDNA, or with 2 μg Oxd.mtDNA and infected with PA103ΔUΔT (MOI 25) for 4 hrs. The panels show Western blot of pro-caspase-1, the caspase-1 p10 subunit, Pro-IL-1β, mature IL-1β in cells supernatant and β-tubulin as a loading control. Graphs show IL-1β and TNF secretion. Columns are means of triplicate independent determinations; error bars are SEM. *, ** and *** indicate significant difference at a level of $p < 0.05$, 0.01 or 0.001 respectively for the indicted comparison or from the result with oxidised DNA. Representative of two independent experiments.

5.2.5 NLRC4 Interacts with and is activated by Mitochondrial DNA

We hypothesised that the activation of the NLRC4 inflammasome by mitochondrial DNA was mediated by binding to the NLRC4 protein. To test this, we grew cells in BrdU and prepared cell lysates before and after infection. NLRC4 was immunoprecipitated from the lysates and bound DNA in the immunoprecipitates detected by probing slot blots of the eluates with antibody to BrdU (Fig. 5-30). We added 3-MA to some of the cells prior to lysis to block autophagy and thus enhance the release of mitochondrial DNA. In lysates prepared from uninfected cells, no DNA was detected in the NLRC4 immunoprecipitates., even in the presence of 3-MA (Fig. 5-30a). Following infection, NLRC4, but not control, immunoprecipitates contained DNA; the amount was further increased in the presence of 3-MA (Fig. 5-30a). We repeated this experiment, but probed the slot blot with an antibody to 8-OH deoxyguanosine, a modified deoxynuceloside found commonly in oxidised DNA (Fig. 5-30b) (Maki and Sekiguchi, 1992). NLRC4, but not control, immunoprecipitates contained material reacting with this antibody. Thus, following infection with *P. aeruginosa*, NLRC4 has a direct or indirect interaction with DNA, including DNA that has undergone oxidation. To demonstrate that this DNA is mitochondrial in origin, we performed NLRC4 immunoprecipitation from both infected J774A.1 and ρ^0J774A.1 that lack mitochondria. In lysates from infected cells lacking mitochondria, immunoprecipitates of NLRC4 did not contain DNA (Fig. 5-31).
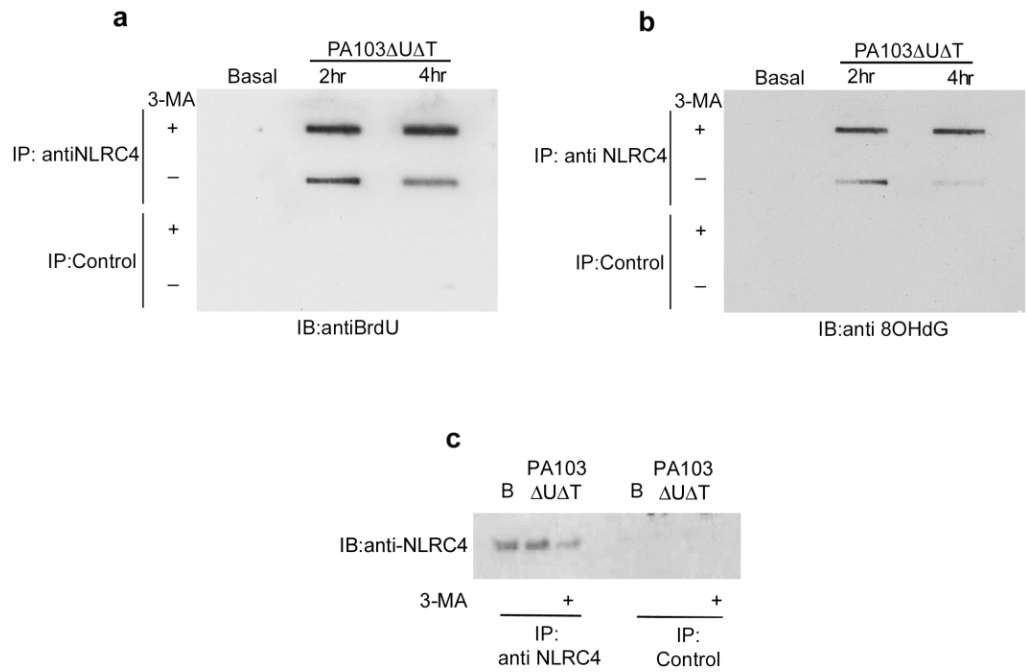
Figure 5.30; NLRC4 binds mtDNA following *P.aeruginosa* PA103ΔUΔT infection.

a, BMDMs were grown in BrdU (10 mM) and infected for 4hr (MOI 25) with PA103ΔUΔT in the absence and prescence of 3-MA as shown before lysates were immunoprecipitated with anti-NLRC4 or control rabbit serum as indicated. Bound material was slot-blotted to nitrocellulose and then blotted with anti-BrdU. **b**, as in **a**, but re-probed with antibody to 8OHdG. **c**, The panel shows separate immunoblot of eluted material from NLRC4 immunoprecipitates blotted for NLRC4. Representative of three independent experiments.
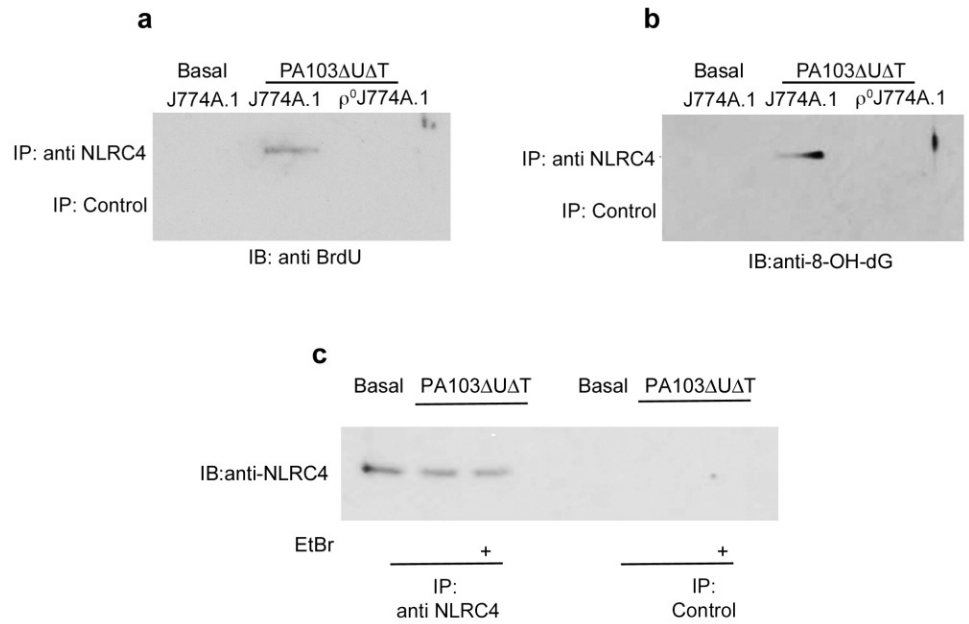
a , J774A.1 and ρ°J77A.1 cells were grown in the presence of (10mM) of BrdU to label DNA and then left uninfected or infected with PA103ΔUΔT(MOI 25) for 4 hr. Panel shows slot blot of elutes immunoprecipitated with anti-NLRC4 or control rabbit serum as indicated. **b**, as in **a** but re-probed with anti- 8OHdG. **c**, The panel shows separate immunoblot of eluted material from NLRC4 immunoprecipitates blotted for NLRC4. Representative of two independent experiments.

Next, we set out to determine if the interaction between NLRC4 and mitochondrial DNA was important in initiating inflammasome activation. To determine if mitochondrial DNA could directly activate NLRC4, we tested the effect of mitochondrial DNA on caspase-1 activation in a reconstituted cell based assay. This work was performed by Dr. Lee Hopkins in Professor Clare Bryant's laboratory in Cambridge. This comprised of HEK cells transfected with expression plasmids encoding NLRC4 and NAIP. These cells were then transfected with mitochondrial DNA and activation of caspase-1 detected by a fluorescent probe, FLICA^{Casp1}. Using a variety of transfection reagents, we detected 'spots' of activated caspase-1 in cells following transfection of mitochondrial DNA, but not in control cells transfected without DNA (Fig. 5-32). Thus, mitochondrial DNA alone is sufficient in this assay to result in NLRC4 inflammasome activation.
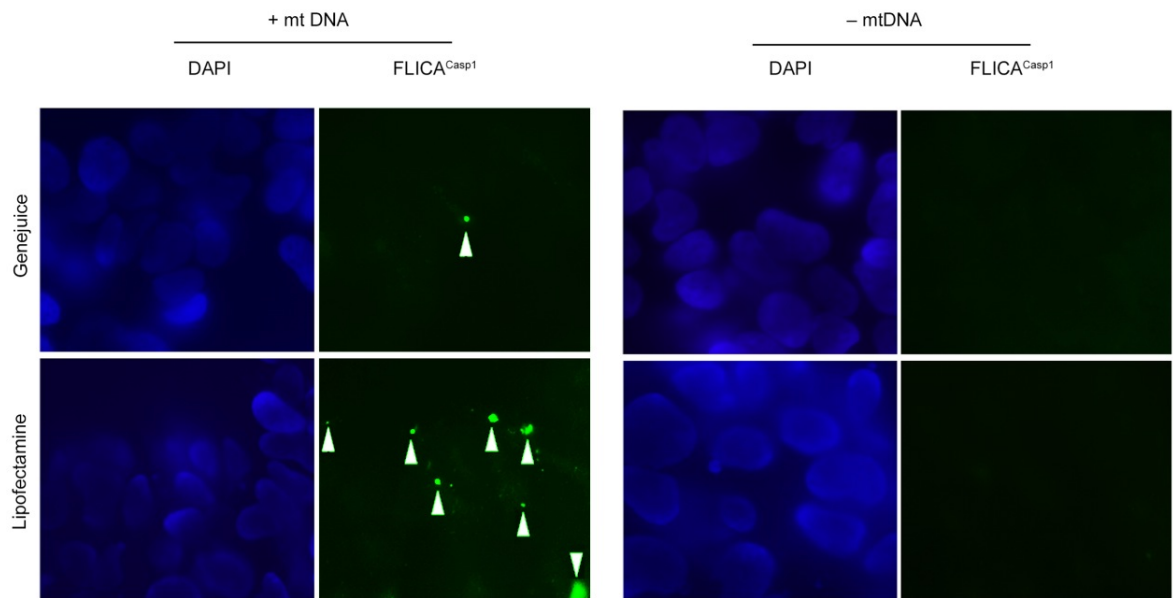
Figure 5.32; Mitochondrial DNA activates NLRC4 in HEK cells.

HEK cells transfected with NLRC4 and NAIP were transfected with and without mitochondrial DNA and active caspase-1 localised by immunofluorescent imaging using FLICA^{Casp1}. Panels show representative images of cells stained with FLICA^{Casp1} (green) and nuclei stained with DAPI (blue) using the indicated transfection reagents. Arrows show 'spots' of active Caspase-1 formation.

5.2.6 Manipulation of autophagy alters inflammasome activation in *vivo* following *P.areuginosa* infection

Given that autophagy attenuates the activation of the inflammasome by *P. aeruginosa* infection, we hypothesised that by drug manipulation of autophagy we could alter inflammasome activation *in vivo*. Firstly, we tested the effect of adding the known inducer of autophagy, rapamycin, to *P. aeruginosa* infected BMDMs as well as the macrophage lines J774A.1 and THP-1. We found that rapamycin augmented the degree of autophagy observed during infection, by assay of LC3 containing puncta, also LC3 II determination using a validated flow cytometric assay (Fig. 5-33a, b), and formation of the LC3 II isoform by Western blot assay (Fig. 5-34). In all cells studied, the addition of rapamycin significantly reduced the amount of IL-1β produced during infection (Fig. 5-34). Neither rapamycin nor 3-MA had any significant effect on the growth of *P. aeruginosa* in culture broth (data not shown).

Next, we tested the effect of altering autophagy on an *in vivo* model of *P. aeruginosa* infection in mice. Animals were infected with the microbe intraperitoneally and the effects of augmenting autophagy with rapamycin and inhibiting autophagy with 3-MA studied. These treatments boosted and inhibited respectively the degree of autophagy in cells recovered from the peritoneal cavity as assayed by levels of LC3 II and LC3 puncta per cell (Fig. 5-35). We found that rapamycin treatment significantly reduced the amount of IL-1β recovered from the peritoneal cavity after infection, but had no effect on levels of TNF (Fig. 5-36). Inhibiting autophagy with 3-MA significantly enhanced IL-1β levels, with no effect on TNF (Fig. 5-36). As an

indicator of disruption to the peritoneal barrier, we measured protein concentration in peritoneal fluid recovered after infection. Rapamycin significantly reduced the protein concentration while 3-MA enhanced it (Fig. 5-37). We also measured the numbers of viable bacteria recovered from the peritoneal cavity following infection (Fig. 5-38). This showed that Rapamycin reduced the numbers of bacteria while 3-MA increased these numbers. Thus, increasing the degree of autophagy with rapamycin reduces the amount of inflammasome activation and resulting inflammatory response following infection *in vivo.* Inhibiting autophagy with 3-MA has the opposite effect. However, increasing the degree of autophagy with rapamycin results in lower numbers of bacteria remaining after infection; again inhibition of autophagy with 3-MA had the opposite effect.
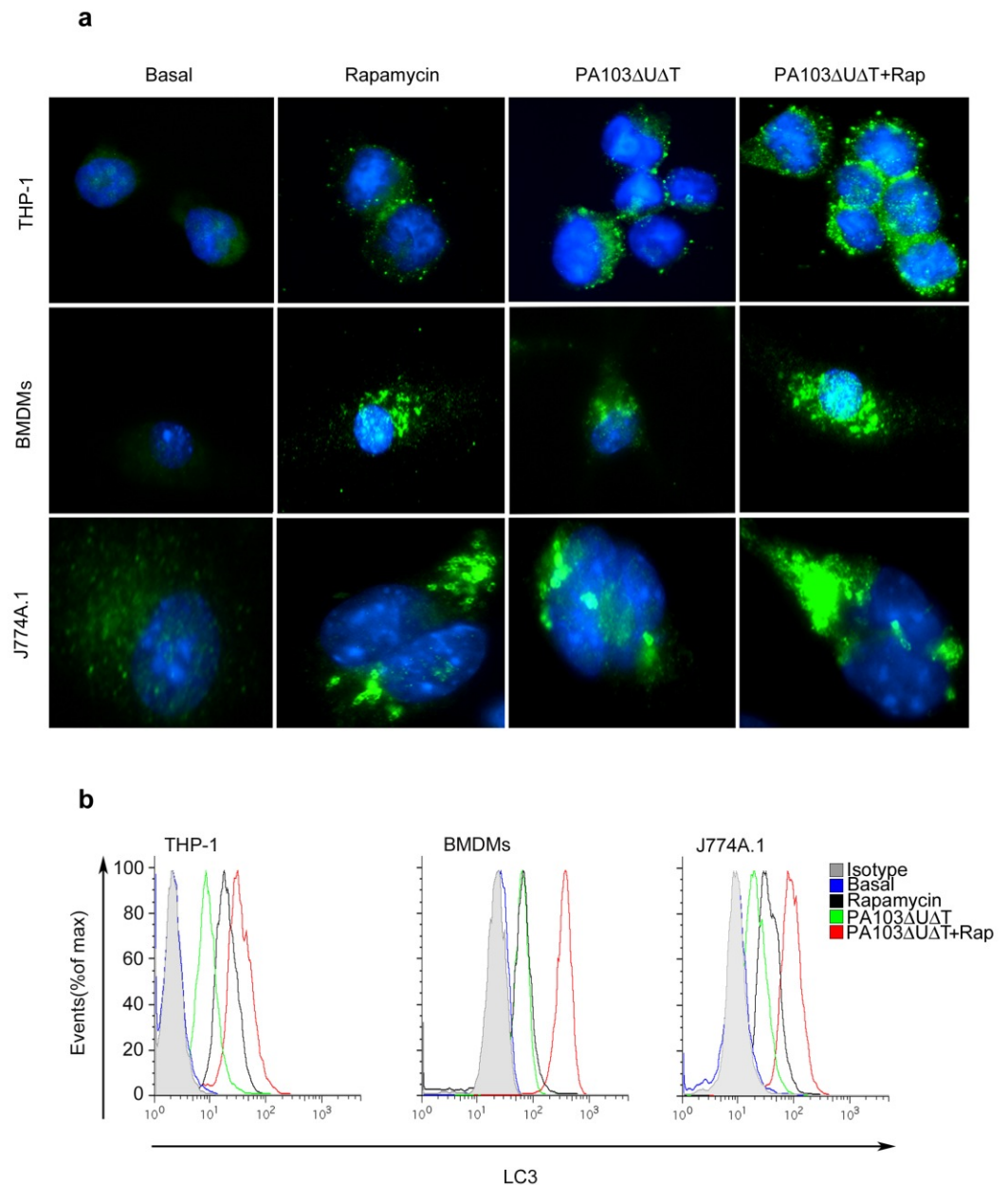
Figure 5.33; Rapamycin augments autophagy following *P.aeruginosa* PA103ΔUΔT infection.

a, representative immunofluorescence images of LC3 in THP-1, BMDM, and J774A.1cells. Cells left uninfected (Basal), treated with rapamycin (50µg/ml) for 4 h, or infected with PA103ΔUΔT or PA103ΔUΔT+rapamycin for 4hrs at a MOI of 25. Cells were stained with DAPI to visualize nuclei (blue), and LC3 staining is shown as green. Scale bar 10 µm. Representative of three independent experiments. **b**, FACS analysis for LC3 protein following infection with PA103ΔUΔT (MOI 25 for 4h), in the presence and absence of rapamycin. Representative of two independent experiments.
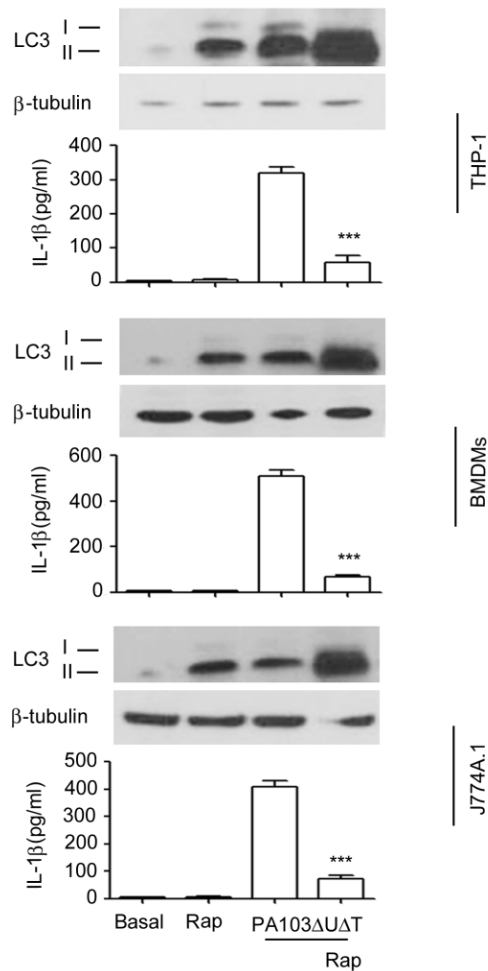
Figure 5.34; Induction of autophagy inhibits inflammasome activation *in vitro.*

The panels show representative Western blot of LC3 isoforms, and β-tubulin as a loading control following infection and rapamycin treatment as indicated. Graphs are means (with SEM as error bars) of IL-1β secretion in the same experiment. THP-1, BMDM, and J774A.1cells were used as indicated. *** indicate significant differences between the levels in the presence and absence of rapamycin during infection, $p < 0.001$. Representative of two independent experiments.
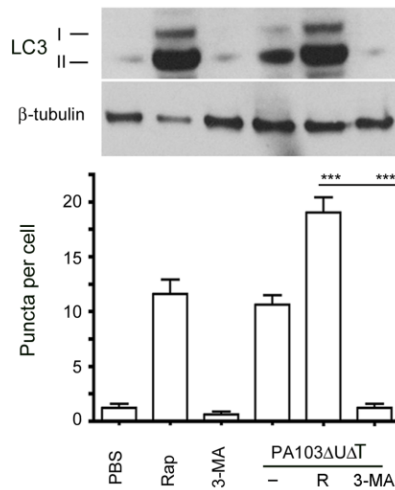
Figure 5.35; Pharmacological manipulation modulates autophagy following infection *in vivo*.

Results from intraperitoneal infection of female C57/BL6 mice with PA103ΔUΔT treated with rapamycin (R), or 3-methyl adenine as indicated. Panel shows level of LC3 I and II in peritoneal cells recovered following infections and treatments as shown; lower panel shows mean (±SEM) numbers of LC3 containing puncta per cell. Representative of two independent experiments.
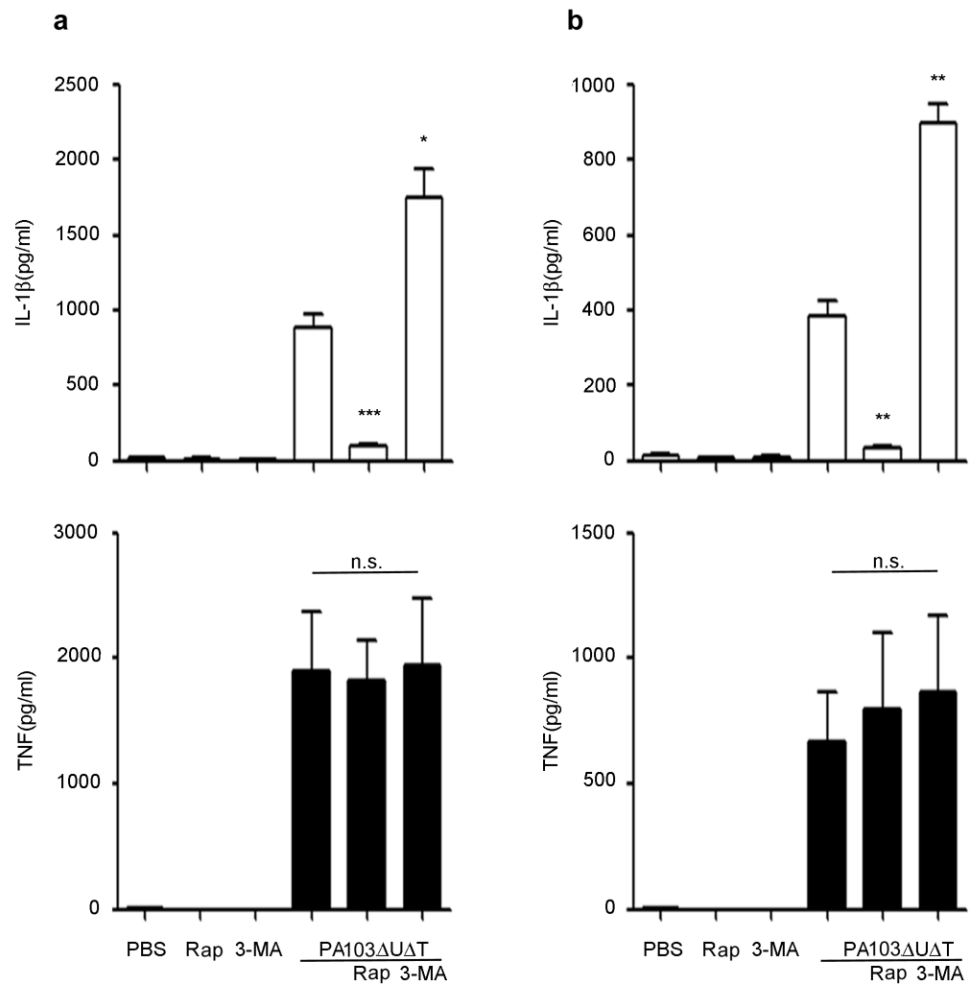
Figure 5.36; Induction of autophagy inhibits inflammasome activation *in vivo* following *P. aeruginosa* PA103ΔUΔT infection.

Results from intraperitoneal infection of female C57/BL6 mice with PA103ΔUΔT treated with rapamycin (R), or 3-methyl adenine as indicated. Graphs shows mean levels (n=3) of IL-1β and TNF (error bars are SEM) in the blood (**a**) and peritoneal washings (**b**) before and 6 hr after infection with the indicated treatments. *and ** and *** indicate significant differences from the levels in infected animals with no pre-treatment. Representative of two independent experiments.
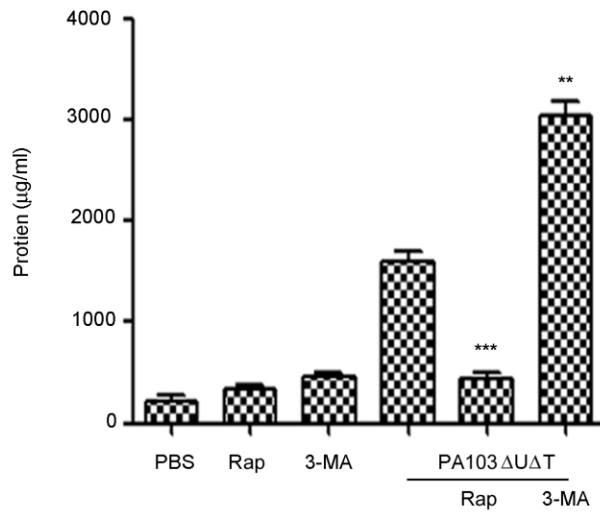
Figure 5.37; Protein concentration following intraperitoneal fluid infection.

Protein concentration in peritoneal fluid following infection and treatments as in figure 5-36. Representative of two independent experiments.
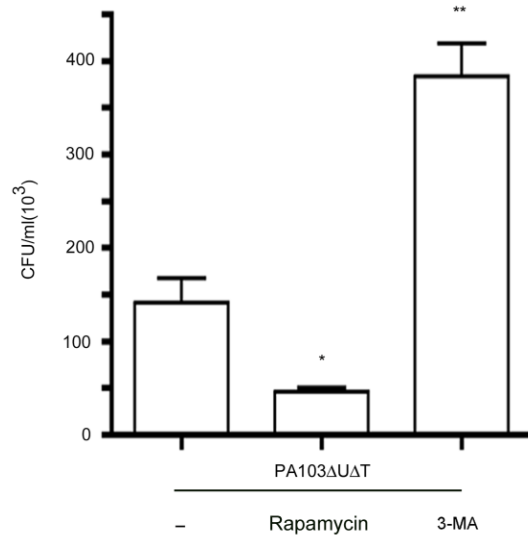
Figure 5.38; Autophagy contributes to bacterial killing *in vivo* following *P. aeruginosa* infection.

Bacterial colony counts per ml of recovered fluid from the peritoneal cavity with treatments as shown. Columns are means of triplicate determinations; error bars SEM. Representative of two independent experiments.

5.3 Discussion

We have shown here that mitochondria play an essential role in the activation of the NLRC4 inflammasome by the pathogen *P. aeruginosa*. Taken together, these data establish a novel pathway of NLRC4 activation dependent on mitochondrial sensing of infection. Flagellin (Miao et al., 2006) and components of the T3SS rod and needle complex have been reported to activate the NLRC4 inflammasome, utilising proteins of the NAIP family as adaptors (Miao et al., 2010, Zhao et al., 2011, Kofoed and Vance, 2011). We propose that these bacterial interactions with NAIP proteins are upstream of a subsequent initiation of mitochondrial damage and release of mitochondrial DNA. Given that NLRP3 activation has also been shown to be dependent on mitochondrial DNA release. The mechanism by which *P. aeruginosa* produces this mitochondrial damage is unclear. However, the initiation of inflammasome activation and pyroptosis has many similarities to apoptosis, in which mitochondria play a key role. For example, the Fas apoptosis pathway can results in cleavage of the protein Bid to a form that moves from the cytoplasm to mitochondria where it initiates damage and release of cytochrome c, amplifying the apoptotic signal (Billen et al., 2008). We speculate that in a similar fashion NAIP proteins may translocate to mitochondria after activation by flagellin or T3SS rod proteins.

The interaction of the T3SS of the microbe with its target cell results in mitochondrial production of reactive oxygen intermediates and the release of mitochondrial DNA. Through a number of independent approaches we have shown that this mitochondrial damage is essential to subsequent activation of the NLRC4 inflammasome by this pathogen and

that it can be attenuated by selective mitophagy, also triggered by the T3SS. We have shown that mitochondrial DNA is sufficient to activate the NLRC4 inflammasome separately from other DNA sensors; oxidised DNA is more potent in this regard than the native form. NLRC4 complexes can bind mitochondrial DNA and results in inflammasome activation. Manipulation of the autophagocytic pathway *in vivo* can alter the activation of the inflammasome by *P. aeruginosa* infection and the subsequent inflammatory response.

P. aeruginosa that lack a functional T3SS can activate the NLRP3 inflammasome by a mechanism that requires a TRIF-dependent activation of caspase-11 (Rathinam et al., 2012, Kayagaki et al., 2011). This is a slower process than activation via the T3SS as it requires transcriptional activation of caspase-11, which typically takes some hours. All the work described here was with *P. aeruginosa* that has an active T3SS which produces rapid inflammasome activation that is independent of caspase-11 and NLRP3 and is abolished in the absence of NLRC4 (Rathinam et al., 2012, Arlehamn and Evans, 2011). Thus, the involvement of mitochondria in the activation of the inflammasome that we describe here is quite independent of caspase-11 and NLRP3 involvement.

Several groups have shown the importance of mitochondrial damage and sensing of released mitochondrial DNA in NLRP3 inflammasome activation (Nakahira et al., 2011, Shimada et al., 2012); removal of damaged mitochondria by selective autophagy (mitophagy) inhibits this activation. Thus, the question remains as to how specific NLRP3 or NLRC4 inflammasome activation can be achieved through an identical signal. We

propose that additional proteins must be involved in triggering either a NLRC4 or NLRP3 response. These might be NAIP family members that in the context of binding to flagellin or T3SS rod/needle proteins direct a NLRC4 response over NLRP3 activation. As the original description of the inflammasome makes clear, an activating signal is required to bring together an inflammasome complex (Martinon et al., 2002). Thus, the presence of particular activated binding partners, such as NAIPs, may lead to assembly of the NLRC4 inflammasome, while different protein interactions may produce a NLRP3 inflammasome. For example, the guanylate binding protein GBP5 has been shown to be important for assembly of the NLRP3 inflammasome for some, but not all triggering stimuli (Shenoy et al., 2012). Indeed, different inflammasomes may assemble at different times during a triggering event such as an infection. A role for mitochondrial damage and sensing of mitochondrial DNA may therefore be a common factor that is required for the final activation of the assembled inflammasome.

We show here that immunoprecipitated NLRC4 contains bound mitochondrial DNA (Fig. 5-30). Similar results have been found for NLRP3. We do not know whether DNA is binding directly to the NLR proteins or if it binds to an associated protein. Direct binding to these different NLRs might suggest a role for the common central NOD domain of these proteins as DNA binding elements; equally, other interacting proteins may be involved. Further experiments to define the exact element that interacts with DNA are required.

The results presented in this chapter show that autophagy regulates NLRC4 activation following *P. aeruginosa* infection, by selective removal of damaged mitochondria – mitophagy. The T3SS of the *P. aeruginosa* triggers a process that leads to the accumulation of full-length PINK-1 on the surface of mitochondria (Fig. 5-9) and their removal by mitophagy. This acts to abrogate the activation of the NLRC4 inflammasome. We have also found that there is a reciprocal effect of inflammasome activation on the process of autophagy, such that caspase-1 activation leads to proteolytic processing of the signalling intermediate TRIF and hence down-regulates autophagy (chapter 4). This is important to consider when evaluating the effects of interrupting NLRC4 activation on the production of mitochondrial reactive oxygen intermediates and release of mitochondrial DNA. Inhibiting NLRC4 activation results in attenuated caspase-1 activity and hence a reduction in TRIF processing and increased autophagy. This will lead to a reduction in mitochondrial reactive oxygen production and release of mitochondrial DNA. We suggest that this is the mechanism that accounts for the apparent dependence of mitochondrial damage on NLRP3 as reported by (Nakahira et al., 2011).

We show using an *in vivo* peritoneal infection model with *P. aeruginosa* that manipulation of the autophagocytic pathway with rapamycin and 3-MA can alter the degree of activation of the inflammasome and subsequent inflammation. This reinforces the physiological relevance of the mechanisms we have described in this work. Additionally, it suggests that manipulation of autophagy could be exploited therapeutically to modify the IL-1β response following infection. Clearly, IL-1β plays an important role in host defense, but excess production of inflammatory mediators is

deleterious as found in sepsis and septic shock. Down-regulating inflammasome activation by promoting autophagy in sepsis might therefore be a useful therapeutic strategy. Autophagy also has a role in clearance of *P. aeruginosa*; in our model of infection, augmenting or inhibiting autophagy decreased or increased respectively the numbers of bacteria recovered from peritoneal cavity (Fig. 5-38).

In conclusion, the work described here establishes a novel pathway by which infection activates the NLRC4 inflammasome, by inducing mitochondrial damage and release of mitochondrial DNA. This pathway is similar to that described for the activation of the NLRP3 inflammasome by LPS and ATP. Further work will be required to establish how each pathway operates independently. This study serves to underscore the importance of mitochondria in initiating an inflammatory response through activation of the inflammasome, and how control of mitochondrial quality through autophagy is central in limiting this response.

6   General discussion and Conclusions

It has been proved that mutation of autophagy genes increases susceptibility to infection by intracellular organisms in plants, flies worms, mice, and possibly to humans. It is suggested that autophagy pathway functions of autophagy proteins also have major role in controlling other aspects of immunity in multicellular organisms. The autophagy machinery is thought to have evolved as a stress response to allow eukaryotic organisms to survive in unfavourable conditions probably by regulating energy homeostasis and quality control of proteins and organelles. The autophagy machinery interacts with cellular stress response pathways (Kroemer et al., 2010), including those responsible for controlling immune responses and the process of inflammation. There is direct interaction between autophagy proteins and immune signalling molecules (Saitoh et al., 2009).

To know whether autophagy is induced by *P. aeruginosa*, we studied this degradative mechanism in BMDMs, dendritic cells, the macrophage cell lines J774A.1, and RAW264.7, and the human cell line THP-1 cells. Our study revealed that autophagy is induced by *P. aeruginosa* in BMDMs through different pathways including Atg8 (LC3), Atg5 and Atg7. The results in chapter 3 and chapter 4 show that *Pseudomonas aeruginosa* induced autophagy and the PA103 pcrV mutant appears to show more autophagy than the PA103ΔUΔT strain, that was not dependent on functional T3SS but was dependent on TLR4 and the signaling molecule TRIF. *PA* infection also strongly induced activation of the inflammasome which was absolutely dependent on a functional T3SS. We found that inhibition of inflammasome activation increased autophagy, suggesting that the inflammasome normally inhibits this process. Further experiments showed that this inhibitory effect

was due to the proteolytic action of caspase-1 on the signaling molecule TRIF. Using a construct of TRIF with a mutation in the proteolytic cleavage site prevented caspase-1 cleavage and increased autophagy. TRIF is also involved in the production of interferon-β following infection. We also found that caspase-1 cleavage of TRIF down-regulated this pathway as well. Caspase-1 mediated inhibition of TRIF-mediated signaling is a novel pathway in the inflammatory response to infection. It is potentially amenable to therapeutic intervention.

Induction of autophagy following *PA* infection was determined using different methods: - electron microscopy, immunostaining of the autophagocytic marker, LC3 and post-translational conjugation of phosphatidyl-ethanoloamine (PE) to LC3 using Western blot, RT-PCR, and FACS for LC3 intracellular staining. We hypothesized the reciprocal link between autophagy and inflammasome activation. To test this hypothesis, we studied autophagy in the mouse BMDMs, dendritic cells, the macrophage cell lines J774A.1, and RAW264.7, and human cell line THP-1 cells. Cells were infected with *Pseudomonas aeruginosa* PA103ΔUΔT, which has a fully functional T3SS but lacks translocated toxins and the PA103ΔpcrV strain which lacks a functional T3SS and is known not to activate the inflammasome. Incubations were conducted using different (MOI) and different time, and with Rapamycin 50µg/ml for 4 hours as positive control. This led to the redistribution of microtubule-associated protein 1 light chain (LC3) from diffuse to punctate staining, which is typical of autophagosome vacuoles (Ogawa et al., 2005); (Gutierrez et al., 2004). A well-recognised marker of activation of the autophagic mechanism within a cell is the conjugation of microtubule associated protein 1 light chain 3

(LC3-I) with phosphatidylethanolamine to generate LC3-II, which becomes bound to the membrane of the autophagosome (Kabeya et al., 2000). During the autophagy process, (LC3-I) undergoes processing to (LC3-II), and then the new form is targeted to autophagosomal membranes (Tanida et al., 2004). LC3-I and LC3-II are separated by SDS-PAGE 12% due to a mobility shift, and the amount of LC3-II correlates with the number of autophagosome vesicles (Mizushima and Yoshimori, 2007).To further prove induction of autophagic vesicles in *Pseudomonas aeruginosa* infected cells, western blotting with an antibody against LC3 was done to monitor conversion of endogenous LC3-I to LC3-II. The conversion of the cystolic form of LC3-I to the lipid conjugated form of LC3-II increased when BMDM were treated with 50 µg/ml Rapamycin for 4 h. Similarly, infection of BMDM with *Pseudomonas aeruginosa* wild-type PA103ΔUΔT and mutant strain PA103ΔpcrV also led to a rapid increase in cellular levels of LC3-II within 1 hour compared to uninfected cells. Our data showed that conversion of LC3-I to LC3-II, number of autophagic vacuoles, and LC3 intracellular staining was increased when cells pre-treated with lysosomal inhibitors such as Pepstatin A, E64d, and Bafilomycin A which prevent loss of LC3-II during lysosomal degradation and recycling of the lipid conjugated form LC3-II to the cystolic form LC3-I after fusion of autophagosome with lysosomes. Therefore these inhibitors increase the autophagy marker (LC3 protein) via blocking autophagy flux (Mizushima and Yoshimori, 2007).

Numerous studies have demonstrated a role of potassium efflux in both NLRP3, and NLRC4 inflammasome activation (Sharp et al., 2009), (Hornung et al., 2008), (Gurcel et al., 2006) (Arlehamn et al., 2010). We found that treating of BMDMs, dendritic cells, J774A.1, and human cell line

THP-1cells with a high concentration of KCl 140mM/ml during infection with PA increased autophagy.

The results in chapter 5 show the inhibition of autophagy by other means increases the activation of the inflammasome and production of the active IL-1β. Thus, autophagy acts normally to limit activation of the inflammasome and production of IL-1β. We also addressed another important question: How does autophagy limit inflammasome activation? Our hypothesis was the production of reactive oxygen intermediates (ROI) from mitochondria would be a force driving inflammasome activation, and that autophagy could remove sick mitochondria produced in infection and thus limit the production of ROI and hence inflammasome activation. We tested this hypothesis using specific inhibitors of mitochondrial ROS production. These did inhibit inflammasome activation, supporting our hypothesis. They were specific as they had no effect on cellular TNF production following bacterial infection. Activation of the NLRC4 inflammasome by pathogenic bacteria is a central event in the innate immune response. We set out to determine the role of autophagy in controlling the activation of the NLRC4 by the pathogenic bacterium, *Pseudomonas aeruginosa.* We show that infection results in mitochondrial damage with increased production of reactive oxygen intermediates and release of mitochondrial DNA. This free cytoplasmic mitochondrial DNA activates the NLRC4 inflammasome. Autophagy attenuates this activation by removal of damaged mitochondria. NLRC4 immunoprecipitates bind mitochondrial DNA and transfection of mitochondrial DNA can activate a reconstituted NLRC4 inflammasome. Manipulation of autophagy alters the degree of inflammasome activation in an *in vivo* model of *P. aeruginosa*

infection, with modulation of the inflammatory response generated. These data demonstrate a novel mechanism by which the NLRC4 inflammasome can be activated, with similarities for mechanisms proposed for activation of the NLRP3 inflammasome.

The mechanism (s) by which the autophagy pathway inhibits inflammasome activation are not yet understood. One possibility includes direct interactions between autophagy proteins and inflammasome components, or indirect inhibition of inflammasome activity through autophagic suppression of mitochondrial ROS accumulation, or autophagic degradation of danger signals that activate the inflammasome. In line with the latter model, the autophagic degradation of amyotrophic-lateral-sclerosis-linked mutant superoxide dismutase has been proposed to limit caspase 1 activation and IL-1β production (Meissner et al., 2010).

3-MA inhibits autophagy by blocking autophagosome formation through the inhibition of type III Phosphatidylinositol 3-kinases PI3KIII which is required in the early stage of autophagy process for autophagosome generation (Petiot et al., 2000). Inhibition of PI3KIII by 3-methyladenine (3MA) or Wortmannin (Wm) has been shown to inhibit starvation-induced autophagy (Lum et al., 2005). Our results showed that 3MA (10 mM) is able to block *Pseudomonas aeruginosa* infection -induced autophagy. A previous study showed that LPS plays a crucial role in inducing inflammasome activation and IL-1β secretion in embryonic liver macrophages from Atg16L $^{-/-}$ mice, suggesting a role for autophagy in dampening the inflammatory response to endotoxin (Saitoh et al., 2008). Autophagy has also been linked to augmenting and inhibiting inflammatory

responses. In inflammasome activation and induction of cell death by pyroptosis, autophagy has been shown to have a marked inhibitory effect (Saitoh et al., 2008).

To demonstrate the crucial role of autophagic proteins during inflammasome activation following infection with *PA*, we isolated macrophages from mice with deletion of autophagy gene Vav-Atg7$^{-/-}$, and infected the cells with PA103 ΔUΔT. First, we examined the effect of deficiency of the autophagic protein Atg7 on the activation of the inflammasome by measuring caspase-1 in BMDM WT, and Vav-Atg7$^{-/-}$ animals. Our results show the macrophages from mice lacking *Atg7* had more of the active, cleaved form of caspase-1 in response to treatment with PA103 ΔUΔT than did wild-type macrophages. Additionally, the cleaved form of IL-1β, produced from the precursor pro-IL-1β through the action of activated caspase-1, was greater in abundance in the lysates and culture medium of Vav-Atg7$^{-/-}$ knockout macrophages. To prove induction of autophagic vesicles in *Pseudomonas aeruginosa* infected cells, immunofluorescence, western blotting, and FACS with an antibody against LC3 as well as RT-PCR was done in Vav-Atg7$^{-/-}$ compared with WT BMDMs. Similarly, knockdown of Atg5, and *Lc3b* mediated by small interfering RNA also enhanced IL-1β secretion and activation of caspase- 1 in BMDM. In addition, secretion of tumour necrosis factor (TNF) in response to PA103 ΔUΔT was similar among the genotypes. Collectively these results demonstrate that depletion of autophagy proteins enhances caspase-1 activation and the secretion of IL-1β in BMDMs macrophages in response to PA103 ΔUΔT. Our results agree with the other studies (Castillo et al., 2012), their results showed *M.tuberculosis* infection of *Atg5*$^{fl/fl}$ LysM-

Cre$^+$ mice increased IL-1β levels. Other studies have shown inhibition of autophagy increases inflammasome activation by increase caspase-1, IL-1α,β , and IL-18 secretion (Kleinnijenhuis et al., 2011) (Nakahira et al., 2011). According to (Fujishima et al., 2011) the deletion of *Atg*7 in intestinal epithelium cells treated with LPS induces higher levels of IL-1β mRNA, compared to wild type mice. These results suggest that the autophagy pathway normally controls and regulates endogenous factors that would otherwise induce inflammasome assembly and activation (Harris, 2013).

According to recent studies, there is a complex relation between autophagy and inflammasome activation. According to Newman etal. 2009, there is unclear information about the mechanism that accounts for autophagy producing inflammasome inhibition is not clear. In the study of (Harris et al., 2011) , autophagosomes were proposed to attack the inflammasome for the purpose of degradation. Though, since NLRP3 inflammasome action is concealed by reactive oxygen species (ROS) obstruction and autophagy negatively controls ROS generation, it is likely that autophagic suppression of ROS restrains inflammasome activity indirectly (Okamoto and Kondo-Okamoto, 2012) .

Another complexity in the relation between autophagy and inflammasome was put forward in a study by (Suzuki and Nunez, 2008). According to this study, inflammasome activation has a negative regulation on autophagy. This study found that caspase-1 deficiency promotes autophagy in macrophages infected with Shigella. However, the report failed to provide complete information about the reciprocal nature of the relation between the two concepts.

According to (Shi et al., 2012), and (Harris et al., 2011), the induction of autophagy results in the reduction of IL-1β processing and secretion. According to Harris et al., 2011, the reduction was shown in cells that were treated with LPS or PAM3CysK4. They suggested that induction of autophagy is inducing degradation of pro-IL-1β, rather than processing and secretion of the mature (p17) form. Similarly, rapamycin abrogated IL-1 β secretion in response to treatment with LPS and ATP. The combination of rapamycin and LPS powerfully forced the formation of autophagosome in LC3-GFP iBMMs. These authors propose that autophagy acts to minimize the accessibility of pro-IL-1β under stimulated cells and represents a novel mechanism for self-regulation of inflammatory responses by macrophages and dendritic cells.

Mitochondrial DNA has recently been emerged as the main element that can take active part in the establishment of inflammasome. A study of (Nakahira et al., 2011) showed that mitochondrial DNA has an involvement in NLRP3 inflammasome activation. Mitochondrial DNA directly induced NLRP3 inflammasome activation, because ρ° J774A.1cells lacking mitochondrial DNA after treatment with EtBr had severely attenuated IL-1β production, yet still underwent apoptosis. Thus, the data reveal that oxidized mitochondrial DNA released during programmed cell death causes activation of the NLRP3 inflammasome. These data supply or expand a missing link between apoptosis and inflammasome activation, through binding between cytosolic oxidized mitochondrial DNA and the NLRP3 inflammasome (Shimada et al., 2012).

There could be an inverse relationship between the Atg proteins and immunity and inflammation and these proteins function both in induction and suppression of immune and inflammatory responses and similarly the immune and inflammatory signals function in both the induction and suppression of autophagy (Levine and Kroemer, 2008). The discovery of autophagy proteins and the relation between autophagy, immunity and Inflammation will reshape the understanding of immunity and disease. The autophagy proteins not only arrange the lysosomal degradation of unwanted cargo, but also help in the control of immunity and inflammation. Thus, the autophagy pathway and autophagy proteins may function as a balance between the beneficial and harmful effects of the host response to infection and immunological stimuli. Autophagy has been implicated in either the pathogenesis or response to a wide variety of diseases, chronic bacterial infections, viral infections, cancers, neurodegenerative diseases, and atherosclerosis (Kundu et al., 2008).

Future work

1- Further studies are necessary to determine how the immune responses are altered and specifically and interact with other critical innate and acquired immune responses (in *vivo* model).

2- Investigate role of autophagy in Ag presentation following PA infection. Does blocking or enhancing the autophagy mechanism alter antigen presentation following PA infection?

3- Further studies are needed to understand the molecular link between inflammasome activation, pyroptosis, and autophagy, as well as their

role in regulating host innate immune response against extracellular bacteria.

4- Further studies are needed to understand how endogenous cytosolic mitochondrial DNA connects mitochondrial dysfunction to caspase-1 activation following PA infection.

5- Further studies are needed to understand how the pharmacological manipulation of the autophagy pathway could be of therapeutic benefit in the treatment of PA infection *in vivo*.

AACHOUI, Y., LEAF, I. A., HAGAR, J. A., FONTANA, M. F., CAMPOS, C. G., ZAK, D. E., TAN, M. H., COTTER, P. A., VANCE, R. E., ADEREM, A. & MIAO, E. A. 2013. Caspase-11 protects against bacteria that escape the vacuole. *Science,* 339**,** 975-8.

AGOSTINI, L., MARTINON, F., BURNS, K., MCDERMOTT, M. F., HAWKINS, P. N. & TSCHOPP, J. 2004. NALP3 forms an IL-1beta-processing inflammasome with increased activity in Muckle-Wells autoinflammatory disorder. *Immunity,* 20**,** 319-25.

AKIRA, S., UEMATSU, S. & TAKEUCHI, O. 2006. Pathogen recognition and innate immunity. *Cell,* 124**,** 783-801.

ALLURED, V. S., COLLIER, R. J., CARROLL, S. F. & MCKAY, D. B. 1986. Structure of exotoxin A of Pseudomonas aeruginosa at 3.0-Angstrom resolution. *Proc Natl Acad Sci U S A,* 83**,** 1320-4.

AMER, A., FRANCHI, L., KANNEGANTI, T. D., BODY-MALAPEL, M., OZOREN, N., BRADY, G., MESHINCHI, S., JAGIRDAR, R., GEWIRTZ, A., AKIRA, S. & NUNEZ, G. 2006. Regulation of Legionella phagosome maturation and infection through flagellin and host Ipaf. *J Biol Chem,* 281**,** 35217-23.

ARLEHAMN, C. S. & EVANS, T. J. 2011. Pseudomonas aeruginosa pilin activates the inflammasome. *Cell Microbiol,* 13**,** 388-401.

ARLEHAMN, C. S., PETRILLI, V., GROSS, O., TSCHOPP, J. & EVANS, T. J. 2010. The role of potassium in inflammasome activation by bacteria. *J Biol Chem,* 285**,** 10508-18.

BAEHRECKE, E. H. 2005. Autophagy: dual roles in life and death? *Nat Rev Mol Cell Biol,* 6**,** 505-10.

BANDYOPADHYAY, U., KAUSHIK, S., VARTICOVSKI, L. & CUERVO, A. M. 2008. The chaperone-mediated autophagy receptor organizes in dynamic protein complexes at the lysosomal membrane. *Mol Cell Biol,* 28**,** 5747-63.

BARRETT, J. C., HANSOUL, S., NICOLAE, D. L., CHO, J. H., DUERR, R. H., RIOUX, J. D., BRANT, S. R., SILVERBERG, M. S., TAYLOR, K. D., BARMADA, M. M., BITTON, A., DASSOPOULOS, T., DATTA, L. W., GREEN, T., GRIFFITHS, A. M., KISTNER, E. O., MURTHA, M. T., REGUEIRO, M. D., ROTTER, J. I., SCHUMM, L. P., STEINHART, A. H., TARGAN, S. R., XAVIER, R. J., LIBIOULLE, C., SANDOR, C., LATHROP, M., BELAICHE, J., DEWIT, O., GUT, I., HEATH, S., LAUKENS, D., MNI, M., RUTGEERTS, P., VAN GOSSUM, A., ZELENIKA, D., FRANCHIMONT, D., HUGOT, J. P., DE VOS, M., VERMEIRE, S., LOUIS, E., CARDON, L. R., ANDERSON, C. A., DRUMMOND, H., NIMMO, E., AHMAD, T., PRESCOTT, N. J., ONNIE, C. M., FISHER, S. A., MARCHINI, J., GHORI, J., BUMPSTEAD, S., GWILLIAM, R., TREMELLING, M., DELOUKAS, P., MANSFIELD, J., JEWELL, D., SATSANGI, J., MATHEW, C. G., PARKES, M., GEORGES, M. & DALY, M. J. 2008. Genome-wide association defines

more than 30 distinct susceptibility loci for Crohn's disease. *Nat Genet,* 40**,** 955-62.

BARTON, G. M. 2008. A calculated response: control of inflammation by the innate immune system. *J Clin Invest,* 118**,** 413-20.

BAUERNFEIND, F., BARTOK, E., RIEGER, A., FRANCHI, L., NUNEZ, G. & HORNUNG, V. 2011. Cutting edge: reactive oxygen species inhibitors block priming, but not activation, of the NLRP3 inflammasome. *J Immunol,* 187**,** 613-7.

BEHRENDS, C., SOWA, M. E., GYGI, S. P. & HARPER, J. W. 2010. Network organization of the human autophagy system. *Nature,* 466**,** 68-76.

BEJARANO, P. A., LANGEVELD, J. P., HUDSON, B. G. & NOELKEN, M. E. 1989. Degradation of basement membranes by Pseudomonas aeruginosa elastase. *Infect Immun,* 57**,** 3783-7.

BENSAAD, K., CHEUNG, E. C. & VOUSDEN, K. H. 2009. Modulation of intracellular ROS levels by TIGAR controls autophagy. *EMBO J,* 28**,** 3015-26.

BERGER, S. B., ROMERO, X., MA, C., WANG, G., FAUBION, W. A., LIAO, G., COMPEER, E., KESZEI, M., RAMEH, L., WANG, N., BOES, M., REGUEIRO, J. R., REINECKER, H. C. & TERHORST, C. 2010. SLAM is a microbial sensor that regulates bacterial phagosome functions in macrophages. *Nat Immunol,* 11**,** 920-7.

BERGSBAKEN, T., FINK, S. L. & COOKSON, B. T. 2009. Pyroptosis: host cell death and inflammation. *Nat Rev Microbiol,* 7**,** 99-109.

BERTHELOT, P., GRATTARD, F., MAHUL, P., PAIN, P., JOSPE, R., VENET, C., CARRICAJO, A., AUBERT, G., ROS, A., DUMONT, A., LUCHT, F., ZENI, F., AUBOYER, C., BERTRAND, J. C. & POZZETTO, B. 2001. Prospective study of nosocomial colonization and infection due to Pseudomonas aeruginosa in mechanically ventilated patients. *Intensive Care Med,* 27**,** 503-12.

BILLEN, L. P., SHAMAS-DIN, A. & ANDREWS, D. W. 2008. Bid: a Bax-like BH3 protein. *Oncogene,* 27 Suppl 1**,** S93-104.

BOYDEN, E. D. & DIETRICH, W. F. 2006. Nalp1b controls mouse macrophage susceptibility to anthrax lethal toxin. *Nat Genet,* 38**,** 240-4.

BRODSKY, I. E. & MONACK, D. 2009. NLR-mediated control of inflammasome assembly in the host response against bacterial pathogens. *Semin Immunol,* 21**,** 199-207.

BROWN, G. D. 2006. Dectin-1: a signalling non-TLR pattern-recognition receptor. *Nat Rev Immunol,* 6**,** 33-43.

BROZ, P., RUBY, T., BELHOCINE, K., BOULEY, D. M., KAYAGAKI, N., DIXIT, V. M. & MONACK, D. M. 2012. Caspase-11 increases susceptibility to Salmonella infection in the absence of caspase-1. *Nature,* 490**,** 288-91.

BROZ, P., VON MOLTKE, J., JONES, J. W., VANCE, R. E. & MONACK, D. M. 2010. Differential requirement for Caspase-1 autoproteolysis in pathogen-induced cell death and cytokine processing. *Cell Host Microbe,* 8**,** 471-83.

BRYANT, C. & FITZGERALD, K. A. 2009. Molecular mechanisms involved in inflammasome activation. *Trends Cell Biol,* 19**,** 455-64.

BURCKSTUMMER, T., BAUMANN, C., BLUML, S., DIXIT, E., DURNBERGER, G., JAHN, H., PLANYAVSKY, M., BILBAN, M., COLINGE, J., BENNETT, K. L. & SUPERTI-FURGA, G. 2009. An orthogonal proteomic-genomic screen identifies AIM2 as a cytoplasmic DNA sensor for the inflammasome. *Nat Immunol,* 10**,** 266-72.

BURDETTE, D. L., YARBROUGH, M. L., ORVEDAHL, A., GILPIN, C. J. & ORTH, K. 2008. Vibrio parahaemolyticus orchestrates a multifaceted host cell infection by induction of autophagy, cell rounding, and then cell lysis. *Proc Natl Acad Sci U S A,* 105**,** 12497-502.

CAI, S., BATRA, S., WAKAMATSU, N., PACHER, P. & JEYASEELAN, S. 2012. NLRC4 inflammasome-mediated production of IL-1beta modulates mucosal immunity in the lung against gram-negative bacterial infection. *J Immunol,* 188**,** 5623-35.

CAMPOY, E. & COLOMBO, M. I. 2009. Autophagy in intracellular bacterial infection. *Biochim Biophys Acta,* 1793**,** 1465-77.

CARRIERE, V., ROUSSEL, L., ORTEGA, N., LACORRE, D. A., AMERICH, L., AGUILAR, L., BOUCHE, G. & GIRARD, J. P. 2007. IL-33, the IL-1-like cytokine ligand for ST2 receptor, is a chromatin-associated nuclear factor in vivo. *Proc Natl Acad Sci U S A,* 104**,** 282-7.

CASTILLO, E. F., DEKONENKO, A., ARKO-MENSAH, J., MANDELL, M. A., DUPONT, N., JIANG, S., DELGADO-VARGAS, M., TIMMINS, G. S., BHATTACHARYA, D., YANG, H., HUTT, J., LYONS, C. R., DOBOS, K. M. & DERETIC, V. 2012. Autophagy protects against active tuberculosis by suppressing bacterial burden and inflammation. *Proc Natl Acad Sci U S A,* 109**,** E3168-76.

CELADA, A., GRAY, P. W., RINDERKNECHT, E. & SCHREIBER, R. D. 1984. Evidence for a gamma-interferon receptor that regulates macrophage tumoricidal activity. *J Exp Med,* 160**,** 55-74.

CESEN, M. H., PEGAN, K., SPES, A. & TURK, B. 2012. Lysosomal pathways to cell death and their therapeutic applications. *Exp Cell Res,* 318**,** 1245-51.

CHASTRE, J. & FAGON, J. Y. 2002. Ventilator-associated pneumonia. *Am J Respir Crit Care Med,* 165**,** 867-903.

CHAVARRIA-SMITH, J. & VANCE, R. E. 2013. Direct proteolytic cleavage of NLRP1B is necessary and sufficient for inflammasome activation by anthrax lethal factor. *PLoS Pathog,* 9**,** e1003452.

CHEN, Y., AZAD, M. B. & GIBSON, S. B. 2009. Superoxide is the major reactive oxygen species regulating autophagy. *Cell Death Differ,* 16**,** 1040-52.

CHU, J., THOMAS, L. M., WATKINS, S. C., FRANCHI, L., NUNEZ, G. & SALTER, R. D. 2009. Cholesterol-dependent cytolysins induce rapid release of mature IL-1beta from murine macrophages in a NLRP3 inflammasome and cathepsin B-dependent manner. *J Leukoc Biol,* 86**,** 1227-38.

COHEN, T. S. & PRINCE, A. S. 2013. Activation of inflammasome signaling mediates pathology of acute P. aeruginosa pneumonia. *J Clin Invest,* 123**,** 1630-7.

COLOMBO, M. I. 2007. Autophagy: a pathogen driven process. *IUBMB Life,* 59**,** 238-42.

COONEY, R., BAKER, J., BRAIN, O., DANIS, B., PICHULIK, T., ALLAN, P., FERGUSON, D. J., CAMPBELL, B. J., JEWELL, D. & SIMMONS, A. 2010. NOD2 stimulation induces autophagy in dendritic cells influencing bacterial handling and antigen presentation. *Nat Med,* 16**,** 90-7.

CRUZ, C. M., RINNA, A., FORMAN, H. J., VENTURA, A. L., PERSECHINI, P. M. & OJCIUS, D. M. 2007. ATP activates a reactive oxygen species-dependent oxidative stress response and secretion of proinflammatory cytokines in macrophages. *J Biol Chem,* 282**,** 2871-9.

DELGADO, M. A., ELMAOUED, R. A., DAVIS, A. S., KYEI, G. & DERETIC, V. 2008. Toll-like receptors control autophagy. *EMBO J,* 27**,** 1110-21.

DERETIC, V. 2011. Autophagy in immunity and cell-autonomous defense against intracellular microbes. *Immunol Rev,* 240**,** 92-104.

DERETIC, V. & LEVINE, B. 2009. Autophagy, immunity, and microbial adaptations. *Cell Host Microbe,* 5**,** 527-49.

DESVAUX, M., HEBRAUD, M., HENDERSON, I. R. & PALLEN, M. J. 2006. Type III secretion: what's in a name? *Trends Microbiol,* 14**,** 157-60.

DI VIRGILIO, F. 2007. Liaisons dangereuses: P2X(7) and the inflammasome. *Trends Pharmacol Sci,* 28**,** 465-72.

DIACOVICH, L. & GORVEL, J. P. 2010. Bacterial manipulation of innate immunity to promote infection. *Nat Rev Microbiol,* 8**,** 117-28.

DINARELLO, C. A. 2009. Immunological and inflammatory functions of the interleukin-1 family. *Annu Rev Immunol,* 27**,** 519-50.

DORN, B. R., DUNN, W. A., JR. & PROGULSKE-FOX, A. 2002. Bacterial interactions with the autophagic pathway. *Cell Microbiol,* 4**,** 1-10.

DUEWELL, P., KONO, H., RAYNER, K. J., SIROIS, C. M., VLADIMER, G., BAUERNFEIND, F. G., ABELA, G. S., FRANCHI, L., NUNEZ, G., SCHNURR, M., ESPEVIK, T., LIEN, E., FITZGERALD, K. A., ROCK, K. L., MOORE, K. J., WRIGHT, S. D., HORNUNG, V. & LATZ, E. 2010. NLRP3 inflammasomes are required for atherogenesis and activated by cholesterol crystals. *Nature,* 464**,** 1357-61.

DUPONT, N., LACAS-GERVAIS, S., BERTOUT, J., PAZ, I., FRECHE, B., VAN NHIEU, G. T., VAN DER GOOT, F. G., SANSONETTI, P. J. & LAFONT, F. 2009. Shigella phagocytic vacuolar membrane remnants participate in the cellular response to pathogen invasion and are regulated by autophagy. *Cell Host Microbe,* 6**,** 137-49.

EITEL, J., SUTTORP, N. & OPITZ, B. 2010. Innate immune recognition and inflammasome activation in listeria monocytogenes infection. *Front Microbiol,* 1**,** 149.

ENG, K. E., PANAS, M. D., KARLSSON HEDESTAM, G. B. & MCINERNEY, G. M. 2010. A novel quantitative flow cytometry-based assay for autophagy. *Autophagy,* 6**,** 634-41.

EVANS, T. J. 2009. Bacterial triggering of inflammation by intracellular sensors. *Future Microbiol,* 4**,** 65-75.

FANG, R., HARA, H., SAKAI, S., HERNANDEZ-CUELLAR, E., MITSUYAMA, M., KAWAMURA, I. & TSUCHIYA, K. 2014. Type I interferon signaling regulates the activation of the absent in melanoma 2 inflammasome during Streptococcus pneumoniae infection. *Infect Immun*.

FAUSTIN, B., LARTIGUE, L., BRUEY, J. M., LUCIANO, F., SERGIENKO, E., BAILLY-MAITRE, B., VOLKMANN, N., HANEIN, D., ROUILLER, I. & REED, J. C. 2007. Reconstituted NALP1 inflammasome reveals two-step mechanism of caspase-1 activation. *Mol Cell,* 25**,** 713-24.

FERNANDES-ALNEMRI, T., WU, J., YU, J. W., DATTA, P., MILLER, B., JANKOWSKI, W., ROSENBERG, S., ZHANG, J. & ALNEMRI, E. S. 2007. The pyroptosome: a supramolecular assembly of ASC dimers mediating

inflammatory cell death via caspase-1 activation. *Cell Death Differ,* 14**,** 1590-604.

FERNANDES-ALNEMRI, T., YU, J. W., DATTA, P., WU, J. & ALNEMRI, E. S. 2009. AIM2 activates the inflammasome and cell death in response to cytoplasmic DNA. *Nature,* 458**,** 509-13.

FERRERO-MILIANI, L., NIELSEN, O. H., ANDERSEN, P. S. & GIRARDIN, S. E. 2007. Chronic inflammation: importance of NOD2 and NALP3 in interleukin-1beta generation. *Clin Exp Immunol,* 147**,** 227-35.

FINK, S. L., BERGSBAKEN, T. & COOKSON, B. T. 2008. Anthrax lethal toxin and Salmonella elicit the common cell death pathway of caspase-1-dependent pyroptosis via distinct mechanisms. *Proc Natl Acad Sci U S A,* 105**,** 4312-7.

FRANCHI, L., AMER, A., BODY-MALAPEL, M., KANNEGANTI, T. D., OZOREN, N., JAGIRDAR, R., INOHARA, N., VANDENABEELE, P., BERTIN, J., COYLE, A., GRANT, E. P. & NUNEZ, G. 2006. Cytosolic flagellin requires Ipaf for activation of caspase-1 and interleukin 1beta in salmonella-infected macrophages. *Nat Immunol,* 7**,** 576-82.

FRANCHI, L., EIGENBROD, T., MUNOZ-PLANILLO, R. & NUNEZ, G. 2009. The inflammasome: a caspase-1-activation platform that regulates immune responses and disease pathogenesis. *Nat Immunol,* 10**,** 241-7.

FRANCHI, L., KAMADA, N., NAKAMURA, Y., BURBERRY, A., KUFFA, P., SUZUKI, S., SHAW, M. H., KIM, Y. G. & NUNEZ, G. 2012a. NLRC4-driven production of IL-1beta discriminates between pathogenic and commensal bacteria and promotes host intestinal defense. *Nat Immunol,* 13**,** 449-56.

FRANCHI, L., MUNOZ-PLANILLO, R. & NUNEZ, G. 2012b. Sensing and reacting to microbes through the inflammasomes. *Nat Immunol,* 13**,** 325-32.

FRANCHI, L., STOOLMAN, J., KANNEGANTI, T. D., VERMA, A., RAMPHAL, R. & NUNEZ, G. 2007. Critical role for Ipaf in Pseudomonas aeruginosa-induced caspase-1 activation. *Eur J Immunol,* 37**,** 3030-9.

FRANK, D. W. 1997. The exoenzyme S regulon of Pseudomonas aeruginosa. *Mol Microbiol,* 26**,** 621-9.

FRANK, D. W., VALLIS, A., WIENER-KRONISH, J. P., ROY-BURMAN, A., SPACK, E. G., MULLANEY, B. P., MEGDOUD, M., MARKS, J. D., FRITZ, R. & SAWA, T. 2002. Generation and characterization of a protective monoclonal antibody to Pseudomonas aeruginosa PcrV. *J Infect Dis,* 186**,** 64-73.

FUJISHIMA, Y., NISHIUMI, S., MASUDA, A., INOUE, J., NGUYEN, N. M., IRINO, Y., KOMATSU, M., TANAKA, K., KUTSUMI, H., AZUMA, T. & YOSHIDA, M. 2011. Autophagy in the intestinal epithelium reduces endotoxin-induced

inflammatory responses by inhibiting NF-kappaB activation. *Arch Biochem Biophys,* 506**,** 223-35.

FUJITA, N., ITOH, T., OMORI, H., FUKUDA, M., NODA, T. & YOSHIMORI, T. 2008. The Atg16L complex specifies the site of LC3 lipidation for membrane biogenesis in autophagy. *Mol Biol Cell,* 19**,** 2092-100.

FUJITA, N., SAITOH, T., KAGEYAMA, S., AKIRA, S., NODA, T. & YOSHIMORI, T. 2009. Differential involvement of Atg16L1 in Crohn disease and canonical autophagy: analysis of the organization of the Atg16L1 complex in fibroblasts. *J Biol Chem,* 284**,** 32602-9.

GASPAR, M. C., COUET, W., OLIVIER, J. C., PAIS, A. A. & SOUSA, J. J. 2013. Pseudomonas aeruginosa infection in cystic fibrosis lung disease and new perspectives of treatment: a review. *Eur J Clin Microbiol Infect Dis,* 32**,** 1231-52.

GE, J., GONG, Y. N., XU, Y. & SHAO, F. 2012. Preventing bacterial DNA release and absent in melanoma 2 inflammasome activation by a Legionella effector functioning in membrane trafficking. *Proc Natl Acad Sci U S A,* 109**,** 6193-8.

GHAYUR, T., BANERJEE, S., HUGUNIN, M., BUTLER, D., HERZOG, L., CARTER, A., QUINTAL, L., SEKUT, L., TALANIAN, R., PASKIND, M., WONG, W., KAMEN, R., TRACEY, D. & ALLEN, H. 1997. Caspase-1 processes IFN-gamma-inducing factor and regulates LPS-induced IFN-gamma production. *Nature,* 386**,** 619-23.

GOLDBACH-MANSKY, R. & KASTNER, D. L. 2009. Autoinflammation: the prominent role of IL-1 in monogenic autoinflammatory diseases and implications for common illnesses. *J Allergy Clin Immunol,* 124**,** 1141-9; quiz 1150-1.

GROSS, O., THOMAS, C. J., GUARDA, G. & TSCHOPP, J. 2011. The inflammasome: an integrated view. *Immunol Rev,* 243**,** 136-51.

GUARDA, G., BRAUN, M., STAEHLI, F., TARDIVEL, A., MATTMANN, C., FORSTER, I., FARLIK, M., DECKER, T., DU PASQUIER, R. A., ROMERO, P. & TSCHOPP, J. 2011. Type I interferon inhibits interleukin-1 production and inflammasome activation. *Immunity,* 34**,** 213-23.

GUO, B. & CHENG, G. 2007. Modulation of the interferon antiviral response by the TBK1/IKKi adaptor protein TANK. *J Biol Chem,* 282**,** 11817-26.

GURCEL, L., ABRAMI, L., GIRARDIN, S., TSCHOPP, J. & VAN DER GOOT, F. G. 2006. Caspase-1 activation of lipid metabolic pathways in response to bacterial pore-forming toxins promotes cell survival. *Cell,* 126**,** 1135-45.

GUTIERREZ, M. G., MASTER, S. S., SINGH, S. B., TAYLOR, G. A., COLOMBO, M. I. & DERETIC, V. 2004. Autophagy is a defense mechanism inhibiting BCG and Mycobacterium tuberculosis survival in infected macrophages. *Cell,* 119**,** 753-66.

HAILEY, D. W., RAMBOLD, A. S., SATPUTE-KRISHNAN, P., MITRA, K., SOUGRAT, R., KIM, P. K. & LIPPINCOTT-SCHWARTZ, J. 2010. Mitochondria supply membranes for autophagosome biogenesis during starvation. *Cell,* 141**,** 656-67.

HAN, J. W., ZHENG, H. F., CUI, Y., SUN, L. D., YE, D. Q., HU, Z., XU, J. H., CAI, Z. M., HUANG, W., ZHAO, G. P., XIE, H. F., FANG, H., LU, Q. J., LI, X. P., PAN, Y. F., DENG, D. Q., ZENG, F. Q., YE, Z. Z., ZHANG, X. Y., WANG, Q. W., HAO, F., MA, L., ZUO, X. B., ZHOU, F. S., DU, W. H., CHENG, Y. L., YANG, J. Q., SHEN, S. K., LI, J., SHENG, Y. J., ZUO, X. X., ZHU, W. F., GAO, F., ZHANG, P. L., GUO, Q., LI, B., GAO, M., XIAO, F. L., QUAN, C., ZHANG, C., ZHANG, Z., ZHU, K. J., LI, Y., HU, D. Y., LU, W. S., HUANG, J. L., LIU, S. X., LI, H., REN, Y. Q., WANG, Z. X., YANG, C. J., WANG, P. G., ZHOU, W. M., LV, Y. M., ZHANG, A. P., ZHANG, S. Q., LIN, D., LOW, H. Q., SHEN, M., ZHAI, Z. F., WANG, Y., ZHANG, F. Y., YANG, S., LIU, J. J. & ZHANG, X. J. 2009. Genome-wide association study in a Chinese Han population identifies nine new susceptibility loci for systemic lupus erythematosus. *Nat Genet,* 41**,** 1234-7.

HARRIS, J. 2013. Autophagy and IL-1 Family Cytokines. *Front Immunol,* 4**,** 83.

HARRIS, J., HARTMAN, M., ROCHE, C., ZENG, S. G., O'SHEA, A., SHARP, F. A., LAMBE, E. M., CREAGH, E. M., GOLENBOCK, D. T., TSCHOPP, J., KORNFELD, H., FITZGERALD, K. A. & LAVELLE, E. C. 2011. Autophagy controls IL-1beta secretion by targeting pro-IL-1beta for degradation. *J Biol Chem,* 286**,** 9587-97.

HASHIGUCHI, K. & ZHANG-AKIYAMA, Q. M. 2009. Establishment of human cell lines lacking mitochondrial DNA. *Methods Mol Biol,* 554**,** 383-91.

HAUSER, A. R. 2009. The type III secretion system of Pseudomonas aeruginosa: infection by injection. *Nat Rev Microbiol,* 7**,** 654-65.

HAUSER, A. R., COBB, E., BODI, M., MARISCAL, D., VALLES, J., ENGEL, J. N. & RELLO, J. 2002. Type III protein secretion is associated with poor clinical outcomes in patients with ventilator-associated pneumonia caused by Pseudomonas aeruginosa. *Crit Care Med,* 30**,** 521-8.

HAWKINS, P. N., LACHMANN, H. J. & MCDERMOTT, M. F. 2003. Interleukin-1-receptor antagonist in the Muckle-Wells syndrome. *N Engl J Med,* 348**,** 2583-4.

HEATH, R. J. & XAVIER, R. J. 2009. Autophagy, immunity and human disease. *Curr Opin Gastroenterol,* 25, 512-20.

HIGA, N., TOMA, C., KOIZUMI, Y., NAKASONE, N., NOHARA, T., MASUMOTO, J., KODAMA, T., IIDA, T. & SUZUKI, T. 2013. Vibrio parahaemolyticus effector proteins suppress inflammasome activation by interfering with host autophagy signaling. *PLoS Pathog,* 9**,** e1003142.

HOGQUIST, K. A., NETT, M. A., UNANUE, E. R. & CHAPLIN, D. D. 1991. Interleukin 1 is processed and released during apoptosis. *Proc Natl Acad Sci U S A,* 88**,** 8485-9.

HOLDER, I. A., NEELY, A. N. & FRANK, D. W. 2001. Type III secretion/intoxication system important in virulence of Pseudomonas aeruginosa infections in burns. *Burns,* 27**,** 129-30.

HORNUNG, V., ABLASSER, A., CHARREL-DENNIS, M., BAUERNFEIND, F., HORVATH, G., CAFFREY, D. R., LATZ, E. & FITZGERALD, K. A. 2009. AIM2 recognizes cytosolic dsDNA and forms a caspase-1-activating inflammasome with ASC. *Nature,* 458**,** 514-8.

HORNUNG, V., BAUERNFEIND, F., HALLE, A., SAMSTAD, E. O., KONO, H., ROCK, K. L., FITZGERALD, K. A. & LATZ, E. 2008. Silica crystals and aluminum salts activate the NALP3 inflammasome through phagosomal destabilization. *Nat Immunol,* 9**,** 847-56.

HUANG, J., CANADIEN, V., LAM, G. Y., STEINBERG, B. E., DINAUER, M. C., MAGALHAES, M. A., GLOGAUER, M., GRINSTEIN, S. & BRUMELL, J. H. 2009a. Activation of antibacterial autophagy by NADPH oxidases. *Proc Natl Acad Sci U S A,* 106**,** 6226-31.

HUANG, M. T., TAXMAN, D. J., HOLLEY-GUTHRIE, E. A., MOORE, C. B., WILLINGHAM, S. B., MADDEN, V., PARSONS, R. K., FEATHERSTONE, G. L., ARNOLD, R. R., O'CONNOR, B. P. & TING, J. P. 2009b. Critical role of apoptotic speck protein containing a caspase recruitment domain (ASC) and NLRP3 in causing necrosis and ASC speck formation induced by Porphyromonas gingivalis in human cells. *J Immunol,* 182**,** 2395-404.

ICHIMURA, Y., IMAMURA, Y., EMOTO, K., UMEDA, M., NODA, T. & OHSUMI, Y. 2004. In vivo and in vitro reconstitution of Atg8 conjugation essential for autophagy. *J Biol Chem,* 279**,** 40584-92.

ICHIMURA, Y., KIRISAKO, T., TAKAO, T., SATOMI, Y., SHIMONISHI, Y., ISHIHARA, N., MIZUSHIMA, N., TANIDA, I., KOMINAMI, E., OHSUMI, M., NODA, T. & OHSUMI, Y. 2000. A ubiquitin-like system mediates protein lipidation. *Nature,* 408**,** 488-92.

JABIR, M. S., RITCHIE, N. D., LI, D., BAYES, H. K., TOURLOMOUSIS, P., PULESTON, D., LUPTON, A., HOPKINS, L., SIMON, A. K., BRYANT, C. & EVANS, T. J. 2014. Caspase-1 Cleavage of the TLR Adaptor TRIF Inhibits Autophagy and beta-Interferon Production during Pseudomonas aeruginosa Infection. *Cell Host Microbe,* 15**,** 214-27.

JIN, S. M. & YOULE, R. J. 2012. PINK1- and Parkin-mediated mitophagy at a glance. *J Cell Sci,* 125**,** 795-9.

KABEYA, Y., MIZUSHIMA, N., UENO, T., YAMAMOTO, A., KIRISAKO, T., NODA, T., KOMINAMI, E., OHSUMI, Y. & YOSHIMORI, T. 2000. LC3, a mammalian homologue of yeast Apg8p, is localized in autophagosome membranes after processing. *EMBO J,* 19**,** 5720-8.

KAHLENBERG, J. M. & DUBYAK, G. R. 2004. Mechanisms of caspase-1 activation by P2X7 receptor-mediated K+ release. *Am J Physiol Cell Physiol,* 286**,** C1100-8.

KAYAGAKI, N., WARMING, S., LAMKANFI, M., VANDE WALLE, L., LOUIE, S., DONG, J., NEWTON, K., QU, Y., LIU, J., HELDENS, S., ZHANG, J., LEE, W. P., ROOSE-GIRMA, M. & DIXIT, V. M. 2011. Non-canonical inflammasome activation targets caspase-11. *Nature,* 479**,** 117-21.

KEIZER, D. W., SLUPSKY, C. M., KALISIAK, M., CAMPBELL, A. P., CRUMP, M. P., SASTRY, P. A., HAZES, B., IRVIN, R. T. & SYKES, B. D. 2001. Structure of a pilin monomer from Pseudomonas aeruginosa: implications for the assembly of pili. *J Biol Chem,* 276**,** 24186-93.

KELLY-SCUMPIA, K. M., SCUMPIA, P. O., DELANO, M. J., WEINSTEIN, J. S., CUENCA, A. G., WYNN, J. L. & MOLDAWER, L. L. 2010. Type I interferon signaling in hematopoietic cells is required for survival in mouse polymicrobial sepsis by regulating CXCL10. *J Exp Med,* 207**,** 319-26.

KIM, I., RODRIGUEZ-ENRIQUEZ, S. & LEMASTERS, J. J. 2007. Selective degradation of mitochondria by mitophagy. *Arch Biochem Biophys,* 462**,** 245-53.

KIM, S., BAUERNFEIND, F., ABLASSER, A., HARTMANN, G., FITZGERALD, K. A., LATZ, E. & HORNUNG, V. 2010. Listeria monocytogenes is sensed by the NLRP3 and AIM2 inflammasome. *Eur J Immunol,* 40**,** 1545-51.

KIM, W. Y., NAM, S. A., SONG, H. C., KO, J. S., PARK, S. H., KIM, H. L., CHOI, E. J., KIM, Y. S., KIM, J. & KIM, Y. K. 2012. The role of autophagy in unilateral ureteral obstruction rat model. *Nephrology (Carlton),* 17**,** 148-59.

KIMURA, S., NODA, T. & YOSHIMORI, T. 2008. Dynein-dependent movement of autophagosomes mediates efficient encounters with lysosomes. *Cell Struct Funct,* 33**,** 109-22.

KIRISAKO, T., BABA, M., ISHIHARA, N., MIYAZAWA, K., OHSUMI, M., YOSHIMORI, T., NODA, T. & OHSUMI, Y. 1999. Formation process of autophagosome is traced with Apg8/Aut7p in yeast. *J Cell Biol,* 147**,** 435-46.

KLEINNIJENHUIS, J., OOSTING, M., PLANTINGA, T. S., VAN DER MEER, J. W., JOOSTEN, L. A., CREVEL, R. V. & NETEA, M. G. 2011. Autophagy

modulates the Mycobacterium tuberculosis-induced cytokine response. *Immunology,* 134**,** 341-8.

KLIONSKY, D. J. 2008. Autophagy revisited: a conversation with Christian de Duve. *Autophagy,* 4**,** 740-3.

KOFOED, E. M. & VANCE, R. E. 2011. Innate immune recognition of bacterial ligands by NAIPs determines inflammasome specificity. *Nature,* 477**,** 592-5.

KRAFT, C., PETER, M. & HOFMANN, K. 2010. Selective autophagy: ubiquitin-mediated recognition and beyond. *Nat Cell Biol,* 12**,** 836-41.

KROEMER, G., MARINO, G. & LEVINE, B. 2010. Autophagy and the integrated stress response. *Mol Cell,* 40**,** 280-93.

KUMAR, H., KAWAI, T. & AKIRA, S. 2009. Pathogen recognition in the innate immune response. *Biochem J,* 420**,** 1-16.

KUNDU, M. & THOMPSON, C. B. 2008. Autophagy: basic principles and relevance to disease. *Annu Rev Pathol,* 3**,** 427-55.

LAMKANFI, M., KANNEGANTI, T. D., VAN DAMME, P., VANDEN BERGHE, T., VANOVERBERGHE, I., VANDEKERCKHOVE, J., VANDENABEELE, P., GEVAERT, K. & NUNEZ, G. 2008. Targeted peptidecentric proteomics reveals caspase-7 as a substrate of the caspase-1 inflammasomes. *Mol Cell Proteomics,* 7**,** 2350-63.

LARA-TEJERO, M., SUTTERWALA, F. S., OGURA, Y., GRANT, E. P., BERTIN, J., COYLE, A. J., FLAVELL, R. A. & GALAN, J. E. 2006. Role of the caspase-1 inflammasome in Salmonella typhimurium pathogenesis. *J Exp Med,* 203**,** 1407-12.

LATZ, E., XIAO, T. S. & STUTZ, A. 2013. Activation and regulation of the inflammasomes. *Nat Rev Immunol,* 13**,** 397-411.

LAU, G. W., HASSETT, D. J., RAN, H. & KONG, F. 2004. The role of pyocyanin in Pseudomonas aeruginosa infection. *Trends Mol Med,* 10**,** 599-606.

LEBEIS, S. L., POWELL, K. R., MERLIN, D., SHERMAN, M. A. & KALMAN, D. 2009. Interleukin-1 receptor signaling protects mice from lethal intestinal damage caused by the attaching and effacing pathogen Citrobacter rodentium. *Infect Immun,* 77**,** 604-14.

LEE, E. J., EVANS, D. J. & FLEISZIG, S. M. 2003. Role of Pseudomonas aeruginosa ExsA in penetration through corneal epithelium in a novel in vivo model. *Invest Ophthalmol Vis Sci,* 44**,** 5220-7.

LEE, V. T., SMITH, R. S., TUMMLER, B. & LORY, S. 2005. Activities of Pseudomonas aeruginosa effectors secreted by the Type III secretion system in vitro and during infection. *Infect Immun,* 73**,** 1695-705.

LEI, X., SUN, Z., LIU, X., JIN, Q., HE, B. & WANG, J. 2011. Cleavage of the adaptor protein TRIF by enterovirus 71 3C inhibits antiviral responses mediated by Toll-like receptor 3. *J Virol,* 85**,** 8811-8.

LEVINE, B. & KROEMER, G. 2008. Autophagy in the pathogenesis of disease. *Cell,* 132**,** 27-42.

LEVINE, B., MIZUSHIMA, N. & VIRGIN, H. W. 2011. Autophagy in immunity and inflammation. *Nature,* 469**,** 323-35.

LI, N., RAGHEB, K., LAWLER, G., STURGIS, J., RAJWA, B., MELENDEZ, J. A. & ROBINSON, J. P. 2003. Mitochondrial complex I inhibitor rotenone induces apoptosis through enhancing mitochondrial reactive oxygen species production. *J Biol Chem,* 278**,** 8516-25.

LIGHTFIELD, K. L., PERSSON, J., BRUBAKER, S. W., WITTE, C. E., VON MOLTKE, J., DUNIPACE, E. A., HENRY, T., SUN, Y. H., CADO, D., DIETRICH, W. F., MONACK, D. M., TSOLIS, R. M. & VANCE, R. E. 2008. Critical function for Naip5 in inflammasome activation by a conserved carboxy-terminal domain of flagellin. *Nat Immunol,* 9**,** 1171-8.

LIVAK, K. J. & SCHMITTGEN, T. D. 2001. Analysis of relative gene expression data using real-time quantitative PCR and the 2(-Delta Delta C(T)) Method. *Methods,* 25**,** 402-8.

LU, Y. C., YEH, W. C. & OHASHI, P. S. 2008. LPS/TLR4 signal transduction pathway. *Cytokine,* 42**,** 145-51.

LUM, J. J., BAUER, D. E., KONG, M., HARRIS, M. H., LI, C., LINDSTEN, T. & THOMPSON, C. B. 2005. Growth factor regulation of autophagy and cell survival in the absence of apoptosis. *Cell,* 120**,** 237-48.

LYCZAK, J. B., CANNON, C. L. & PIER, G. B. 2000. Establishment of Pseudomonas aeruginosa infection: lessons from a versatile opportunist. *Microbes Infect,* 2**,** 1051-60.

MAKI, H. & SEKIGUCHI, M. 1992. MutT protein specifically hydrolyses a potent mutagenic substrate for DNA synthesis. *Nature,* 355**,** 273-5.

MARIATHASAN, S., NEWTON, K., MONACK, D. M., VUCIC, D., FRENCH, D. M., LEE, W. P., ROOSE-GIRMA, M., ERICKSON, S. & DIXIT, V. M. 2004. Differential activation of the inflammasome by caspase-1 adaptors ASC and Ipaf. *Nature,* 430**,** 213-8.

MARTINON, F. 2012. Dangerous liaisons: mitochondrial DNA meets the NLRP3 inflammasome. *Immunity,* 36**,** 313-5.

MARTINON, F., BURNS, K. & TSCHOPP, J. 2002. The inflammasome: a molecular platform triggering activation of inflammatory caspases and processing of proIL-beta. *Mol Cell,* 10**,** 417-26.

MARTINON, F., GAIDE, O., PETRILLI, V., MAYOR, A. & TSCHOPP, J. 2007. NALP inflammasomes: a central role in innate immunity. *Semin Immunopathol,* 29**,** 213-29.

MARTINON, F., MAYOR, A. & TSCHOPP, J. 2009. The inflammasomes: guardians of the body. *Annu Rev Immunol,* 27**,** 229-65.

MARTINON, F., PETRILLI, V., MAYOR, A., TARDIVEL, A. & TSCHOPP, J. 2006. Gout-associated uric acid crystals activate the NALP3 inflammasome. *Nature,* 440**,** 237-41.

MEISSNER, F., MOLAWI, K. & ZYCHLINSKY, A. 2010. Mutant superoxide dismutase 1-induced IL-1beta accelerates ALS pathogenesis. *Proc Natl Acad Sci U S A,* 107**,** 13046-50.

MIAO, E. A., ALPUCHE-ARANDA, C. M., DORS, M., CLARK, A. E., BADER, M. W., MILLER, S. I. & ADEREM, A. 2006. Cytoplasmic flagellin activates caspase-1 and secretion of interleukin 1beta via Ipaf. *Nat Immunol,* 7**,** 569-75.

MIAO, E. A., ERNST, R. K., DORS, M., MAO, D. P. & ADEREM, A. 2008. Pseudomonas aeruginosa activates caspase 1 through Ipaf. *Proc Natl Acad Sci U S A,* 105**,** 2562-7.

MIAO, E. A., MAO, D. P., YUDKOVSKY, N., BONNEAU, R., LORANG, C. G., WARREN, S. E., LEAF, I. A. & ADEREM, A. 2010. Innate immune detection of the type III secretion apparatus through the NLRC4 inflammasome. *Proc Natl Acad Sci U S A,* 107**,** 3076-80.

MIAO, E. A., RAJAN, J. V. & ADEREM, A. 2011. Caspase-1-induced pyroptotic cell death. *Immunol Rev,* 243**,** 206-14.

MIZUSHIMA, N. & LEVINE, B. 2010. Autophagy in mammalian development and differentiation. *Nat Cell Biol,* 12**,** 823-30.

MIZUSHIMA, N. & YOSHIMORI, T. 2007. How to interpret LC3 immunoblotting. *Autophagy,* 3**,** 542-5.

MORTENSEN, M., FERGUSON, D. J., EDELMANN, M., KESSLER, B., MORTEN, K. J., KOMATSU, M. & SIMON, A. K. 2010. Loss of autophagy in erythroid cells leads to defective removal of mitochondria and severe anemia in vivo. *Proc Natl Acad Sci U S A,* 107**,** 832-7.

MORTENSEN, M., SOILLEUX, E. J., DJORDJEVIC, G., TRIPP, R., LUTTEROPP, M., SADIGHI-AKHA, E., STRANKS, A. J., GLANVILLE, J., KNIGHT, S., JACOBSEN, S. E., KRANC, K. R. & SIMON, A. K. 2011. The autophagy protein Atg7 is essential for hematopoietic stem cell maintenance. *J Exp Med,* 208**,** 455-67.

MUNOZ-PLANILLO, R., KUFFA, P., MARTINEZ-COLON, G., SMITH, B. L., RAJENDIRAN, T. M. & NUNEZ, G. 2013. K(+) efflux is the common trigger of NLRP3 inflammasome activation by bacterial toxins and particulate matter. *Immunity,* 38**,** 1142-53.

MURUVE, D. A., PETRILLI, V., ZAISS, A. K., WHITE, L. R., CLARK, S. A., ROSS, P. J., PARKS, R. J. & TSCHOPP, J. 2008. The inflammasome recognizes cytosolic microbial and host DNA and triggers an innate immune response. *Nature,* 452**,** 103-7.

NAKAHIRA, K., HASPEL, J. A., RATHINAM, V. A., LEE, S. J., DOLINAY, T., LAM, H. C., ENGLERT, J. A., RABINOVITCH, M., CERNADAS, M., KIM, H. P., FITZGERALD, K. A., RYTER, S. W. & CHOI, A. M. 2011. Autophagy proteins regulate innate immune responses by inhibiting the release of mitochondrial DNA mediated by the NALP3 inflammasome. *Nat Immunol,* 12**,** 222-30.

NAKHAEI, P., GENIN, P., CIVAS, A. & HISCOTT, J. 2009. RIG-I-like receptors: sensing and responding to RNA virus infection. *Semin Immunol,* 21**,** 215-22.

NARENDRA, D., WALKER, J. E. & YOULE, R. 2012. Mitochondrial quality control mediated by PINK1 and Parkin: links to parkinsonism. *Cold Spring Harb Perspect Biol,* 4.

NARENDRA, D. P., JIN, S. M., TANAKA, A., SUEN, D. F., GAUTIER, C. A., SHEN, J., COOKSON, M. R. & YOULE, R. J. 2010. PINK1 is selectively stabilized on impaired mitochondria to activate Parkin. *PLoS Biol,* 8**,** e1000298.

NEDJIC, J., AICHINGER, M., EMMERICH, J., MIZUSHIMA, N. & KLEIN, L. 2008. Autophagy in thymic epithelium shapes the T-cell repertoire and is essential for tolerance. *Nature,* 455**,** 396-400.

NODA, T., FUJITA, N. & YOSHIMORI, T. 2009. The late stages of autophagy: how does the end begin? *Cell Death Differ,* 16**,** 984-90.

OGAWA, M., NAKAGAWA, I., YOSHIKAWA, Y., HAIN, T., CHAKRABORTY, T. & SASAKAWA, C. 2009. Streptococcus-, Shigella-, and Listeria-induced autophagy. *Methods Enzymol,* 452**,** 363-81.

OGAWA, M., YOSHIMORI, T., SUZUKI, T., SAGARA, H., MIZUSHIMA, N. & SASAKAWA, C. 2005. Escape of intracellular Shigella from autophagy. *Science,* 307**,** 727-31.

OHSUMI, Y. & MIZUSHIMA, N. 2004. Two ubiquitin-like conjugation systems essential for autophagy. *Semin Cell Dev Biol,* 15**,** 231-6.

OKAMOTO, K. & KONDO-OKAMOTO, N. 2012. Mitochondria and autophagy: critical interplay between the two homeostats. *Biochim Biophys Acta,* 1820**,** 595-600.

ORVEDAHL, A. & LEVINE, B. 2009. Eating the enemy within: autophagy in infectious diseases. *Cell Death Differ,* 16**,** 57-69.

PATTERSON, N. L. & MINTERN, J. D. 2012. Intersection of autophagy with pathways of antigen presentation. *Protein Cell,* 3**,** 911-20.

PETIOT, A., OGIER-DENIS, E., BLOMMAART, E. F., MEIJER, A. J. & CODOGNO, P. 2000. Distinct classes of phosphatidylinositol 3'-kinases are involved in signaling pathways that control macroautophagy in HT-29 cells. *J Biol Chem,* 275**,** 992-8.

PETRILLI, V., PAPIN, S., DOSTERT, C., MAYOR, A., MARTINON, F. & TSCHOPP, J. 2007. Activation of the NALP3 inflammasome is triggered by low intracellular potassium concentration. *Cell Death Differ,* 14**,** 1583-9.

PIER, G. B. & AMES, P. 1984. Mediation of the killing of rough, mucoid isolates of Pseudomonas aeruginosa from patients with cystic fibrosis by the alternative pathway of complement. *J Infect Dis,* 150**,** 223-8.

PIER, G. B. A. R., R. 2005. Prenciples and practice of infectious disesases. *In:Mandell, G.L., Bennett,J.E.and Dolin, R. (eds).* Pliladelphia: Elsevvier Churchill Livingstone.

POLAGER, S., OFIR, M. & GINSBERG, D. 2008. E2F1 regulates autophagy and the transcription of autophagy genes. *Oncogene,* 27**,** 4860-4.

POOLE, K. & MCKAY, G. A. 2003. Iron acquisition and its control in Pseudomonas aeruginosa: many roads lead to Rome. *Front Biosci,* 8**,** d661-86.

QU, Y., MISAGHI, S., IZRAEL-TOMASEVIC, A., NEWTON, K., GILMOUR, L. L., LAMKANFI, M., LOUIE, S., KAYAGAKI, N., LIU, J., KOMUVES, L., CUPP, J. E., ARNOTT, D., MONACK, D. & DIXIT, V. M. 2012. Phosphorylation of NLRC4 is critical for inflammasome activation. *Nature,* 490**,** 539-42.

RATHINAM, V. A., JIANG, Z., WAGGONER, S. N., SHARMA, S., COLE, L. E., WAGGONER, L., VANAJA, S. K., MONKS, B. G., GANESAN, S., LATZ, E., HORNUNG, V., VOGEL, S. N., SZOMOLANYI-TSUDA, E. & FITZGERALD, K. A. 2010. The AIM2 inflammasome is essential for host defense against cytosolic bacteria and DNA viruses. *Nat Immunol,* 11**,** 395-402.

RATHINAM, V. A., VANAJA, S. K., WAGGONER, L., SOKOLOVSKA, A., BECKER, C., STUART, L. M., LEONG, J. M. & FITZGERALD, K. A. 2012.

TRIF licenses caspase-11-dependent NLRP3 inflammasome activation by gram-negative bacteria. *Cell,* 150**,** 606-19.

RAVIKUMAR, B., MOREAU, K., JAHREISS, L., PURI, C. & RUBINSZTEIN, D. C. 2010. Plasma membrane contributes to the formation of pre-autophagosomal structures. *Nat Cell Biol,* 12**,** 747-57.

REBSAMEN, M., MEYLAN, E., CURRAN, J. & TSCHOPP, J. 2008. The antiviral adaptor proteins Cardif and Trif are processed and inactivated by caspases. *Cell Death Differ,* 15**,** 1804-11.

SADIKOT, R. T., BLACKWELL, T. S., CHRISTMAN, J. W. & PRINCE, A. S. 2005. Pathogen-host interactions in Pseudomonas aeruginosa pneumonia. *Am J Respir Crit Care Med,* 171**,** 1209-23.

SAITOH, T. & AKIRA, S. 2010. Regulation of innate immune responses by autophagy-related proteins. *J Cell Biol,* 189**,** 925-35.

SAITOH, T., FUJITA, N., HAYASHI, T., TAKAHARA, K., SATOH, T., LEE, H., MATSUNAGA, K., KAGEYAMA, S., OMORI, H., NODA, T., YAMAMOTO, N., KAWAI, T., ISHII, K., TAKEUCHI, O., YOSHIMORI, T. & AKIRA, S. 2009. Atg9a controls dsDNA-driven dynamic translocation of STING and the innate immune response. *Proc Natl Acad Sci U S A,* 106**,** 20842-6.

SAITOH, T., FUJITA, N., JANG, M. H., UEMATSU, S., YANG, B. G., SATOH, T., OMORI, H., NODA, T., YAMAMOTO, N., KOMATSU, M., TANAKA, K., KAWAI, T., TSUJIMURA, T., TAKEUCHI, O., YOSHIMORI, T. & AKIRA, S. 2008. Loss of the autophagy protein Atg16L1 enhances endotoxin-induced IL-1beta production. *Nature,* 456**,** 264-8.

SALMOND, G. P. & REEVES, P. J. 1993. Membrane traffic wardens and protein secretion in gram-negative bacteria. *Trends Biochem Sci,* 18**,** 7-12.

SCHENTEN, D. & MEDZHITOV, R. 2011. The control of adaptive immune responses by the innate immune system. *Adv Immunol,* 109**,** 87-124.

SCHMITZ, J., OWYANG, A., OLDHAM, E., SONG, Y., MURPHY, E., MCCLANAHAN, T. K., ZURAWSKI, G., MOSHREFI, M., QIN, J., LI, X., GORMAN, D. M., BAZAN, J. F. & KASTELEIN, R. A. 2005. IL-33, an interleukin-1-like cytokine that signals via the IL-1 receptor-related protein ST2 and induces T helper type 2-associated cytokines. *Immunity,* 23**,** 479-90.

SHAHNAZARI, S., YEN, W. L., BIRMINGHAM, C. L., SHIU, J., NAMOLOVAN, A., ZHENG, Y. T., NAKAYAMA, K., KLIONSKY, D. J. & BRUMELL, J. H. 2010. A diacylglycerol-dependent signaling pathway contributes to regulation of antibacterial autophagy. *Cell Host Microbe,* 8**,** 137-46.

SHARP, F. A., RUANE, D., CLAASS, B., CREAGH, E., HARRIS, J., MALYALA, P., SINGH, M., O'HAGAN, D. T., PETRILLI, V., TSCHOPP, J., O'NEILL, L. A. & LAVELLE, E. C. 2009. Uptake of particulate vaccine adjuvants by dendritic cells activates the NALP3 inflammasome. *Proc Natl Acad Sci U S A,* 106**,** 870-5.

SHENOY, A. R., WELLINGTON, D. A., KUMAR, P., KASSA, H., BOOTH, C. J., CRESSWELL, P. & MACMICKING, J. D. 2012. GBP5 promotes NLRP3 inflammasome assembly and immunity in mammals. *Science,* 336**,** 481-5.

SHI, C. S., SHENDEROV, K., HUANG, N. N., KABAT, J., ABU-ASAB, M., FITZGERALD, K. A., SHER, A. & KEHRL, J. H. 2012. Activation of autophagy by inflammatory signals limits IL-1beta production by targeting ubiquitinated inflammasomes for destruction. *Nat Immunol,* 13**,** 255-63.

SHIMADA, K., CROTHER, T. R., KARLIN, J., DAGVADORJ, J., CHIBA, N., CHEN, S., RAMANUJAN, V. K., WOLF, A. J., VERGNES, L., OJCIUS, D. M., RENTSENDORJ, A., VARGAS, M., GUERRERO, C., WANG, Y., FITZGERALD, K. A., UNDERHILL, D. M., TOWN, T. & ARDITI, M. 2012. Oxidized mitochondrial DNA activates the NLRP3 inflammasome during apoptosis. *Immunity,* 36**,** 401-14.

SLOBODKIN, M. R. & ELAZAR, Z. 2013. The Atg8 family: multifunctional ubiquitin-like key regulators of autophagy. *Essays Biochem,* 55**,** 51-64.

SMITH, D. E. 2011. The biological paths of IL-1 family members IL-18 and IL-33. *J Leukoc Biol,* 89**,** 383-92.

SMITH, R. A., HARTLEY, R. C. & MURPHY, M. P. 2011. Mitochondria-targeted small molecule therapeutics and probes. *Antioxid Redox Signal,* 15**,** 3021-38.

SONGANE, M., KLEINNIJENHUIS, J., NETEA, M. G. & VAN CREVEL, R. 2012. The role of autophagy in host defence against Mycobacterium tuberculosis infection. *Tuberculosis (Edinb),* 92**,** 388-96.

SOSCIA, C., HACHANI, A., BERNADAC, A., FILLOUX, A. & BLEVES, S. 2007. Cross talk between type III secretion and flagellar assembly systems in Pseudomonas aeruginosa. *J Bacteriol,* 189**,** 3124-32.

STROMHAUG, P. E. & KLIONSKY, D. J. 2001. Approaching the molecular mechanism of autophagy. *Traffic,* 2**,** 524-31.

SUTTERWALA, F. S., MIJARES, L. A., LI, L., OGURA, Y., KAZMIERCZAK, B. I. & FLAVELL, R. A. 2007. Immune recognition of Pseudomonas aeruginosa mediated by the IPAF/NLRC4 inflammasome. *J Exp Med,* 204**,** 3235-45.

SUZUKI, T., FRANCHI, L., TOMA, C., ASHIDA, H., OGAWA, M., YOSHIKAWA, Y., MIMURO, H., INOHARA, N., SASAKAWA, C. & NUNEZ, G. 2007.

Differential regulation of caspase-1 activation, pyroptosis, and autophagy via Ipaf and ASC in Shigella-infected macrophages. *PLoS Pathog,* 3**,** e111.

SUZUKI, T. & NUNEZ, G. 2008. A role for Nod-like receptors in autophagy induced by Shigella infection. *Autophagy,* 4**,** 73-5.

TAL, M. C., SASAI, M., LEE, H. K., YORDY, B., SHADEL, G. S. & IWASAKI, A. 2009. Absence of autophagy results in reactive oxygen species-dependent amplification of RLR signaling. *Proc Natl Acad Sci U S A,* 106**,** 2770-5.

TANIDA, I., UENO, T. & KOMINAMI, E. 2004. LC3 conjugation system in mammalian autophagy. *Int J Biochem Cell Biol,* 36**,** 2503-18.

TERADA, L. S., JOHANSEN, K. A., NOWBAR, S., VASIL, A. I. & VASIL, M. L. 1999. Pseudomonas aeruginosa hemolytic phospholipase C suppresses neutrophil respiratory burst activity. *Infect Immun,* 67**,** 2371-6.

TING, J. P., LOVERING, R. C., ALNEMRI, E. S., BERTIN, J., BOSS, J. M., DAVIS, B. K., FLAVELL, R. A., GIRARDIN, S. E., GODZIK, A., HARTON, J. A., HOFFMAN, H. M., HUGOT, J. P., INOHARA, N., MACKENZIE, A., MALTAIS, L. J., NUNEZ, G., OGURA, Y., OTTEN, L. A., PHILPOTT, D., REED, J. C., REITH, W., SCHREIBER, S., STEIMLE, V. & WARD, P. A. 2008. The NLR gene family: a standard nomenclature. *Immunity,* 28**,** 285-7.

TRAVASSOS, L. H., CARNEIRO, L. A., GIRARDIN, S. E., BONECA, I. G., LEMOS, R., BOZZA, M. T., DOMINGUES, R. C., COYLE, A. J., BERTIN, J., PHILPOTT, D. J. & PLOTKOWSKI, M. C. 2005. Nod1 participates in the innate immune response to Pseudomonas aeruginosa. *J Biol Chem,* 280**,** 36714-8.

VALLIS, A. J., FINCK-BARBANCON, V., YAHR, T. L. & FRANK, D. W. 1999. Biological effects of Pseudomonas aeruginosa type III-secreted proteins on CHO cells. *Infect Immun,* 67**,** 2040-4.

VANCE, R. E., RIETSCH, A. & MEKALANOS, J. J. 2005. Role of the type III secreted exoenzymes S, T, and Y in systemic spread of Pseudomonas aeruginosa PAO1 in vivo. *Infect Immun,* 73**,** 1706-13.

VIRGIN, H. W. & LEVINE, B. 2009. Autophagy genes in immunity. *Nat Immunol,* 10**,** 461-70.

WANG, Y. H., GORVEL, J. P., CHU, Y. T., WU, J. J. & LEI, H. Y. 2010. Helicobacter pylori impairs murine dendritic cell responses to infection. *PLoS One,* 5**,** e10844.

WEBER, D. J., RUTALA, W. A., SICKBERT-BENNETT, E. E., SAMSA, G. P., BROWN, V. & NIEDERMAN, M. S. 2007. Microbiology of ventilator-associated pneumonia compared with that of hospital-acquired pneumonia. *Infect Control Hosp Epidemiol,* 28**,** 825-31.

WITZENRATH, M., PACHE, F., LORENZ, D., KOPPE, U., GUTBIER, B., TABELING, C., REPPE, K., MEIXENBERGER, K., DORHOI, A., MA, J., HOLMES, A., TRENDELENBURG, G., HEIMESAAT, M. M., BERESWILL, S., VAN DER LINDEN, M., TSCHOPP, J., MITCHELL, T. J., SUTTORP, N. & OPITZ, B. 2011. The NLRP3 inflammasome is differentially activated by pneumolysin variants and contributes to host defense in pneumococcal pneumonia. *J Immunol,* 187**,** 434-40.

WOODS, D. E., STRAUS, D. C., JOHANSON, W. G., JR., BERRY, V. K. & BASS, J. A. 1980. Role of pili in adherence of Pseudomonas aeruginosa to mammalian buccal epithelial cells. *Infect Immun,* 29**,** 1146-51.

WU, J. J., QUIJANO, C., CHEN, E., LIU, H., CAO, L., FERGUSSON, M. M., ROVIRA, II, GUTKIND, S., DANIELS, M. P., KOMATSU, M. & FINKEL, T. 2009. Mitochondrial dysfunction and oxidative stress mediate the physiological impairment induced by the disruption of autophagy. *Aging (Albany NY),* 1**,** 425-37.

XU, Y., JAGANNATH, C., LIU, X. D., SHARAFKHANEH, A., KOLODZIEJSKA, K. E. & EISSA, N. T. 2007. Toll-like receptor 4 is a sensor for autophagy associated with innate immunity. *Immunity,* 27**,** 135-44.

YAMAGUCHI, H., NAKAGAWA, I., YAMAMOTO, A., AMANO, A., NODA, T. & YOSHIMORI, T. 2009. An initial step of GAS-containing autophagosome-like vacuoles formation requires Rab7. *PLoS Pathog,* 5**,** e1000670.

YAMAMOTO, M., SATO, S., MORI, K., HOSHINO, K., TAKEUCHI, O., TAKEDA, K. & AKIRA, S. 2002. Cutting edge: a novel Toll/IL-1 receptor domain-containing adapter that preferentially activates the IFN-beta promoter in the Toll-like receptor signaling. *J Immunol,* 169**,** 6668-72.

YANG, J., ZHAO, Y., SHI, J. & SHAO, F. 2013. Human NAIP and mouse NAIP1 recognize bacterial type III secretion needle protein for inflammasome activation. *Proc Natl Acad Sci U S A,* 110**,** 14408-13.

YOSHIHARA, E. & EDA, S. 2007. Diversity in the oligomeric channel structure of the multidrug efflux pumps in Pseudomonas aeruginosa. *Microbiol Immunol,* 51**,** 47-52.

YU, H. B. & FINLAY, B. B. 2008. The caspase-1 inflammasome: a pilot of innate immune responses. *Cell Host Microbe,* 4**,** 198-208.

YUAN, K., HUANG, C., FOX, J., LATURNUS, D., CARLSON, E., ZHANG, B., YIN, Q., GAO, H. & WU, M. 2012. Autophagy plays an essential role in the clearance of Pseudomonas aeruginosa by alveolar macrophages. *J Cell Sci,* 125**,** 507-15.

ZAMBONI, D. S., KOBAYASHI, K. S., KOHLSDORF, T., OGURA, Y., LONG, E. M., VANCE, R. E., KUIDA, K., MARIATHASAN, S., DIXIT, V. M., FLAVELL,

R. A., DIETRICH, W. F. & ROY, C. R. 2006. The Birc1e cytosolic pattern-recognition receptor contributes to the detection and control of Legionella pneumophila infection. *Nat Immunol,* 7**,** 318-25.

ZHANG, J., RANDALL, M. S., LOYD, M. R., DORSEY, F. C., KUNDU, M., CLEVELAND, J. L. & NEY, P. A. 2009. Mitochondrial clearance is regulated by Atg7-dependent and -independent mechanisms during reticulocyte maturation. *Blood,* 114**,** 157-64.

ZHAO, Y., YANG, J., SHI, J., GONG, Y. N., LU, Q., XU, H., LIU, L. & SHAO, F. 2011. The NLRC4 inflammasome receptors for bacterial flagellin and type III secretion apparatus. *Nature,* 477**,** 596-600.

ZHAO, Y. O., KHAMINETS, A., HUNN, J. P. & HOWARD, J. C. 2009. Disruption of the Toxoplasma gondii parasitophorous vacuole by IFNgamma-inducible immunity-related GTPases (IRG proteins) triggers necrotic cell death. *PLoS Pathog,* 5**,** e1000288.

ZHAO, Z., FUX, B., GOODWIN, M., DUNAY, I. R., STRONG, D., MILLER, B. C., CADWELL, K., DELGADO, M. A., PONPUAK, M., GREEN, K. G., SCHMIDT, R. E., MIZUSHIMA, N., DERETIC, V., SIBLEY, L. D. & VIRGIN, H. W. 2008. Autophagosome-independent essential function for the autophagy protein Atg5 in cellular immunity to intracellular pathogens. *Cell Host Microbe,* 4**,** 458-69.

ZHOU, R., YAZDI, A. S., MENU, P. & TSCHOPP, J. 2011. A role for mitochondria in NLRP3 inflammasome activation. *Nature,* 469**,** 221-5.

ZOU, H., LI, Y., LIU, X. & WANG, X. 1999. An APAF-1.cytochrome c multimeric complex is a functional apoptosome that activates procaspase-9. *J Biol Chem,* 274**,** 11549-56.